Sant'Anna
School of Advanced Studies – Pisa

Accademic Year 2018/2019
Phd Course
in BioRobotics

Soft and Flexible Sensors: technologies and biomedical applications

Author
Martina Maselli
Supervisor
Prof. Cecilia Laschi
Tutor
Dr. Francesca Cecchi
Co-Tutor
Eng. Cristina Frà

ABSTRACT

The study of pressure distribution over a not-defined surface, as well as the detection of stretching capability, are subjects matter of great interest in many fields as biomedical measurements, human motion detection, human-machine interfaces, and soft robotics. Novel and smart sensing solutions are research topics of great interest since the need for sensors with properties of flexibility and stretchability is growing. The emerging class of smart textiles holds great potential for developing new concepts of transducers and sensors, and investigations about their prospects deserve rising attention.

The aim of this research is the study of concepts and applications of textile sensors for strain and pressure detection. An example of matrix textile sensor has been designed and developed, by sandwiching a piezoresistive fabric sheet between two outer fabric layers embedding conductive rows and columns. The location of the applied pressure can be identified by detecting the position where the change of resistances occurs between the external conductive paths. Tests regarding its metrological properties have been carried out to highlight the sensor advantages and drawbacks and to establish general guidelines for its use. Also, a strain-resistance sensor based on commercial knitted textile has been designed and developed. Firstly, a methodology to characterize and to calibrate the strain-resistance sensor is proposed, suitable also for analysing the behaviour of any conductive and stretchable fabrics and useful to establish general guidelines for its use. Secondly, a new mathematical model is proposed to compensate for hysteresis and relaxation in strain sensors made of conductive textile.

The wide selection of advantages exhibited by this class of sensors, e.g. thinness, lightness, flexibility, stretchability and wearability, suggests their exploitation in a huge number of applications, especially concerning the biomedical field. In this thesis, smart fabric sensors based on a piezoresistive detecting principle have been employed to monitor single planes neck movements and to develop a new cognitive technological tool for physical and cognitive training. Development, testing and data analysis phases have been accomplished, confirming the versatility and potentiality of the sensing solutions based on smart textiles.

Contents

List of Figures

List of Tables

Introduction

Strain and pressure sensing with smart textiles

Conventional electronic devices, fabricated on rigid yet brittle semiconductor wafers, have evolved towards miniaturization with the aim of realizing faster, smaller and more integrated devices. An alternative approach to future electronics is to integrate the attributes of flexibility and stretchability to realize soft and human-friendly devices. Stretchability — the ability to conform to and cover movable and arbitrarily shaped objects — could be exploited in the development of wearable devices, as well as biomedical applications, that can be embedded into clothes and garments or even attached directly to the skin. Possible applications of this include the detection of human motion, monitoring personal health and therapeutics.

Owing to the difficulties in developing stretchable electric materials, the current mainstream strategy in attempting to achieve stretchability is not to develop new materials, but instead is to engineer new structural constructs from established materials. Device of particular interest are soft and flexible sensors that are enveloped in arbitrarily shaped soft matrices, which are both highly conformable and extensible. The goal is to gain valuable sensing information while minimizing the physical impact on the host system.

The study of pressure distribution over a not-defined surface, as well as the detection of stretching capability, are subjects matter of great interest in many fields, such as biomedical measurements, human motion detection, human-machine interfaces, and soft robotics.

Since commonly employed commercial products tend to be expensive and application specific, it would be worthwhile to develop a thin, versatile and flexible sensing device, free from geometry constraints, stretchable and able to perform multi-touch detection. For these reasons numerous recent research studies have been aimed to obtain sensing solutions low-cost and versatile from the point of view both of hardware (e.g. shape and dimension) and software (e.g. direct management of data reading and resolution settings). They are asked to be not only thin and pliable, as polyester- and PCB-based products, but also flexible and attachable over curved and narrow surfaces, like robotic joints and fingers. They also need to

be customizable, suitable to be embedded in wearable systems and possibly based on affordable technologies.

A large amount of different types of sensors have already been proposed for the aforesaid applications, mainly relying on the capacitive, piezoelectric and piezoresistive transduction principle.

The latest class of smart textiles is a promising candidate to meet the above mentioned conditions, making the manufacturing of lightweight, soft and low cost sensors possible. Smart textiles are fabrics that can sense and react to mechanical, thermic, chemical, magnetic and electric stimuli, by means of extrinsic and intrinsic modifications. In the last years the development of conductive/piezoresistive fabrics has been a common research topic in the areas of chemistry and smart materials, leading to widespread commercial products. To date, conductive/piezoresistive textiles are employed to develop a wide group of Smart Fabrics Transducers (SFT), e.g. actuators, energy harvesting solutions and sensors. Specifically, conductive textiles that change their electrical properties because of the environmental impact can be used as sensors, and in particular as stretch or pressure sensors.

In this framework, the present thesis aims at analysing possible smart solutions for both pressure and strain sensors that can be manufactured with commercial conductive/piezoresistive fabrics. In particular, studies on matrix multilayer textile-based pressure sensors and on textile-based strain sensors have been carried out. The last part of the thesis involved the use of smart fabric sensors in two different biomedical applications that can actually benefit from their properties (i.e. flexibility, thinness, lightness, wearability, streatchability, customizability of shape, dimension and resolution). For each application, the proper sensor design was studied considering the specific requirements. Development, testing and data analysis were carried out.

Chapters organization

This thesis is devoted to the design, development and employment of textile sensors for pressure mapping and strain detection, and it is divided into seven chapters.

Chapter one presents a general discussion on the state of the art of soft and flexible sensors for pressure and strain measurements. The aim is to highlight the fundamental domain

of interest (biomedical) for this thesis that make use of pressure and strain profiles and the mainly employed detecting principles. A final part is dedicated to the smart fabrics description, focusing on their potentialities for the manufacturing of a wide class of transducers and sensors.

Chapter two describes the design, development and characterization of a rectangular-shaped textile matrix sensor, composed of two external fabric layers with a further piezoresistive fabric layer (EeonTexTM LG-SL-PA, Eeonyx Corp., Pinole, CA, US) interposed between the former ones. The two external layers consisted of a nonconductive textile on which parallel conductive stripes were obtained by sewing multiple copper threads, so that a pattern of alternate conductive and insulating bands was created. The stripes of each layer were oriented at 90° with respect to the stripes of the other layer. Thanks to this arrangement, the sensing units, called sensels, were placed at each intersection of rows and columns. Thus, the pressure measurements were obtained by evaluating the resistance changes for each sensel: when the fabrics were compressed near the crossing point, the electrical resistance of the interposed piezoresistive layer decreased proportionally to the applied pressure values. The electric measurement of the sensels was achieved according to a powering/reading scanning sequence based on possible circuital solutions that are reviewed in the text. The developed sensor was characterized in both static and dynamic conditions and also under stretch and fixed on curved surfaces. This study was accomplished to obtain a complete metrological overview of the sensor, which is fundamental for managing it with a deeper awareness of both its benefits and drawbacks.

Chapter three proposes a methodology to characterize and to calibrate a strain-resistance sensor based on commercial knitted textile. This characterization procedure represents an interesting result per se. It has been conducted on a single material, but its general characteristics make it suitable for analyzing the behaviour of any conductive and stretchable fabrics. Secondly, the design of an innovative wearable device for long-term and minimally invasive joint angular measurements has been described. Electrolycra (Mindsets Ltd) was selected as the sensing element of the device because of its electromechanical properties and because it is elastic, highly conductive, inexpensive, light and not cumbersome. The validation of the wearable sensor (a goniometer) was performed using the humanoid robot SABIAN. Dynamic tests demonstrated that the wearable device is suitable for scenarios where the accuracy of measurements is less relevant than the ability to continuously track joint movements in a not-obtrusive way.

Chapter four is concerned with modelling of smart textiles, aimed at compensating their intrinsic nonlinearities. In particular, a new model is proposed to compensate for hysteresis and relaxation in strain sensors made of Electrolycra. These sensors are increasingly employed in emerging areas such as wearable electronics and soft robotics for their simple transduction mechanism and low cost. However, being intrinsically nonlinear, the signals measured from these devices need some processing, in order to increase their sensing accuracy. Here, a new model was proposed for the compensation of the main distortions intrinsic in these soft sensors, which are mainly caused by hysteresis and relaxation, whose combined effect produces rate-dependent hysteresis. The model capabilities are tested on experimental data measured on Electrolycra. The comparisons with the results obtained with two different models witness the good behaviour of the proposed model.

Chapter five presents the development of a "wear and forget" device able to monitor head posture. This chapter consists of three parts: 1) characterization of the piezoresistive textile employed both in static and dynamic conditions; 2) development of the sensor design; and 3) validation study concerning the investigation of sensor performances using Vicon measurements, as the reference standard. The proposed smart textile allowed the development of a light, comfortable, and non-invasive wearable system. The sensor accuracy and repeatability in measuring cervical range of motion in each primary plane (lateral bending, axial rotation, and flexion/extension) for five healthy subjects were evaluated. The results show a good accuracy and satisfactory repeatability with maximum standard deviation value close to 10°. The effectiveness of the wearable system as a valid, accurate, and suitable device for evaluating single plane neck movements was demonstrated.

Chapter six is about the creation of a new cognitive tool able to provide training for cognitive functions that take advantage of the physical activity involved in the execution of the task. In the present chapter, a study concerning the application of a new cognitive tool for episodic memory is presented and divided in two parts. The first one aims at developing a new sensorized device based on smart textiles, called SmartTapestry, for physical and cognitive training. The second part aims at understanding its technical viability and level of sensitivity in stimulating the same cognitive domain covered by the standardized tests, despite the introduction of the physical activity variable. The SmartTapestry device was tested with a total of 53 subjects, 29 healthy subjects and 24 subjects suffering from Mild Cognitive Impairment. The results show a good correlation between the two approaches ($p<0.005$),

suggesting that SmartTapestry can stimulate the same cognitive functions of traditional cognitive tasks, with the addition of physical exercise.

Chapter seven reports the conclusion of the work, reporting the main obtained results, a critical discussion of the proposed sensors, the advantages of the approach and the possible future works.

Chapter 1

Soft and flexible sensors: state of the art

Since the advent of electronics, advances in fabrication techniques have driven the development of smaller, faster, and more efficient devices. To date, the primary focus has been on rigid electronics. Recent interest in wearable electronics [1][2], human/machine interfaces [3], and soft robotics [4], among other areas [5], has led to an entirely new class of electronic devices – known as stretchable electronics. These emerging devices require new fabrication schemes that enable integration of heterogeneous soft functional materials [6]. One device of particular interest is soft and flexible sensors that are enveloped in arbitrarily shaped soft matrices, which are both highly conformal and extensible. The goal is to gain valuable sensing information while minimizing the physical impact on the host system. In addition to their compliance, these sensors have the advantages over more traditional sensors including impact resistance, reduced-cost, low power, and tolerance to strains over 100%.

Due to the disparate mechanical properties of soft objects and conventional rigid electronics, integrating electronic devices within highly stretchable matrices has proven difficult. Soft sensors are typically composed of a deformable conducting material patterned onto, attached to, or encapsulated within an inactive stretchable material. Generally, the material used for fabrication of sensors is decided from some factors like the application of the sensor, its availability, total cost of manufacturing, and so forth. Moreover, there are different kinds of techniques with which the flexible sensors are developed. The dimensions of the final products dictate the procedure used to make the sensor prototype. Photolithography [7], screen-printing [8], inkjet printing [9], laser cutting [10] are some of the most common ones.

Strain and pressure sensors are one of the most standardized applications of those innovative flexible sensors. Nowadays, a wide number of commercial and research products have been developed as sensitive thin skins that are able to adapt their properties and

performances according to the specific application. Particularly, various pressure and strain sensors have been developed because of their broad applications in personalized heath-monitoring, human motion detection, human-machine interfaces, and soft robotics. The fundamental domain that makes use of force and deformation profiles and of interest for this thesis project is described in the following section.

1.1 Biomedical Applications

There are numerous potential biomedical applications for flexible strain and pressure sensors. Below there are the most promising examples in the field of biomedical engineering.

1.1.1 Pressure sensors

Arrays of force sensors of different configurations have been used also for an incredibly wide variety of medical applications [11], from robotic surgery and drug delivery systems to orthopaedics and physical therapy devices.

First of all, minimal invasive surgery (MIS) benefits from a haptic feedback from sensorized tools [12]. Having a complete tactile feedback for the laparoscopic tools would enable the analysis of tissue characteristics and pathological conditions, maintaining the same time reduced anatomical openings and also improving remote-control manipulation of instruments. Similarly, force feedback permits collision detection with rigid structures but does not prevent damage to soft tissues or tearing of sutures and it reduces the force applied for suture sewing. Also the Vinci surgical system by Intuitive Surgical, Inc. (the only master-slave MIS system approved by US Food and Drug Administration), that has been successfully used in the last years for general, urological, gynaecological, thoracoscopic, and thoracoscopically assisted cardiotomy procedures, provides force feedback also if it lacks feedback of tactile sensation [13].

Gait analysis can also benefit from pressure sensors use, in particular employing in-shoe sensor developed for providing information regarding the symmetry in foot function during gait. Asymmetry in foot function during gait can generate undesired torque and stress components that, over-time, place wear and tear on body tissues and can potentially cause symptoms of discomfort and pain [14][15]. Commercial products like F-Scan and iShoe insoles and MatScan® pressure mat by Tekscan, Inc. are commonly used by doctors to

analyse patients' gait [16], and in particular the force distribution on their foot, in order to increase their comfort level while walking, decrease lower back and chronic knee pain, prevent falls and assess balance problems.

An interesting pressure-sensitive foot insole for real-time monitoring of plantar pressure distribution during walking based on an optoelectronic technology was developed at Scuola Superiore Sant'Anna [17]. The device consisted of a flexible insole with 64 pressure-sensitive elements and an integrated electronic board for high-frequency data acquisition, pre-filtering, and wireless transmission to a remote data computing/storing unit. The transduction unit was made of independent silicone cells that had the shape of a pyramidal frustum with a square basis and an internal central curtain (Figure 1.1). Each cell covered a light emitter and a light receiver diodes, soldered on the PCB. The light emitter was a high-luminosity green LED and the receiver was an ambient-light photodiode equipped with an embedded temperature-compensation circuit. The sensor worked as a force-to-voltage transducer: when a load was applied on the top surface of the cover, the silicone bulk deformed itself and the curtain gradually closed the light path between the emitter and the receiver, and thus the output voltage changed.

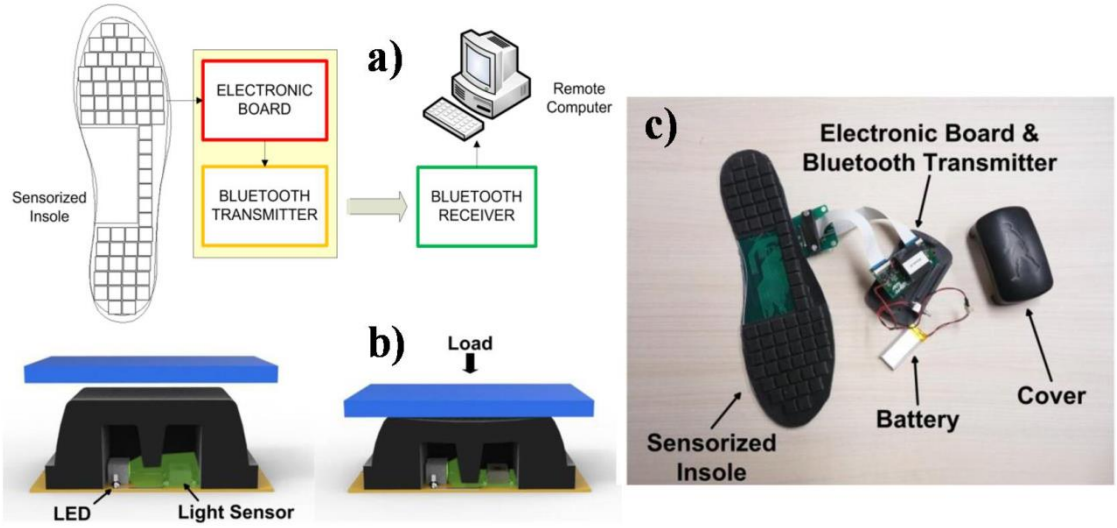

Figure 1.1 Overview of the system architecture of the pressure-sensitive foot insole developed at the Scuola Superiore Sant'Anna, b) representation of the sensitive element and its functioning principle, c) components of the device: sensorized insole connected to the electronic board through flat cables, Bluetooth transmitter, Li-Ion battery [17].

1. Soft and flexible sensors: state of the art

Pressure sensing has been commercially introduced to evaluate dental implants and for digital occlusal analysis to create long-lasting restorations, control bite forces during full mouth restorations and protect veneers during orthodontic treatment [18]. In addition, Electropalatography (EPG) is also another domain of application, which is a technique employed to monitor patterns of tongue contacts with the hard palate, especially during articulation and speech. Recently, textile-based sensing technologies were employed to realize an innovative EPG tool (Figure 1.2) able to both maintain the proper spatial resolution and perform quantitative pressure detection [19].

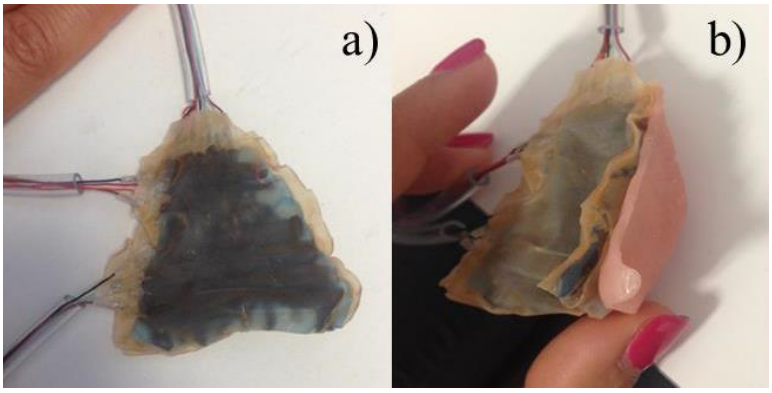

Figure 1.2 a) The sensor shielded in the latex cover and b) lateral views of the complete prototype with the sensor fixed on the acrylic support obtained from the plaster cast of a volunteer [19].

Force sensitive bed monitoring for the elderly is the cornerstone of methods to prevent bed shores incidence and promote healing, allowing clinicians to screen areas for potential ulcers, display peak pressure profiles and contact area [20]. Main commercial products for the aim are by Tekscan, Inc. (COMFORTMat System® and Body Pressure Measurement System®, see Figure 1.3) [16], Pressure Profile Systems, Inc. [21] and Sensor Products, Inc. (Tactilus® Bodyfitter®) [22].

Interface pressure sensing is exploited also for the sensorization of medical devices and simulators for clinical training. A commercial example is the MammaCare PAD system by Tekscan, Inc. that is a training platform comprised of tactually accurate breast models and instrumented with force sensors [16]. An example in literature is the modification of the Laerdal ®Neonatal Intubation Trainer by applying pressure sensors on areas that are mainly subject to stress and potential injuries (force sensing resistors-FSRs on the dental arches and epiglottis, a matrix textile sensor on the tongue) [23]. The device is able to provide an

instrumented neonatal intubation skill trainer and an objective feedback for the improvement of clinical competences required for such a delicate procedure.

Pressure distribution provides important information in case of pressure garments employment, since the application of a correct pressure on skin portions is useful for the treatment of scars, ulcers and muscle pain after training [24][25].

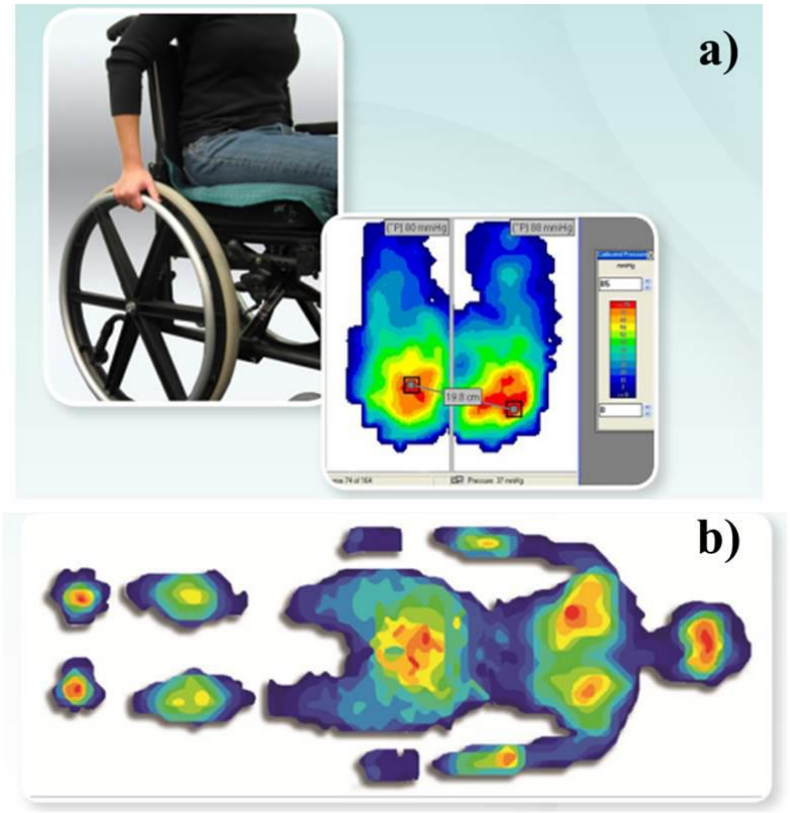

Figure 1.3 a) Seating pressure profile with Tekscan's CONFORMat System®, b) full body pressure measurement profile with Tekscan's Body Pressure Measurement System (BPMS) [16].

Orthotic and orthopaedic prosthesis research and fitting benefits from determining loading forces, pressures, and contact areas at the joint interfaces, in order to provide data for dynamic and finite stress analysis, study implant design and articulating joints, view and assess the impact of various joint compartment geometries and materials [26][27].

1.1.2 Strain sensors

Flexible strain sensors can potentially function for several biomedical applications; they could be utilized as body-integrated electronic devices, attached onto the clothing or directly

laminated on the human skin for the body strain measurement, ranging from minute skin motions induced by respiration and heartbeat to human body large strains like bending/straightening of body joints. Indeed, as largely demonstrated in the research field, highly stretchable and flexible strain sensors have been used especially as wearable sensors.

Wearable sensors have revolutionized the way the activities of a person are being monitored [28]. They provide the information accurately and efficiently regarding the behaviour and actions of a person. Figure 1.4 shows a schematic of a monitoring system to sensing the physiological parameters like heart rate and respiratory rate or motion parameters of a person and transmit the data wirelessly to the cloud via any information gateway [29]. This is a quick and efficient system because any abnormality in the transmitted data can generate a notification to the healthcare or family members.

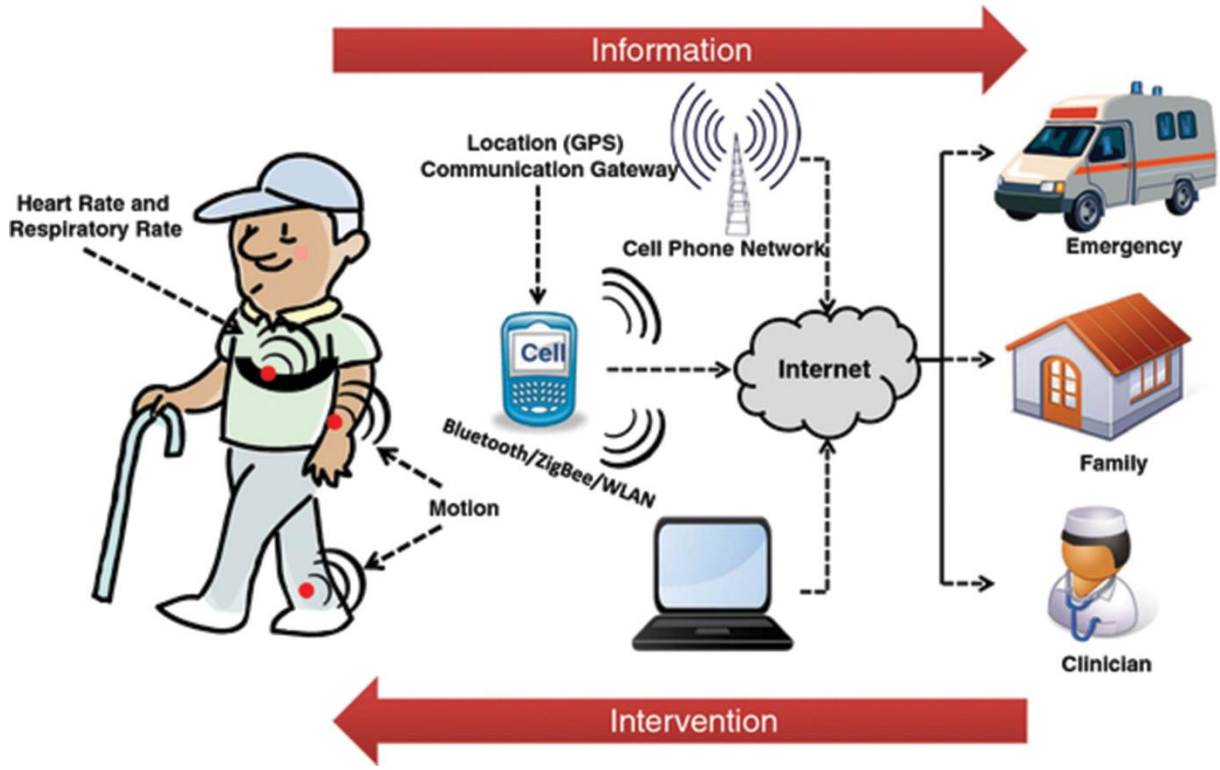

Figure 1.4 Schematic representation of the use of wearable sensors for physiological and motion parameter monitoring for remote and personalized health-care systems [29].

Wearable sensors have many potential applications in rehabilitation, personal health, sport performance monitoring and entertainment. The majority of these applications require long-term wearing of these sensors; therefore it is essential to assign an equal priority of sensor performance to wearability and comfort [30]. The challenge is thus the development of

technologies capable of monitoring continuously, similar to the “wear and forget” concept [31]. This means that the technology should not hinder movements, instead offering a comfortable wearability similar to everyday cloths. The human body is mainly composed of soft tissues; therefore, wearable sensors designed to interact with human bodies should be soft, light and conform to body geometry without obstructing natural motion [32]. Within this framework, solutions based on soft or flexible strain sensors represent the most promising approach [5].

Such sensors should be highly stretchable and flexible to mimic complex and large deformations of the human skin or clothing and sufficiently possess high sensitivity to be able to detect minute skin strains induced by blood flow pulse or respiration [33].

Figure 1.5 (a) shows in vitro blood pressure monitoring using a flexible capacitive-type sensor. The sensor was wrapped around the carotid artery of a pig and changes on the diameter of the vessel due to the blood flow pressure were measured [34]. In another approach, highly sensitive and wearable strain sensors have been developed for the tiny skin motion detection induced by phonation, facial expression, tissue swelling, wound healing, breathing, and pulse [35][36][37][38]. Inset of Figure 1.5 (b) illustrates a resistive-type sensor fixed to the chest area and its response to the breathing both in still (black) and movement (red) sates. The same sensor attached to the wrist was also used for heartbeat measurement [36]. Long-term monitoring of blood flow pulse and respiration rate, as vital signs, can be potentially employed for the personalized health-monitoring and early diagnosis of diseases.

Patellar reflex test was conducted by using a stretchable sensor attached onto the knee while the person was sat with naturally relaxed leg (Figure 1.5 (c)) [39]. At this state, a large strain was accommodated by the sensor since the knee was fully bent. To test the patellar reflex, a hammer was used to tap the patellar tendon ligament. As a normal response, the leg should straighten and then come to its initial position quickly (Figure 1.5 (d)). Therefore, flexible strain sensors are able to detect physiological data, such as blood pressure and oxygen saturation [34], breathing rate [1] [36] [40], heartbeat [2] [36], and beyond.

As another application, flexible strain sensors can be used for the body movement analysis [41], generally implemented for joint angular measurement. Yamada et al. [1] used aligned carbon nanotubes (CNT) encapsulated in silicone rubber, with ten films being assembled on a commercial stocking over the knee joint (Figure 1.6 (a)). Similarly, Ryu et al. [42] adopted

CNT fibers fabricated by the dry-spinning process for human motion detection (Figure 1.6 (b)).

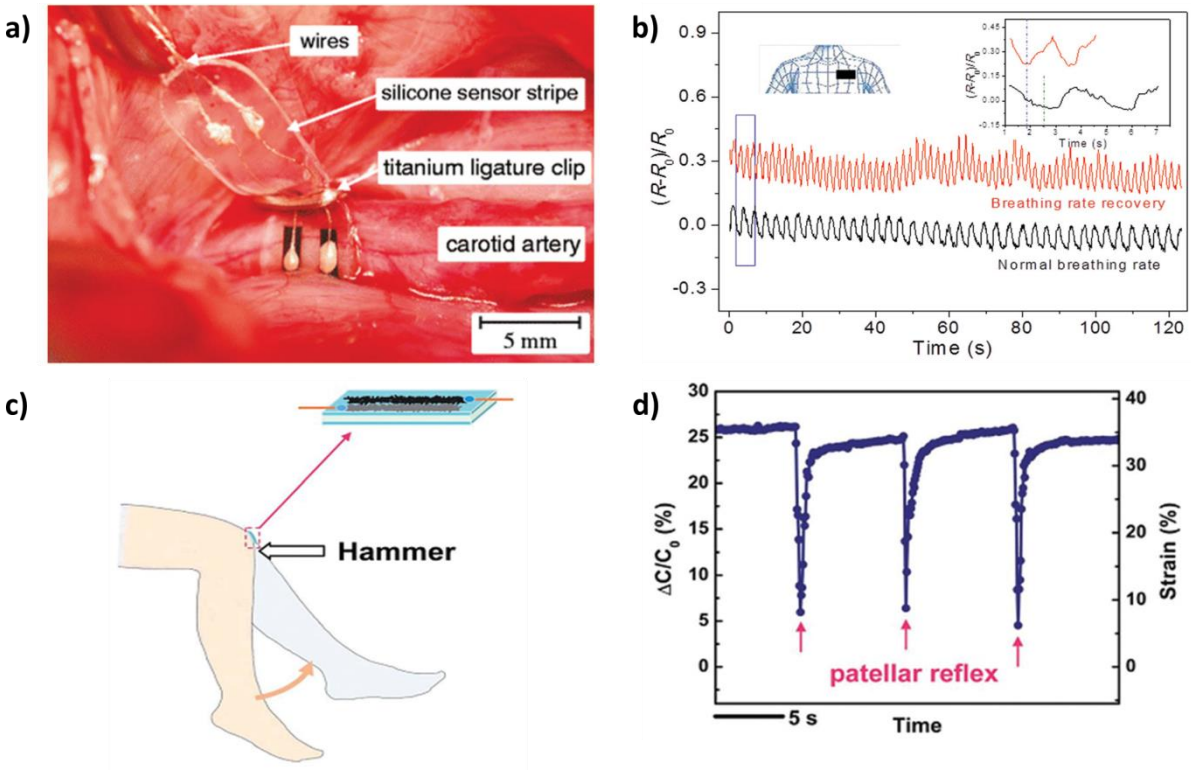

Figure 1.5 a) A capacitive-type strain sensor wrapped around the carotid artery of a pig [34]; b) breathing monitoring by attaching a wearable strain sensor in the chest; inset, location of attached strain sensor [36]; c) schematic of the patellar reflex test, a capacitive-type sensor is mounted on the knee for the strain measurement [39]; d) response from a strain sensor during the patellar reflex test [39].

These sensors are highly stretchable, but materials and fabrication are still expensive. In contrast, Mengüç et al. [43][44] presented a soft suit to measure leg joint angles that was based on a liquid metal, eutectic gallium indium alloy, embedded in the elastomer (Figure 1.6 (c)).

Tognetti et al. [45] described a goniometer for knee motion detection based on knitted piezoresistive fabrics (single- and double-layer), whereas Shyr et al. [46] developed an elastic conductive webbing composed of conductive yarns (polyamide fibers coated with carbon particles) and elastic yarns.

As a conclusion, the possible applications of pressure interface monitoring and strain sensing in biomedical field are impossible to count in an exhaustive manner, being limited only by imagination.

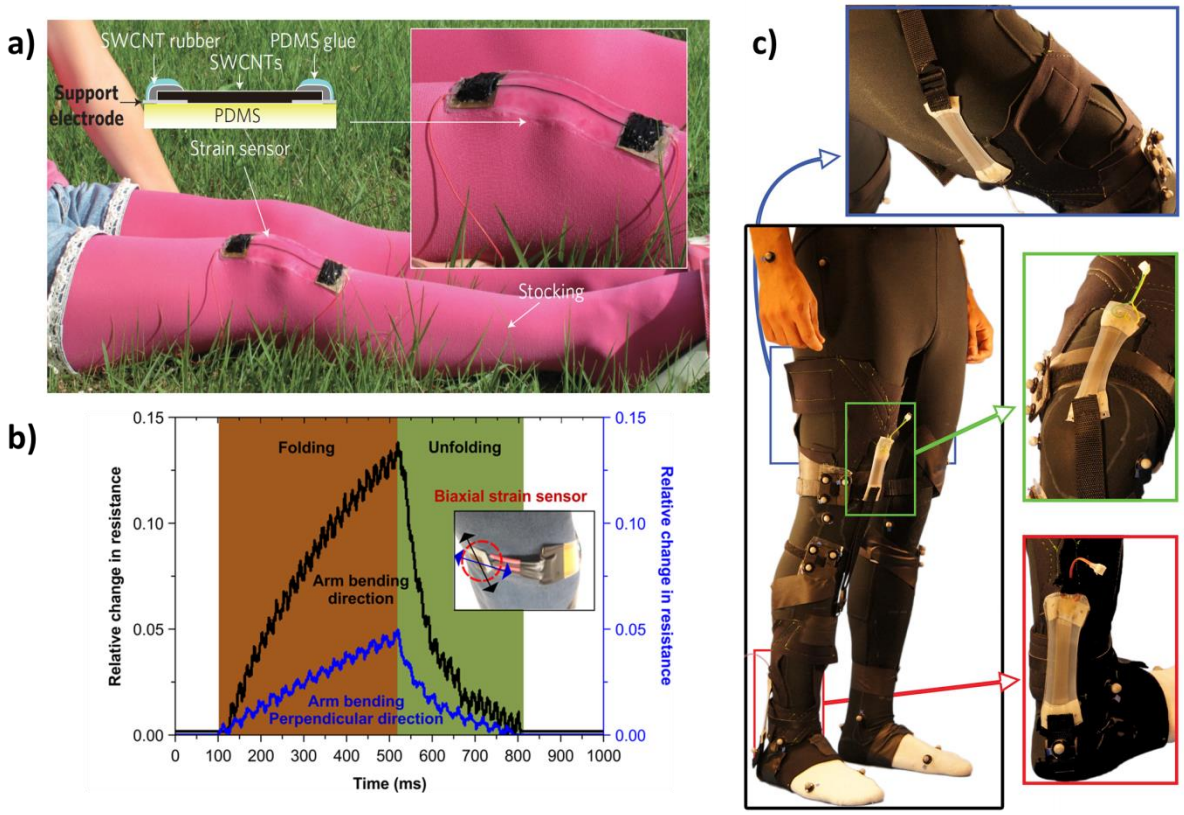

Figure 1.6 a) Strain sensor fixed to a stocking [1]; b) relative changes in resistance versus time for a biaxial strain sensor placed over an elbow, with the x-axis parallel to the arm (black) and the y-axis parallel to joint's axis of rotation (blue) [42]; c) photograph of the prototype sensing suit worn by a participant, from top to bottom: the hip sensor, the knee sensor and the ankle sensor [43].

1.2 Detecting principle for pressure and strain sensing

A large amount of different types of sensors have already been proposed for the aforesaid applications, mainly relying on the capacitive, optical, piezoelectric and piezoresistive detecting principles. The main requirements are flexibility and enhanced stretch capabilities. Flexible pressure sensors are currently available based on different transduction methods, but stretch capability is less common. On the other hand, different types of flexible and stretchable strain sensors have been proposed. Other requirements include simple mounting or adhesion mechanism, minimal wiring, temperature independence, low cost and well established fabrication techniques.

1. Soft and flexible sensors: state of the art

In spite of the variety of technical solutions currently used to implement pressure and strain sensors, we mention here just those that are more common or more promising. The advantages and disadvantages of the main transduction methods were summarized in Table 1.1 and explained in the following sections.

Table 1.1 Transduction techniques and their relative advantages and disadvantages.

Type	*Modulated parameter*	*Advantages*	*Disadvantages*
mechanical deformation-based	resistance	-low cost -realized as MEMS -easy to integrate in PDMS layers	-hysteresis -non linearity -temperature and humidity susceptibility
capacitive	capacitance	-excellent sensitivity -large dynamic range -good spatial resolution	-hysteresis -complex electronics -noise susceptibility
piezoelectric	stress polarization	-high frequency response -high sensitivity -high dynamic range	-dynamic sensing only -temperature sensitivity -poor spatial resolution
optical	light intensity/spectrum	-good sensing range -high spatial resolution -immunity from EMI	-bulkiness -high power consumption -fragility
magnetic	magnetic field	-high sensing range -good dynamic range -physical robustness	-sensitivity to EMI -bulkiness -high power consumption
piezoresistive	resistance	-good sensitivity -low noise -simple electronics -high spatial resolution	-hysteresis -non linearity -drift -temperature sensitivity

1.2.1 Mechanical deformation-based sensors

Mechanical deformation based sensors, or strain gauges, consist of a structure that elastically deforms when subject to a force which in turn leads to a change in its resistance. To optimise the change in resistance due to applied mechanical stress, strain gauges are typically long winding snakelike structures. In this way, when deformed, the cross-section of the strain gauge decreases while its conduction length increases. Here, typically, the change in resistance of the strain gauge material itself is secondary to the change due to its mechanical deformation.

Strain gauges can also be employed to design pressure sensing units [47]. They are made either from resistive elements or from semiconducting materials and bonded to the stressed material. Since they are very sensitive and highly susceptible to humidity and temperature changes, strain gauges are often used with a conditioning circuit that includes a Wheatstone bridge followed by an amplification stage. Due to their mechanical nature, they have high hysteresis and often are non-linear in response. Strain gauge development is currently optimized through the use of micro-machined fabrication techniques, to be directly integrated with readout electronics and other microelectromechanical systems (MEMS) elements.

In order to develop flexible strain gauge sensors that should be adaptable on curved surfaces, silicon-based or metallic strain gauges can be adapted on flexible printed circuit boards [48] or on flexible polyimide films and covered with polydimethylsiloxane (PDMS) layers [49]. An example of highly stretchable and soft strain gauge sensors were reported by Muth et al. [50] using embedded 3D printing technique where the viscous nanomaterial ink was directly embedded in elastomer films through a deposition nozzle (Figure 1.7). The ink forms a resistive sensing element, while the reservoir serves as a matrix material.

In [51] a fully printable sensorized bending actuator was presented with a flexible resistive strain sensor directly 3D printed using easily accessible FDM printer hardware with a dual-extrusion tool head.

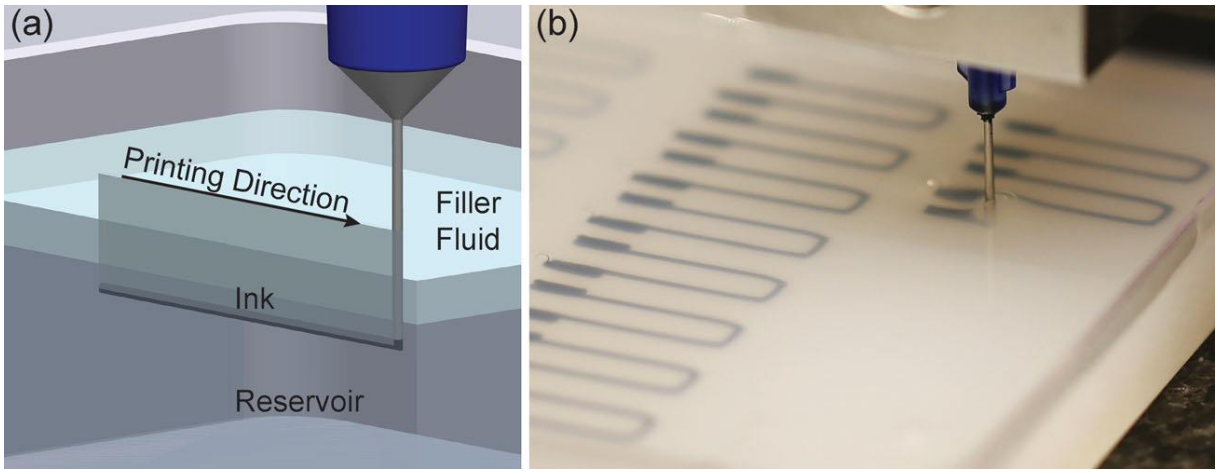

Figure 1.7 (a) Schematic illustration of the embedded 3D printing process. A conductive ink is printed into an uncured elastomeric reservoir, which is capped by filler fluid; (b) photograph of 3D printing process for a planar array of soft strain sensors [50].

1.2.2 Capacitive sensors

A capacitive sensor consists of two conductive plates with a dielectric material sandwiched between them. The applied force or strain can cause either the change in the distance between electrodes or in its area, modifying the capacitance. To measure the variation, several conditioning circuits can be used depending also on the type of the desired output signal.

To date, capacitive sensors have primarily been used in pressure, tactile, or shear sensing. In addition, they seem to be temperature independent and they generally exhibit a good frequency response, high spatial resolution, shear sensitivity and have a large dynamic range. However, these sensors are more susceptible to noise, especially in a matrix configuration because of crosstalk noise. They suffer from severe hysteresis and require relatively complex electronics to filter out this noise: careful and dedicated conditioning circuitry is required to take advantage of the excellent sensitivity and repeatability achieved by some of their implementations. Another disadvantage of capacitive sensing is its susceptibility to parasitic capacitance. Several designs have emerged specifically for the robotic skin application, especially relying on MEMS and silicon micromachining [52]. In particular, a capacitive sensor manufactured using photolithography on a flexible substrate is presented in [53][54][55].

For flexible strain sensors, capacitive-type sensors generally employ a highly compliant dielectric layer sandwiched between a pair of stretchable electrodes [33]. Hydrogels, swollen

with ionic liquids are electrically conductive and have become a popular choice for electrodes in soft capacitive sensing devices [56]. Usually, hydrogels suffer from failure due to ionic migration and eventual electrochemical breakdown at relatively low voltages, but it was recently shown that incorporation of a dielectric and use with AC fields limits the voltage drop at the electrical double layer [57]. As these materials improve and new ones become available, the key considerations are the conductivity of the material at necessary strains, as well as its temporal stability due to solvent volatility. Additionally, the change in conductivity as a function of stimulus is relevant. For example, resistive strain sensors require a large change in conductivity associated with the application of strain; whereas capacitive sensors are dependent on the change in distance between the electrodes. Hydrogels have large potential in this space, as they are inexpensive to fabricate, potentially bio-compatible and biodegradable; furthermore, they can be optically transparent [4] [58].

Capacitive sensors depend heavily on what dielectric materials they use. Design considerations include the dielectric constant, dielectric loss, and dielectric mechanical properties. It is important that the thickness of the dielectric layer remains uniform, using techniques such as spin coating [59], or alternatively using commercial dielectric tapes further allowing easy fabrication via lamination [60]. Most of these materials have interesting hyperelastic and viscous properties that must be taken into account for high strain applications. In some cases, using advanced micro- or nano-structured geometries in the dielectric structure can allow for devices with enhanced sensitivity [61].

1.2.3 Piezoelectric sensors

Piezoelectric materials have the ability to convert mechanical energy into electrical energy and have long been used for pressure and strain sensing. Among other types of sensors, piezoelectric sensors have the lowest power requirements [62] and the charge output from piezoelectric sensors lies within the range of measurement capabilities of commercially available analog/digital sensors.

Piezoelectric sensors are made of crystal materials like quartz, ceramics and polymers showing piezoelectric properties. This means that those materials produce a voltage potential when the crystal lattice is deformed. The sensitivity of the crystal depends on its structure, allowing it to distinguish between transverse, longitudinal and shear forces. The generated voltage is directly proportional to the applied force, pressure or strain. Polymer polyvinylidene fluoride (PVDF) and ceramic lead zirconium titanate (PZT) are the mainly

used materials for their mechanical flexibility, high piezoelectric coefficients, dimensional stability, low weight and chemical inertness.

In pressure sensing applications, the sensing element is obtained by applying a thin layer of metallization to both sides of the piezoelectric material, constituting a parallel plate capacitor. Its conditioning circuit is based on ultra-high input impedance amplifiers and the bandwidth of the circuit does not go down to DC, which means that piezoelectric transducers are not adequate for static force transduction but just for detecting dynamic forces. This problem can be overcome by vibrating the sensor and detecting the difference in the vibration frequency due to the applied force [63], however they are preferably employed as switches.

In [64], PVDF film sensors were fabricated separately and embedded into a silicone layer that was moulded onto a robotic fingertip. In [65], the sensor system was further developed into a prototype for tactile skin for flat areas such as the palm of the hand. It showed potential for biomimetic artificial skin, with the ability to sense texture and forces. However, the sensor suffered from several limitations, as the fabrication constraints when moving to larger areas such a full anthropomorphic hand and the pyroelectric effect which required continuous compensation based on the temperature.

Wang and co-workers fabricated a ZnO piezoelectric fine-wire-based strain sensor, wherein ZnO fine wires were laterally bonded with a polystyrene substrate and used to measure strain [66]. Pure crystalline forms of piezoelectric materials such as PZT or ZnO, when used as strain sensors, are usually bonded on the surface or embedded inside the host structure for strain measurement and have limitations to measure strain at discrete points and in a fixed direction. Pure piezoelectric materials are mostly brittle ceramics that are not amenable to flexible applications and are very weak in tension [67]. Furthermore, it is observed in the literature that combined mechanical and electrical loading might lead to premature cracking in piezoelectric materials, which markedly affects their behaviour [68].

In [69] Gullapalli et al. demonstrated a low temperature solvothermal method for the synthesis of a nanocomposite material consisting of ZnO nanostructures embedded in a paper (cellulose) matrix. They fabricated a flexible piezoelectric nanocomposite strain sensor and also demonstrated strain sensing under both static and dynamic loading. Whereas, certain studies have demonstrated the fabrication of flexible piezoelectric sensors but require special techniques, thus making it uneconomical for large-scale synthesis [70].

1.2.4 Optical sensors

Optical sensors employ a light source, a transduction medium and a photodetector, the latter often in the form of a camera or a photodiode. Their operating principles include modulation by the applied force of the transmitted light intensity, phase, or polarization and interaction of the applied force with the light external to the primary light path. In robotic tactile sensing, the optical sensor is generally based on intensity measurement because of its simplicity of construction, signal conditioning and information processing. Moreover, optical sensors have high spatial resolution and low susceptibility to electromagnetic noise, intrinsically safety and low electrical wire demand. Although they have many benefits, optical sensors do not allow a great spatial sensitivity and are bulky in terms of thickness. Their size and rigidness are the major disadvantages.

Optical fibers have also been used as macrobend stretch sensors for pose sensing in soft continuum robot arms [71]. In addition, optical sensors [72] [73] are used widely for measuring strain of greater magnitude but are often bulky and difficult to integrate into soft structures.

Prototypes of optical sensors are often composed of glass or Plastic Optical Fibers (POF) in conjunction with an LED and a Charge Coupled Device (CCD) camera, and forces are detected on the base of a change in the reflective wavelength. In this case optical fibers are not used just for light transmission, but as the sensor itself. The idea is that, when a mechanical bend or perturbation (of the order of few microns) is applied to the outer surface of the fiber, the light is attenuated in the core. The attenuation depends not only on the radius of curvature and spatial wavelength of the bend but also on the fiber parameters. Generally, the main disadvantages that incurred when using optoelectronics are micro-bending and fragility. POF-based microbending optical fiber sensors were presented in [74][75].

Intrinsic POF sensors have also a great potential for large-strain applications. POFs provide a large elastic strain range, are more flexible than silica optical fibres, and are more durable in harsh chemical or environmental conditions. Xiong et al demonstrated 6% strain before failure of a POF and cites a potential 13% increase with the improvement of manufacturing techniques [76]. Thus, for structural health monitoring applications, POF sensor systems potentially offer a larger strain range measurement capability along with more long-term survivability. The greater flexibility of the POF as compared to silica optical fibres allows larger curvatures before failure of the sensor [72]. Intensity-based measurements,

however, are limited in application due to the presence of multiple modes propagating through the optical fiber and therefore produce lower measurement accuracy and resolution [77].

1.2.5 Magnetic sensors

Sensors based on magnetic transduction measure the change in flux density, magnetic induction of an inductor or magnetic coupling between circuits, caused by applied force on a small magnet. The flux measurement can be made by either a Hall Effect or a magneto resistive device, it means a device whose magnetic properties are force dependent, or a magnetoelastic material [78].

Magnetorestrictive or magnetoelastic based pressure sensors may have some positive characteristics, namely high sensitivity, wide dynamic range, no measurable mechanical hysteresis, a linear response and physical robustness. Nevertheless, a few tactile sensors that use the magnetic mode of transduction have been reported in literature, since they still are not a valuable alternative to the above-mentioned types of sensors. The major drawback of magnetic based tactile sensors is the fact that they cannot be used in a magnetic medium and they involve complex computations.

A recently proposed method to detect soft body deformation is to measure changes in local magnetic fields generated by embedded miniature magnets in an elastomeric substrate [79][80]. Magnetic sensors have little to no effect on the mechanical response of the substrate, or hysteresis or dynamic artefacts, due to the noncontact nature of measurement. Furthermore, magnetic fields form closed 3D curves that vary continuously with the relative pose of the magnet embedded in the elastomer. Integrated custom magnetic curvature sensors provide the possibility of proprioceptive feedback motion control for soft robotic systems and have the potential to be extended to other sensing modalities such as tactile/force or axial deformation sensing following the same integration process with minimal variations [81].

1.2.6 Piezoresistive sensors

Piezoresistive sensors are among the most widely used for both pressure mapping and strain sensing.

Resistive-type strain sensors are typically composed of electrically conductive sensing films coupled with flexible substrates. When composite structures are stretched,

microstructural changes in the sensing films lead to the change of electrical resistance as a function of the applied strain. After release of the strain, reestablishment of the sensing films to their original states recovers the electrical resistance of sensors. Whereas, a possible solution to implement a pressure sensitive resistor is using a conductive elastomer or foam or elastomer cords in a grid pattern [82], with the resistance measurements being taken at the point of intersection, called sensel or taxel in analogy to a pixel (picture element) in an image sensing array. Also pressure sensitive elements change their resistance upon the application of forces.

In the typical working configuration the current is fixed and a change in resistance is observed by a change in the voltage. Piezoresistive sensors take the advantages of robustness, low susceptibility to noise (therefore they are adequate for mesh configurations), ability to measure both static and dynamic loads. In addition, they generally require simple electronics as change in resistance can easily be quantified and therefore they are fairly easy to manufacture and integrate [83]. However, resistive sensors suffer from hysteresis and have a lower frequency response when compared to capacitive sensors. Moreover, dedicated strategies have to be applied to reduce hysteresis and crosstalk among sensels in the matrix structures.

Micro-machined sensors

Piezoresistors can be obtained using micromachining techniques, considering that silicon and other semiconductor materials have high piezoresistive responses, also if they are brittle and fragile. Embedding them in an elastomer, as commonly done with strain gauges, allows for mechanical flexibility even if decreasing sensitivity.

An example was presented in [84], in which a silicon-based piezoresistive sensor was embedded directly into a soft fingertip. It was composed of four cross-beams with piezoresistors on its surface for detecting longitudinal and shear stresses. After packaging, the sensor chip was moulded into a polyurethane hemisphere representing a fingertip and it demonstrated high accuracy for both pushing (vertical) and sliding (lateral). The direction and magnitude of shear forces were detected by measuring the change in resistance of two perpendicularly placed standing silicon-based cantilevers embedded in PDMS.

1. Soft and flexible sensors: state of the art

Conductive elastomers and foams

A conductive elastomer is a composite containing both flexible material and conductive material. A common way to fabricate a conductive elastomer is by mixing flexible material and conductive material, and then curing the composites by baking. Generally, highly extensible elastomers are loaded with electrically conductive additives, such as carbon black [85], metal nanoparticles [86], carbon nanotubes [35], or graphene [87]. The most commonly used flexible material for conductive elastomer fabrication is PDMS [88][89]. Typically, the additives significantly stiffen the materials, so a balance must be met between the desired conductivity and maintaining sufficiently soft conductors. When an external force or strain is applied to the sensor deforming the elastomer composite layer, its resistivity changes depending on the type of conductive particles, the resulting material stiffness and their volume percentage in the elastomer. Additionally, the motion of the conductive particles relative to the matrix elastomer is hysteretic and results in varying conductivities during cyclic loading.

There are many methods to fabricate flexible sensors with conductive elastomers, including carbon nanotube growth, photolithography, and soft lithography [90]. Examples of these sensors used for strain sensing or pressure mapping are reported in [35][91][92][93].

Such sensors have been quite popular because of the simplicity of their design: elastomers are highly stretchable, so they are excellent candidates for application on curved surfaces and moving parts. On the other side, elastomer-based sensors are affected by a long nonlinear time constant. Moreover, the resistance characteristic of elastomer based sensors is highly nonlinear and with severe hysteresis, low dynamic ranges and permanent deformation and fatigue.

Conductive fluids

Another approach is to confine a conductive liquid metal, such as eutectic gallium indium (EGaIn) inside microchannels embedded within the silicone rubber body, to create more resilient soft and stretchable sensors that are less prone to hysteresis. These sensors have demonstrated relatively high accuracy and reliability for measuring large strains [94][95].

Similar to conventional strain gauges, the change of the resistance of these soft sensors is a function only of the change in geometry, that is, the length and the cross sectional area of the microchannels. Their output is nearly linear over a wide range of strain and hence easily

predicted. Therefore, the measured change in resistance from those sensors can then be related to different physical parameters such as multiaxis forces [96] or multimodal strain and curvature [97].

Sensors with conductive liquid metal channels offer soft and highly stretchable sensors that can well bond to actuators made from similar silicone rubber materials. However, the conductive liquid metal material is expensive and injecting it to intricate channels in a soft body requires manual skills or custom printing hardware to automate the process as demonstrated more recently [50][98]. Unfortunately, EGaIn is also costly and the creation of such microchannels with subsequent imbibing also increases the fabrication complexity of the sensor.

Conductive polymers

Resistive sensors can also be made of conductive polymers or semi-conductive coatings (inks).

In the first case the polymer is made piezoresistive by adding conductive and non-conductive micron particles. Polymer-based sensors are flexible, robust, and can be chemically resistant. They can be manufactured using large area and low cost fabrication techniques such as roll-to-roll fabrication and screen printing [99]. A few conductive polymers and their use in tactile sensing are reviewed in [82].

As one of the promising conductive polymers, polypyrrole (PPy) has attracted extensive attention, due to its ease of preparation, high conductivity, nontoxicity, and good adhesion with diverse substrates. An example of polymeric and mechanically flexible piezoresistive sensor, presented in [100], was made of a porous nylon matrix which is filled with electrodeposited PPy. A series of flexible strain sensors based on PPy were also developed [40][101]. However, these sensors exhibited low sensitivity and unsatisfying conductivity, which depended on the conditions and reagents used in the oxidation. Moreover, PPy is insoluble in any solvent and non-fusible, which has restricted its large-scale applications in construction of conductive networks.

Apart from PPy, PEDOT-based materials are another promising electrode material, due to their excellent air and thermal stability, high transparency in the visible spectral region, and tunable conductivity [102]. The commercially available PEDOT:PSS has been widely used to develop conformal skin sensors [103][104]. Thanks to its solubility in water, it could be

processed easily using conventional techniques and can be used to form homogeneous slurries with some stretchable matrix. However, the existence of hard segments and hydrophilic PSS chains results in destruction of dried PEDOT:PSS film during bending and stretching, and the decay of conductivity with time under humid conditions [105].

In [106] Flemion, an ion-polymermetal composite (IPMC), was used as the sensing layer of a 3D tactile sensor. The membrane was deposited on a patterned electrode on a PDMS tactile bump. When an external force was applied to the bump, the Flemion layer was deformed causing an internal charge redistribution and hence an output potential. Ink-based sensors have been developed by Tekscan (Tekscan, Inc, MA, USA) [16][107] that is the leader in the market of pressure mapping devices. Such sensors consist of two thin and flexible polyester sheets that have electrically conductive electrodes deposited typically in row-column pattern with sensing a location at each intersection and are separated by 0.5 *mm*.

Quantum tunneling composite

Sensors based on Quantum Tunneling Composites (QTC) can be considered as a particular type of piezoresistive materials, since they are conductive and show a decrease of resistance if compressed, twisted or stretched. QTC are composite materials of metals and non-conducting elastomeric binders, generally used as pressure sensors. Their working principle is based on the quantum tunnelling effect: the conductive elements are too far apart to conduct electricity if no pressure is applied, while, in presence of pressure, conductive particles move closer and electrons can tunnel through the insulator.

The effect is far more pronounced than would be expected from classical (non-quantum) effects alone, as classical electrical resistance is linear (proportional to distance), while quantum tunneling is exponential with decreasing distance: the resistance can change by a factor of up to 10^{12} between two different states (e.g. pressured and unpressured states). This is the reason why they tend to be used as switches more than as actual pressure sensors.

A sensor based on the electron tunneling principle is reported in [108]. The system, composed of a thin film with metal and semiconducting nanoparticles, directly turned stress into electroluminescent light and modulation in local current density, in linear proportionality to local stress. A spatial resolution better than that of the human fingertip was reported for the device.

1. **Soft and flexible sensors: state of the art**

The piezoresistive detecting principle is in general preferred for manufacturing flexible pressure and strain sensors, because of its advantages (i.e. robustness, low noise, simple read-out systems and high flexibility and stretchability). Also main commercial products for pressure mapping and strain sensing exploit the piezoresistive detective principle [16] [22]. Products on the market cost thousands of dollars because of the expensive electronics essential to acquire data with a good temporal resolution. Furthermore, the custom acquisition software provided with the product is mandatory to manage pressure and strain information and to overcome problems typical of the piezoresistive transduction mechanism [33][109] (e.g. non linearity, hysteresis, low frequency response and creep) and of the scanning (e.g. crosstalk effect) [110]. Moreover, even if showing high-quality performances, products available on the market are markedly application specific and users are not allowed to access to raw voltage data from the elaboration software.

For these reasons a huge number of recent research studies have been aimed to obtain sensing solutions based on the same working principle, but low cost and versatile from the point of view both of hardware (e.g. shape and dimension) and software (e.g. direct management of data reading and resolution settings). Pressure and strain sensors are asked to be not only thin and pliable, as polyester- and PCB-based products are, but also flexible and attachable over curved and narrow surfaces (e.g. robotic joints and fingers). They also have to be customizable, suitable to be embedded in wearable systems and possibly achievable with affordable technologies.

1.3 Smart Textiles

The recent class of smart textiles is a promising candidate to meet the conditions mentioned in the previous section, making the development of lightweight, wearable, soft and low cost sensors possible [111][112][113]. Smart textiles research represents a new model for generating creative and novel solutions integrating sensing functionalities and electronics into unusual environments and will result in new interesting discoveries. In particular, a pushing reason for this research is the fact that both textile and electronics fabrication processes are capable of automatically creating large area surfaces at very high speeds. In the last years, smart textiles have been attracting more and more attention, especially in the fields of healthcare [114], military [115], aerospace [116], leisure [117] and sports [118]. They provide

technological possibilities which are not possible with conventional electronics, in such a versatile way to be defined as the new silicon wafers [111].

A brief introduction to the textiles structure is mandatory for a better understanding of their potentialities. A textile is a drapeable and fibrous material that can be processed on textile machinery. It is usually made of fine and flexible fibers and threads with a high L/D ratio, inserted into a hierarchical structure. In particular, a fabric is generally composed of bundles of fibers interlaced to form a thread (first level of integration). Those are then twisted to create yarns (second level of integration). Yarns get turned into what is called fabric (third level of integration), using different techniques such weaving and knitting. Then two or more layers can be assembled into composite fabric units (fourth level of integration). Basic levels of fabric construction hierarchy are shown in Figure 1.8.

Knitted fabrics are easily deformable while woven textiles are usually more stable and hard to deform. Wovens are typically manufactured using straight interconnections of wefts (transverse threads) and warps (longitudinal threads). Knits are typically made up of looped interconnections of courses and wales, where the wales are the threads that run vertically and the courses run horizontally across the fabric (Figure 1.9).

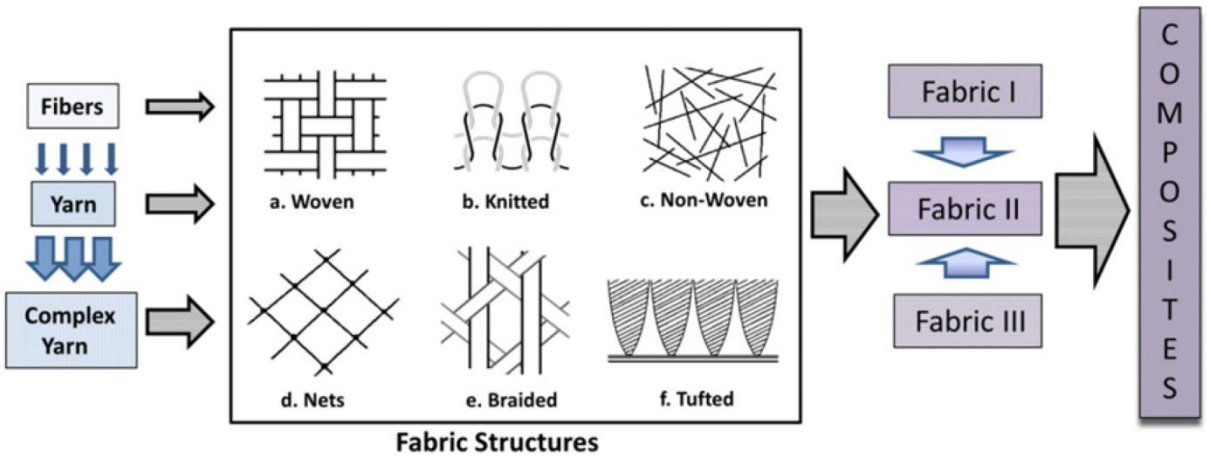

Figure 1.8 Fabric construction platform and hierarchy. Fabric structures: (a) woven, (b) knitted, (c) nonwoven, (d) nets, (e) braided and (f) tufted, which can be assembled in layers (e.g. three layers) to form composite structures [111].

Another widespread category is the one of non-woven fabrics, normally made from filaments that are strengthened by different bonding techniques, as adhesive or thermal bonding, mechanical interlocking or fluid jet entanglement.

1. Soft and flexible sensors: state of the art

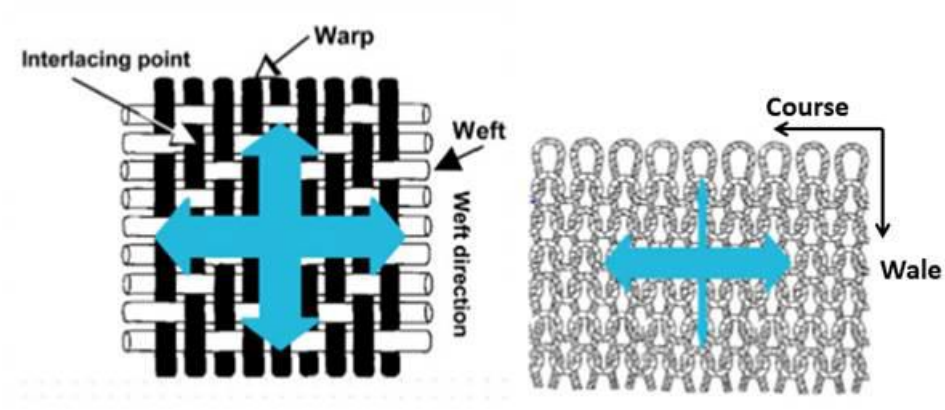

Figure 1.9 Typical interconnection paths of wefts and warps in wovens (a) and of wales and courses in knits (b) [117].

Smart textiles, also known as intelligent textiles, electro or e-textiles, are fabrics that can sense and react to mechanical, thermic, chemical, magnetic and electric stimuli, by means of extrinsic and intrinsic modifications at any level of integration. In case of extrinsic modifications, fabrics can be altered by attaching discrete or self-contained sensing elements like resistors or integrated circuit chips to the fabric (those are usually referred to as electronic textiles) or by coatings application.

Coating techniques are other types of extrinsic or external modification to the fabric substrates. They can involve fibers, yarns or fabrics and include screen printing, ink-jet printing, electrodeposition, vapor deposition of thin films, and sputtering. Coatings alter the fabrics mechanics in their tensile, shear and bending properties, because of the change in the yarn mobility after the coating application [119]. In case of intrinsic modifications, fibers and yarns are directly made of materials that are sensitive to different mechanical or chemical stimuli. Some of the commonly employed methods to make fibers out of sensitive materials are electrospinning, wet-spinning, self-assembly and die extrusion.

Intelligent textiles can show several particular properties. They may be phase changing materials, shape memory materials, or thermochromatic materials, according to their smart performances [120]. However, the main class of smart fabrics involved in a huge number of applications is the one of conductive/piezoresistive textiles. The development of conductive/piezoresistive fabrics has been a common research topic in the areas of chemistry and smart materials [121]. There are different ways to produce electrically conductive fabrics. One method is to integrate conductive yarns in a textile structure, e.g. by weaving.

1. Soft and flexible sensors: state of the art

Conductive properties can be given to threads by several techniques during and after the thread manufacturing process. The different conductive thread types are enumerated in Figure 1.10 and showed in Figure 1.11: extruded wires (the conductive yarn consists of metal multifilaments), twisted metal wire (the metal wire is twisted around the polymer yarn), and yarn with metal coating (the polymer yarn is physically/ chemically coated with a thin metal layer).

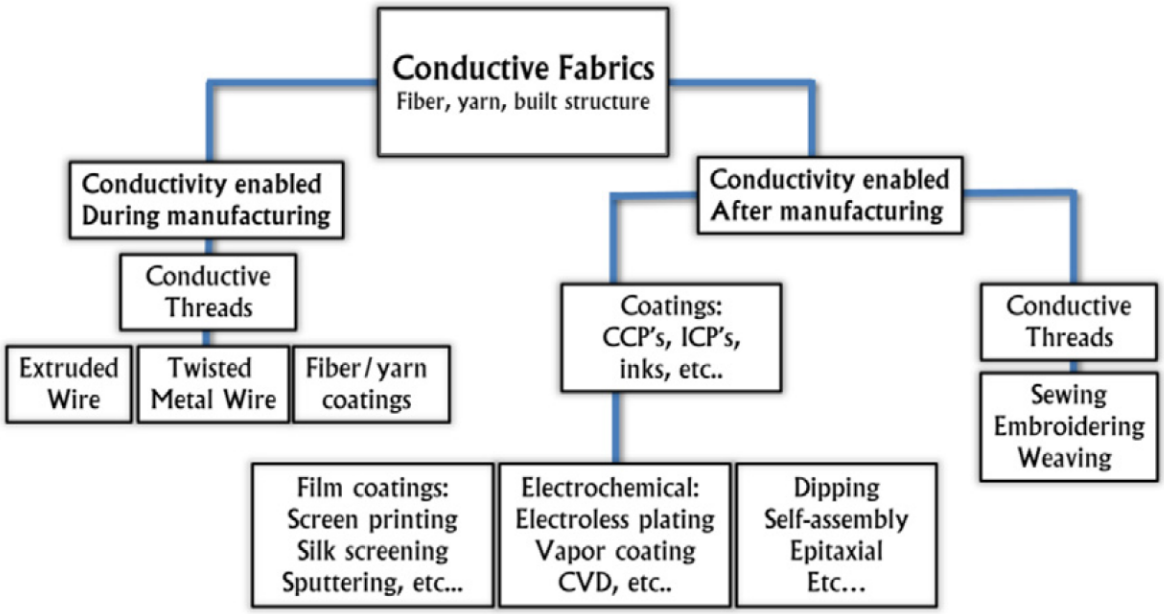

Figure 1.10 Techniques to enable conductivity in fabrics [111].

Figure 1.11 (a) Twisted metal wire: The metal wire is twisted around the polymer yarn; (b) Metal coating: The polymer yarn is physically/chemically coated with a thin metal layer; (c) Metal fibers: The conductive yarn consists of metal multifilaments [112].

Another very common technique entails the application of metal or conductive polymer coatings to the fabric surface. Coatings can be water-based conductive inks that have to

contain an appropriate highly conductive metal precursor such as Ag, Cu and a carrier vehicle. These specialized inks can be printed onto various materials, and in particular onto textiles, to create electrically active patterns.

Other types of piezoresistive coatings typically entail either conductive particle polymers (CPP) or inherently conductive polymers (ICP). CPP are also referred to as conductive doped polymers, since they can be made either of organic or inorganic constituents: organic (i.e. carbon) particles and inorganic (i.e. metal) particles can be mixed in with polymeric matrices. On the contrary, ICP do not need to be doped to achieve conductivity. Most ICP (e.g. PANi, polypyrrole (PPy), polyacetylene, polythiophene and PEDOT-PSS) are prepared via chemical or electrochemical oxidation of the monomer in solution or in the vapor phase.

It is important to remember that using proper coatings can provide textiles also with electrostrictive, pH sensitive, and humidity sensitive properties. Methods for applying coatings onto fibers and fabric depend on the consistency of the coatings themselves. Liquid polymers can be applied by electrochemical deposition, sputtering (Au, Cu), electrospinning, spinning, printing, electroplating, spraying, or wet-spinning. More solid coatings such as carbon loaded pastes or other organically doped polymers can be applied by screening, dip-coating, soft lithography, by hand or using masking techniques.

The main commercial piezoresistive textiles are the EeonTex^{TM} Conductive Textiles by Eeonyx Corp. [122] and the Electrolycra by Mindsets Ldt [123] (Figure 1.12).

The first are made using a proprietary coating technology developed by the Eeonyx company. Individual fibers within a fabric or yarn are completely and uniformly coated using the aqueous process with doped PPy, an inherently conducting polymer, or with carbon loaded polymers [124]. Available fabrics can be woven, knitted, and nonwoven and typical substrates include polyester, nylon, glass, and Kevlar®. Different products show particular resistance variation if stretched or pressed. On the other hand, the Electrolycra looks and feels like ordinary lycra but it is highly conductive because it is weaved with Silver plated 76% Nylon 24% elastic fibers. Its conductivity depends on how tightly it is stretched, showing increasing resistance if pulled [125].

Generally, the resistance provided by a smart fabric is measured with two electrodes placed in contact with the same side of a material under test. Measured values depend on the type of material and, for non-homogeneous fabrics, even from the orientation of the specimen.

Because of the lack of standards, manufacturers often adopt their own measurement protocols and give the user the value of the surface or linear resistance.

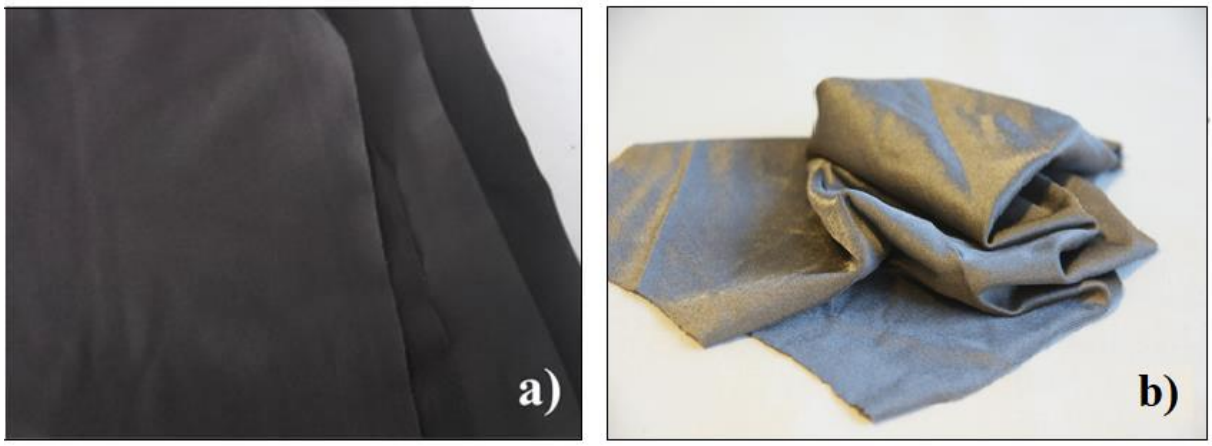

Figure 1.12 a) EeonTex™ Conductive Textiles by Eeonyx Corp. [122] and b) Electrolycra by Mindsets Ldt [123].

Fabrics that have been treated or modified to act as sensors, actuators and/or other types of transducers create a generalized category of smart fabric transducers (SFT), which allow to either measure or influence the environment where they are employed. SFT can be used as actuators (e.g. electroactive fabrics and auxetic fabrics) [126] or as antennas [127], for EMI shielding [128], for heat regulation [129] and as batteries and energy harvesting solutions [130] (i.e. exploiting the kinetic or the thermal energy of the wearer or their environment to generate electrical power).

Next to these possible employments, smart fabrics are mainly used as sensors. In particular, fabrics that have sensing properties of diverse physical nature, such as capacitive, resistive, optical and solar are usually refereed as Smart Fabric Sensors (SFS) [111]. Actually they can be employed as temperature/humidity sensors [131], optical sensors [132], shape memory sensors [133], sensors for gases and chemicals detection [134], pressure/force and strain/motion sensors [135][136] (Figure 1.13). The last two classes are those that are of fundamental importance for the present thesis and they will be deeply described in the next section.

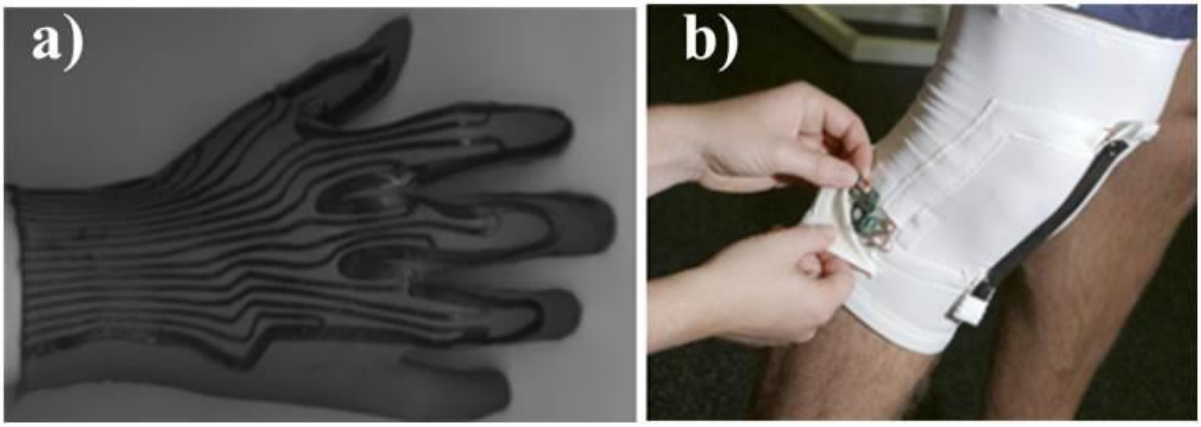

Figure 1.13 Examples of textile wearable sensors for motion detection: a) sensorized glove made of strain sensing fabric for hand posture and gesture monitoring [135], and b) an intelligent knee sleeve used to provide feedback on the knee flexion angle for injury prevention programs [136].

1.3.1 Smart fabric *pressure* sensors

Fabric pressure sensors are extremely advantageous for their lightness, softness, flexibility and even wearability. For these reason such sensors are present also as patented commercial products [137].

Fabric pressure sensors can be presented in either capacitive or resistive configurations:

- *capacitive fabric pressure sensors:*

Capacitive designs range from adapted electronics to intrinsically modified materials. In the first case, e-textiles employ conventional capacitors that are mounted on a frame which can be sewn or glued to a fabric substrate and soldered to other wires or electronics components. Otherwise, fabric capacitors can be constructed using compliant conductive materials that act as electrode plates separated by dielectric layers of different kind. In the case of conductive thread/fabrics, the plates can be woven or sewn [138], while in case of conductive inks or polymers they can be painted, printed and sputtered [139]. Dielectric spacers are typically synthetic foams, non-conductive fabrics or soft polymers.

Fabric sensor capacitors can be used either as a single element or they can also be placed in arrays to obtain distributed measurements [140]. In array configurations, capacitance is measured at intersecting rows and columns of electrodes, which are connected to multiplexers, DAQ systems and microcontrollers. As previously explained, capacitive sensors

suffer from low SNR, crosstalk in case of matrix structure for the presence of parasitic capacitances and severe hysteresis.

- *resistive fabric pressure sensors:*

Finding a correlation between pressure and electrical resistance is another way of constructing fabric pressure sensors and the electrical resistivity can be quantified by measuring resistance, conductance or resistivity changes. These types of sensors can be manufactured at all fabric structure levels, i.e. yarn, fiber, or coatings.

The main design employed to create pressure sensing large areas with textiles is the matrix-based approach inspired by Tekscan products [117]. This means that the piezoresistive fabrics are sensed laying them into interdigitated grids of conductors, that can be simply arranged in parallel lines placed in orthogonal directions on the top and bottom of a single fabric sheet, thus creating a matrix.

Matrix fabric sensors can rely on several configurations (namely sandwich or multilayer, machine sewn, trapped conductor and woven topographies) that can be grouped into two main categories. In the first class the piezoresistive sheet can be sensed by sandwiching it between two layers embedding conductive elements, while in the second class conductive components (i.e. conductive threads) are directly sewn in the sensing fabric (Figure 1.14).

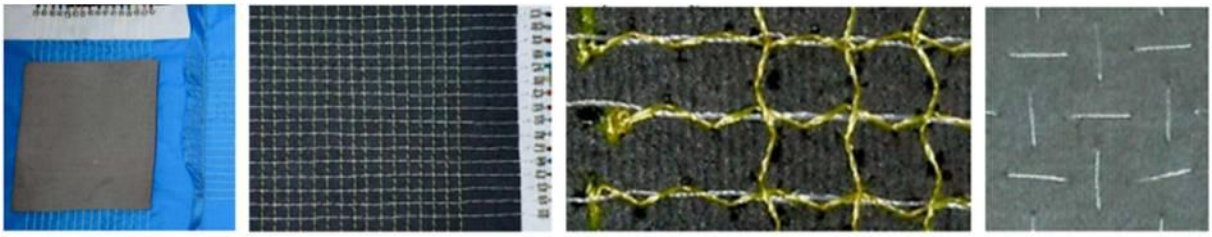

Figure 1.14 Four possible topographies to sense the piezoresistive fabric layer creating a matrix structure: a) sandwich, b) machine sewn, c) trapped conductor, and d) woven [117].

Actually the last described sensors, also available on the market [141], are not provided with studies about either well-defined metrological properties or improving strategies that support their use in dynamic multitouch modality. Thus, one of the aims of the present thesis will be the description of a piezoresistive multilayered matrix pressure sensor with the

analysis of its properties for both static and dynamic measurement conditions, with the realization of a thorough sequence of experimental tests.

1.3.2 Smart fabric *strain* sensors

Fabric strain sensors are predominantly used for sensing and monitoring body parameters, as the textile is in contact with the skin over a large body area. This means that monitoring can take place at several locations on the body. A specific structure of textile sensors is that integrating fibers featuring piezo-resistive properties, enabling their use as strain or deformation sensor.

Fabrics can be made sensitive to mechanical strain by different methods at the different levels of the structure hierarchy; fibers can become strain sensitive when made out of strain sensing materials, yarns can have different topologies by interlacing sensing fibers with no sensing fibers and fabrics can be modified by introducing sensing fibers or by applying a coating with strain sensing materials to achieve the same goal [111].

Metal fibers such as stainless-steel fibers can be knitted to construct a piezoresistive textile [142], as shown in Figure 1.15. When stretched in the wale direction, the resistance of the knitted sensor initially increases and then decreases. The initial increase in resistance is due to the increased length that the current sees. However, in the decreasing resistance phase, the gaps between the strands of yarn reduce, allowing better contact adding parallel conductivity paths which results in a lowered net resistance. Other mechanisms that enable strain sensing entail inserting sensing fibers into nonconductive knits. In a similar way, yarns can become sensing elements by wrapping piezoresistive fibers around an elastic core [143]. However, hysteresis and linearity are also problems need to be solved. Generally, linearity increases at the expense of sensor sensitivity [144].

- *Piezocoatings to enable sensing features*

Fabrics can be converted to ‘smart fabrics’ by applying piezoresistive [145], piezoelectric [146] or piezocapacitive [147] coating materials, usually in the form of polymers due to their elastic properties. Coatings are usually either externally modified by conductive fillers or intrinsically sensitive to changes in elongation, pressure and other mechanical stimuli. Sensing coatings are typically applied to stretchable substrates such as fibers, yarns and fabrics to make them strain sensitive.

1. Soft and flexible sensors: state of the art

For intrinsically conductive coatings the most important conductive polymers applied to fabrics are PPy [148], polythiophenes [149], PEDOT-PSS [150] and PANi [151]. The application technique as well as the nature of the substrate will have an impact on the sensor properties. However, intrinsically conductive polymer coatings by themselves are typically not as flexible as other polymeric based matrices with conductive inclusions [152]. This is part of the motivation for exploring extrinsically conductive polymers. These consist of mixtures of conductive or semiconductive fillers and nonconductive insulating matrices. Coatings of these mixtures can be applied to fabrics to give them sensing properties. The particles can be of any size; in particular, nanocomposites have been shown to possess special sensing properties.

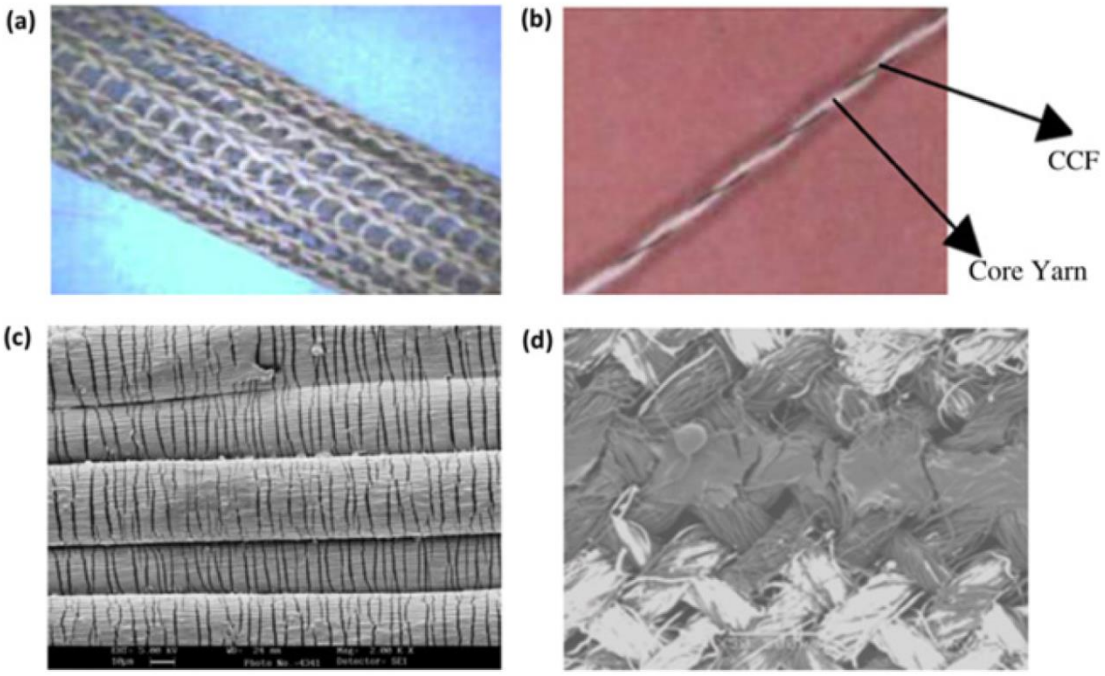

Figure 1.15 Strain fabric sensors. (a) Stainless-steel knitted fabric sensor. (b) Yarn sensor composed of a single wrapping of carbon-coated fiber (CCF) with elastic fibers and polyester fibers. (c) SEM micrograph of polypyrrole-coated Lycra fibers at 6% strain (d) PEDOT-printed sensor on woven cotton fabric [111].

Coated sensor characteristics will depend on several factors; internal mechanics and geometry of the yarn or fabric substrate; the thickness, consistency, brittleness, elasticity and composition of the coating; and the coating mechanism. In the case of piezoresistive coatings, a change in electrical resistance will be observed as a result of the application of strain to the substrate. This change can be quantified by the gauge factor, which is a measure of the

sensitivity of a given strain sensor. It relates the normalized change in resistance with the applied strain. Positive or negative gauge factors are obtained depending on the material itself and depending on how the fabric substrate deforms under applied load. A positive gauge factor indicates an increase in resistance with applied strain, typical of metals. A negative gauge factor in turn indicates that there is more conductivity when the fabric sensor undergoes strain.

In the case of coated fabric sensors, the relationship between resistance and strain is often obtained experimentally. A gauge length is chosen and a conventional tensile test is conducted for such a characterization [153].

Also these types of sensors, available on the market [123] too, are not provided with studies about either well-defined metrological properties or improving strategies that aim at compensating their intrinsic nonlinearities. Therefore, the further objective of the present thesis will be the description of a piezoresistive textile strain sensor with the analysis of its properties for both static and dynamic measurement conditions. Moreover, such study will enable the identification of novel challenging applications.

Chapter 2

Multilayer matrix textile-based pressure sensor

2.1 Introduction

Matrix textile sensors hold great potential for measuring pressure distribution in applications of modern daily lives, mainly regarding the biomedical field, but also robotics, automotive systems, wearable and consumer electronics. However, an experimental analysis of their metrological properties is lacking in literature, thus compromising their widespread acceptance.

In the present Chapter, an 8x8 textile sensor was assembled by sandwiching a piezoresistive fabric sheet between two outer fabric layers embedding conductive rows and columns. The sensor structure, its electrical circuit and characteristics are described in detail, analyzing its properties for both static and dynamic measurement conditions with the execution of a thorough sequence of experimental tests. The knowledge of the proposed sensor metrological features and its possible optimizing solutions may help the user in managing the sensor with a deeper awareness of both its benefits and drawbacks.

2.2 Sensor development

2.2.1 The three layers matrix structure

The textile sensor assembled for the metrological characterization has a multilayer (or sandwich) matrix structure. This topography is the most employed, since it offers a simple and easily fixable implementation and allows a large volume production.

2. Multilayer matrix textile-based pressure sensor

The piezoresistive textile employed is a stretchable and knitted fabric (EeonTex™ LG-SL-PA, Eeonyx Corp., Pinole, CA, US [122]) composed of 91% of nylon and 9% of elastane. The fibers within the fabric are coated with conductive polymers to provide both superficial and transversal electrical resistance (respectively 30–50 $k\Omega$/100 *mm* and ~0.05 $M\Omega$ [154] through the 0.5 *mm* thickness) that tend to decrease with stretch or pressure application. If the fabric fibers are stretched, the yarns diameters get thinner and the impedance lowers since the contact areas among the fibers decreases [124]. The EeonTex structure was analyzed using the scanning electron microscope (FEI Helios NanoLab™ 600 DualBeam FIB/SEM, Hillsboro, Oregon, US) provided of a detector for EDS microanalysis (Bruker, Billerica, Massachusetts, US), to study both the integration levels of the hierarchical structure [111] and the composition of the material.

The resistive sheet was sandwiched between two layers that consisted of a non-conductive textile on which parallel conductive strips (20 *mm* wide) were obtained by sewing multiple copper threads (with a diameter of 110 μm), so that a pattern of alternate conductive and insulating bands was created. Outside layers (each one 0.65 *mm* thick) can be cut from long, wide rolls of pre-manufactured fabric (Texe srl, Firenze, Italy). They were placed so that the conductive stripes on the top and the bottom layers were orthogonal to each other, creating a grid (Figure 2.1 (a)). The crossing of row *i* with column *j* produces the pressure sensitive element *ij*.

The three components were held together with a series of stitches that did not alter the electrical properties of the fabrics and additional outer layers of felt were applied to protect the conductive elements from wear and tear. The sensor overall thickness resulted around 4.6 *mm*. Slipping between the three layers can occur in case of improper sensor positioning, thus compromising the sensels topography. To overcome this problem, users are recommended to eliminate undesired folding of textiles by fixing the sensor in a stable position. The sensor realized for the study includes 8 rows and 8 columns, for a total of 64 sensels. Being the single sensel area of 400 mm^2 (a value that can be easily customized for different application requirements), the size of the entire sensing area was 160 × 160 mm^2 (Figure 2.1 (b)).

The pressure applied at each sensel is measured by connecting the row of the top layer to an energy supply unit and the column of the bottom layer to a reading circuitry based on inverting amplifiers. If no pressure is applied to the sensor, there is just a negligible contact between the resistive sheet and the conductive stripes: the sensel results as open circuits

exhibiting a high resistance (~0.5 $M\Omega$). When a pressure is applied, a physical contact is created between the conductive stripes and the piezoresistive textile, and the transversal resistivity of the latter tends to decrease in relation to the applied load (down to ~100–500 Ω). The measurement of the electrical resistance at each *ij* crossing allows to reconstruct the applied pressure map (Figure 2.1 (c)). The electric signal was transmitted through metal wires soldered on the boundary of the outer layers in correspondence to each conductive stripe (soldering points are represented in Figure 2.1 (a)), without affecting the sensor wearability and possibility of mass production.

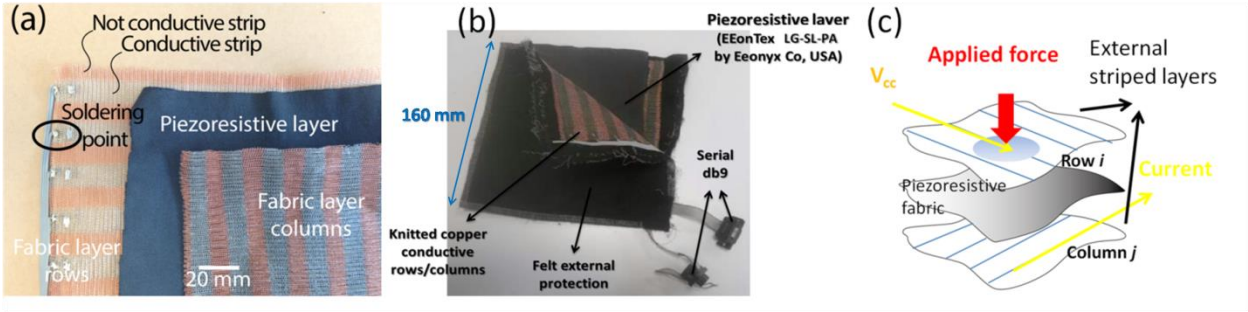

Figure 2.1 (a) The three layers of the flexible matrix textile sensor with indicated soldering points, (b) the complete sensor involved in the study and (c) the description of sensels location: the sensitive areas are at the intersection of conductive rows and columns embedded in the fabric and distanced by a piezoresistive layer.

2.2.2 The powering/reading circuitry

The main problem when dealing with matrix structures is the presence of crosstalk between adjacent elements, since the electrical behaviour of each sensitive element is affected by the presence of the surrounding resistive elements that introduces parallel of currents interfering with measurement. For a better comprehension of the problem, please refer to Figure 2.2. The measurement of $R_{i,j}$ is affected by the other three transversal resistances ($R_{i,j-1}$, $R_{i+1,j-1}$ and $R_{i+1,j}$) in series, that appear in parallel to $R_{i,j}$. This error is particularly evident in case the resistances have the same order of magnitude, which is common in case of multitouch. If resistances among rows and columns are also present (e.g. $R_{i,i+1}$ and $R_{j-1,j}$), other parallel paths must be included for the evaluation of $R_{i,j}$. General methods for preventing these surrounding currents are reported in literature [155].

One possible solution is performing field effect transistor switching at every measuring point, thus measuring elements in a complete independent way. However the solution is very

much expensive to be employed for a large area development. Another possible solution is inserting diodes at all the measuring points; in this case the leak resistances between electrodes still exist and it is also required to create anisotropy in the pressure-sensitive material, i.e. cutting slits in the sheet and inserting insulators between electrodes.

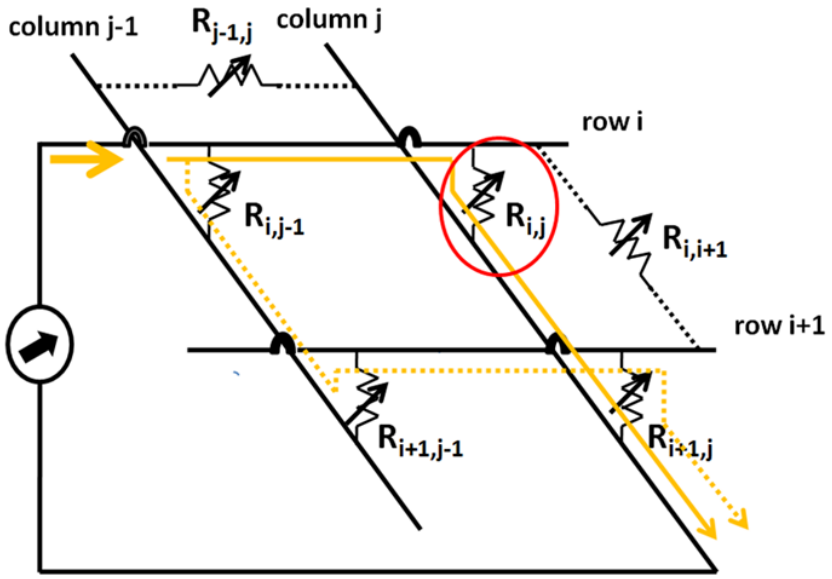

Figure 2.2 Crosstalk analysis scheme for a portion of the matrix while measuring $R_{i,j}$ (right current path: solid arrow, undesired leakage current: dotted arrow).

In 1981 Purbrick proposed the voltage mirror or voltage feedback loop method [110][156]. This solution removes crosstalk currents by setting the drive lines that are not connected to the measuring point at the same potential of the output voltage. In this case the unwanted effects of crosstalk are reduced by including the loop formed by buffers on the rows and switches on the columns: the buffers impose the output voltage on all the rows, except to the powered one, while the switch connects the columns that are not active to V_{out}, so that all the terminals of the resistances of the matrix different from $R_{i,j}$ are at the same potential. Therefore, in ideal conditions, no current can flow across them.

Similar to this approach, Hillis proposed the zero potential/grounding method in 1982 [110][157]. In this solution the voltage of the scanning electrodes different from the measured one is set to a zero potential. In this case, instead of generating equal potential for the respective electrodes, the voltage is zero and the circuit is simplified respect to the voltage mirror solution.

2. Multilayer matrix textile-based pressure sensor

The scanning method used in this work was designed considering the above mentioned points. The conceptual diagram of the scanning circuit is shown in Figure 2.3. The powering voltage V_{cc} was applied to the row to be selected, and other rows were brought to zero voltage. As for column direction, operational amplifiers were connected to all of the columns, grounding all the columns except to the measured one. In this way also the error in measurement due to leak resistance between electrodes was removed.

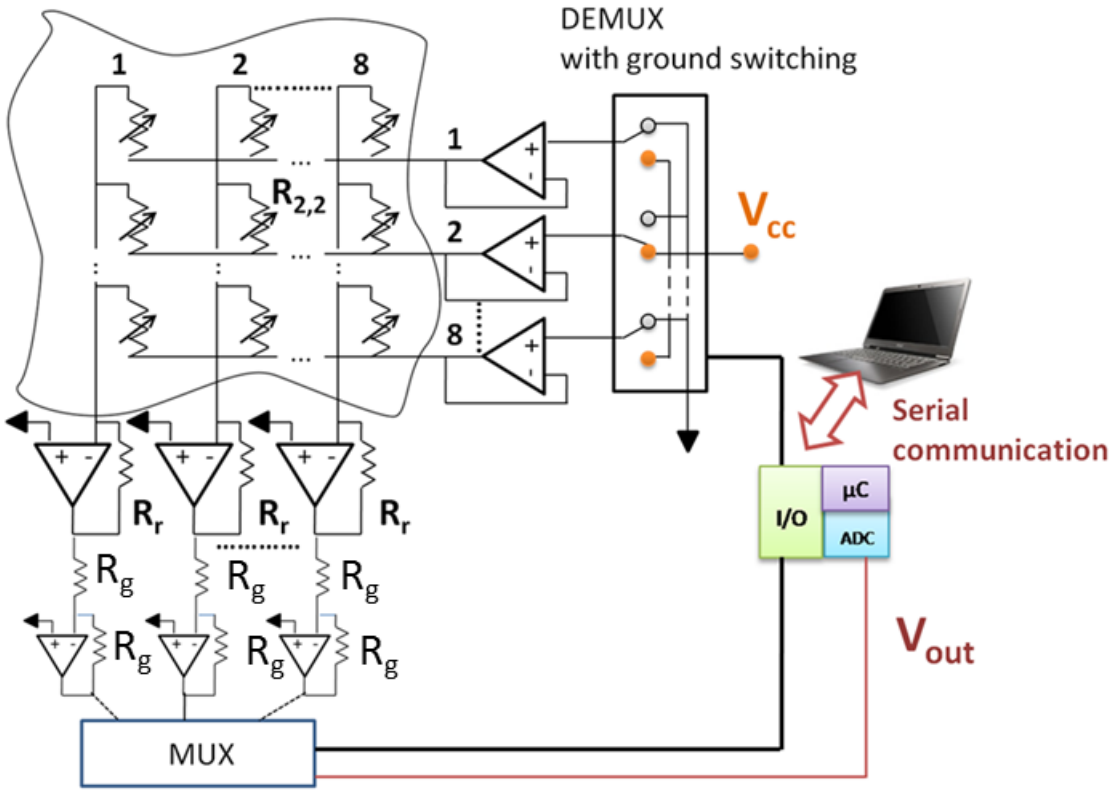

Figure 2.3 The powering/reading circuit based on the grounding method: the powering voltage V_{cc} (5 V) is applied to the rows while the sensel resistance is measured through the acquisition board at the columns. The MUX/DEMUX is employed for row/column scanning. In particular, every row is driven to V_{cc} through independent buffers while the others are switched to ground and the input of the trans-resistance amplifiers acts as a virtual ground so that the columns not active are grounded. The gain of the amplifiers can be tuned to obtain the desired voltage range by varying R_r and additional inverting amplifiers are introduced for measuring positive voltages with the Arduino Mega Board.

LM741 general-purpose operational amplifiers (Texas Instrument Inc., Dallas, Texas, US) were employed and powered with an external dual power supply. Moreover, different inverting resistances R_r were chosen to study different calibration curves. Two multiplexers (ADG732 32:1, Analog Devices, US), connected one to the rows and the other to the

columns, and an Arduino Mega Board (Arduino, Italy) with a 16-bit microcontroller (32 MHz clock) were employed to manage the powering/reading scanning sequence (Figure 2.3). Since the employed microcontroller board was designed just for measuring positive voltages, inverting operational amplifiers with unitary gain were added downstream of the reading circuit. The output voltage measurements were sent via serial communication to the host PC for further processing. An acquisition rate of 10 *Hz* was set.

2.3 Sensor characterization

2.3.1 Static calibration

A static calibration procedure was performed using a mechanical testing machine (Instron Corp, Canton, MA) provided with an electronically calibrated 1 *kN* load cell. Ten loads values equally spaced from 0 to 100 *kPa* were applied on a square area of the sensor, using a rectangular indenter (60 × 60 mm^2). The voltage signals derived from the 9 compressed sensels (rows i = 3, 4, 5 and columns j = 3, 4, 5) were then recorded through the acquisition board (Figure 2.4). Three replicates were performed for each load value.

In particular, the mean values and the standard deviations (SD) of the 9 sensels involved in the calibration were considered for each replicate; then the results were averaged on the three trials and SD were considered to evaluate the static repeatability.

The achievement of a mean calibration curve available for the whole sensor, that is representative of the mean response of each sensor element within the measurement range, is a common approach when dealing with matrix structures [158]. The mean curve can be applied to every active element of the matrix sensor under the hypothesis that each element would respond the same way to the same applied pressure, following the calculated calibration function. The limits of such a hypothesis were quantified and discussed in the results and discussions section where the results of the measurement repeatability among sensels are reported.

The measuring range was chosen in accordance with previous related studies [154], since it covers most possible biomedical applications ranges.

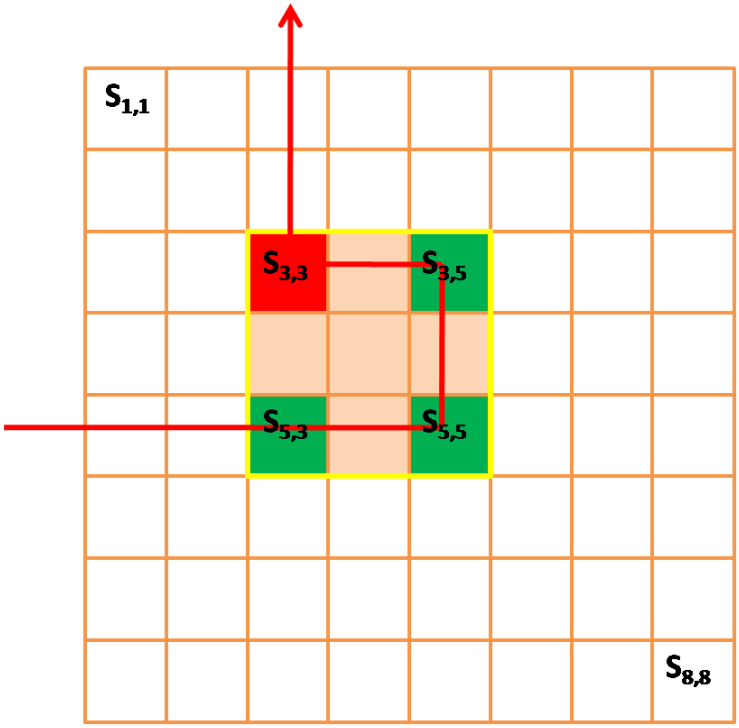

Figure 2.4 Sensor sensels involved in static tests: the 3 × 3 matrix in the yellow frame is the area involved for the static calibration, while $S_{3,5}$, $S_{5,5}$ and $S_{5,3}$ (green sensels) were loaded separately for the shear test and all together to prove the grounding efficacy in case of multitouch. If the current leakage is present, the current path reported with the red arrow would result in the detection of a phantom touch (false output from the red sensel $S_{3,3}$).

Moreover, the whole calibration procedure was repeated using four gain resistances R_r (160, 220, 330, 560 Ω) in order to define different calibration curves and working ranges. The equation relating the sensel resistance $R_{i,j}$ and the output voltage V_{out} is the following:

$$V_{out} = -\frac{R_r}{R_{i,j}} V_{cc} \qquad (2.1)$$

The stage of inverting amplifiers with unity gain assures the measurement of a positive voltage (see Figure 2.3). A complete analysis with the four different R_r was realized only for the static calibration. Other tests that are described in the following sections were obtained just with one representative R_r (i.e. 220 Ω), since in those contexts behaviours are independent from the analog front-end were investigated.

2.3.2 Stretch and curved surface tests

In order to evaluate the sensor behaviour under stretching conditions, the three fabrics were stretched of the 20% of their dimensions in both directions. Higher percentage of stretching could be obtained for the EeonTex fabric (maximum extension ≈150% in both directions) but not for the external layers. The ten static loads employed for the static calibration were applied on the square area covering the 9 sensels involved in the previous test. The experiment was repeated three times.

Differences between mean pressure measurement for the 9 sensels in case and in absence of stretch were calculated as a root mean square error (RMSE, see equation (2.2) [159]), considering the results without stretch as reference.

$$RMSE = \sqrt{\frac{\sum_{i=1}^{n}(p_i - \widehat{p_i})^2}{n}} \qquad (2.2)$$

where p_i and $\widehat{p_i}$ are the measured pressures for the n = 9 sensels with and without stretch, respectively. In addition, thin and flexible pressure sensors are often required to bend around curved surfaces; therefore it is important to understand the effect of such deformation on output.

To this aim, the sensor was fixed on a regular curved surface with a radius of curvature of 45 *mm* and the same apparatus described in the previous section was used to apply the sequence of ten static loads from 10 to 100 *kPa* (three tests). Since a normal load could be applied only on a single column of sensels (rows i = 3, 4, 5 and central column j = 4), just the three sensels voltage outputs could be compared with their corresponding ones for the sensor tested on a flat surface.

2.3.3 Shear test

A novel static load test was performed to study the effect of shear load on the sensor output. Literature rarely reports results indicating how thin-film sensors react to this type of loading. On the contrary shear forces are often present in tasks requiring pressure measurement, therefore it is important to define how these sensors behave under this loading condition. In particular, it is worthwhile to understand if shear load affects normal load measurements. For this reason, a Modular Compact Rheometer 302 (MCR 302, Anton Paar GmbH, Graz, Austria) was employed to apply static normal loads on sensels (from 5 to 25

kPa with steps of 5 *kPa*), using a circular tool (provided with the instrument equipment) with a radius of 25 *mm*. The tool just allowed loadings of a single sensel for each test. The equipment was able to realize tests with controlled shear rate:

a) a constant shear rate of 100 s^{-1};
b) a shear rate linearly increasing from 10 to 300 s^{-1}.

Consequently, the applied shear stress is proportional to the normal stress (0.7 *kPa* of shear stress every 5 *kPa* of normal stress). Differences from the baseline condition (without shear) were considered for 3 sensels voltage outputs ($S_{3,5}$, $S_{5,5}$ and $S_{5,3}$, see Figure 2.4).

2.3.4 Drift test

The same sequence of loads employed for the static calibration was applied three times on the sensor square area for 10 *min* to evaluate the sensor drift properties. Drift is the change in sensor output when a constant force is applied over a period of time. The drift error was calculated according to equation (2.3) [160]:

$$Drift\ error\ (\%) = \frac{p_{mean}(t_{end}) - p_{mean}(t_0)}{p_{mean}(t_0)} 100 \quad (2.3)$$

where $p_{mean}(t_0)$ is the mean sensel voltage output at t = 0 (after reaching the steady state) and $p_{mean}(t_{end})$ is the mean sensel voltage output at t = 10 *min*.

2.3.5 Temperature and noise tests

The dependence of the sensor output on temperature was investigated by applying a constant load of 10 *kPa* on a round area of 2000 mm^2 for 5 *min* and considering the mean value of the loaded sensels (also averaged in time) at three temperatures: 27 °*C*, considered as the room temperature where other tests were performed, 35 °*C* and 42 °*C*. The last two temperatures were reached inserting the device into a laboratory oven and can be considered the extreme thermal conditions that the sensor can experience in case of biomedical applications.

The signal to noise ratio (SNR) was calculated during the same test for the data acquired at the three temperatures, according to equation (2.4) [161]:

$$SNR = 20log_{10}\frac{\overline{V_{mean}}}{SD(V_{mean})} \quad (2.4)$$

$\overline{V_{mean}}$ and SD (V_{mean}) are the mean and the standard deviation of the temporal trend of the output (averaged on the loaded sensels).

2.3.6 Multitouch analysis

Additional tests were performed to prove the actual removal of crosstalk current thanks to the use of the grounding method. Indeed, the solution has been demonstrated just theoretically in literature, but without any experimental proof. To this aim, a sequence of ten equally spaced static loads from 10 to 100 *kPa* was applied to three sensels $S_{3,5}$, $S_{5,5}$ and $S_{5,3}$ (green squares in Figure 2.4) that are at the square vertices of the 3 × 3 matrix involved in the static calibration procedure. Loads were applied using three square indenters (20 × 20 mm^2 each one).

The mean behaviour of the three sensels was compared to the mean behaviour of themselves during the static calibration of the 3 × 3 matrix: if the leakage currents are avoided, the two mean output should be comparable. Moreover, in case of triple touch, a fourth signal output from $S_{3,3}$ should not be present (red square in Figure 2.4). This false pressure detection is the most representative evidence of low accuracy in case the non-active electrodes are not grounded and it is indicated in literature as 'phantom touch' [162].

2.3.7 Hysteresis tests

Calibration with static loads is inadequate for piezoresistive sensors if they have to be employed in dynamic tasks, since they typically suffer from hysteresis [109].

A dynamic analysis was carried out applying on the matrix three loading/unloading cycles (from 0 to 100 *kPa*) at four different rates (v_1 = 0.1 *mm/min*, v_2 = 1 *mm/min*, v_3 = 10 *mm/min*, v_4 = 50 *mm/min*). The three cycles were averaged afterward. The study involved both the same square area and the equipment employed for the static tests and the sensor output was aligned with the load cell output with a sampling frequency of 10 *Hz*. Measurement accuracy respect to the applied pressure trends was analyzed in terms of RMSE. Hysteresis evaluation was performed considering the maximum difference in sensor output during loading and unloading and expressed as a percentage of the working range, as indicated in equation (2.5) [160].

$$Hysteresis\ error = max \frac{|P_{measured\_load} - P_{measured\_unload}|}{P_{measured\_max}} 100 \qquad (2.5)$$

In the literature there are different approaches to compensate for the hysteresis with data processing actions. Chua and Chen successfully adapted the general Preisach model (generally employed in the field of ferromagnetism) to increase the accuracy of their silicon piezoresistive pressure sensor [161] [163]. However the wiping-out and congruency properties that constitute necessary and sufficient conditions for the application of the model scarcely fit with our case study. Hall et al. used a fourth-order polynomial regression equation to predict compression force with terms that depended on both the current output voltage and the loading history represented as a moving integral [164]. The best windows size of the moving integral strictly depends on the loading velocity: a window of 5 *s* can be adequate for a compression velocity of 1 *mm/min*, but completely ineffective for slower signals and disruptive for faster ones.

In this work a quasi-static calibration was realized to compensate for hysteresis, calculating two different fittings for loading ($V_{out}(t_i) \leq V_{out}(t_{i+1})$) and unloading ($V_{out}(t_i) > V_{out}(t_{i+1})$) and using data from tests at v_1, v_2 and v_3 at the same time. This method introduces very small delays (just one sample) and allows to fit data from a wider range of speed solicitation with an improved accuracy.

In the Results session it will be possible to notice that curves at v_4 cannot be related to the other ones without introducing considerable errors. High speed stresses need for ad hoc calibrations that will not be evaluated in the present work.

2.3.8 Long term dynamic stability test

In order to study the long term dynamic stability of the sensor, the 3 × 3 matrix highlighted in Figure 2.4 was tested with loading/unloading cycles from 0 to 50 *kPa*, for 120 *min* and at a velocity of 10 *mm/min*. The same apparatus employed for the hysteresis analysis was used in this test. Peaks were detected and their mean value and SD were reported.

2.4 Results and discussions

2.4.1 SEM/EDS textile structure analysis

The SEM analysis confirmed that the third integration level of the EeonTex™ LG-SL-PA is a knitted structure [111]. Differently from weaving, in knitted fabrics the yarn follows a

meandering path, called course, creating symmetric loops above and below the mean path of the yarn. These meandering loops are easy to be stretched in different directions providing knit fabrics with much more elasticity than woven fabrics (up to 500%). For this reason, knitting is very suitable for garments that must be elastic or stretch in response to the wearer's motions, such as socks and hosiery. Knitted garments are often more form-fitting than woven garments, because their elasticity allows them to contour to the body's outline more closely.

Thanks to their elasticity, knitted structures undergo structural deformations of both the yarns and weaves if compressed or pulled. This lead to measurable changes of their electrical impedance. Figure 2.5 (a) shows that the fabric is made up of looped interconnections of courses and wales, where the wales are the threads that run vertically and the courses run horizontally across the fabric.

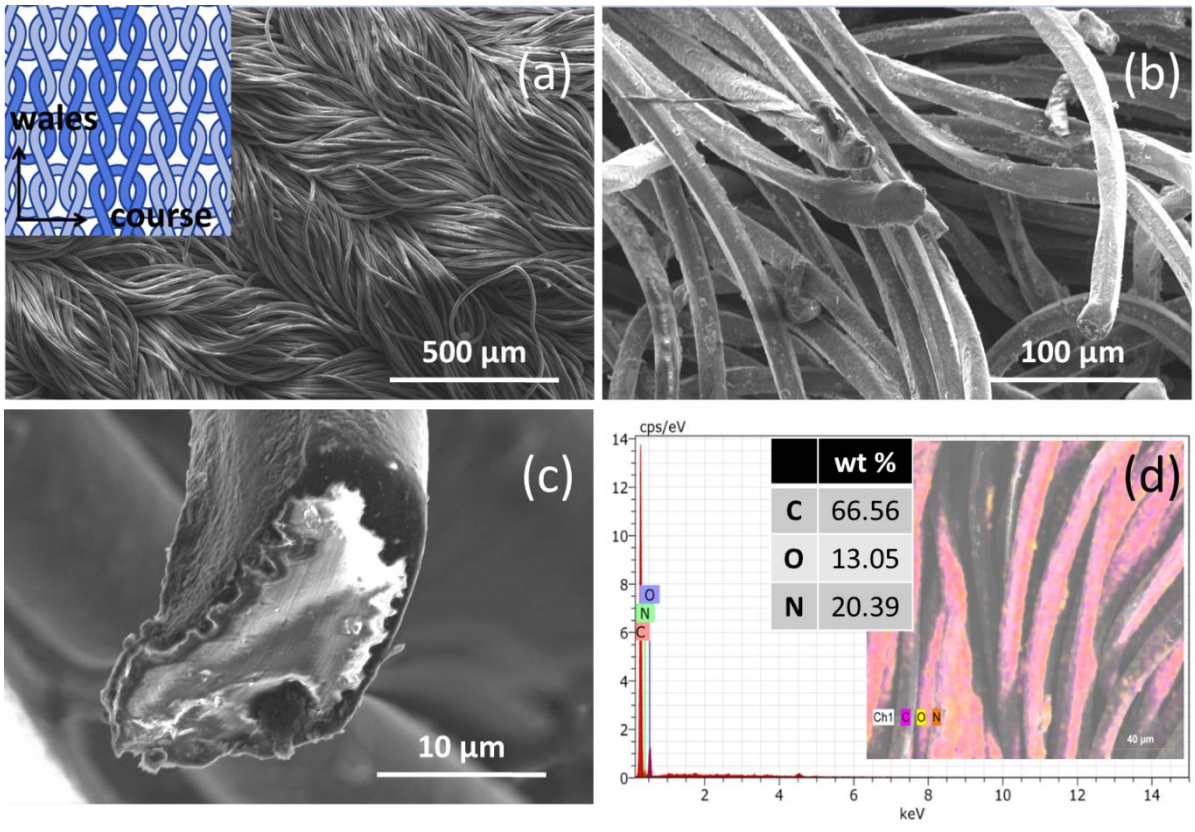

Figure 2.5 SEM images at the fabric level (a) with the knitted structure scheme, at the yarn level (b) and the fiber level (c); EDS microanalysis results are reported in (d).

Regarding the yarn level (second integration level), Figure 2.5 (b) shows that each yarn is composed of multiple fibers running in parallel. Each fiber is composed of a coating around an internal core (Figure 2.5 (c)). The EDS analysis detected the element composition of a

single fiber: it is made of carbon, oxygen and nitrogen (percentages are reported in Figure 2.5 (d)). Hydrogen, obviously present, is too light to be observed. The composition is compatible with the nylon-elastane structure, but it does not give information regarding the conductive formulation of coating. Detected elements are compatible with both polypirrole [165] and carbon coatings [124].

2.4.2 Static calibration

The mean calibration curves calculated for the sensor are reported in Figure 2.6 (a). The selection of a proper gain resistance is fundamental for defining sensitivity and working range adequate for an application: low resistance values (e.g. 160 Ω) are inadvisable for the poor sensitivity, especially at high loadings, while high resistance values (e.g. 560 Ω) assure higher sensitivity but reach saturation at 50 *kPa*. The latter are recommended for low pressure detection tasks, as grasping analysis or compression therapy monitoring [166]. Halfway resistance values provide for both good sensitivity and wide working range. For this reason an intermediate resistance (i.e. 220 Ω) had been chosen for the remaining tests.

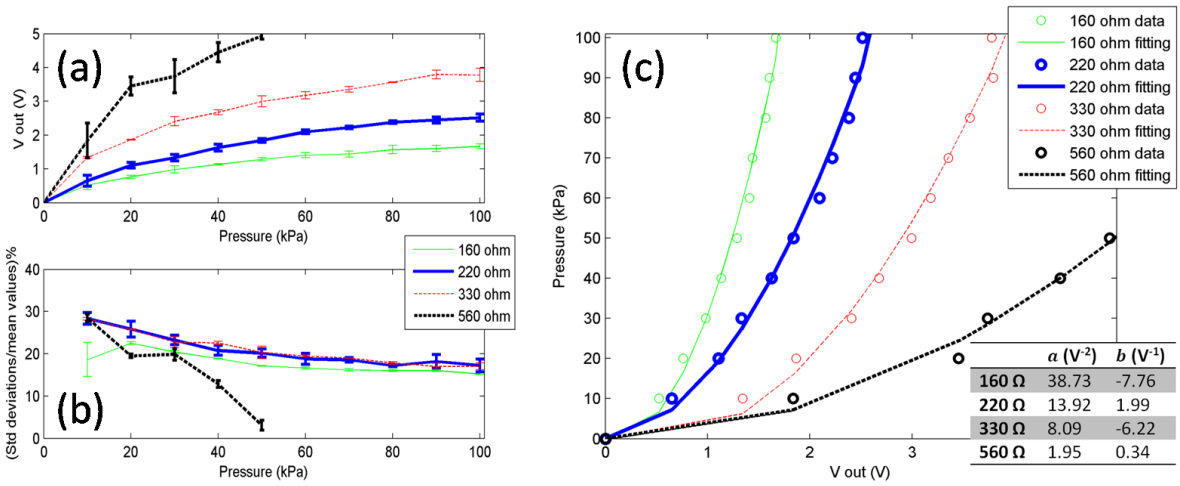

Figure 2.6 (a) Calibration curves obtained considering the mean voltage outputs for 9 matrix sensels for the four gain resistance values (error bars are due to the three performed trials); (b) standard deviations SD (expressed as a percentage) of the single sensels outputs respect to the mean calibration curve versus applied static loads (from 0 to 100 *kPa*) and (c) second order polynomial fittings employed to calculate P from static measurements of V_{out} (all $R^2 \approx 0.99$). Parameters of the second order polynomial fittings are reported in the table for the four resistances.

The percentage deviation (SD%) of the single sensels curves from the overall calibration curve takes into account the spatial repeatability among different active elements. It was

calculated for each resistance (Figure 2.6 (b)). Results indicated an overall error within 30% and 20% of the measured values, decreasing for high pressures. For the case of the highest gain resistance, SD% decreased markedly since output voltages rapidly converged to the saturation value.

Such a simplified but effective approach has been accepted also in prior works [158], allowing the convenient use of one single mean calibration curve for the whole sensor. These deviations may appear of some weight, especially for those cases where the pressure load is applied on a low number of elements. However, when the load is spread over a higher number of elements the application of one single overall calibration curve seems well-justified, although with the approximations set by the measured deviations.

The relationship between the measured pressure P (in *kPa*) and the mean voltage output V_{out} (in *V*) averaged on the 9 pressed sensels resulted in second order polynomial fittings (equation (2.6)). Fitting parameters are reported in Figure 2.6 (c) for the four resistances. They had been applied for all the static analysis reported in the following sections. Fitting results are markedly accurate (all $R^2 \approx 0.99$) and therefore strongly remarkable for static pressure evaluation tasks (e.g. posture analysis and bedsores prevention).

$$P = aV_{out}^2 + bV_{out} \tag{2.6}$$

In Figure 2.6 (a) is possible to notice that the application of lower pressures (within 40 *kPa*) assures a better sensitivity respect to the case of major loads. In addition, in case of low pressures the sensor behaviour can be considered linear. This is considered a good property for sensors management [167].

2.4.3 Stretch and curved surface tests

Static calibration tests with the 20% stretched sensor showed low differences respect to the not stretched condition, with a RMSE equals to 2.63 *kPa* (Figure 2.7 (a)). Regarding test performed on a curved surface, no strong differences with the reference condition were detected on the three loaded sensels (RMSE of 3.11 *kPa*, Figure 2.7 (b)). In particular, results for pressures lower than 40 *kPa* slightly overestimate the applied loads, while higher pressures underestimate them.

The presented results are positive since they allow a simple use for the sensor in case of both moderate stretch and employment on curved surfaces that are not markedly sharp, adding

worth to the sensor flexibility and softness. Conditions of stretching and adaptation on curved surfaces are typical for wearable applications [168].

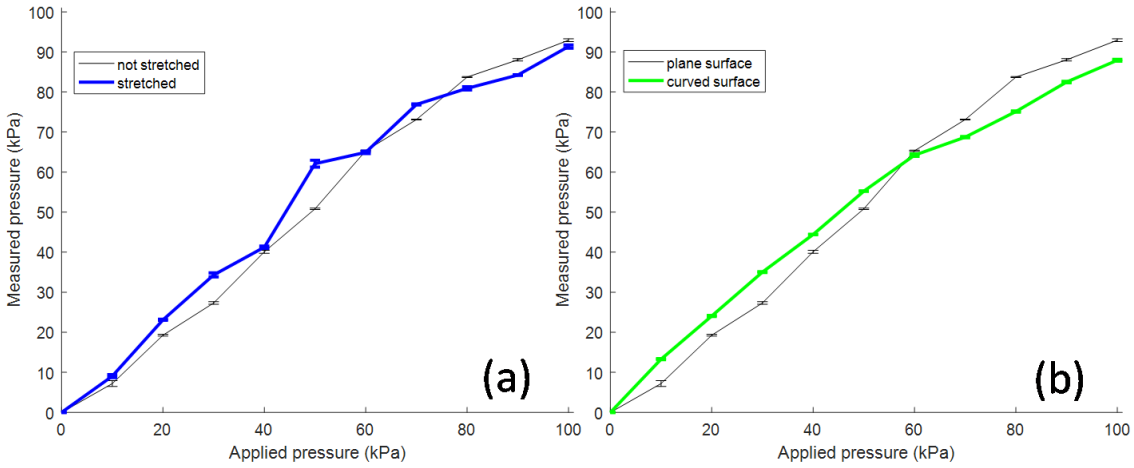

Figure 2.7 (a) Static mean curves for the sensor in case of 20% of stretch in both planar directions versus reference condition (sensor without stretch on a plane), (b) static mean curves for the sensor in case of use on a curved surface versus reference condition. Error bars refer to the trials performer three times.

2.4.4 Shear test

Shear tests showed that sensels response to normal loads is not significantly affected by the additional stress (Figure 2.8): RMSE values respect to the condition with just normal loads are 1.27 *kPa* and 0.69 *kPa* for the constant and linear shear cases, respectively. The fact that normal load detection is not disturbed by shear increases the measurement accuracy. On the other hand, the fact that the sensor is not sensitive to shear (at least for the low stresses that could be produced with the available equipment) can be considered a limit in the sensor potentialities.

2.4.5 Drift test

Drift is generally related to the stress relaxation behaviour typical of elastic materials. For the presented sensor, the percentage drift is more significant for low loads, then it decreases for higher values (Table 2.1). This can be explained considering that the sensitivity of the sensor decreases for pressures higher than 40 *kPa*. Results are compatible with performances of other piezoresistive sensors [169] and confirm the suitability of the sensor for static measurement tasks.

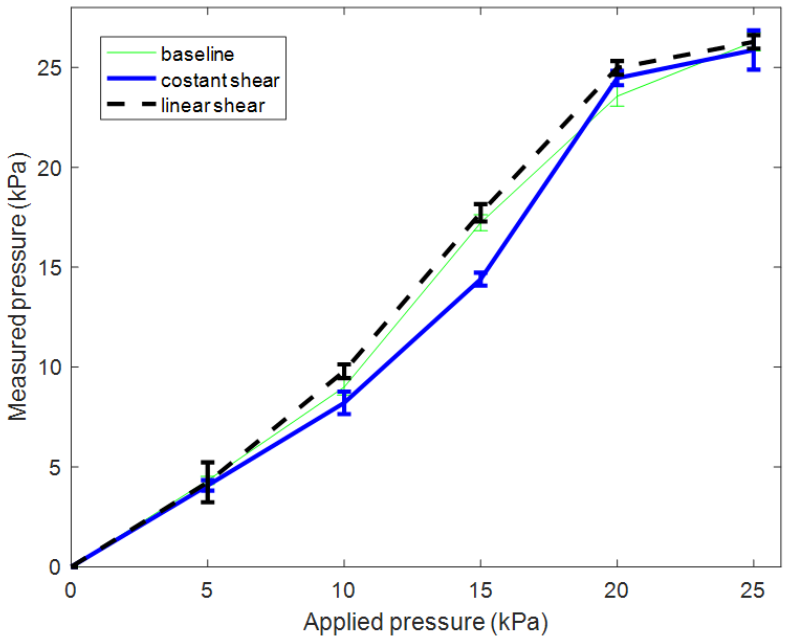

Figure 2.8 Static tests comparing sensels response to just normal load (baseline), normal load with constant shear and normal load with linearly increasing shear. Means and SD values were calculated on three sensels stressed separately.

Table 2.1 Drift errors (in %), averaged over three tests, in correspondence to static loads (in *kPa*) applied for 10 *min* on a 3 × 3 sensels area of the sensor.

Pressure	10	20	30	40	50	60	70	80	90	100
Drift error % (SD)	4.23 (0.33)	3.40 (0.41)	2.36 (0.04)	1.61 (0.09)	1.06 (0.21)	1.09 (0.08)	1.17 (0.27)	0.79 (0.14)	0.73 (0.07)	1.27 (0.05)

2.4.6 Temperature and noise tests

Tests for the evaluation of the sensor output in dependence to temperature showed a voltage variation of 2.65% at 35 °*C* and 14.22% at 42 °*C* respect to *RT*. Temperature dependence is a well-known limit of piezoresistive sensors, since conductive materials resistivity is highly sensitive to temperature changes. This drawback has limited effects for wearable applications that are typical of textile sensors because a narrow range of

temperatures can be experienced. Moreover, the sensor provided very low noise readouts, with a SNR of 41.77 ± 2.58 *dB* that did not exhibit a significant correlation with temperature.

2.4.7 Multitouch analysis

The mean calibration curves obtained averaging the three sensels $S_{3,5}$, $S_{5,5}$ and $S_{5,3}$ outputs during the static loading of the complete 3 × 3 matrix area (see Figure 2.4) and just the three sensitive units produced slight differences, with a RMSE equals to 3.31 *kPa* (Figure 2.9 (a)). The result confirmed that the output voltage of each sensel is not affected by the loading of close sensitive elements. In addition, no phantom touches were present during the triple loading (Figure 2.9 (b)). Therefore, the effectiveness of grounding in the current leakage removal was empirically assessed.

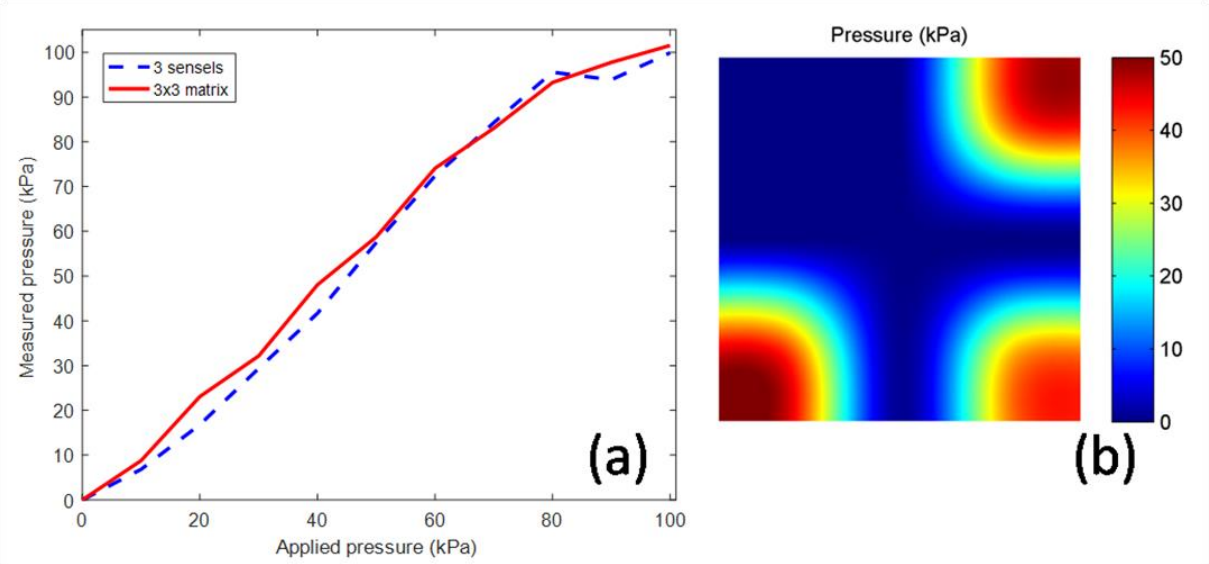

Figure 2.9 (a) The mean static stress curves obtained for the three sensels $S_{3,5}$, $S_{5,5}$ and $S_{5,3}$ during the loading of the 3 × 3 matrix area and the loading of just the three sensels, (b) an image of the 3 × 3 matrix during the loading of $S_{3,5}$, $S_{5,5}$ and $S_{5,3}$ at 50 *kPa*, showing the absence of phantom touches.

2.4.8 Hysteresis tests

The employment of static fittings in case of dynamic analysis (in a wide range of cyclic loading rate, from 0.1 to 50 *mm/min*) entailed low quality measurements, due to hysteresis. The problem is a typical drawback of the piezoresistive detecting principle and it is related to a delay in the material reaction to applied stress, which is depending on its previous conditions [109][158][160][163]. In fact, sensor performances are comparable with other

sensing solution based on the same working rationale [158][160]. Moreover, tests showed that sensor output was higher during unloading than loading in correspondence of identical loads (Figure 2.10), similar to other piezoresistive pressure sensors [160].

Figure 2.10 and Table 2.2 show that hysteresis, evaluated in accordance to equation (2.5), tended to decrease with the loading rate. On the other hand, at higher stress velocity the sensor fails in following and covering the entire required response range. Both behaviours can be explained considering that high dynamic stresses do not allow the electric properties of the sensing material to reach a steady state condition. This double effect balances out accuracy, leading to similar values (calculated as RMSE according to equation (2.2)) for the different loading rates (5.38 *kPa* on average, see Table 2.2).

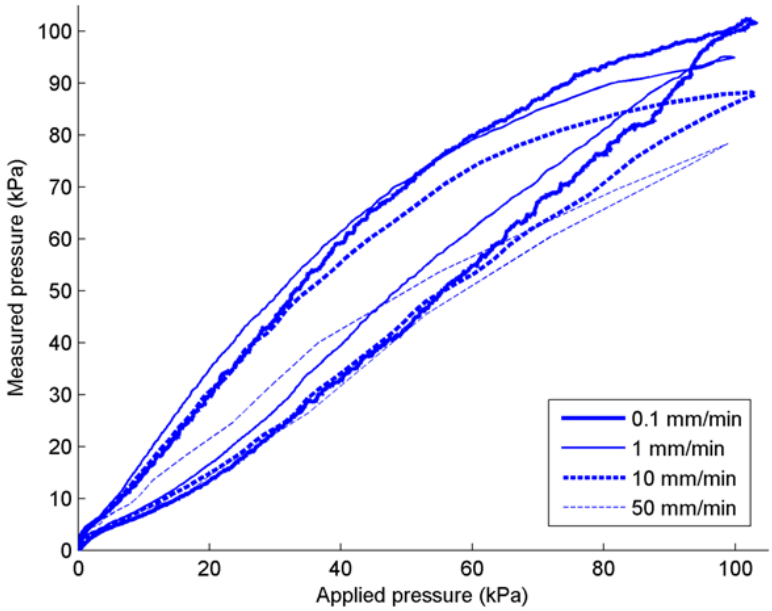

Figure 2.10 Measured versus applied pressure for loading/unloading cycles averaged on three repetitions. Tests were carried out at v_1 = 0.1 *mm/min*, v_2 = 1 *mm/min*, v_3 = 10 *mm/min*, v_4 = 50 *mm/min*.

Table 2.2 Hysteresis and accuracy errors (RMSE) for the different loading rates.

Loading rate (*mm/min*)	Hysteresis (%)	RMSE (*kPa*)
0.1	28.12	5.96
1	23.25	5.64
10	22.22	5.07
50	15.73	4.87

2. Multilayer matrix textile-based pressure sensor

As previously explained, main post-processing techniques employed to compensate hysteresis are not satisfying for the present study. More precisely, moving average methods [164] depend on parameters, as the window size, that are too heavily related to the loading rate. On this basis, in the present work two different calibration curves were considered, both resulting as dual exponential fittings (see equation (2.7)).

$$P = ae^{bV_{out}} + ce^{dV_{out}} \tag{2.7}$$

The first curve was calculated as the best fitting for the loading sections of the cycles at v_1, v_2 and v_3 (Figure 2.11 (a)) and it has to be applied when the sensor is in a unload phase (when $V_{out}(t_i) \leq V_{out}(t_{i+1})$). The second curve was obtained as the best fitting for the unloading sections of the cycles at v_1, v_2 and v_3 (Figure 2.11 (b)) and it has to be applied when the sensor is in a unload phase (when $V_{out}(t_i) > V_{out}(t_{i+1})$). Fitting parameters are summarized in Figure 2.11 (both $R^2 \approx 0.98$).

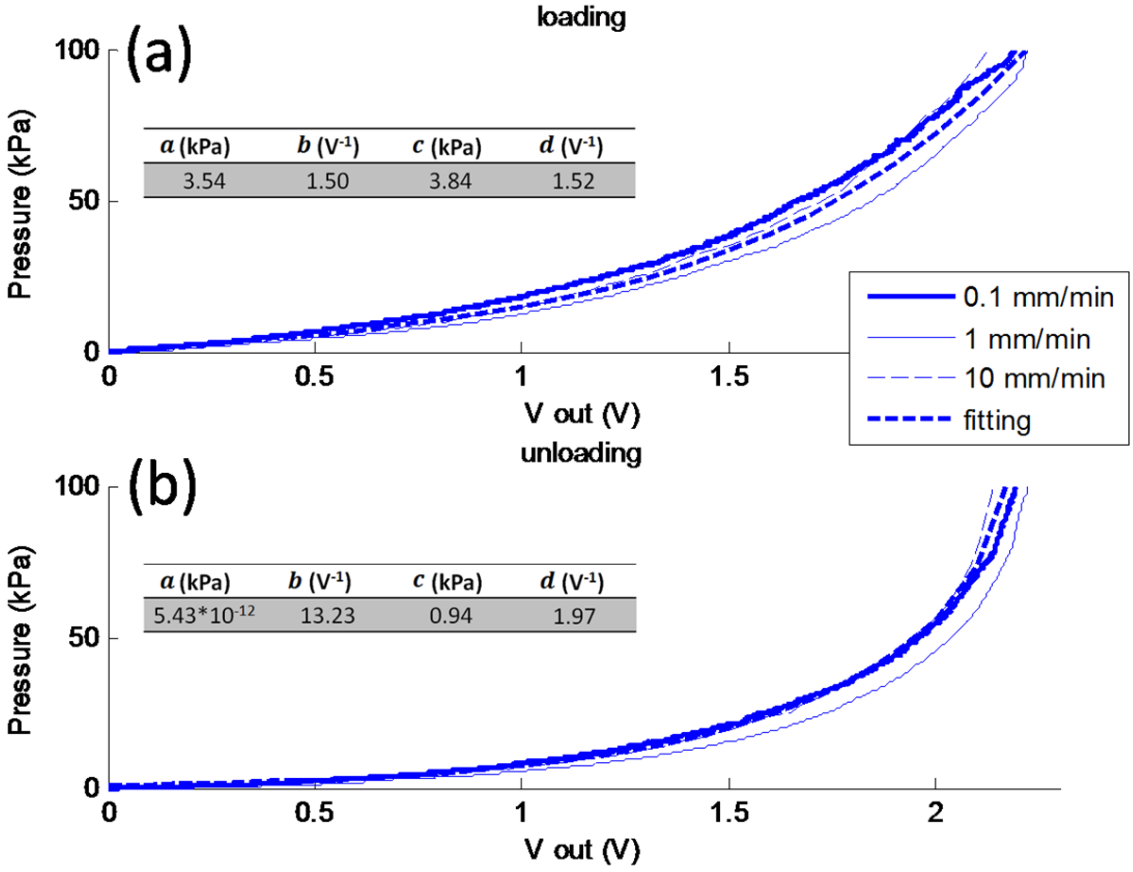

Figure 2.11 Dual exponential fittings and related fitting parameters for the loading (a) and unloading (b) sections of the stress cycles for three different loading rates (v_1 = 0.1 *mm/min*, v_2 = 1 *mm/min*, v_3 = 10 *mm/min*).

The presented fittings allow managing measurement information from a wide range of stress speed, but they are not accurate in case of higher velocities, e.g. 50 *mm/min*. These high dynamic conditions should require further ad hoc studies.

Thereafter, the new calibration curves were applied in repeated load/unload cyclic tests at the three velocities v_1, v_2 and v_3, providing substantial improvements in terms of both hysteresis and accuracy errors (Table 2.3). Results can be easily assessed from Figure 2.12, confirming that an adequate post-processing can enhance the sensor performances in case of dynamic measures. This approach suffers from the limit of requiring additional calibration phases respect to the traditional static ones. Moreover, it needs for different fittings according to the loading velocity range. This condition supposes an approximate prior knowledge of the stress rate that is typical of a particular application.

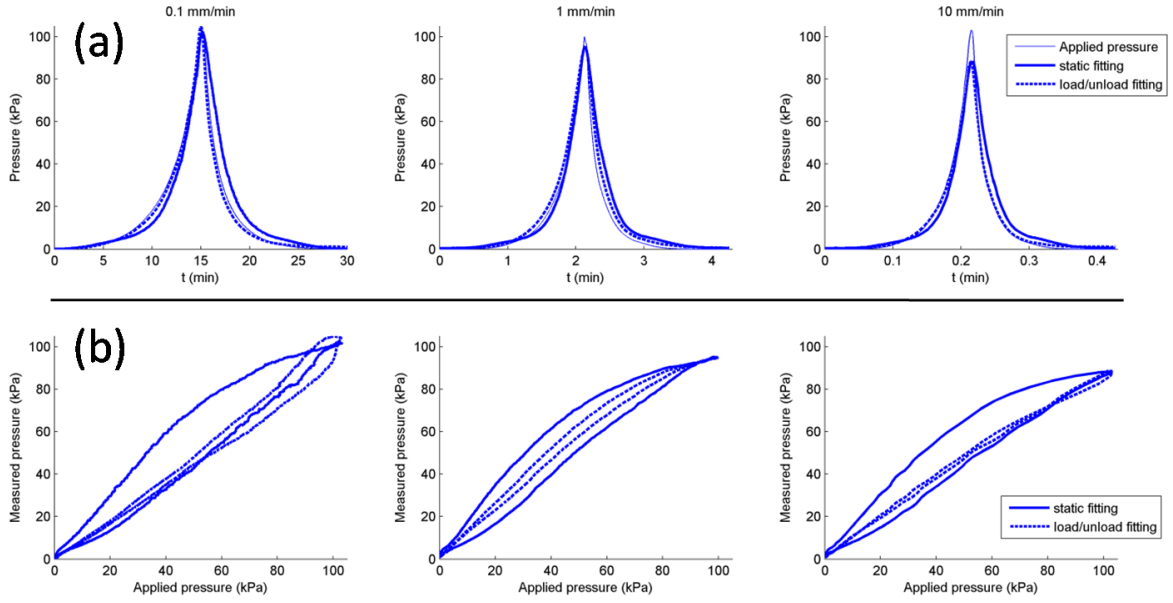

Figure 2.12 (a) Applied pressure curves versus measured pressure curves calculated using both the static and the load/unload fittings for v_1, v_2 and v_3, (b) hysteresis cycles using the static and the load/unload fittings for the three loading rates.

2.4.9 Long term dynamic stability test

Mean and SD values calculated on the 258 detected peaks during the 2 *h* long test are 52.59 *kPa* and 0.77 *kPa*, respectively (Figure 2.13). The reduced deviation proves the dynamic stability of the sensor that is mandatory for long term dynamic and cyclic measurements, as in case of gait analysis.

Table 2.3 Hysteresis and accuracy errors (RMSE) for the different loading rates obtained with the load/unload fitting.

Loading rate (*mm/min*)	Hysteresis (%)	RMSE (*kPa*)
0.1	14.42	2.29
1	6.12	3.74
10	4.03	2.63

Considering the complete pool of presented results, it is possible to confirm the good performances of the sensor for a wide range of applications that can also benefit from its thinness, lightness, flexibility, stretchability and wearability. Presented results provides valuable insights on the design issues and performances of piezoresistive textile pressure sensors, and in particular on their strengths and limitations [170]. Specifically, a better understanding of the loading options, applications and reliability has been obtained, highlighting and partially solving the undesired effects that has to be taken into account in the processing of data. This information should facilitate researchers and users in determining the best design and employment of their smart sensing solutions.

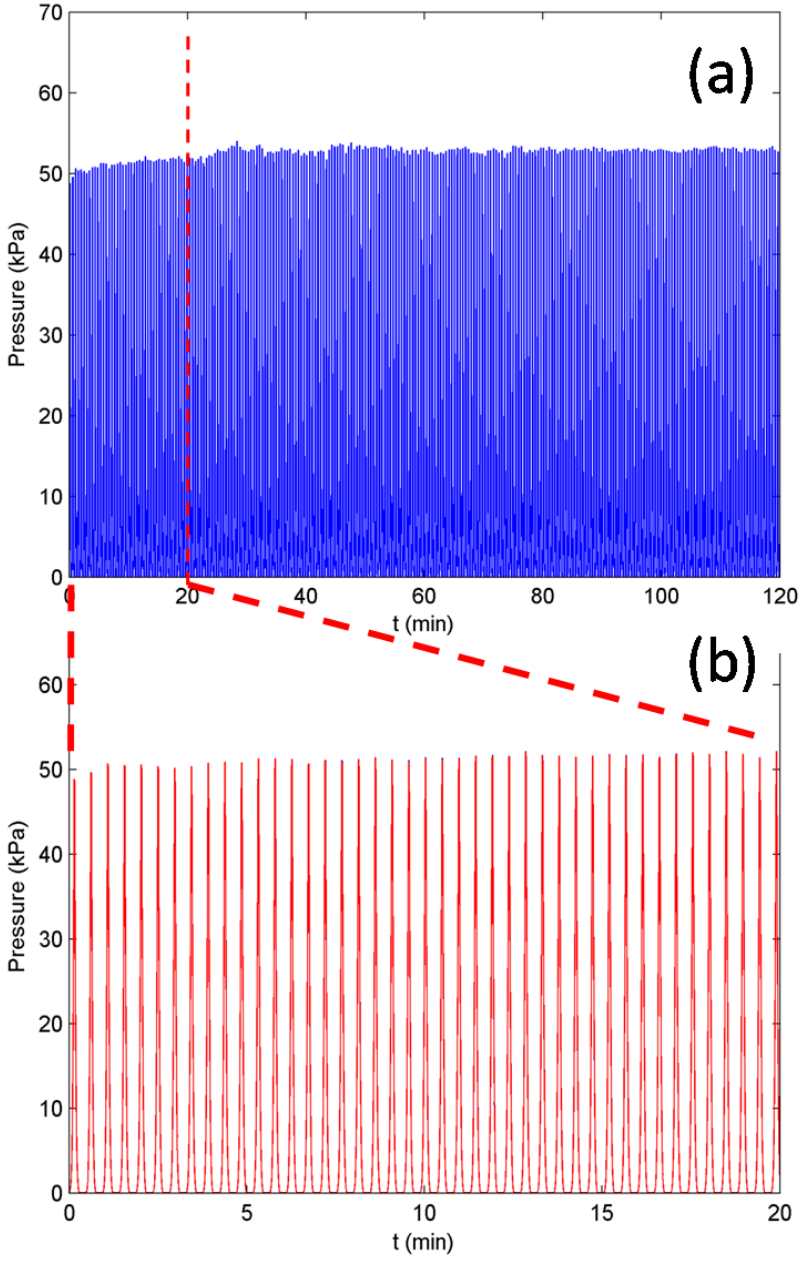

Figure 2.13 Measured pressure (averaged on the 9 loaded sensels) during the dynamic stability analysis: (a) the complete 2 *h* long test, (b) a 20 *min* expanded section of trace (a).

Chapter 3

Textile-based strain sensor

3.1 Introduction

Strain sensors based on smart textiles either have intrinsic electric properties that are not normally associated with traditional textiles or they can act as a substrate for attachment of sensors, output devices and printed circuit boards [113]. To date, several works have been published that summarise textile fabrication techniques [111][112] and applications of these smart fabrics in intelligent clothes, representing a new type of human-machine interface [171].

For the present thesis, we focused our attention on strain-resistant textile sensors. These sensors are based on the piezoresistive effect. Piezoresistive sensor technology is common method of creating textile-based strain sensors along with capacitive, inductive, and impedance sensors. Piezoresistive technology offers advantages respect to other sensor technologies: high responsivity, small size, simplicity and repeatability [172]. Capacitive sensing approach in smart textiles is mainly used for pressure detection [173], and development of these sensors is more complex due to requirement for separation of conductive panels and the usage of dielectric material. Whereas, inductive or impedance sensors in electro-textiles are mainly used for the measurement of physiological parameters of the human body, with a serious problem due to signal interference during trials [174].

Usually, piezoresistive strain sensor exploit the electrical resistance change due to an applied mechanical stretching. This means that forces experienced by everyday clothing during movement can be detected without the need for additional, less-comfortable devices [175].

3. Textile-based strain sensor

Textiles stretch sensors could be divided into two broad groups, stitched and knitted. Stitched sensors are based on conductive thread stitched onto fabric substrates [176][177][178]. The stitched structure creates the sensing mechanism, but the sensor response relies heavily on the physical characteristics of the textile substrate to which it is stitched. For knitted stretch sensors, in contrast, a conductive textile is used in place of a standard thread and generally follows the wales and courses of the common knitted structure. Consequently, with the knitted stretch sensor, it is difficult to create a free-form sensor pattern, but it can be more easily integrated into a wearable device and the final system could be simpler and more comfortable.

These devices have interesting potential uses, but they must overcome limits related to their manual manufacturing, which causes additional variabilities within the well-known limits of these materials: hysteresis and low accuracy. Moreover, the lack of a specific procedure for the electromechanical characterization of these materials complicates the identification of an adequate conductive textile for a specific application.

Mattman et al. [177], Gioberto and Dunne [30], and Guo et al. [179] analysed the mechanical properties using a tensile tester, while simultaneously analysing the electrical properties using a digital multimeter [30][177] or a pre-programmed microprocessor and a computer [179]. In general, the following sensor properties were examined: working range, working function, sensitivity, stability, electrical hysteresis, relaxation behaviour, dependency on strain rate, long-term cycling, ageing and wash-ability. Shyr et al. [180] performed stretch-recovery measurements of elastic-conductive webbings to analyse the effect of webbing structures on tensile hysteresis and the electrical contact resistance. These studies quantified sensors' features, highlighting the relationship between fabrication methodology and the specific material composition. It is evident that a generic, but rigorous approach to the characterization of conductive textiles is required.

Therefore, in the present Chapter we propose a methodology to characterise whatever electrically conductive knitted textile, in order to optimise and calibrate its sensing capabilities. The key aspect of this methodology is that it is not limited to a specific material because it is derived by merging approaches found in literature and mechanical concepts. Moreover, we reported a case study where the tests of the procedure have been used to select a suitable conductive textile and to steer the design of the sensor. Device usability was then assessed by tracking the elbow flexion/extension of an adult participant, and the device's

dynamic performances were validated using the encoder of the knee joint of the SABIAN humanoid robot [181].

Understanding the electro-mechanical features of the proposed sensor and its possible use as wearable device may help the user in managing the sensor with a deeper awareness of both its benefits and drawbacks.

3.2 Material characterization

A warp-knitted textiles have been taken into consideration and the investigation started with the description of the three integration levels of their hierarchical structure [113]: the fabric (the third integration level) composed by turned yarn knitted or weaved, the yarn itself (second level) composed of twisted fibers, and the fibers (first level).

To clarify the three level hierarchy, in Figure 3.1 (a) we reported the example of Electrolycra [123] that shows a typical knitted structure. It is made up of looped interconnections of courses and wales, where the wales are the threads that run vertically and the courses run horizontally across the fabric [111]. There are two major varieties of knitting: weft and warp. Weft knitting, the most common, presents wales perpendicularly to courses, whereas in warp knitting, wales and courses run in parallel. Electrolycra strained at 50% is presented in Figure 3.1 (c), clearly showing its warp knitted structure.

In relation to the yarn level, Figure 3.1 (e) and Figure 3.1 (f) show that each yarn strand is composed of multiple fibers running in parallel, with each fiber (Figure 3.1 (g)) being composed of a coating around an internal core (Figure 3.1 (h) and Figure 3.1 (i)). The element composition analysis of a single fiber was conducted using energy-dispersive X-ray spectroscopy (BRUKER). Figure 3.1 (j) shows the results of a single fiber, and Figure 3.1 (k) and Figure 3.1 (l) demonstrate that each fiber has a non-conductive core with a silver particle coating. The coating represents the extrinsic modification introduced to enable conductivity of the fabric substrate at the fiber level.

In order to determine the mechanical and electrical properties of the fabric, uniaxial cyclic strain tests have to be conducted using a material testing machine. Resistance values need to be simultaneously recorded with force and elongation. The complete description of the

electromechanical behaviour of the conductive textile can be obtained through the evaluation of the following nine factors and parameters.

1) Preferential direction

Courses and wales of the knitted structure could offer different paths to the current, thus resistance change should be assessed horizontally, (along courses direction - CD) and vertically (along wales direction - WD). This factor is important to identify the most appropriate deformation direction of the fibers during strain cycles.

2) Pre-stretching

The history of stretching range can determine the electromechanical behaviour of an elastomeric material (e.g. Mullins effect). Measurements are necessary to assess the influence of high deformations, so-called pre-stretching, applied before cyclic strains in the desired range.

3) Strain rate

Tests have to be carried out to measure the dependence of the textile behaviour on the rate of applied strain. This parameter is crucial and usually set in a range that depends on the specific application.

4) Sample dimensions

This consists in assessing whether the sensor behaviour depends on its size. This is important especially when there are limitations in the sensor dimensions.

5) Temporal stability

The long-term behaviour and thus the reliability of the sensors have to be estimated by measuring basic performances at different times (often known as “test-retest” approach). Aging and other degrading effects have to be investigated to assess the working life of the device.

3. Textile-based strain sensor

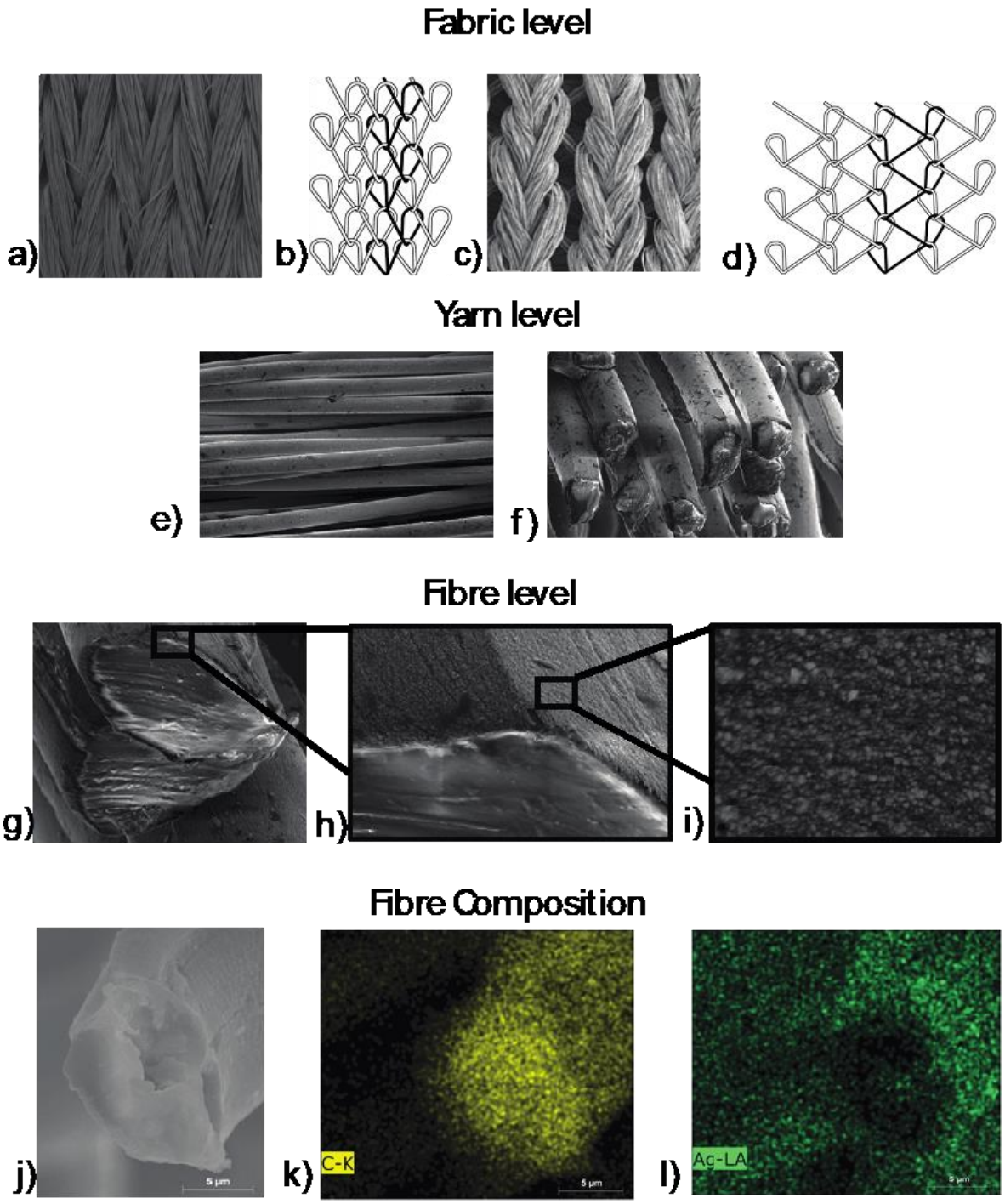

Figure 3.1 SEM images (HELIOS NANOLAB 600i DualBeam FIB/SEM). Fabric level: a) Electrolycra at 0% of strain and b) its corresponding warp knitting scheme, c) 50% strained Electrolycra, and d) its corresponding scheme. Yarn level: e) surface and f) cross-section of the fibers that compose a single strand of yarn; Fiber level: g) single fiber cross-section and h) the external conductive layer with i) the particle coating; j) Fiber composition: k) nonconductive fiber and l) external silver particle coating.

6) Hysteresis

This refers to the dependence of the state of the system on its history and it is important to quantify the sensor capability of following the changes of the input parameter (strain) regardless the direction (loading or unloading) the change is made.

7) Working range

The maximum and minimum values of applied strain that can be measured by the sensor. The designer has to compare this working range and the expected deformation to be sure that the material is able to cover the entire range and without damages.

8) Relaxation behaviour

This is visible as a temporal decrease of resistance in response to a fixed amount of strain applied to the sensor. When this drift is significant the sensor reaches low levels of reliability for prolonged static conditions.

9) Curve fitting

The experimental data have to be described with an analytical function that relates strain and resistance values. This is crucial to derive the calibration curve of the sensor.

The electro-mechanical tests described above were performed at room temperature by using a material testing machine (model 4464, Instron Inc., Norwood, MA), which allows imposing a desired strain to the textile. Each end of the sample was fixed mechanically using clamps with copper sheets and welded wires to detect the sensor voltage. These wires were connected to a data acquisition board (DAQ, National Instrument®) to measure the electrical resistance values, which were simultaneously recorded for different strains with a sampling frequency of 10 *Hz*. The resistance value *R*, in particular, is measured by means of the voltage divider shown in Figure 3.2, as $R = R_1 \frac{V_{in} - V_R}{V_R}$, with V_{in} = 3.2 *V* and R_1 = 10.5 *Ω*. We cut the conductive textiles into pieces of different sizes using a Laser cutter (VLS 3.50, Universal Laser Systems), as laser cutting guarantees high precision without affecting the sample's functionality. If not otherwise specified, we tested a different sample (2 *cm* width × 3 *cm* length) for each measurement, with a strain rate of 60 *mm/min*.

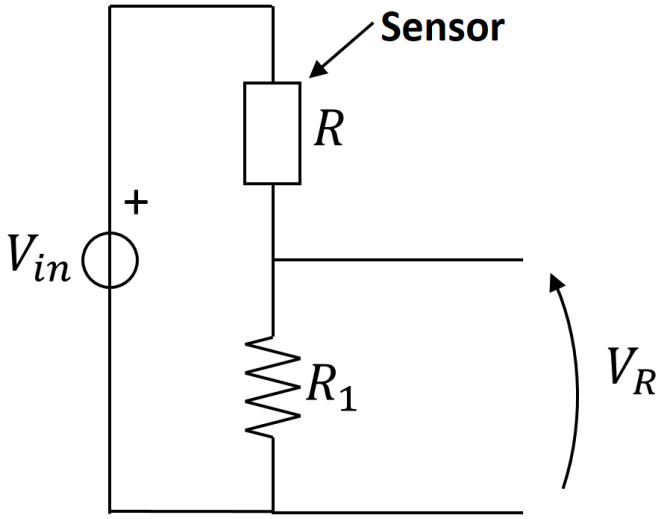

Figure 3.2 Voltage divider used to measure the resistance of the sensor.

The nine factors reported above have been investigated through a series of tests. Preferential direction has been evaluated by testing the resistance-strain behaviour along both directions. Pre-stretching was evaluated as follows: after five cycles of 60% of strain, each sample was respectively pre-strained at 100%, 150%, 200% and 250%, then another five cycles of 60% strain were performed. To evaluate the strain rate, different deformation velocities (50, 60, 100, 200, 400, 600 *mm/min*) were applied, in order to cover the typical motion speed range of the human body [177]. The sample dimension was tested through cyclic measurements using samples of different length-width ratios (1.5, 2, 3, and 6). Temporal stability of the sensor was evaluated once a week for two months, more specifically, uniaxial cyclic strain tests were executed for 10 *min*. In order to measure the relaxation behaviour, each sample was stretched at a speed of 60, 200 or 600 *mm/min*, and held at increasing values of strain (20, 30, 40, and 50 %) for 2 *min*.

3.3 Sensor development

Device usability was assessed by tracking the flexion/extension of human joints, in order to offer a possible simple and wearable solution for continuous monitoring.

3.3.1 Sensor design

Prior to designing the device, it is important to briefly analyse the quantitative parameters necessary for monitoring human joint angles. In this work, the elbow joint was investigated, which has two degrees of freedom (DOF): flexion-extension and prono-supination. The attention was focused on the humeroulnar joint that supports flexion-extension of the elbow. Literature findings [138] showed that the elbow's centre of rotation is not fixed during flexion-extension, however human motion studies often simplify the analysis with acceptable approximation [182]. The human body is schematically represented as a system of rigid links, connected by ideal joints. The simplified biomechanical model of the elbow adopted in this study, composed of two cylinders connected by a spherical shell with fixed radius and rotational axis, is shown in Figure 3.3 [183].

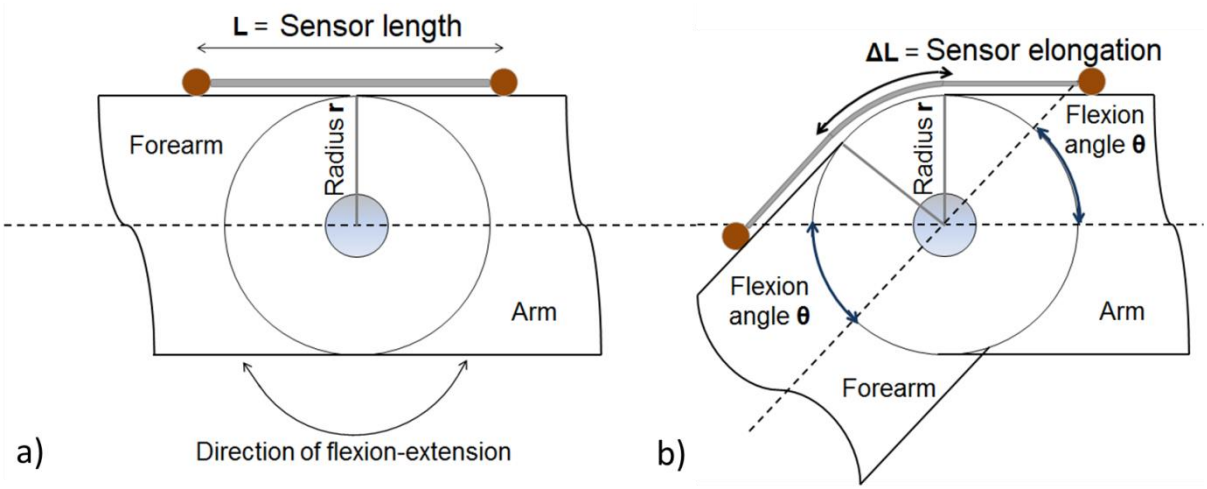

Figure 3.3 A biomechanical model of the elbow joint. a) full extended; b) bent at a ϑ angle.

A single sensor, fixed in correspondence with the joint, is sufficient to measure the elbow joint flexion-extension. The sensor location should be carefully evaluated, however, such that the entire range of sensor extension is utilised for maximising the sensitivity range [178]. The strain, particularly the elongation (ΔL, where L represents the sensor length), is directly related to the circular arch length (see Figure 3.3). Based on the simplified biomechanical model, elongation L is related to the bending angle θ and scaled by the joint radius r:

$$\Delta L = r\theta \tag{3.1}$$

The radius of the elbow joint is an anthropometric parameter, specific to each subject. By combining equation (3.1) and a linearized characteristic of the sensor, it is possible to estimate the relationship between the bending angle (in degrees) and the sensor resistance:

$$\theta = \frac{L_0}{100ar}\left(\frac{\Delta R}{R_0} - b\right)\frac{180}{\pi} \qquad (3.2)$$

where the parameters *a* and *b* are specific for each sample, and R_0 is the initial resistance corresponding to the length L_0. This biomechanical model could be extended to measure the rotation angle of each single axis joint, such as the knee or wrist.

The integration of the textile into a wearable device was a key point. The idea was to design a goniometer sensing system to allow monitoring of joint motion in a non-intrusive and comfortable way. For this purpose, the Lycra textile was selected for its favourable features: it is light, comfortable, skin-tight and highly stretchable. To begin, we verified that the double-layer conductive textile/Lycra does not influence the electrical characteristic of the sensor and that the tensile force increases by an acceptable value.

Two hooks, each one constituted of two coaxial cylinders, were designed to fix the sensing material on a Lycra elbow sleeve and set up the electrical connections. The hooks were produced by a 3D printer (PROJET HD 3000 3D Systems) using an acrylic resin (see Figure 3.4 (a)).

The final sensing device is composed of a strip (2×14 *cm*) of conductive material fixed on a customised Lycra sleeve by two hooks. Electrical resistance values were acquired using the same setup adopted during the characterization phase. A graphical user interface was designed to make using the device simple and suitable for a wide range of users. Flexion/extension angles were shown in real-time and were stored for off-line analysis.

3.3.2 Early Evaluation of Human and Robot Motion Detection

Preliminary qualitative tests were performed to assess the usability of the wearable goniometer and its capability to track the elbow joint movement of an adult volunteer during cyclic flexion/extension tasks (Figure 3.4 (a)).

For validation, dynamic tests were performed using the humanoid robot SABIAN, developed by the Scuola Superiore Sant'Anna in collaboration with the Waseda University of Tokyo [181]. SABIAN was built with a total of 16 DOF, 14 for the legs and two for the waist.

Its joints are actuated by DC Maxon motors and each joint is equipped with an encoder integrated with the corresponding actuator. These encoders provide 1024 pulses per rotation, giving a resolution of 0.35°.

For these tests, we designed a custom sleeve for SABIAN's knee and applied the sensor in correspondence with the robot joint (Figure 3.4 (b)). Flexion/extension cycles were performed by rotating the knee joint with a sinusoidal trajectory at 0.15 *Hz*. This movement frequency was chosen in relation to the robot's capabilities. Flexion/extension angles measured with our sensor and the encoder data were collected simultaneously, and all data were synchronised and analysed using a custom MATLAB® code.

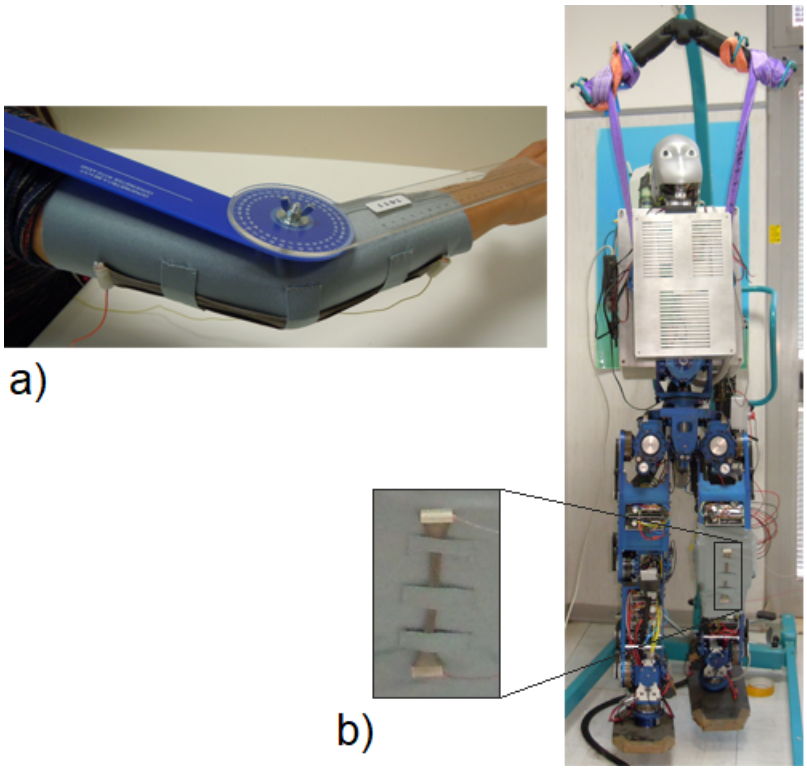

Figure 3.4 a) Wearable goniometer sensing device: conductive material fixed on a Lycra sleeve with two specially designed cylindrical hooks. An adult volunteer tested the performance of the device with a traditional goniometer. b) Validation tests using the humanoid robot SABIAN: the wearable device is fixed in correspondence with the knee joint.

3.4 Results and discussions

3.4.1 Material characterization

The first phase of this work concerned the electromechanical characterization of the smart fabric. Four textiles were taken into consideration: Electrolycra (Mindsets Ltd), EeonTex™LG-SL-PA (Eeonix), EeonTex™LR-SL-PA (Eeonix) and 4900 Stretch Conductive Fabric (Holland Shielding Systems B.V). This approach offers a very simple and compact sensing solution that relies on commercially available conductive fabric and does not require complex hardware or skills to implement. To explore the electromechanical responses of these conductive fabrics for their applications in stretch sensing, preliminary stretch-resistance tests were conducted:

- EeonTex™LR-SL-PA (Eeonix) is not a stretchable material and it can be used only for compression, as a pressure sensor;
- The fabric 4900 Stretch Conductive Fabric (Holland Shielding Systems B.V) can be stretched up to twice its length, but its conductivity increases only up to 25%;
- The EeonTex™LG-SL-PA (Eeonix) showed resistance change only after a 30% strain and the initial resistance value suffered from drifting (it was different after each flexion-extension cycle);
- Electrolycra (Mindsets Ltd) showed a repeatable resistance-strain behaviour with an appropriate working range, compatible with human joint movements.

Because of these preliminary suitable electro-mechanical properties, the Electrolycra was analysed in-depth. The manufacturer [123] declares the material's resistance to be 5 Ω per 100 *mm*. This value increases to 20 Ω when the material is stretched to 150 *mm* along one axis, but drops to 2.5 Ω when stretched at a 90° angle. Previous works have adopted Electrolycra as a strain sensor to reconstruct the spatial configuration of a soft octopus inspired robot arm [125] and as the electrodes of a capacitive transduction mechanism [138], but neglecting much information on the material behaviour.

1) Preferential direction

Five stretch-recovery cycles were performed along the CD and the WD (Figure 3.5). Since the results were not repeatable and presented hysteresis and drift between the cycles, additional characterization steps were required to choose a preferential direction.

2) Pre-stretching

The effect of increasing values of pre-stretching on the resistance-strain behaviour was evaluated along both the CD and the WD. These high values of pre-stretching caused two effects: damage and breakage of the textiles along the WD, and improvement of the sensor behaviour along the CD.

A comparison of the mean value of five stretch-recovery cycles before and after 100%, 150% and 200% of a single strain cycle along the CD is shown in Figure 3.6 (a). The 250% pre-stretching results are not reported because the textile was significantly damaged. It is noteworthy that a trade-off was necessary: whereas 100% pre-stretching improved linearity and decreased the hysteresis, 200% caused a higher resistance change range, but also slightly wider hysteresis. The SEM analysis (Figure 3.6 (b)) demonstrated that the 200% pre-stretching reduced the yarn tension; consequently, the density of wales and courses decreases after the pre-stretching. This caused a plastic deformation of the knitted strain sensor; therefore, the initial length and resistance values for the next characterization steps and application were set to these pre-stretching values.

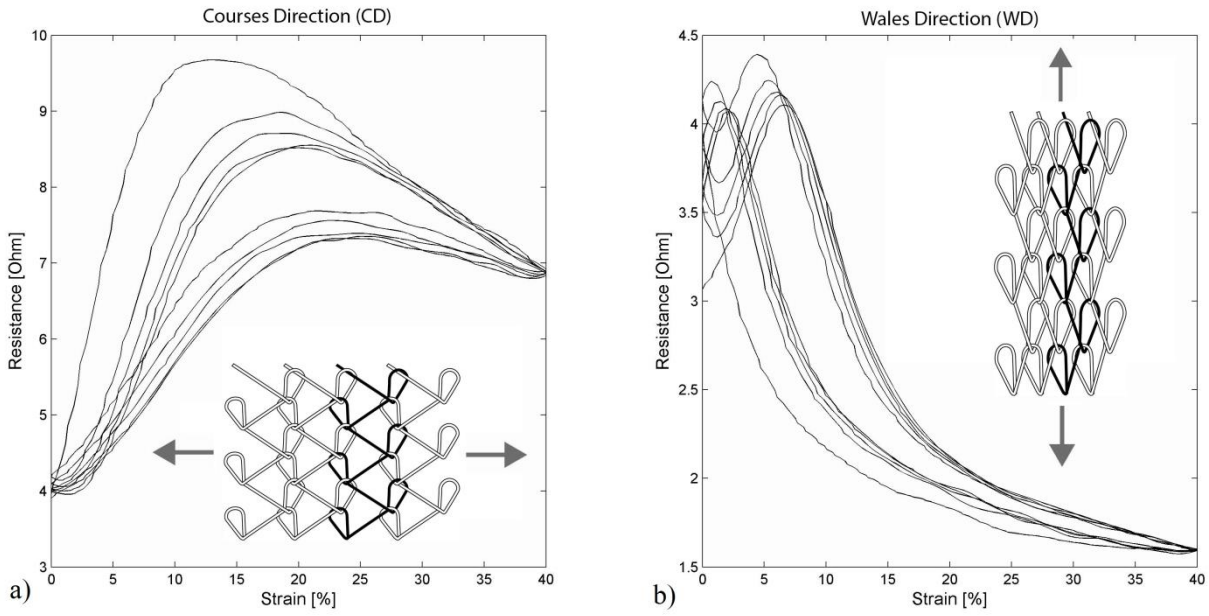

Figure 3.5 Resistance change along the a) courses direction (CD) and b) wales direction (WD) of Electrolycra fabric.

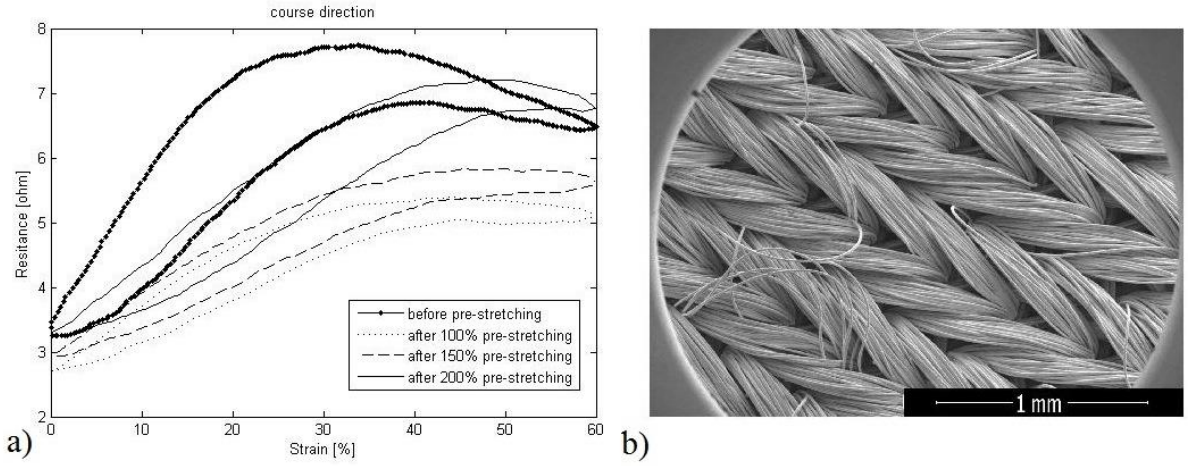

Figure 3.6 Pre-stretching: a) mean stretch-recovery cycle of five cycles performed before and after a single cycle of pre-stretching by 100%, 150% and 200%; b) SEM image of a sample that was pre-stretched with a single cycle of 200% strain.

3) Strain rate

The sensor possessed similar trends when strain velocity was increased from 60 *mm/min* to 200 *mm/min*, with marginal changes in resistance and hysteresis (Figure 3.7). The trend was also similar in the case of 50 *mm/min*, but resistance values remained slightly higher in the second part of the plot (on the right of Figure 3.7). This could be related to relaxation time (analysed in one of the following characterization tests); however, these results demonstrate that the sensor behaviour is practically independent from the deformation velocity. This result is important for the design since it means that the sensor can be used to track body movements at a wide range of velocities.

4) Sample dimensions

The sensor behaviour for different length-width ratios (*r*) is reported in Figure 3.8. Electrolycra's capacity for sensing appears to be slightly dependent on the ratio. Specifically, a higher ratio (r = 6) improves its performance in terms of a higher sensing range and a lower hysteresis.

5) Temporal stability

The results of tests performed over two months are presented in Figure 3.9. It can be observed that there was a slow decline in the sensor resistance range during this time.

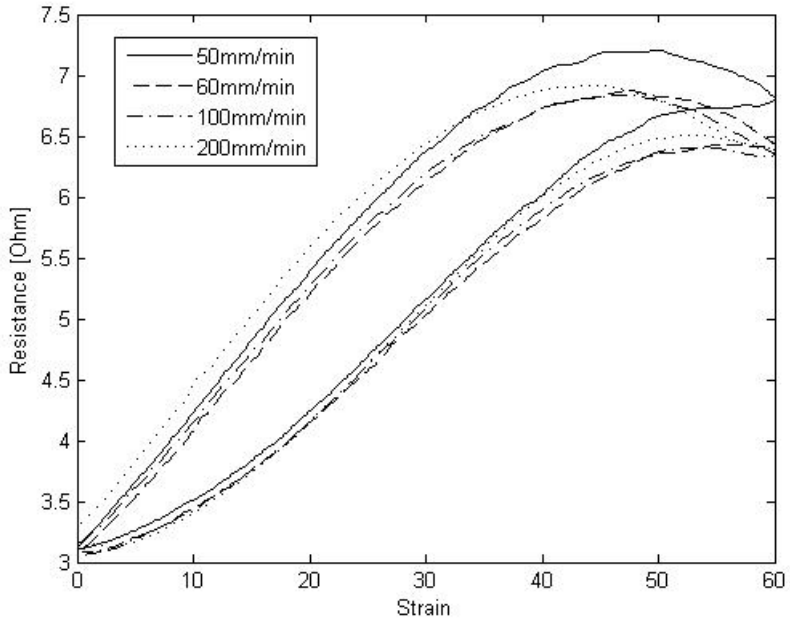

Figure 3.7 Sensor resistance at increasing strain rate (50, 60, 100, 200 *mm/min*), covering a typical motion speed range for the human body.

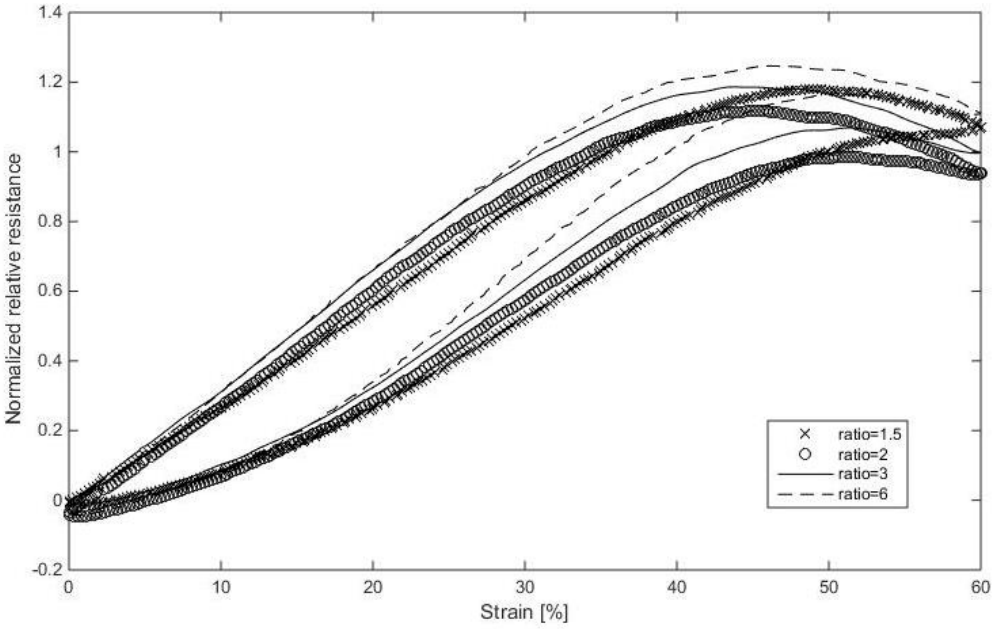

Figure 3.8 Dependency between different length-width ratios (*r*).

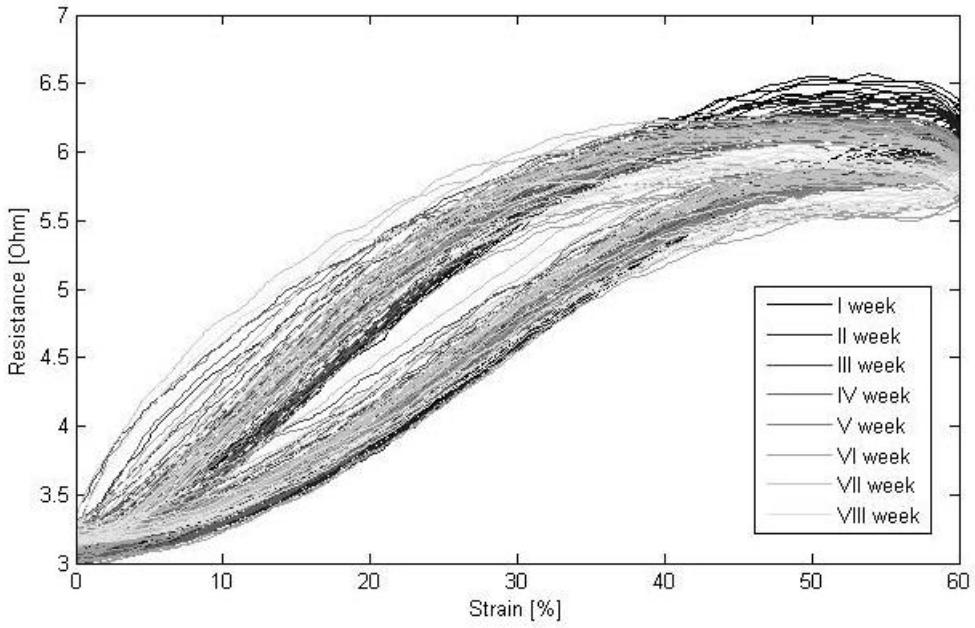

Figure 3.9 Long-term stability of the sensor over eight weeks.

6) Hysteresis

Hysteresis, typically caused by friction and structural change in materials, is crucial for the strain sensor due to its negative influence on sensor durability [180]. Typically, elastic materials have higher hysteresis because they require longer recovery time. Both tensile and electrical hysteresis were measured, the former for a strain-force curve (Figure 3.10 (a)) and the latter for a strain-resistance curve (Figure 3.10 (b)). The tensile hysteresis was calculated as in [125] and the mean hysteresis (see Figure 3.10 (a)) was approximately 17.8%. A resistance vs. strain plot (Figure 3.10 (b)) showed how to calculate the electrical hysteresis (see also equation 2.5) of the sensor and presented the maximal hysteresis error, 14.8% of the full-scale, at 28% strain. Piezoresistive hysteresis is known for a major drawbacks of resistance-type sensors, which makes the calibration of the materials for their use very difficult. Few studies were conducted to compensate piezoresistive hysteresis through structural modification or using mathematical modelling. However, in this first phase of Electrolycra characterization the hysteresis was only quantified and examined qualitatively. Whereas, a thorough study of the hysteresis compensation with a comparison between different mathematical models used will be dealt with in the next Chapter.

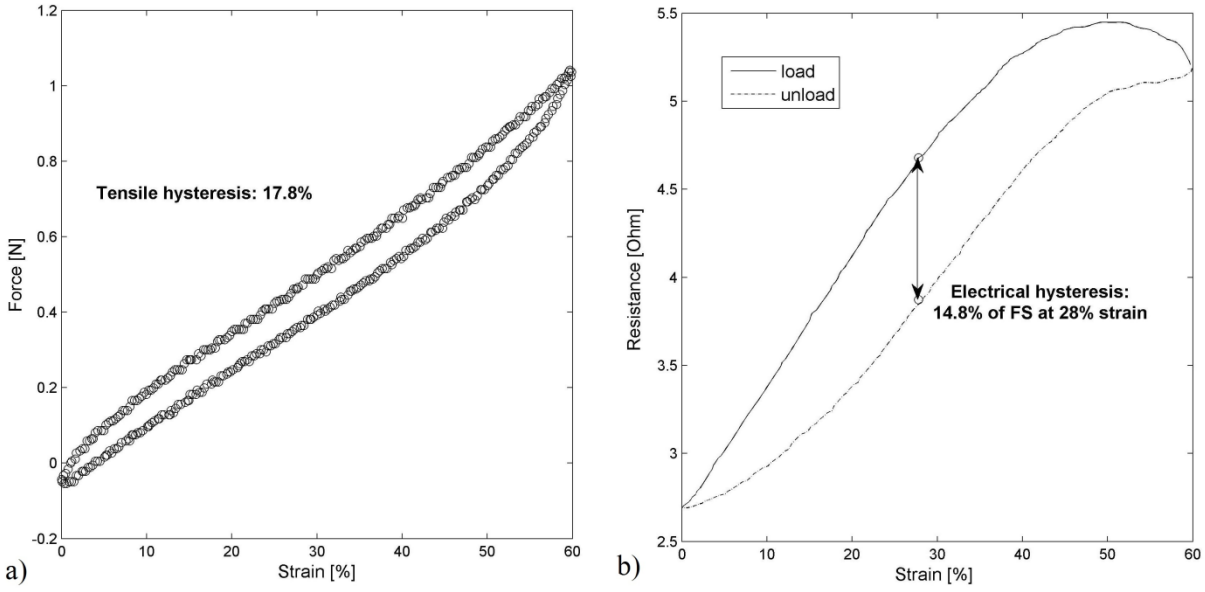

Figure 3.10 Hysteresis: (a) mechanical and (b) electrical.

7) Working range

The resistance-strain behaviour of the sensor was maximised at 50% strain and then, after a plateau, began to decrease for higher strain values (Figure 3.10 (b)). Consequently, Electrolycra's usable working range could be considered to be between 0 and 50% strain.

The relationship between resistance and deformation is due to the specific fabric structure. The electrical current must pass from one conductive yarn strand to another because of the warp knitted structure and the preferential direction along the courses. Consequently, the overall resistance is determined by the resistance of the yarn plus the contact resistance of the strand-to-strand contacts. When the fabric was subjected to stretching along the courses, as shown in Figure 3.1 (c), there is the transformation of yarn strands into loops. This transformation allows for the elongation of the fabric, resulting in an increase in resistance.

Meanwhile, stretching causes the contact resistance to change. According to Holm's contact theory [184], contact resistance is inversely proportional to the number of contact points and the contact pressure. As the load applied on the fabric increases, the yarn strands are more distant and the contact points lessen, but the contacting pressure on the overlapped yarn strands increases. Up to 50% fabric elongation, the overall resistance of the sensor therefore increased due to two factors: yarn strand elongation and the decrease of the number of contact points. After approximately 50% elongation, the overall resistance shows a plateau,

followed by a decrease. This behaviour could partly be explained by the increase in contact pressure. The contact pressure becomes more influential on the overall resistance, which decreases with the applied strain.

Comparing the resistance change without the pre-stretching along the courses direction (in Figure 3.5 (a) and Figure 3.6 (a)), and the resistance change after the pre-stretching, it is clear that the relationship between resistance and deformation, previously described, affects not only the material structure, but also the sensor behaviour. The textiles show less hysteresis, a larger working range and more linearity. Consequently, this characterization step will influence the sensor design in relation to the specific application.

8) Relaxation behaviour

Figure 3.11 reports resistance vs. time plots for increasing strain (20, 30, 40, 50%) reached at one of three different speeds (60, 200, 400 *mm/min*). After the target strain was reached, it was kept constant. The plots clearly show that the initial overshoot and the corresponding steady state increased with increasing speed.

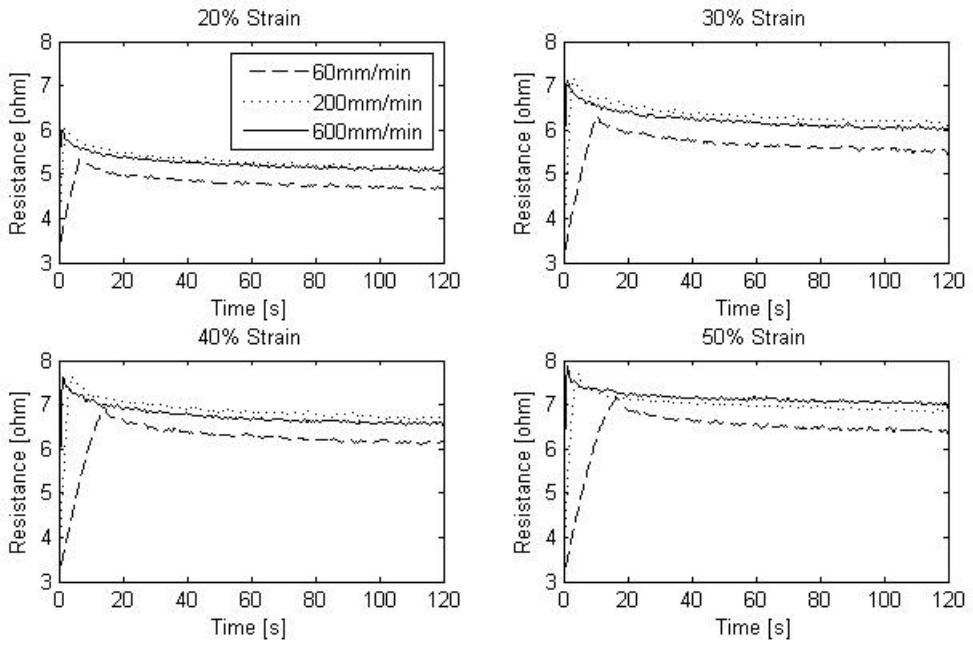

Figure 3.11 Relaxation behaviour of Electrolycra fabric at 20, 30, 40 and 50% strain applied at three speeds (60, 200, 600 *mm/min*), with waiting times of 2 *min*.

The total difference between the highest value during the overshoot and the lowest value after 120 *s* was lowest for 50% strain at 60 *mm/min* (0.82 *Ω*), where the long-term drift was

most dominant (0.58 Ω). In contrast, this difference was highest for 40% strain at 600 *mm/min* (1.15 Ω), where the overshoot was most dominant (0.75 Ω). In general, there was an increase in resistance with an increase in strain for all different speeds.

9) Curve fitting

Finally, the strain-resistance linear characteristic of the Electrolycra sensor was calculated (Figure 3.12). After 200% pre-stretching, eight stretch-recovery cycles within the sensor working range were performed and data were averaged. Resistance was expressed as a normalised relative resistance: $\frac{R-R_0}{R_0}$, where R_0 is the resistance at zero value strain. For each 5% of strain, the standard deviation was calculated (vertical bars in Figure 3.12); the maximum standard deviation value was 0.2, in correspondence with 30% strain. The results show that Electrolycra's normalised resistance was proportional to the strain during the tensile stretch-recovery cycles, in which the coefficient of determination (R^2) of the linear regression curve was 0.998. The linear characteristic of the Electrolycra shows a gauge factor ($GF = \frac{\Delta R}{\varepsilon R_0}$, where ΔR is the variation of the sensor resistance and ε is the applied strain) of about 2.56. The GF for metallic strain gauges is usually around 2. Conductive fabric strain sensors comparable to Electrolycra show a GF of 1.42, in linear range (7.6–26% of elongation) [111]. Considering that a high GF value is a positive factor for strain gauge realization, and Electrolycra GF is about 2.56 in linear range (up to 50% of deformation), this can be considered a further advantage of the proposed sensor.

The first phase of this work resulted in a characterization methodology based on nine steps. In general, this methodology can be adopted to characterise, design and calibrate a strain sensor to fulfil the application requirements.

The first evaluation steps are relevant to understand how the electrical properties of the material are related to the strain changes. The following three steps: i) preferential direction, ii) working range and iii) sample dimension offer important information about how to size the sensor. In particular, both the horizontal and vertical directions should be measured. In fact, as shown with Electrolycra, the material could present a preferential direction, meaning that the material presents a linear trend along this direction, and the working range must be measured. The sample dimension can be chosen in relation to the application and the working range;

however, a test is necessary to prove that the material's behaviour is independent from the sample dimensions.

The pre-stretching test, during the calibration phase, could improve the sensor properties, as it did with the Electrolycra. In such a case, it is necessary to find the percentage of pre-stretching that offers the most benefits in terms of linearity and repeatability, and without damaging the textile.

Once sized the sample, the following steps are relevant to evaluate time dependency: i) temporal stability, ii) relaxation behaviour, iii) hysteresis. These tests offer information about how to design the acquisition system. It is useful to know if the measurements are temporally stable and if they are affected by the stress relaxation of the textile material.

Finally, in relation to the specific application of the textile sensor, it is relevant to know how it behaves with a range of strain rates and to identify the best curve fitting of the electrical-strain relationship of the sensor.

The above reported role of each measured parameter has been used for the design of the wearable device for measuring joint angle and our resulting choices are summarized in Table 3.1.

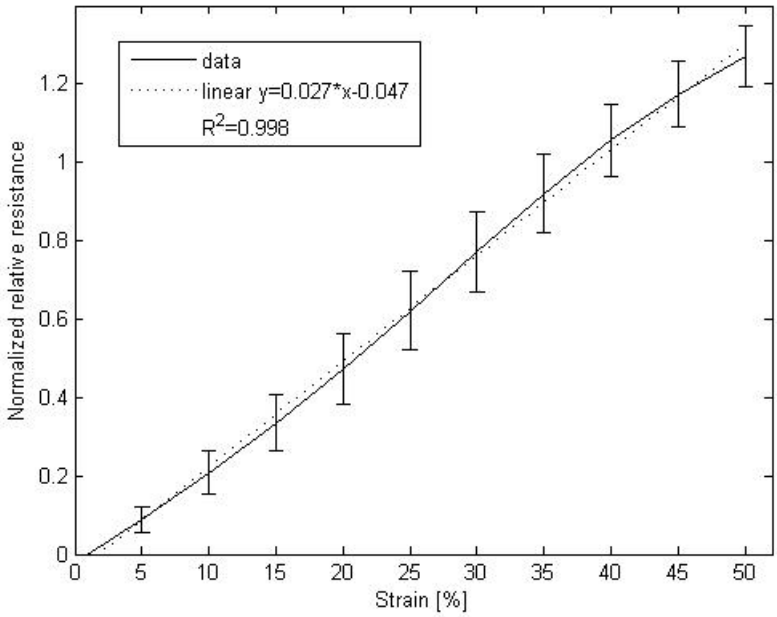

Figure 3.12 The normalised relative resistance-strain relationship of Electrolycra. Data were averaged from eight stretch-recovery cycles measured within the sensor working range.

Table 3.1 Design choices for the wearable device deriving from the characterization procedure performed on Electrolycra.

Parameter	Role in the design	Choice for the wearable device
Preferential direction	-Different behaviour -Not completely reliable tests	Deformation along CD for the higher resistance change (after evaluating pre-stretching performances)
Pre-stretching	-100%: low resistance change, medium linearity, low hysteresis -150%: medium resistance change, medium linearity, low hysteresis -200%: high resistance change, low linearity, medium	200% was selected to maximize the sensitivity of the sensor
Strain rate	Almost independent in the relevant velocity range	No choice needed
Sample dimension	Slightly dependent on length-width ratio	Ratio set to 6 for maximizing sensing range and minimizing hysteresis
Temporal stability	Slow decline of performances	No choice needed
Hysteresis	Evaluated for possible compensation	No choice needed
Working range	The resistance-strain curve has a plateau and then a decrease after 50% of deformation	Working range set to: 0-50% Sensor dimension set to: 2 *cm* width x 12 *cm* length
Relaxation behaviour	Stability evaluated	No choice needed
Curve fitting	Simple modelling: easy to implement, low accuracy Complex modelling: difficult to implement, high accuracy	Linear model fitting experimental data is enough reliable to describe the dynamics of the movement

3.4.2 Device performance

Experimental tests conducted with the adult volunteer qualitatively proved the usability of the developed device as a wearable goniometer. The device resulted easy to wear and comfortable during motion, without affecting the natural motion of the elbow joint.

3. Textile-based strain sensor

The device realised for the SABIAN's knee joint was customised starting from the known geometrical features of the robot and calculating the linear characteristic of the Electrolycra sensor to find coefficients *a* and *b* of equation (3.2).

Data acquired from our fabric-based sensor and from the SABIAN encoder during the flexion/extension tasks are shown in Figure 3.13. The root-mean-square error (RMSE) was 8.9°. This error is not negligible, and therefore it is important to briefly discuss its causes. The linear fitting is an approximation of the sensor behaviour and does not take into account the hysteresis. In particular, the results presented in Figure 3.13 show an overestimation of the higher angle values and an underestimation of the lower angle values. The acceptability of this RMSE is related to the intended application. If the priority is to acquire more accurate angle measurements, another curve fitting or a different modelling technique should be applied that accounts for the hysteresis error. The drawbacks in such a case would be a more complicated model and the higher computational cost required.

Another limit to this process was due to the approximation of the SABIAN knee joint radius *r*, which, unlike the human joint, was not easy to quantify. In addition, some errors may also come from the wearable sleeve sliding on the skin. Any skin-mounted sensor will likely suffer from soft-tissue artefacts, however, even without sliding error.

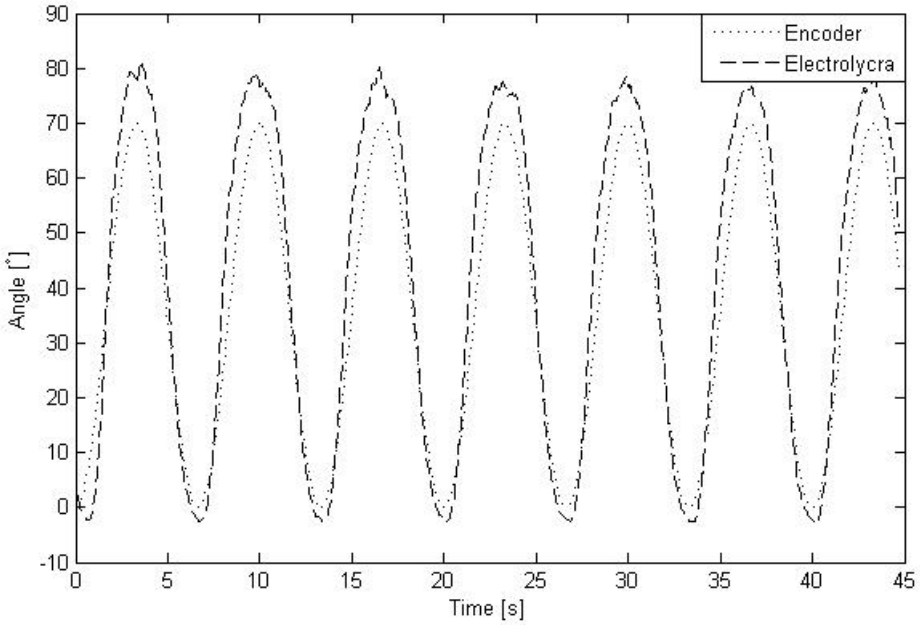

Figure 3.13 The plot shows 2 *min* of the SABIAN knee flexion/extension, both the encoder output and the wearable goniometer output.

3. Textile-based strain sensor

Considering the first results presented in this Chapter, it is possible to confirm that the introduction of a general approach can be used for the assessment of the electro-mechanical properties of a piezoresistive conductive textile, applied as a stretch sensor. This approach is easy to follow and could be employed for other textile strain sensors for their design, characterization and optimization (e.g. the pre-stretching that increases accuracy and repeatability). The second results shown that the developed wearable goniometer possesses the necessary wearability and sensing capabilities for long-term monitoring, following the "wear and forget" concept. Indeed, even though the RMSE is not negligible, the sensor signal still provides sufficient motion measurement capabilities that could be useful for specific applications. The developed device is an example of the application of Electrolycra to monitor human joint movements, which shows the potential of this sensor to be used as a wearable sensor without being stressful for the wearer.

Next Chapters focus on the improvement of the sensor performance (in particular rate-dependent hysteresis) and on the development of a new wearable sensing device whose application could be extended to different scenarios, as tracking neck movements.

Chapter 4

Model-based compensation of rate-dependent hysteresis in a textile-based strain sensor

4.1 Introduction

This Chapter is concerned with modelling of conductive textiles, aimed at compensating their intrinsic nonlinearities. In particular, a new model is proposed to compensate for hysteresis and relaxation in strain sensors made of Electrolycra. These sensors have interesting potential uses, but they present remarkable electro-mechanical hysteresis.

Piezoresistive hysteresis is known for a major drawbacks of resistance-type sensors. Depending on the magnitude of the effect, it makes the calibration of the materials for their use very difficult, limiting severely the applicability of these materials as sensors. A system with hysteresis is defined as a system whose output does not only depend on the current input but also on the history of the input. Friction force and structural changes in the material are regarded as the main causes of this undesirable behaviour [185].

Some approaches have been introduced to reduce the impacts of these factors through structural modification [186] or by varying the production parameters applied to specific designs [187]. However, the correction of nonlinear hysteresis using mathematical modelling is unavoidable to improve the stretch sensing accuracy. Few studies were conducted to compensate piezoresistive hysteresis. For strain sensing application, a hysteresis compensator based on a modified dynamic Preisach model was applied on a strain sensor made of conductive polymer nanocomposites [188]. This model could compensate for both the static effect and the relaxation and input-rate dependence of conductive polymers. In [189] a modified Prandtl-Ishilinskii (MPI) model was adopted to compensate for piezoresistive hysteresis of the nanocomposite for skin-mountable stretch sensing. The MPI model

formulates rate-independent and monotonic hysteresis behaviour. This means this model can compensate velocity independent and monotonic piezoresistive characteristics of the nanocomposite. However, these studies presented limited results in terms of performance and generalizability.

This Chapter present a thorough experimental investigation probing the electromechanical response of the Electrolycra subjected to cyclic loading and propose a new model to compensate for its intrinsic nonlinearities, thus improving its sensing accuracy and paving the way to precise strain measurement in soft highly stretchable sensors. The new model was developed in collaboration with the University of Genoa (Department of Naval, Electric, Electronic and Telecommunications Engineering), and it is a variant of a power-law (PL) model recently proposed [190] to reproduce hysteresis and creep (another rate-dependent phenomenon) in piezoelectric actuators (PEAs), which are largely used for micro- and nano-positioning applications [191][192]. In this work the PL model is properly modified in order to compensate for the rate-dependent hysteresis of the conductive textile. The model can be exploited to accurately estimate the strain of the textile, given the measurement of its electrical resistance and is valid at different strain rates. The model parameters are identified on a set of experimental data and its accuracy is validated on a different set. In addition, the model is also validated by using experimental data sets foreseen the use of the elbow joint of the iCub robot. Comparisons with the well-known MPI model and an algebraic model that relates strain and resistance through a third-order polynomial are also provided, to benchmark the performances of the proposed model.

4.2 Experimental setup

After a thorough characterization of the electro-mechanical properties of the Electrolycra presented in the previous Chapter, here we focus our attention on the compensation of its hysteresis.

Electrolycra looks and feels like ordinary lycra but it is highly conductive because it is weaved with silver plated 76% nylon 24% elastic fibers [125]. Its conductivity depends on how tightly it is stretched; if it is stretched, its resistance R increases. In particular, we are interested in the relationship between strain $S = 100\frac{L-L_0}{L_0}\%$ and resistance R, where L is the current sample length, whereas L_0 is the sample resting length.

As demonstrated in the previous Chapter, Electrolycra can be stretched beyond its initial length, with better performances after pre-stretching of 200% [193]. Moreover, this material has a preferential direction along which resistance significantly changes and a major strain is possible, with a working range of strain *S* from 0% to 50%.

Additional tests were performed for the present work to better understand Electrolycra electromechanical behaviour and to validate the developed model with new experimental datasets. The electromechanical tests were performed at room temperature by using the Instron material testing machine (model 4464, Instron Inc., Norwood, MA), with the same setup adopted during the characterization phase and presented previously.

Due to material preferential direction [125][193], uniaxial cyclic strain tests have been conducted along this direction on a specimen 20 *mm* wide and with length L_0 = 100 *mm* along the preferential direction. The dimensions of the specimen were chosen arbitrarily, as the sensor behaviour depends only slightly on the length-width ratio [193].

4.3 Experimental protocol

13 datasets of applied strain *S* and corresponding resistance *R* were collected, belonging to three different classes:

- **Different strain patterns** (datasets SP1, SP2 and SP3): three strain profiles composed of pieces of triangular waves with 5 periods each (see Figure 4.1). The sample is stretched at a constant rate of 50 *mm/min*. In SP1 each piece is characterized by a different offset (10%, 20%, 20% and 30%) and amplitude (20%, 20%, 30% and 20%); in SP2 the offset is constant (10%) and only the amplitude changes (10%, 20%, 30% and 40%); in SP3 the amplitude is constant (20%) and the offset changes (10%, 20% and 30%).
- **Different strain rate** (datasets from SR1 to SR9): nine strain profiles composed of triangular waves. For each dataset, the sample is stretched at a different rate, from 20 *mm/min* (SR1) to 100 *mm/min* (SR9), with an increasing step of 10 *mm/min*. Figure 4.2 shows the time evolution of strain and resistance (left panels) and the relationship between *S* and *R* (right panel) for datasets SR1 and SR9. The other datasets, not shown to improve the visibility of the graph, are distributed among the

curves of datasets SR1 and SR9. Notice that this relationship is hysteretic and, as the strain rate increases, the loop rotates counterclockwise around its low-left corner. Moreover, each loop is traveled clockwise, as marked by the arrows in Figure 4.2. These datasets allow to evaluate the influence of the strain rate on the sensor characteristics.

- **Relaxation behaviour** (dataset RB1): in this case the sample was stretched at a speed of 1000 *mm/min*, and held at increasing values of strain (10%, 20%, 30%, 40%, and 50%) for 30 *sec* (see Figure 4.3). Notice the temporal decrease (relaxation) of the resistance in response to a constant strain applied to the sensor. This effect is particularly visible when the textile is stretched (black ellipse), whereas it is negligible when the textile is relaxed (gray ellipse).

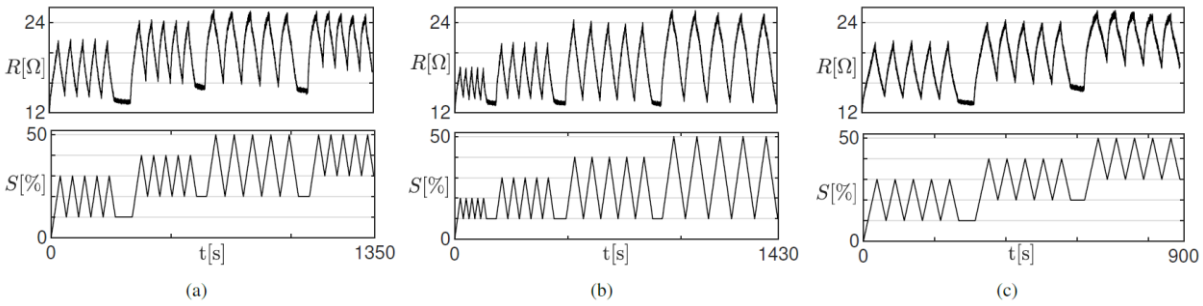

Figure 4.1 Measurements of applied strain (bottom panels) and corresponding resistance (top panels) as a function of time, for datasets SP1 (a), SP2 (b) and SP3 (c).

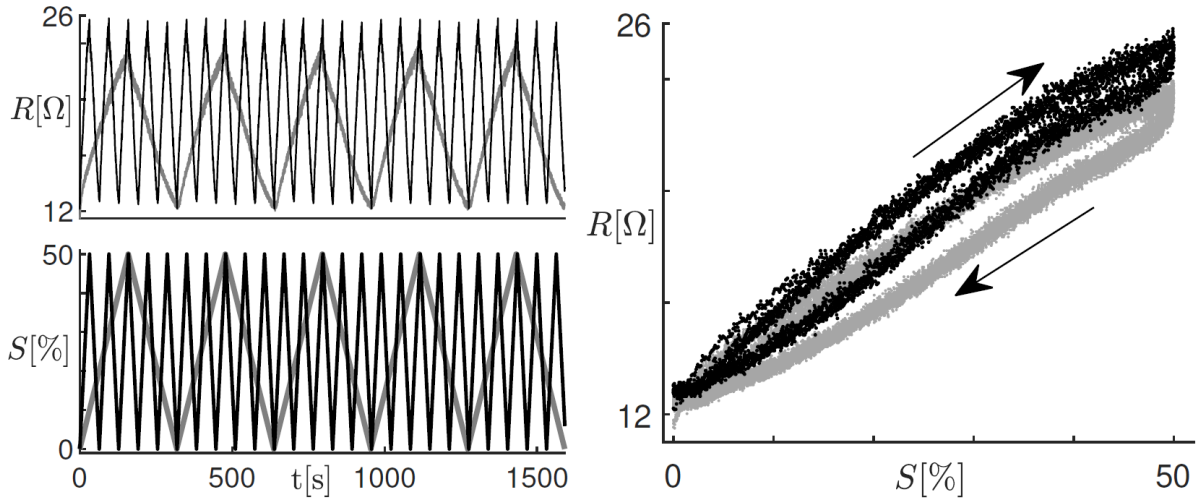

Figure 4.2 Measurements of applied strain (left bottom panel) and corresponding resistance (left top panel) as a function of time for datasets SR1 (gray curves) and SR9 (black curves). The right panel shows the same measurements in the (*S*;*R*) plane.

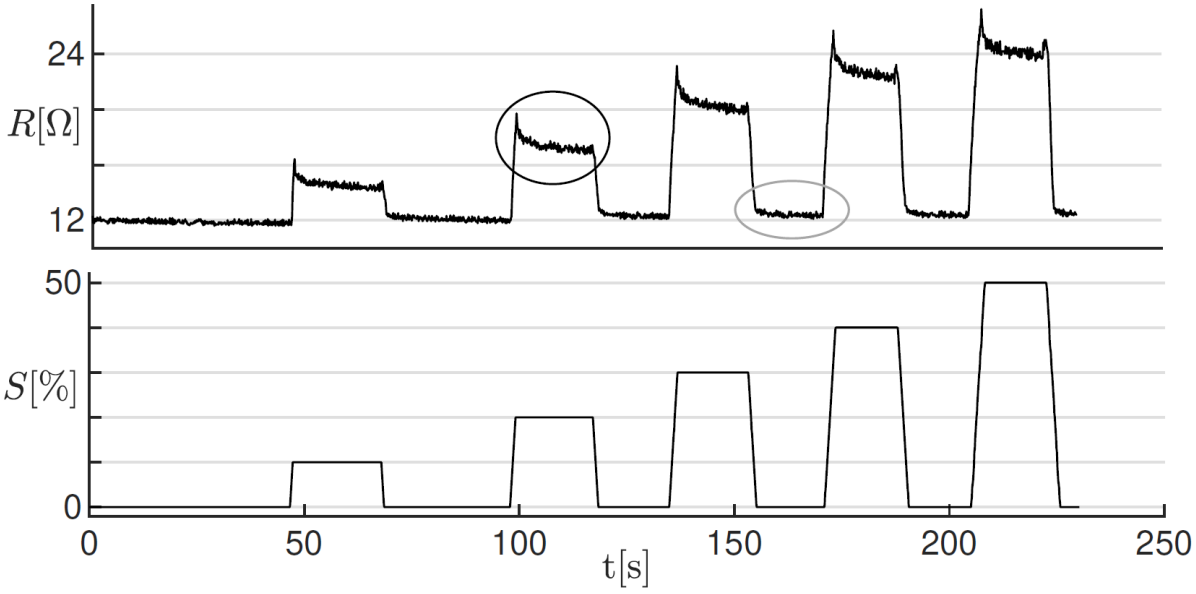

Figure 4.3 Measurements of applied strain (bottom panel) and corresponding resistance (top panel) as a function of time for datasets RB1. Notice (see the black ellipse) the relaxing behaviour of the resistance in response to a constant strain, when the textile is stretched.

4.4 Hysteresis model

In order to accurately employ the Electrolycra as a strain sensor, S must be estimated based on the measurement of the resistance R. An inverse model (simply referred to as model, in the following) able to reproduce both the hysteresis characteristic and the relaxation dynamics, is therefore necessary, which takes in input the measured resistance R and provides an estimation $\hat{S}$ of the corresponding strain S. To estimate the strain, the model must be connected in cascade to the sensor, as shown in Figure 4.4.

The model must be able to compensate for the typical nonlinear behaviours of Electrolycra:

1) the relationship between Electrolycra input S and output R is hysteretic, and the hysteresis loop is traveled clockwise;
2) the hysteresis loop rotates counterclockwise around its lower-left corner as the strain rate increases;
3) in the presence of a constant strain, Electrolycra resistance slowly drifts (relaxing dynamics);
4) the relaxation is negligible for up-down strain steps.

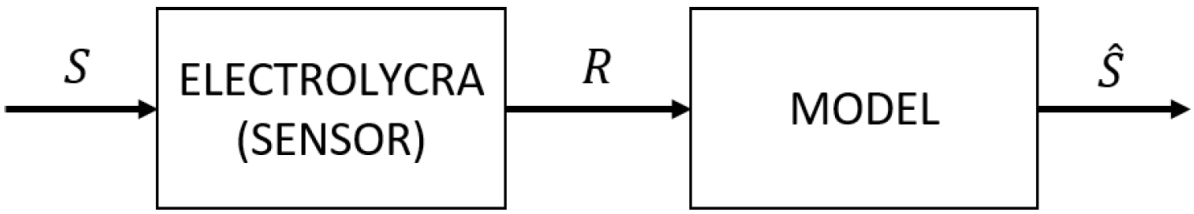

Figure 4.4 Block scheme showing how to connect the model to the Electrolycra in order to estimate the strain *S* based on the measurement of the resistance *R*.

This section describes a new model developed in collaboration with the University of Genoa (Department of Naval, Electric, Electronic and Telecommunications Engineering), henceforth called asymmetric power-law model (APL), able to compensate for these behaviours. The normalized version of model input R and output $\hat{S}$ are $\xi = R/R_0 + \alpha$ and $\psi = \hat{S}/S_0 + \beta$, respectively, being ξ and ψ dimensionless quantities in the range [-1, 1].

The model is composed of a set of N elementary hysteretic cells each one characterized by a state variable x_k whose dynamics is defined through the implicit formulation $h_k(x_k, \dot{x}_k, t) = 0$, $k = 1, \ldots, N$. Functions h_k are defined as follows:

$$h_k(x_k, \dot{x}_k, t) = \begin{cases} \dot{x}_k - \sigma\left(\frac{\xi(t) - x_k(t) + 1}{\rho_k + 1}\right) if\ -1 \le \xi(t) - x_k \le \rho_k \\ x_k - \xi(t) - 1\ if\ \dot{x}_k \le 0 \\ x_k - \xi(t) + \rho_k\ if\ \dot{x}_k \ge \sigma \end{cases} \quad (4.1)$$

where $\rho_k = \frac{2k}{N+1} - 1$ (k = 1, …, N) are thresholds equally spaced in the range (-1, 1).

The corresponding nonlinear vector field is shown in Figure 4.5 (left panel), and its shape is determined by parameters $\sigma > 0$ and $p > 0$.

The model output ψ is computed as:

$$\psi(t) = f^{-1}(\omega_0 \xi + \sum_{k=1}^{N} \omega_k x_k + \omega_{N+1}) \quad (4.2)$$

where f is assumed to be a strictly-increasing piecewise-affine (PWA) function, defined as a weighted sum of an odd number M of PWA basis-functions ϕ_j(j = 1, …, M) [190]:

$$f(\psi) = \sum_{j=1}^{M} \mu_j \phi_j(\psi) \quad (4.3)$$

Coefficients ω_k (k = 0, …, N+1) and μ_j (j = 1, …, M) are obtained by solving a quadratic programming problem based on experimental measurements of model inputs and outputs.

By applying a high-frequency triangular input ξ, the relationship between the state x_k of the k-th APL cell and the input ξ is the trapezoidal hysteresis loop shown in black in Figure 4.5 (right panel). As the rate of the input increases, the loops are hinged at the lower-left corner. By summing states x_k as in equation (4.2), it results (see Figure 4.6, left panel) that the hysteresis loop between the model output ψ and ξ is traveled counterclockwise (see arrows) and rotates clockwise around its lower-left corner as input rate increases. This allows to compensate for the Electrolycra's nonlinearities. The right panels in Figure 4.6 show instead the response (bottom panel) of the model to a stepwise input (top panel). Notice that the relaxation dynamics is exhibited only for increasing input steps.

Model parameters are N, M, σ, p, ω_k, and μ_j and can be optimized with a procedure completely similar, *mutatis mutandis*, to the one proposed in [194] for the model of piezoelectric materials.

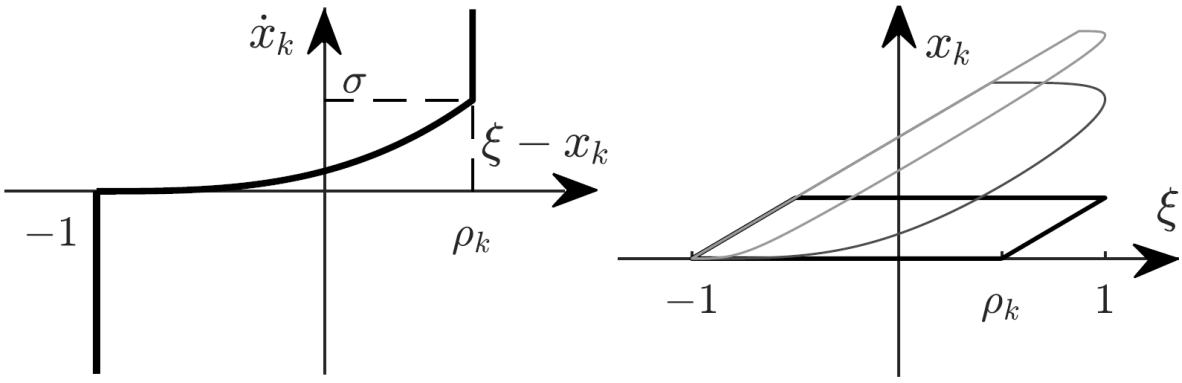

Figure 4.5 Vector field (left panel) and hysteresis loops at different input rates (right panel) of the *k*-th cell of the APL model. In the left panel, curve colors become darker as the input rate increases.

4.5 Tests on iCub

Preliminary tests (reported in the previous Chapter) were performed to assess the usability of the conductive textile as wearable goniometer and its capability to track the elbow joint movement during cyclic flexion/extension tasks. For model validation, Electrolycra strain sensor was applied to a robot iCub (Figure 4.7) to estimate elbow angle rotation. Because the sensor attached to the robot changes its length following elbow angle rotation, the change in

resistance measured by the sensor can be used to estimate the rotation angle. In this process, hysteresis behaviour of resistance change was compensated by the APL model, and MPI and polynomial curve fitting models for comparison.

The iCub is a 53 degree-of-freedom (dof) humanoid robot of the same size as a three or four year-old child. The total number of dof for the upper body was set to 38 (seven for each arm, nine for each hand and six for the head) [195]. The elbow is driven by Kollmorgen medium-power motor (20 Nm) occupying almost the entirety of the upper arm link, and it is equipped with relative position sensing (Hall effect sensors integrated within the motors) and miniature 12-bit absolute magnetic encoders (AS5045; Austria Microsystems) [196]. The iCub is an open systems platform: researchers can use it and customize it freely since both hardware and software are licensed under the GNU General Public Licence (GPL). For the tests, flexion/extension cycles were performed by rotating the elbow joint with aperiodic movements that simulate the natural human elbow movements. Electrolycra was applied in correspondence with the robot joint (Figure 4.7 (b)) and the change in resistance was measured using the same acquisition circuit adopted during the tests on Instron. Sensor resistance variation and the encoder data were collected simultaneously, and all data were synchronised and analysed using a custom MATLAB® code. The change in resistance of the stretch sensor was converted to the flexion angle using the APL model. The parameters of the APL model were estimated using reference data obtained from the encoder.

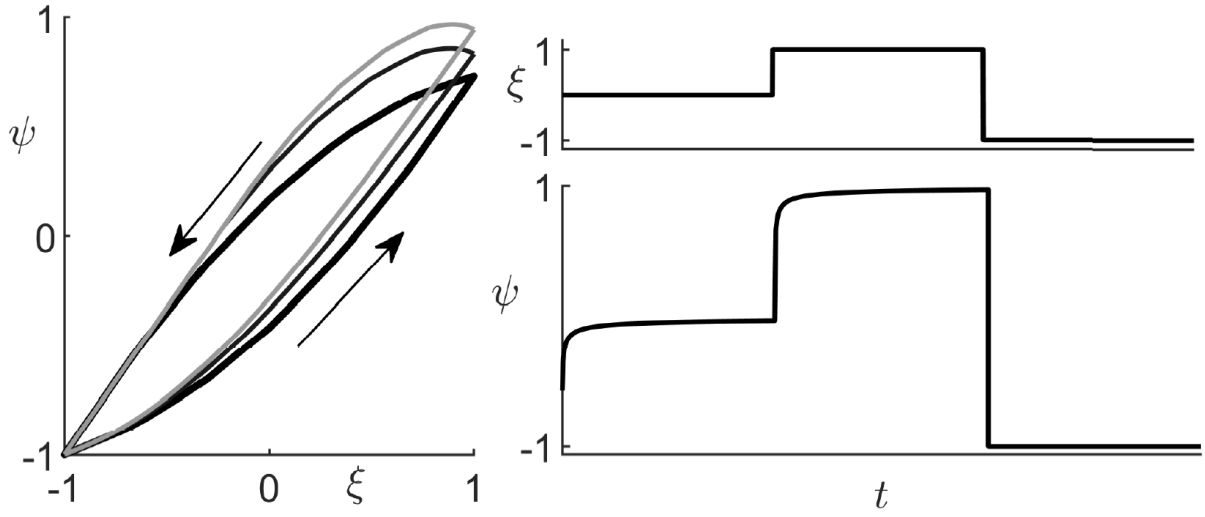

Figure 4.6 Left panel: hysteresis loops ψ vs ξ. Curve colors become darker as the input rate increases. Right panels: applied input (top) and APL model output (bottom).

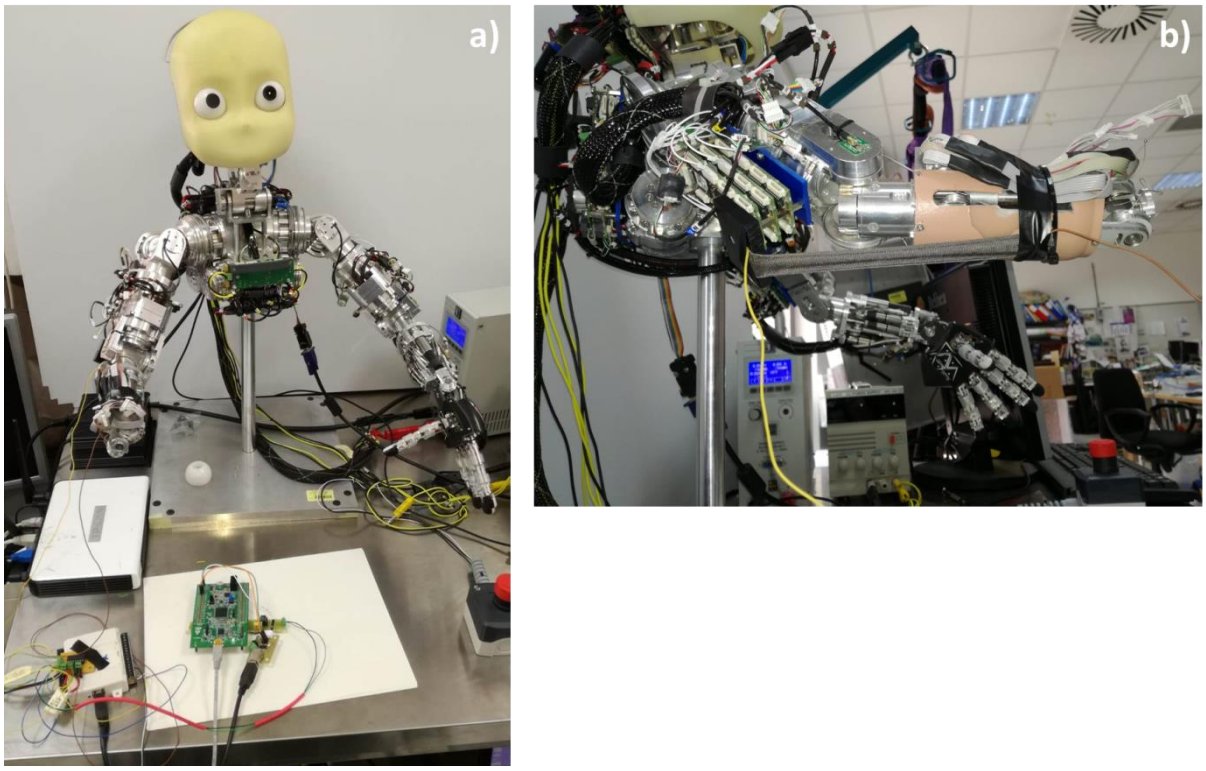

Figure 4.7 Validation tests using the humanoid robot iCub: a) experimental setup; b) Electrolycra fixed in correspondence with the elbow joint.

4.6 Results and discussions

The APL model was added to the MATLAB toolbox HystTool [197], which automatically fits its parameters to experimental data. We chose to use as training set the datasets SP1, SR1, SR4, SR7, SR9, whereas the other sets are used for validation purposes. The model inputs ξ and outputs ψ have been obtained by normalizing the values of R and S contained in the training set, with R_0 = 7.16 Ω, α = -2.61, S_0 = 25% and β = -1. Through HysTool we set N = 11 and M = 9 (a further increase of their values does not decreases significantly the estimation error), σ = 2.15 * 10^{-2} and p = 0.73. The other fitting parameters (obtained by solving a quadratic problem) are listed in Table 4.1 (left columns).

HysTool has been also used to fit the MPI model (already implemented in the tool), in order to perform a comparison with the solution adopted in [189]. The MPI model relies on the same parameters of the APL model, with the exception of σ and p. By setting a priori N = 11 and M = 9, the resulting optimal parameters are listed in Table 4.1 (right columns).

Table 4.1 APL and MPI model parameters.

	APL model		MPI model	
k, j	ω_k ($\times 10^{-6}$)	μ_j ($\times 10^{5}$)	ω_k ($\times 10^{-6}$)	μ_j ($\times 10^{5}$)
0	2.523		1.483	
1	0.843	0.412	0.510	0.518
2	1.522	0.014	0.808	-0.143
3	0.522	0.092	0.337	0.295
4	0.513	0.190	0.220	0.506
5	0.002	1.405	0.233	2.516
6	0.022	0.293	0.102	0.692
7	0.041	0.056	0.070	0.131
8	0.106	0.716	0.043	0.841
9	0.276	-0.160	0.038	-0.367
10	0.457		0.068	
11	0.695		0.070	
12	3.827		0.026	

A third model (used as benchmark also in [189]) has been considered, which simply expresses the strain as a cubic (CU) function of the resistance, by neglecting the hysteresis:

$$S = c_3 R^3 + c_2 R^2 + c_1 R + c_0 \tag{4.4}$$

Coefficients c_0, …, c_3 are obtained through least squares optimization on the considered data, leading to c_0 = -69.5, c_1 = 7.816 Ω^{-1}; c_2 = -0.2112 Ω^{-2} and c_3 = 0.003512 Ω^{-3}.

Figure 4.8 shows the root mean square error (RMSE) obtained with the APL, MPI and CU models on all the 13 available datasets, being t_k (k = 1, …, K) the sampling times. The RMSE is defined as:

$$RMSE = \sqrt{\frac{1}{K}\sum_{k=1}^{K}(\hat{S}(t_k) - S(t_k))^2} \tag{4.5}$$

As expected, the CU model leads to larger errors, since it does not represent hysteresis, whereas the APL model outperforms in most cases the MPI model, as it is able to reproduce

rate-dependent effects. In the following sections, more detailed results are shown for each class of datasets.

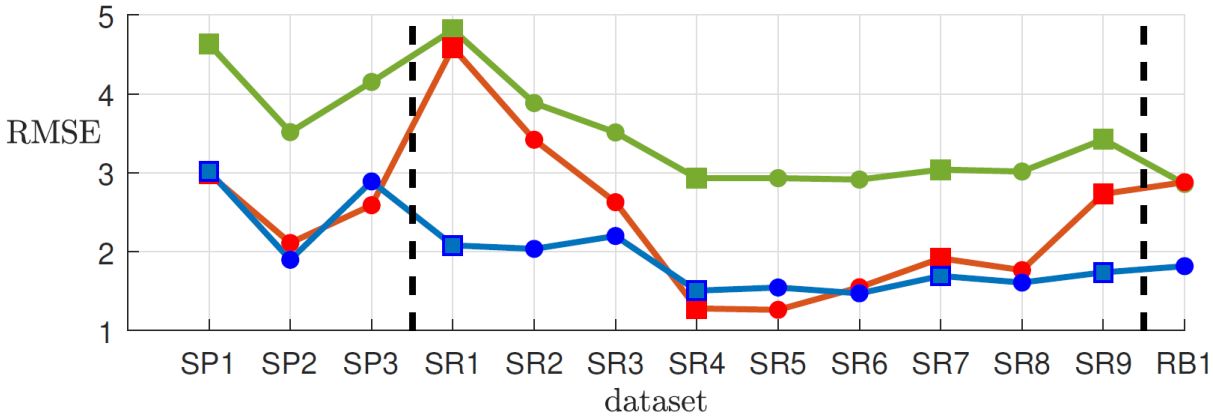

Figure 4.8 RMSE obtained on all the 13 datasets employing APL model (blue curve), MPI model (red curve) and CU model (green curve). Squares mark the datasets used also to train the models.

4.6.1 Different strain patterns

On datasets SP1, SP2 and SP3 the performances of the APL and MPI models are comparable. Indeed, in these datasets the strain rate is constant, and therefore also the MPI model (which only models rate-independent hysteresis) is accurate. The absolute error $e(t) = |S(t) - \hat{S}(t)|$ as a function of time on datasets SP2 and SP3 (not used to train the model) is shown in Figure 4.9, confirming that the accuracies of APL and MPI models are comparable and higher with respect to the CU model.

4.6.2 Different strain rate

The APL model, instead, outperforms the MPI model on datasets SR1-SR9, since the MPI model is not able to reproduce the rotation of the hysteresis loops as the strain rate increases. This is clearly visible in Figure 4.10, which shows the time evolution of the measured and estimated strains (one period) for datasets SR2 (left) and SR9 (right). The bottom panels show the corresponding absolute errors. It can be noticed that the APL model is the only one able to correctly estimate the strain at both low and high rate with an error always lower than 4%, as it reproduces the loop rotation, as visible in Figure 4.11.

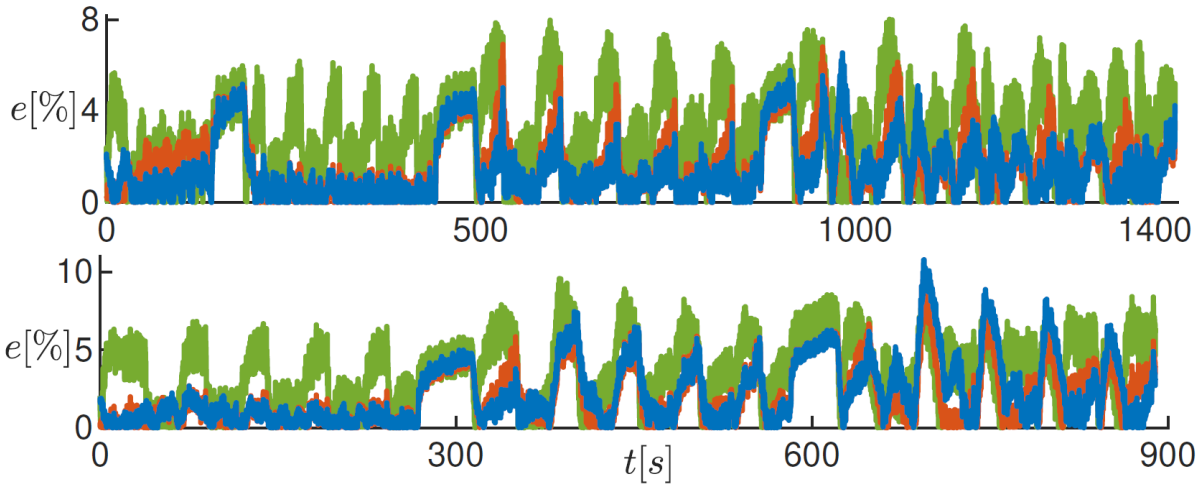

Figure 4.9 Time evolution of e(t) = |S(t) - Ŝ(t)| for dataset SP2 (top panel) and SP3 (bottom panel) with APL (blue), MPI (orange) and CU (green) model.

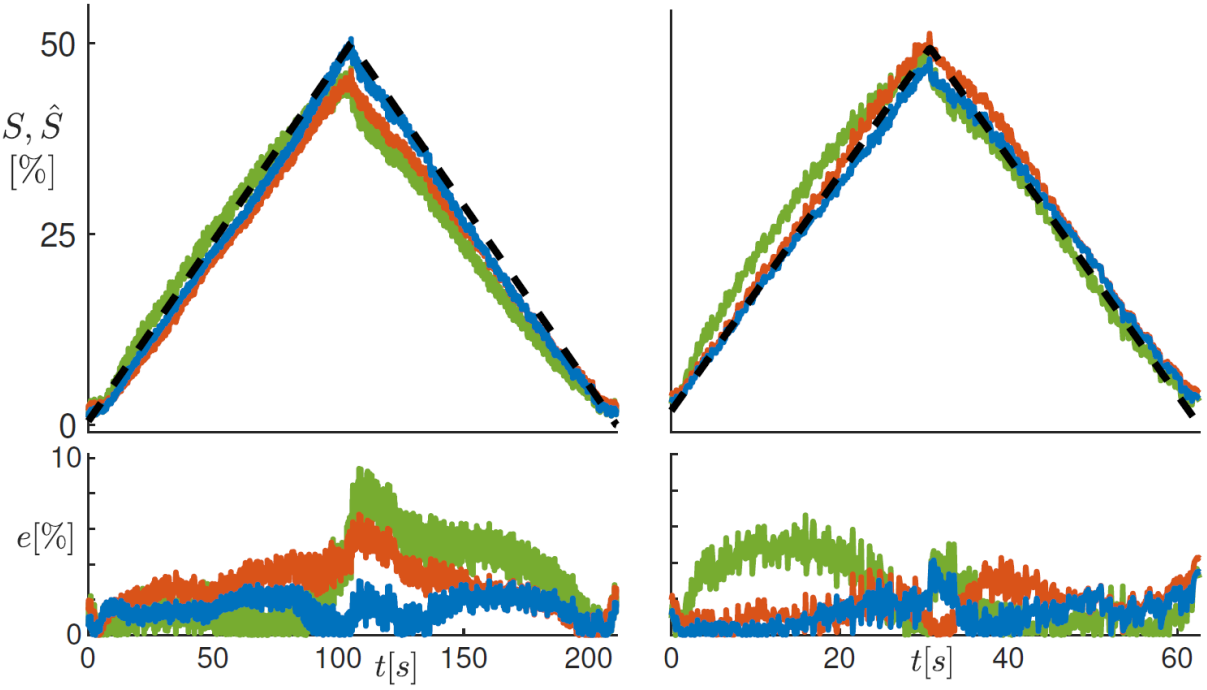

Figure 4.10 Measured (black dashed curves) and estimated (color curves) strain *S* for datasets SR2 (top left panel) and SR9 (top right panel). The bottom panels show the corresponding absolute errors. Blue curves: APL model; orange curves: MPI model; green curves: CU model.

The ideal characteristic of the compensated sensor shown in Figure 4.4 should be $\hat{S} = S$. Figure 4.12 shows the characteristics obtained with the CU (left), MPI (center) and APL (right) models on datasets SR1, …, SR4. If the CU model is used, hysteresis is not compensated, as demonstrated by the loops in the (S, $\hat{S}$) plane. With the MPI model, the loop

areas are greatly reduced, however the characteristics deviate from the ideal one (black dashed line) as the input rate decreases. On the contrary, by exploiting the APL model, hysteresis is well compensated and the characteristics remain close to the ideal one for all the considered input rates.

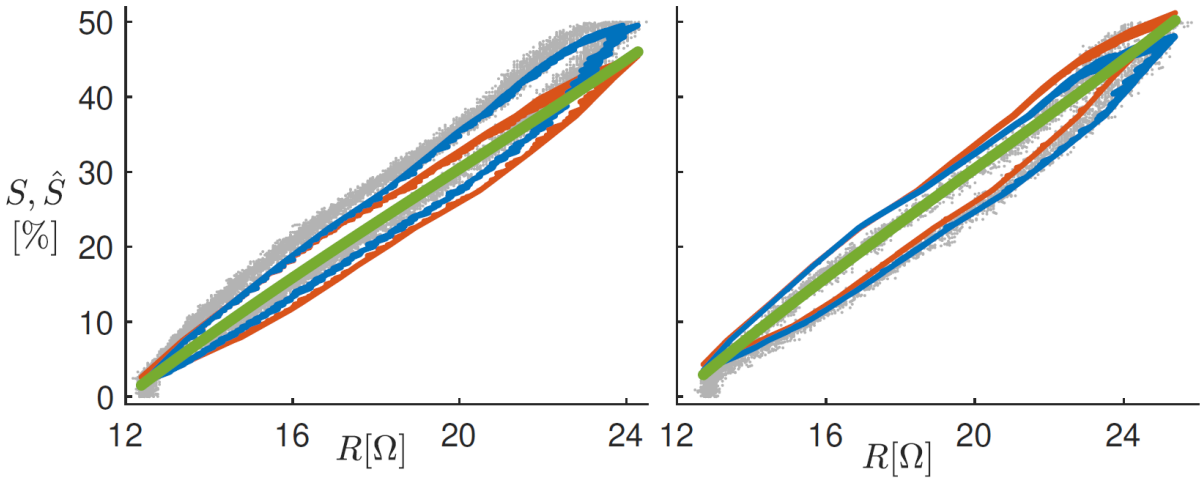

Figure 4.11 Measured (gray points) and estimated (colored curves) strain *S* vs. resistance *R* for the lowest (SR1 – left panel) and the highest (SR9 – right panel) strain rates. Blue curve: APL model; orange curve: MPI model; green curve: CU model.

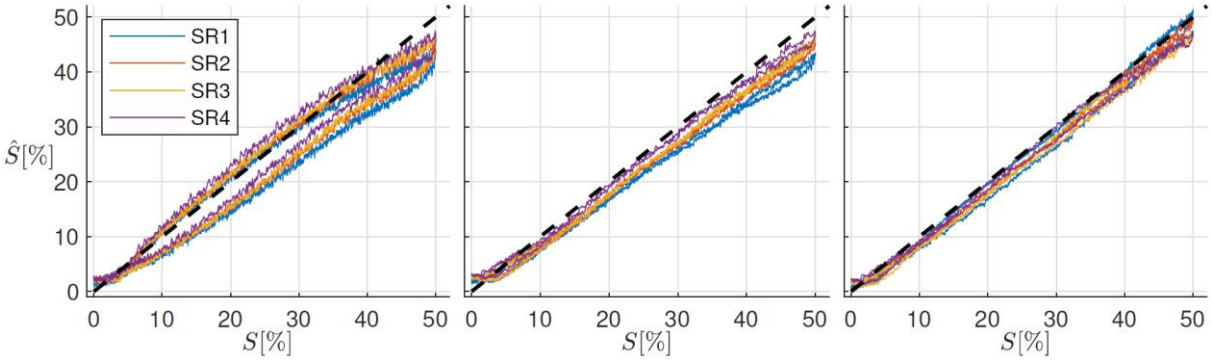

Figure 4.12 Estimated strain $\hat{S}$ with CU (left panel), MPI (middle panel) and APL (right panel) model as a function of the measured strain *S*. The black dashed line represents the ideal characteristic $\hat{S} = S$.

4.6.3 Relaxation behaviour

For dataset RB1, the lowest error is achieved with the APL model because it is the only one able to reproduce the relaxation dynamics. This is also visible in Figure 4.13 (see in

particular the inset), where the APL model estimates an almost constant strain in response to a time decreasing resistance, meaning that the relaxation dynamics is at least partially compensated. In other steps the compensation is worse, especially in the first part of the steps, but anyway it is better than those obtained with the other considered models. It is also important to remark that this dataset has not been used to identify the model parameters; this test is therefore a further proof of the generalization capability of the model.

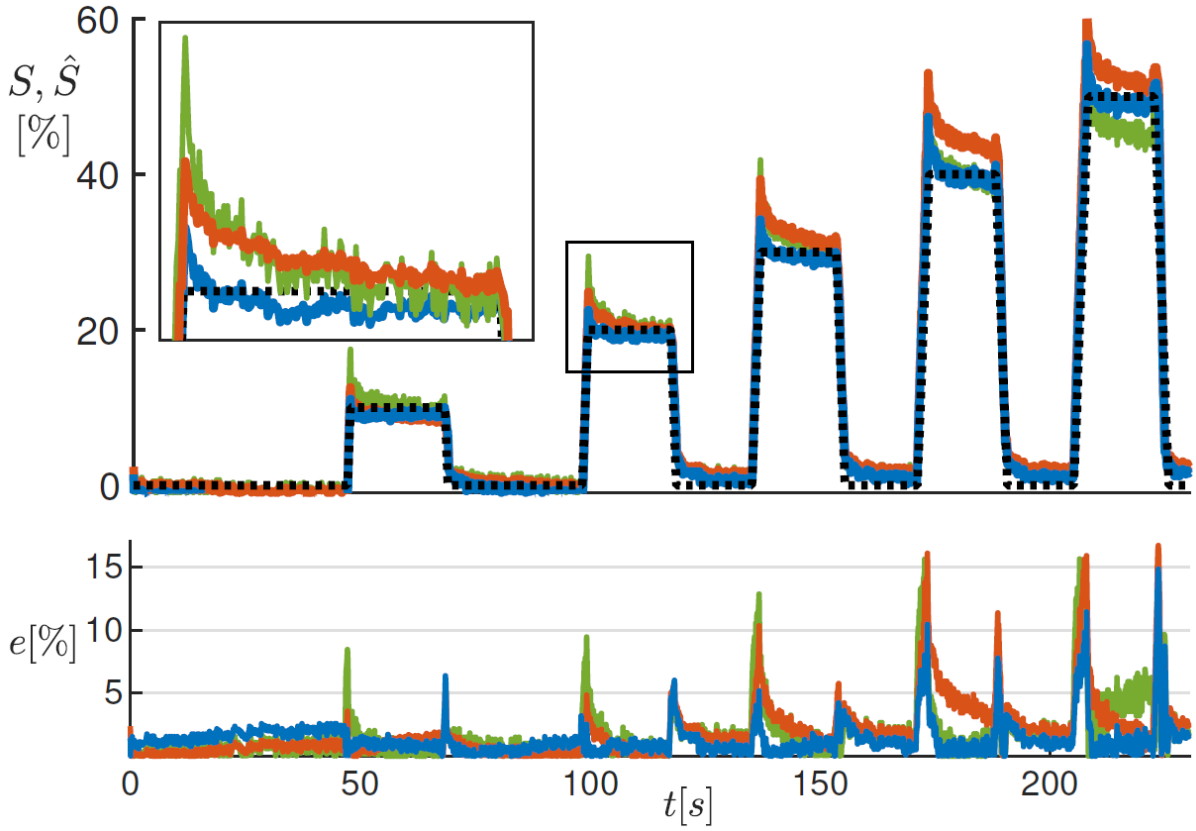

Figure 4.13 Measured (black dashed lines) and estimated (color curves) strain *S* computed on dataset RB1. Blue curve: APL model; orange curve: MPI model; green curve: CU model.

4.6.4 Tests on iCub

The APL model was added to the MATLAB toolbox HystTool [197], which automatically fits its parameters to experimental data. The data used for the robotic application are the three "natural" movements shown in the following figures. We chose to use a portion (highlighted in gray) of movement 1 (Figure 4.14) and of movement 3 (Figure 4.16) to train the 3 models (APL, MPI and CU). The remaining parts of movements 1 and 3 and the entire movement 2

(Figure 4.15) were not used to train the models, but only for validation purposes. The models were trained from R and angle θ measurements (rather than S).

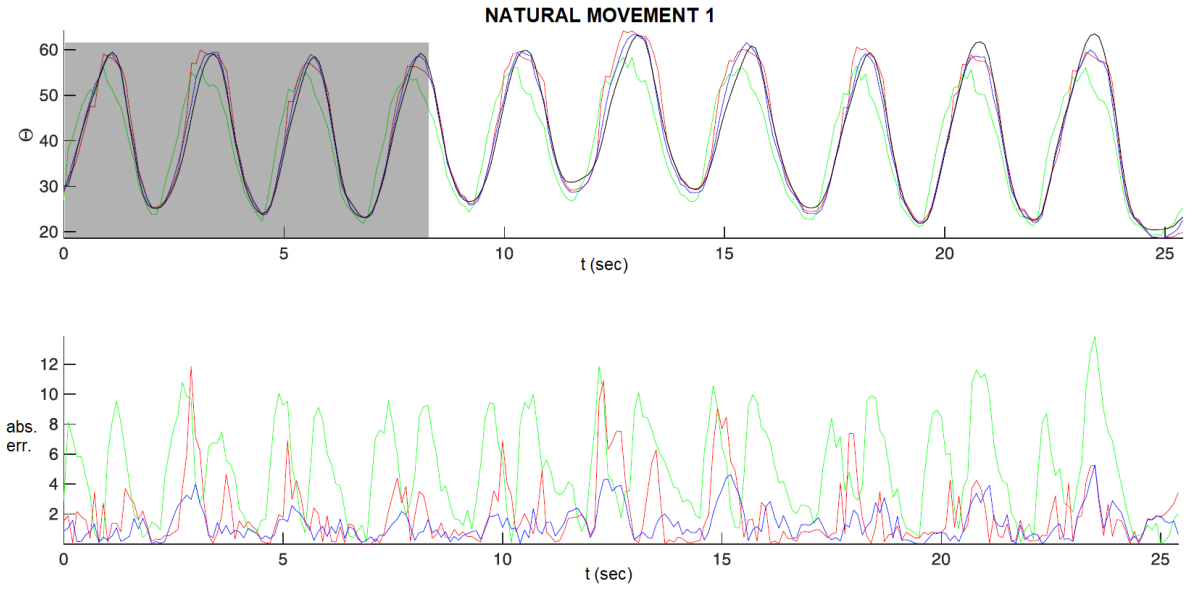

Figure 4.14 Measured (black curves) and estimated (color curves) angle ϑ for natural movement 1 (top panel). The bottom panel shows the corresponding absolute errors. Blue curves: APL model; red curves: MPI model; green curves: CU model.

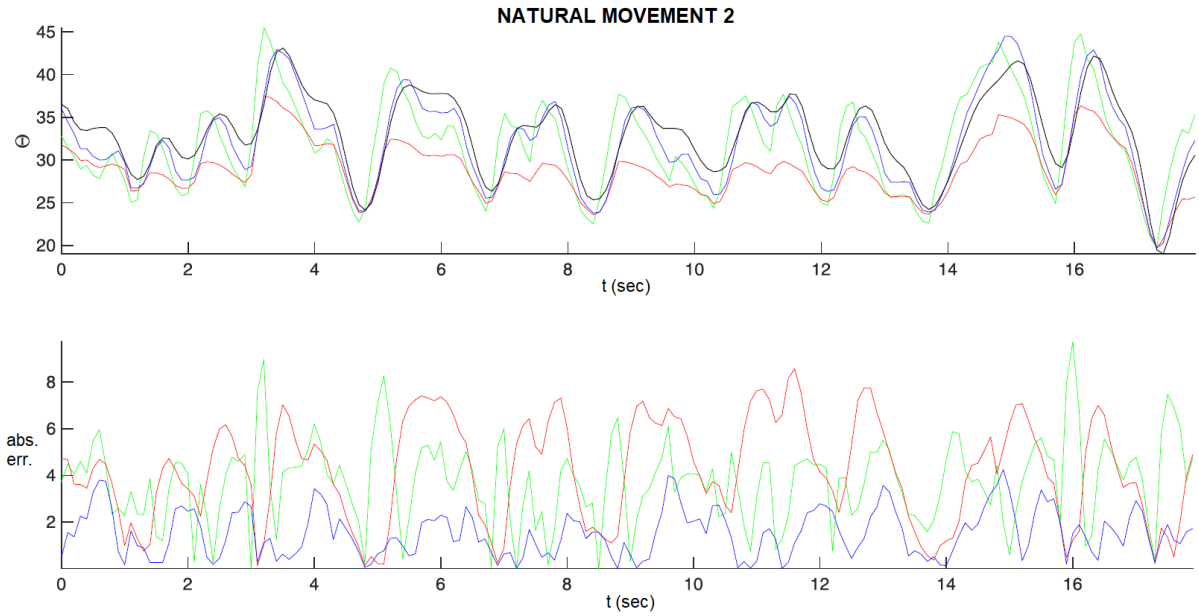

Figure 4.15 Measured (black curves) and estimated (color curves) angle ϑ for natural movement 2 (top panel). The bottom panel shows the corresponding absolute errors. Blue curves: APL model; red curves: MPI model; green curves: CU model.

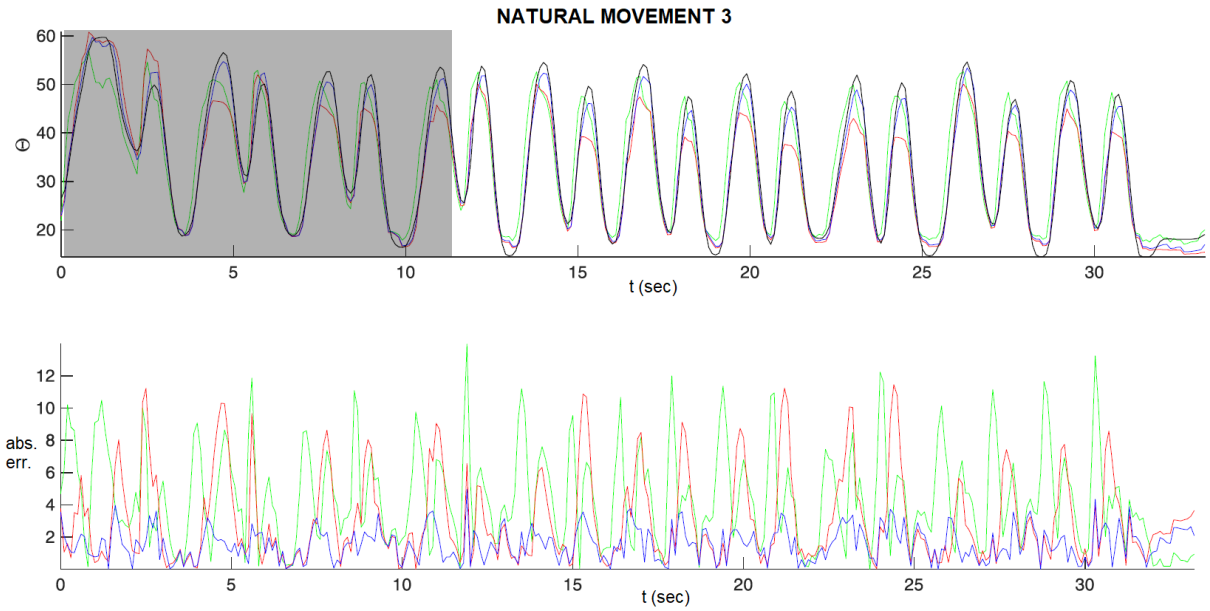

Figure 4.16 Measured (black curves) and estimated (color curves) angle ϑ for natural movement 3 (top panel). The bottom panel shows the corresponding absolute errors. Blue curves: APL model; red curves: MPI model; green curves: CU model.

In some parts of the natural movement 2 the compensation is worse, but anyway it is better than those obtained with the other considered models.

Figure 4.17 shows the RMSE obtained with the APL, MPI and CU models on all the three natural movements.

As expected, the CU model leads to larger errors, since it does not represent hysteresis, whereas the APL model outperforms the MPI model, as it is able to reproduce rate-dependent effects. It can be noticed that the APL model is the only one able to correctly estimate the angle in all the three natural movements with an error always about 4%, as visible in Figure 4.17.

These results confirming that the accuracies of APL model are higher with respect to the MPI and CU models.

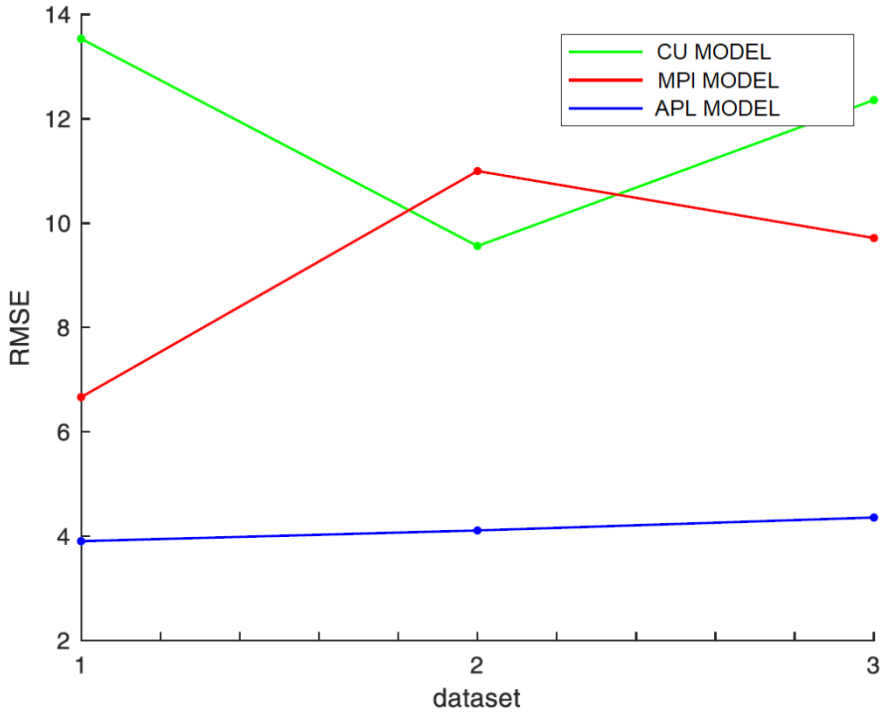

Figure 4.17 RMSE obtained on all the three natural movements employing APL model (blue curve), MPI model (red curve) and CU model (green curve).

In conclusion, the APL model provided a good hysteresis compensation performance even with a small calibration dataset. These results confirm that an adequate processing can enhance the sensor performances in case of dynamic measurements, without a prior knowledge of the strain rate typical for a particular application, extending its general applicability. Moreover, since hysteresis is caused by the intrinsic mechanical properties of the elastic material (that requires longer recovery time) the approach can be extended to all the sensors which are based on elastomer deformations and present rate-dependent hysteresis to improve their estimation performance.

In addition, analogously to the PL model, also the APL model is suitable for implementation on digital devices (e.g., microcontrollers [198]), making it suitable for a real-time estimation of the textile strain, given the measurement of its electrical resistance. This allows to develop accurate strain sensors based on piezoresistive textile, suitable for wearable and soft robotics applications.

Chapter 5

Biomedical application I: a wearable sensing device for monitoring single planes neck movements

5.1 Introduction

Neck mobility is fundamental for many Activities of Daily Living and a reduction in the Range Of Motion (ROM) can reduce the quality of life of the affected subjects. The evaluation of cervical spine mobility and the measurement of cervical ROM are important methods used in clinical settings for diagnosis and prognosis of patients with cervical spine disorders but also to quantify manipulation effects [199]. A reduction of ROM has been found to be a useful indicator of cervical physical impairment [200]. Indeed, modifications of ROM have been observed in subjects with traumas, head and neck problems, disturbances of termporomandibular joints and masticatory muscles, cervicogenic headache, neck pain, cervical dystonia, cervical radiculopathy and Whiplash-Associated Disorders (WADs) [199][200][201][202][203]. Therefore, the measurement of ROM has been used to assess the severity of the disability and the effectiveness of a rehabilitation program [201]. Generally, in clinical settings, physiotherapists and clinicians carry out visual estimation of cervical ROM. However, an adequate tool could be useful for a quantitative measurement of cervical ROM, taking into account that age and gender affect the physiological ROM [200][201].

In literature, different methods have been proposed for ROM measurement based on expensive technologies, such as optoelectronic system [202][203], electromagnetic tracker [200][204][205], and ultrasonic techniques [206]. A recent study investigated the validity of the Coda Motion 3-D Analysis System (Charnwood Dynamics Ltd., Leicestershire, UK) for measuring cervical ROM in healthy adults, with good results [207]. All of them provide accurate data but they need a structured environment and a qualified staff. Another system used to evaluate cervical ROM is the electrogoniometer [208][209], it produces a good

precision of data but an accuracy less than satisfactory [210]. Other wearable devices were proposed, such as a cervical goniometer [211] and a device based on a new iPhone-application [212]. However, these instruments is not so user-friendly and acceptable by patients. Moreover, concerning the iPhone-application, the technology used in smartphones innovates rapidly and then it will need continuous validity and reliability evaluation. Wearable inertial sensors are other systems adopted for monitoring neck movements [213]. In their use, the benefits are that they are wearable and acceptable for patients, inexpensive and provide accurate data. However, the output data require a post-processing with very complex algorithms [214].

Accurate measurement of the cervical ROM is important not only for orthopaedists, who carry out surgeries on the neck, but also for therapists, who provide therapy and treatment of the neck. This parameter allows to evaluate the efficacy of such interventions [215]. However, most of the existing measurement systems evaluate neck ROMs including trunk motion. The measurement of pure neck ROM needs trunk stabilization [202], which makes clinicians or researchers unable to measure neck ROM during Activity of Daily Living. As the new device aims to measure the neck ROM without taking into account the compensating movement of the trunk, it could allow clinicians to assess the effectiveness of interventions for the neck. In addition, a precise measurement of the cervical ROM is also important because a repeatable measurement is suitable for a clinical setting and for research field. In particular, the feature of repeatability should guarantee a valuable tool in the management of patients with a reliable clinical outcome.

In the last years, several studies have employed smart textiles as sensors to monitor physiological parameters or for quantitative analysis of movements. Indeed, smart textiles represent a valid solution to conventional solid-state sensors because of their comfortable wearability, lightweight, and capacity to adapt to different body structures without hindering physiological movements [216], providing satisfying accuracy of the collected data. The main advantages of these textiles are that feature electronics and interconnections woven into them, presenting physical flexibility and typical size that cannot be achieved with other existing electronic manufacturing techniques [112].

In the wearable field, conductive textiles are widely used for a new on-body capacitive sensing approach to derive activity related information. Cheng et al. [217] considered a capacitor build out of a conductive textile based electrodes integrated in a collar and the

human body as dielectric (Figure 5.1 (a)). They investigated electrode positions at the neck for a better recognition of speaking, head motions (shaking, nodding), head positions, deep breathing, chewing and swallowing. In addition, different strain sensors based on piezoresistive textiles have been proposed for neck movement measurement, such as foam sensor composed of polypyrrole-coated polyurethane foam [218] and a fiber-shaped textile knitted with hierarchical polyurethane fibers and coated of silver nanowires and styrene–butadiene–styrene [219] (Figure 5.1 (b)). These studies presented the development of a prototype sensing textile and their potential in measuring neck movement by evaluating resistance changes when the human's neck moves, but a device validation is missing.

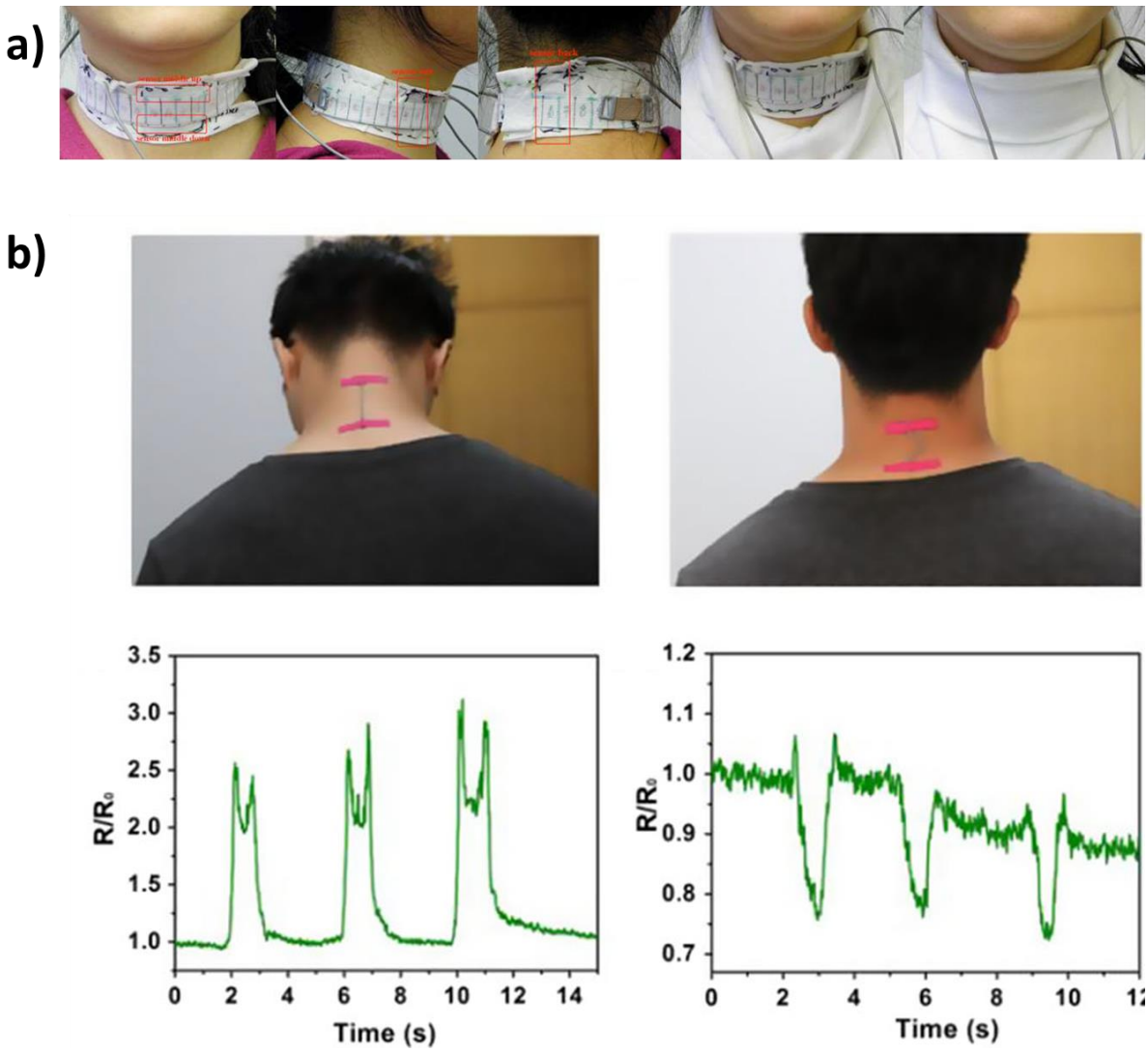

Figure 5.1 a) Sensor placement in an elastic band and integration in a pullover collar are shown [217]; b) e-textile attached on a human's nape and corresponding resistance changes when the human's neck turns down and up [219].

It is clear the wide scope of application of the smart fabrics and their potential employment in diagnosis and monitoring of several diseases. In this framework, the primary objective was to develop a Wearable Sensor Device (WSD) based on smart fabrics that overcomes the limitations of current technologies used for measuring neck movements. Although there are very few studies on the use of smart fabrics for the measurement of cervical ROM, the challenge of the proposed work was the development of a "wear and forget" device for a continuous monitoring of the three-dimensional movement of head and cervical spine. The key idea is to place the WSD along the neck; therefore, the system must be light, non-intrusive and simple to wear.

Thus, the present work consists of three parts. The first aim has been the characterization of the piezoresistive textile employed with the analysis of its properties for both static and dynamic measurement conditions, in order to optimize and calibrate its sensing capabilities. The second part focuses on the identification of a sensor design able to provide a comfortable wearability on subjects' neck. Finally, in the third part of the study, the reliability of the developed WSD for measurement of cervical head movements was investigated, by using Vicon measurements as the Reference Standard (RS).

5.2 Material characterization

Among the available possibilities on the market of conductive textile, the Electrolycra (Mindsets Ltd, United Kingdom) has been selected for this study, also thanks to its features previously studied. Previous works have also adopted Electrolycra as a strain sensor in several applications such as the sensorisation of continuum soft robots for reconstructing their spatial configuration [125], and as to reveal bending and force in a soft body [138].

Electrolycra main characteristics, previously investigated, are that it can be stretched beyond its initial length, with better performances after pre-stretching of 200%. Moreover, this material has a preferential direction along which resistance significantly changes and a major strain is possible, with a working range from 0% to 50% of strain and electrical hysteresis of about 14.8%. Additional tests were performed in the framework of the present work to better understand and characterize Electrolycra electrical and mechanical properties in conditions that are more suitable for this application. Therefore, the electromechanical tests were performed at room temperature by using the Instron material testing machine (model

4464, Instron Inc., Norwood, MA), with the same setup adopted during the characterization phase and presented in the Chapter 3.

Due to material preferential direction [125][193], uniaxial cyclic strain tests have to be conducted along this direction. In order to characterize our material, the first phase consisted in cutting Electrolycra for preparing several specimens with 20 *mm* in wide and 100 *mm* in length along the preferential direction. Tests carried out to extract stress-strain relation have been performed in static and dynamic condition.

A static characterization has allowed to evaluate the sensor behaviour under normal condition, without impact, acceleration and vibration. Twenty strain values equally spaced from 5% to 100% were applied to the sensor, and the output signal was recorded for two minutes. Three replicates were performed for each strain value. In particular, the mean values and the Standard Deviations (SD) were considered for each replicate; then the results were averaged on the three trials and SD were considered to evaluate the static repeatability of the sensor.

In order to describe the behaviour of the sensor for different percentage of deformation, in the absence of stresses at constant strain rate, dynamic tests were performed [177]. Ten strain values equally spaced from 10% to 100% were applied to the sensor, with a strain rate of 50 *mm/min*. For each deformation, five cycles were performed.

In addition, tests included different level of velocity were carried out, in order to evaluate and confirm the influence of the strain rate on the sensor characteristics, previously found. These tests were performed applying on the sensor the same strain (50%) at ten different strain rates (from 10 *mm/min* to 100 *mm/min* equally spaced). This range of strain rate covers reasonably the typical velocity of neck human movements.

5.3 Sensor design identification

The integration of the conductive textile into a wearable device was a key point. The challenge was to realize a wearable sensing system for monitoring neck movements in a non-intrusive and comfortable way. In addition, since the device has to deform or expand by following the neck movement, it is crucial its perfect adhesion on the skin around the joint. For this purpose, an adhesive tape was selected as interface between the sensor and the skin

(Kinesio Tape, Kinesio Co., Ltd, Tokyo). This tape has several advantages: it is not invasive and readily available on the market, it does not limit movement and does not require a complex process of integration with the Electrolycra. The Kinesio Tape is widely used in the sports field for healing purpose of traumatized tissues and muscles. Its favourable features are elasticity, adhesiveness and breathability of the tissues.

The double-layer conductive textile/adhesive tape was characterized to verify the influence on the electrical behaviour of the sensor. Tests were carried out on a 20 *mm* × 100 *mm* sample of double-layer Electrolycra/Kinesio Tape. These tests, performed in a static condition, were compared with those performed on a single layer Electrolycra. Ten strain values equally spaced within the sensor working range were applied, and the output signal was recorded for two minutes. Three replicates were performed for each strain value. In particular, the mean values and the SD were considered for each replicate; then the results were averaged on the three trials and SD were considered to evaluate the static repeatability.

The final sensing system is composed of stripes (20 *mm* × 100 *mm*) of conductive textile fixed on Kinesio Tape using two simple clips placed at the extremities with welded wires to detect the sensor voltage. These wires were connected to the same acquisition circuit adopted during the characterization phase to acquire the electrical resistance value.

5.4 Evaluation of system reliability

Literature findings [220] showed that the neck's center of rotation is not unique; however, despite this result, the human body is often treated as a system of rigid links, connected by the geometrically ideal joints [221]. As such, we can model the neck as a spherical joint with three Degrees Of Freedom (DOF), and not as a kinematic chain. The simplified biomechanical model adopted in this work, is composed of two cylinders connected by a spherical shell with fixed radius and three rotational axes (Figure 5.2).

5. Biomedical application I

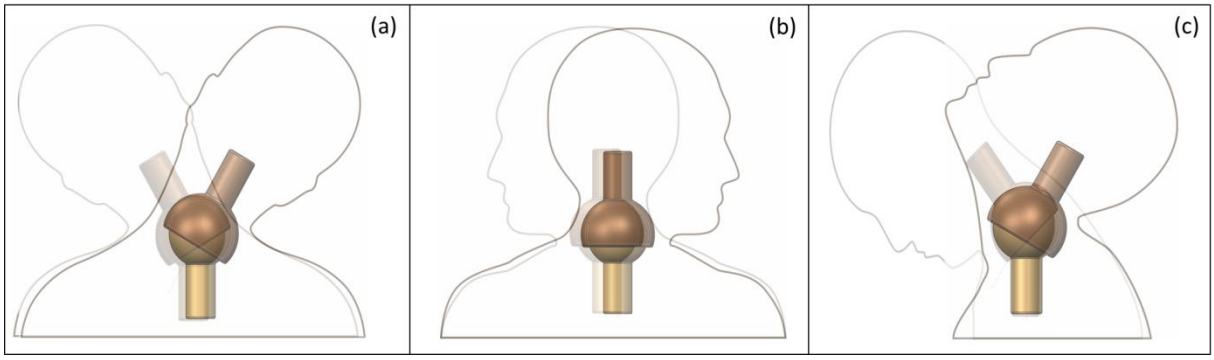

Figure 5.2 A biomechanical model of the neck in a) lateral bending, b) rotation, and c) flexion-extension.

The sensor location should be carefully evaluated and standardized to guarantee comparable measurements and optimize the sensor's capability in detecting head movement. Considering that the sensor can only measure the amount of stretch and in order to measure each movement, it is necessary to place two sensors on the opposite sides of the joint. For the lateral bending, sensors are placed on both sides under the angle of the mandible and in correspondence with the trapezius scapula insertion (Figure 5.3 (a)). In the case of rotation, sensors are placed on both sides on the anterior part of angle of the mandible and in correspondence of the trapezius muscle (Figure 5.3 (b)). Finally, for the flexion-extension movement, one sensor is placed between the hyoid bone and the sternum (extension), the other between C2 and C7 vertebrae (flexion) (Figure 5.3 (c)).

The key advantage of this approach is that it allows the use of the geometric relationship between the elongation of each pair of sensors (ΔL, where L represents the sensor length) and the angle θ relate to each plane [46][193][222] (as also shown in Figure 3.3):

$$\Delta L = r\theta \tag{5.1}$$

where r is the neck joint radius, an anthropometric parameter that is specific for each subject. By combining this equation and the characteristic of the sensor, it is possible to evaluate the relationship between the sensor resistance and the angle (in degrees) of lateral bending, rotation and flexion-extension.

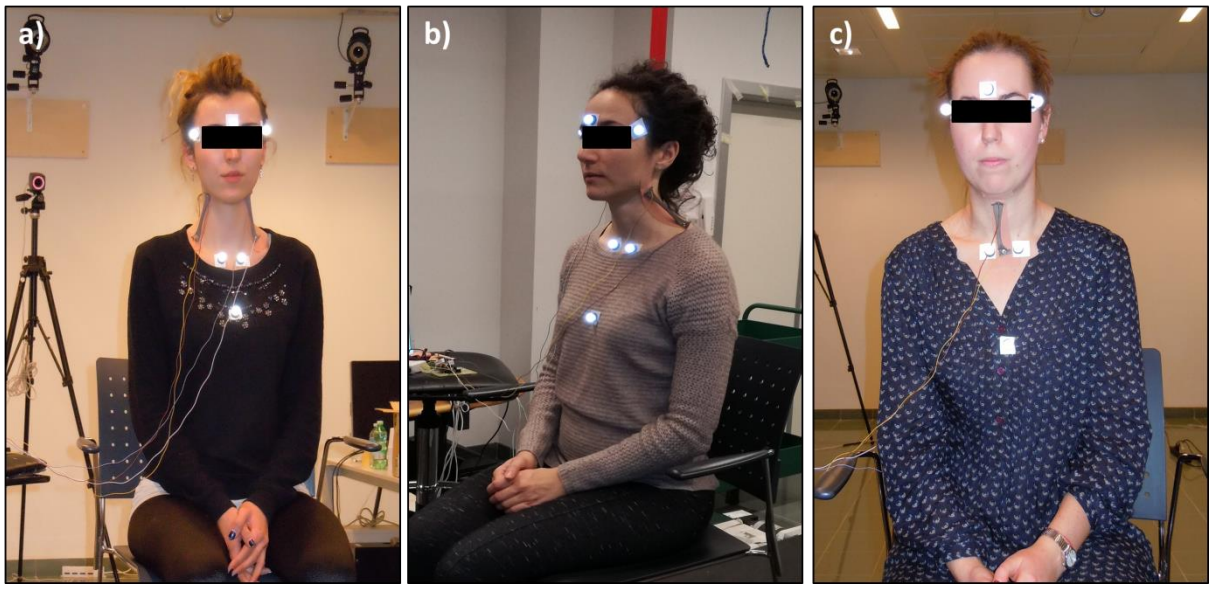

Figure 5.3 Position of the WSDs for the a) lateral bending, b) axial rotation and c) flexion-extension measurements.

5.4.1 Accuracy and repeatability

For the investigation of the *accuracy* and *repeatability* of the developed WSD in measuring the cervical head movement, the optoelectronic system (Vicon Bonita, Vicon Motion System Ltd, Oxford, UK) was used as RS [202][213][215]. It was composed of six infrared cameras acquiring the trajectories of reflective markers at 100 *Hz*. Seven spherical markers (5 *mm* in diameter) were attached on each subject, three were positioned on the head (glabella, right and left sphenofrontal suture) and four on the upper body (body of sternum, right and left sternoclavicular joint and T10 vertebra) (see Figure 5.4). Neck angles measured with both systems (WSD and RS) were synchronized and analyzed using a custom MATLAB® code (MathWorks Inc., Natick, MA, USA).

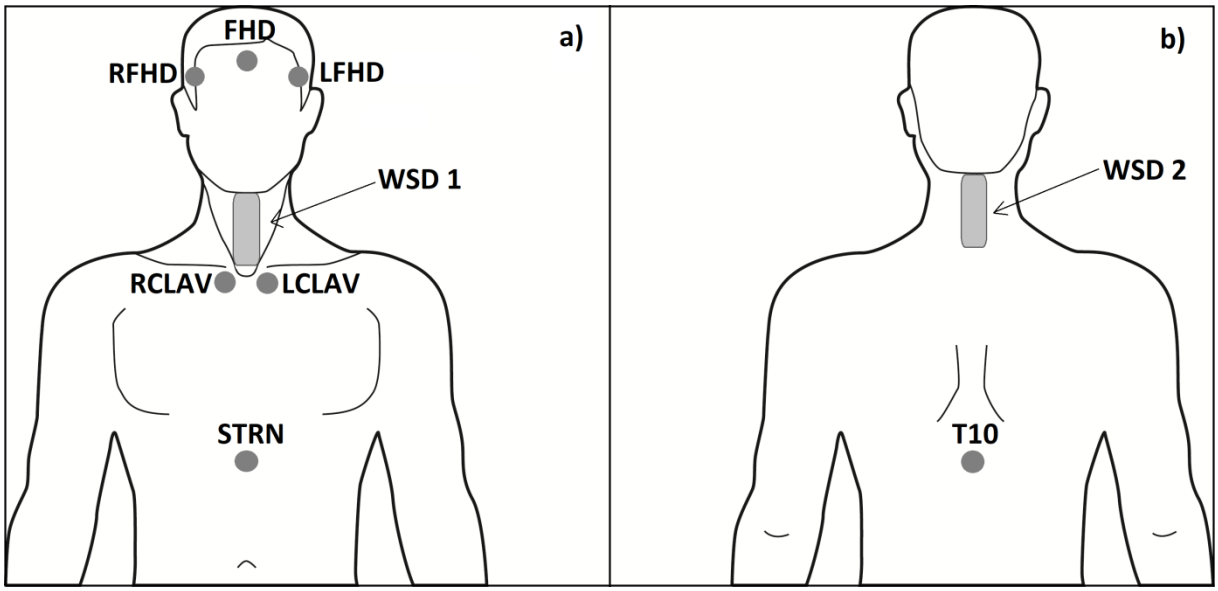

Figure 5.4 Position of the WSD and spherical markers for the flexion/extension measurement during the testing procedure: a) frontal and b) rear view of the subject.

Five young healthy volunteers (one male and four females, mean age 24.8 ± 3.5 *yrs*) were recruited and asked to perform active head movements. They were asked to seat and to assume a natural head and neck position, which was stabilized as reference posture (i.e. still, straight head and looking forwards). The reference posture of each participant was initially recorded by both systems (i.e. WSD and RS) for 5 *s*. They were asked to perform three head movement tasks: right/left Lateral Bending (LB), right/left Axial Rotation (AR), and Flexion/Extension (FE). For each task, the subject started in the reference posture, moved in one direction, moved in the opposite direction, and moved back in the reference posture (e.g. for a FE task, the patient was invited to flex, extend and then return to the reference posture). Two modalities of execution were required for each task:

- the *Amplitude Modality* (AM) according to which subjects were asked to move their head at their best, always keeping inside their 'maximum normal' range, and to carry out each head movement task in 10 *s*;
- the *Continuous Modality* (CM) according to which subjects were asked to move at a comfortable speed repeating the single task three times continuously.

For what concern the AM, five trials were recorded for each movement, whereas for the CM only one. Before testing, written informed consent was obtained from the participants, also for publication of both subjects' data and all accompanying images. All methods

included in the protocol were carried out in accordance with the guidelines laid down in the Declaration of Helsinki.

The angles obtained by the two systems were compared in terms of movement patterns and ROM. The accuracy parameter was estimated on individual subjects' tests (both in AM and CM cases) in terms of Root Mean Square Error (RMSE) between RS and WSD signals. Whereas, to evaluate the validity of our WSD to measure the ROM, the Spearman correlation coefficient r_s and the Mann-Whitney u-test for non-parametric independent variables were performed between ROM calculated from RS measurement and ROM calculated from WSD measurement (in AM case), at the 0.05 significance level.

To evaluate the repeatability of the sensor, it was necessary to firstly consider the intra-subject repeatability during the AM [223]. Therefore, for each movement only tests with RS curves sufficiently overlapped were taken into account. This because it is necessary to have the same input measures in order to monitor the repeatability of the sensor. These selected data intervals were resampled on a 0-600 basis to allow for curve comparison. For each task and variable, the intra-subject repeatability was assessed by the SD at each sample of the curves obtained from five repetitions performed by the subject, averaged over the movement cycle. If movements were correctly repeated the sensor repeatability was evaluated. In addition, a statistical comparison between the mean SD values of averaged RS signals and the mean SD values of averaged WSD signals was performed, to evaluate if there are small differences in repeatability between WSD and the reference Vicon system. Spearman correlation coefficient r_s and Mann-Whitney u-test at the 0.05 significance level were used.

5.5 Results and discussions

5.5.1 Material characterization

The mean calibration curve calculated for the sensor in static condition is reported in Figure 5.5 (a). For each 5% of strain, the SD was calculated (bars) and the maximum standard deviation value was 3.2%, for 35% strain. It is worthwhile to notice in Figure 5.5 (a) that the sensor shows a working range from 0% to 50% of strain in static condition. The sensor behaviour is quite linear and the resistance variation grows up to 93% of strain in correspondence of its maximum working range.

5. Biomedical application I

Whereas a typical normalized relative resistance vs. strain plot in dynamic condition is shown in Figure 5.5 (b), indicating a quite linear rise in resistance when applying strain. Electrolycra's usable working range is confirmed to be between 0% and 50% strain, also in dynamic condition. This is also highlighted by the resistance–strain relationships of the sensor exhibiting a similar shape in the working range, whereas for higher strain values the resistance-strain behaviour tends to decrease. From a visual inspection, it is possible to notice that the sensor's sensitivity is higher in dynamic condition rather than in static condition. Indeed, the resistance variation grows up to 130% of strain in correspondence of its maximum working range.

The electrical hysteresis of the sensor was calculated on the resistance-strain relationship obtained from the mean curve of five cycles at 50 *mm/min* and 50% strain. The hysteresis value is 13.8% of the full-scale, at 25% strain, comparable with the value obtained in the Chapter 3 e presented in [193] (14.8% of the full-scale, at 28% strain). Moreover, the calculated hysteresis confirms that elastic materials have higher hysteresis because they require longer recovery time.

The dependency on the strain rate is shown in Figure 5.6. The strain rate velocity was increased from 10 *mm/min* to 100 *mm/min* equally spaced. The increase in speed has shown a marginal rise in resistance. This trend may be due to sensor drift, rather than a true frequency response. In particular, the sensor drift was investigated in Chapter 3, in which results shown that the initial overshoot and the corresponding steady state increased with increasing speed. Therefore, the sensor behaviour for lower strain velocity is nearer to the static condition. This result is aligned to the literature evidence [177]. In addition, the result shown in Figure 5.6 is important for the design since it means that the sensor could be used to track body movements within a wide range of velocities, but with different calibration procedure. This study aims to monitor cervical head movements and these movements can be considered sufficiently slow compared to the other human joints movements. Despite the dynamic calibration offers a higher sensor's sensitivity compared to the static calibration, tests results suggest the choice of a static calibration procedure as more suitable for this kind of application. In conclusion, Electrolycra textile required a static calibration within its working range along its preferential direction after pre-stretching of 200%. In this way, we are sure that our sensor will be able to detect all neck human movements.

5. Biomedical application I

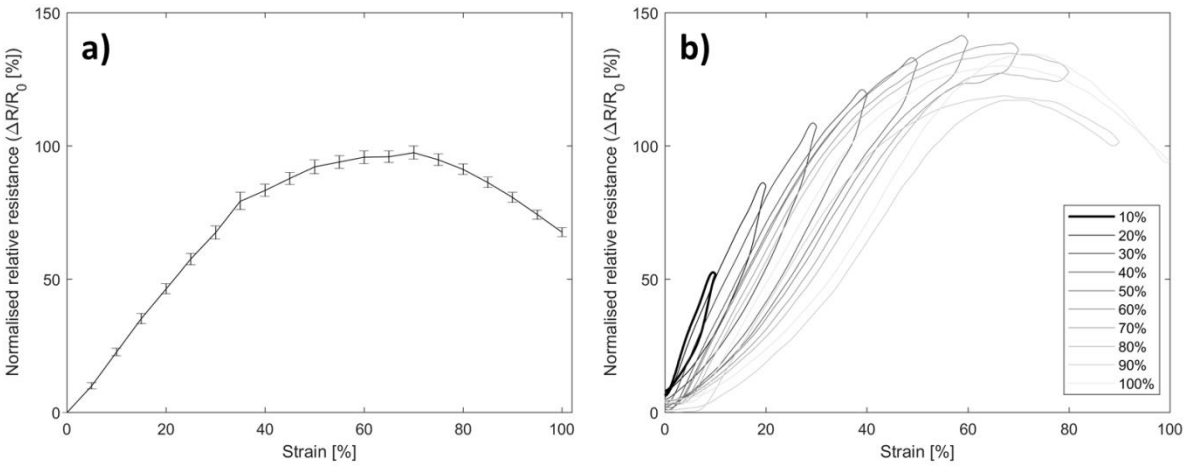

Figure 5.5 (a) Static calibration curve obtained from 5% to 100% of strain equally spaced. For each strain value, three replicates were performed; the mean values and the SD (bars) were showed. (b) Dynamic calibration curves obtained from 10% to 100% of strain equally spaced performed at 50 *mm/min*. For each strain value five cycles were carried out and the mean values of the five cycles were shown.

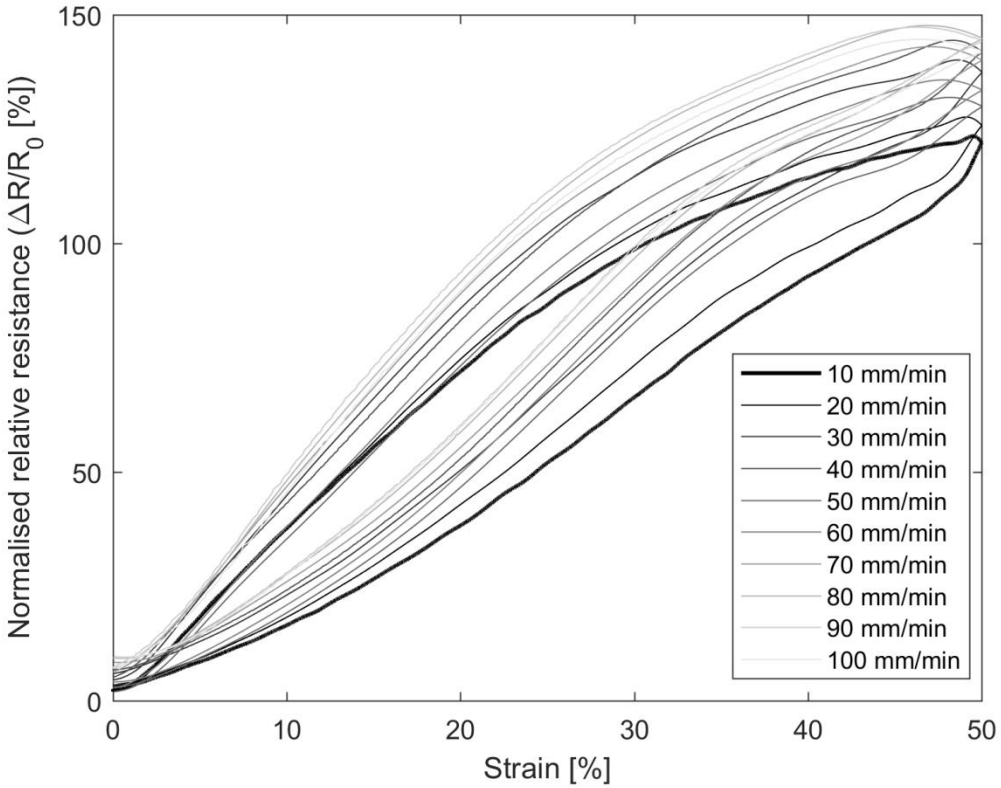

Figure 5.6 Normalized relative resistance of the sensor characteristics at increasing strain rate.

5.5.2 Sensor design identification

The mean static calibration curves calculated for the double-layer (black line) and single layer (gray line) are reported in Figure 5.7 (a). From a visual inspection, it is possible to notice that the double-layer sample influences the static calibration curve with a significant increase in sensitivity. The reasons for the increase in the normal operating range have been credited to the material composition of the adhesive tape. In fact, the Kinesio Tape is made of 100% acrylic fiber [224]. Acrylic fibers are synthetic textile fibers made up of 85% by acrylonitrile and 15% by other co-monomers [225]. The features of these fibers are: low specific weight, high resilience, easy to undergo thermoplastic treatments, surface resistance of 1.9×10^{15} *Ω/cm* and electrical resistivity 1.6×10^{16} *Ω* [226]. Therefore, these features could be the cause of the increase in conductivity of double-layer with an increase in the normal operating range and sensitivity of the sensor. The maximum standard deviation value was 3.5% in correspondence with 30% strain in the calibration curve calculated for the double-layer.

The strain-resistance characteristic of the double-layer conductive textile/adhesive tape was calculated (Figure 5.7 (b)). Resistance was expressed as a normalized relative resistance: $\frac{R-R_0}{R_0}$, where R_0 is the resistance at zero value strain. The relationship between the strain (in %) and the normalized relative resistance resulted in second-order polynomial fittings (equation 5.2). It has been applied for all the analysis reported in the following sections. Fitting result is markedly accurate (R^2 = 0.987) and therefore strongly remarkable for tracking all tasks performed during the measurement protocol (i.e. AM and CM execution modalities).

$$\frac{\Delta L}{L_0} = a * \left(\frac{\Delta R}{R_0}\right)^2 + b * \left(\frac{\Delta R}{R_0}\right) \quad (5.2)$$

By combining this equation and the geometric relationship (equation 5.1), it is possible to evaluate the relationship between the sensor resistance and angle (in degrees) of LB, AR and FE.

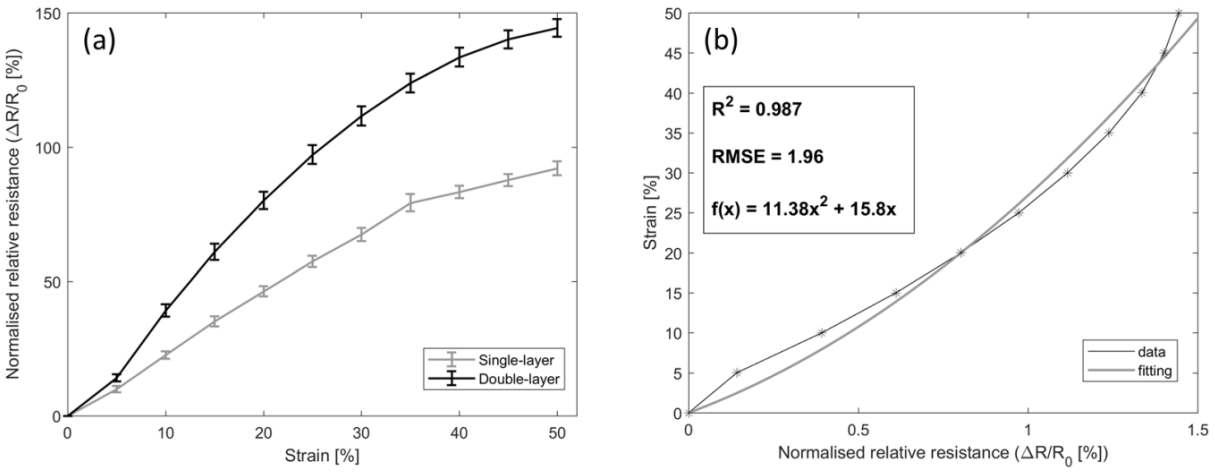

Figure 5.7 (a) Static calibration curve obtained from 5% to 50% of strain equally spaced for the double-layer (black line) and single layer (gray line). For each strain value three replicates were performed; the mean values and the SD (bars) were showed. (b) Second-order polynomial fittings employed to calculate Strain from static measurements of Normalized relative resistance (R^2 = 0.987). Parameters of the second-order polynomial fittings are reported in the textbox.

The final sensing system is composed of stripes (20 *mm* × 100 *mm*) of conductive textile fixed on Kinesio Tape. The sensor length was customized starting from the working range, the maximum ROM of LB, AR, FE [227], and the average circumference of the human neck [228]. The length of the strips had to guarantee the use of the sensor within the working range (0-50% strain) for the expected maximum deformation. A graphical user interface was designed to make using the device simple and suitable for a wide range of users. LB, AR and FE angles were shown in real-time and were stored for off-line analysis.

The main advantage of the final WSD is that it does not limit and restrict the neck movement during usage. The intended features of this WSD other than the cost will be easy of wear to the user with minimum or no assistance. This compact configuration allows user to operate in any environment in a comfortable way.

5.5.3 Evaluation of system reliability

Over the 90 movements measured by both systems, 21 movements were discarded for some problems: (i) 16 movements not correctly performed due to execution of composite movements (i.e. generally AR was paired with a not negligible lateral bending component

and, therefore, it was not a single plane neck movement); (ii) 5 movements for recording problems due to marker occlusions especially during FE movement tasks.

Through the comparison with RS we evaluated the sensor accuracy and repeatability in measuring neck angle and the validity of our WSD to measure the ROM.

1) Accuracy

The mean RMSE values on each head movement task calculated for each subject are reported in Table 5.1. The RMSE value of AR for the subject 1 is not available since all five trials were discarded. Finally, for LB, AR and FE movements the mean RMSE value was 6.04±0.67, 10.16±2.11 and 12.31±3.22, respectively.

Table 5.1 Mean RMSE value over five repetitions in amplitude modality for each subject.

$\overline{RMSE}$ [°]	*LB* *Lateral Bending*	*AR* *Axial Rotation*	*FE* *Flexion/Extension*
Subject 1	6.68	NA	8.49
Subject 2	5.08	10.05	13.13
Subject 3	5.94	12.46	15.39
Subject 4	5.85	10.78	15.16
Subject 5	6.67	7.35	9.38

Three performances of CM in LB, AR and FE cases are reported in Figure 5.8. These tests have allowed to evaluate the response of the WSD in continuous and more dynamic neck movements. The most important aspect, resulting from such tests, is the ability of the WSD to follow the motion dynamics, as can be seen from the RMSE values shown in the Figure 5.8. Indeed, these values are slightly lower than the RMSE values calculated for AM cases.

The RMSE values calculated to assess the sensor accuracy (Table 5.1) are not entirely negligible, but in line with another study [215]. Therefore, results shown a good accuracy in the detection of LB angle, with an average RMSE of 6.04°, whereas in the AR an error of 10.16° is obtained. The performance of the developed WSD in monitoring FE movement is less accurate with RMSE values of 12.31°. These errors resulting from validation of the WSD may be considered acceptable for specific applications. However, if the purpose is to obtain a

more accurate LB, AR and FE angles, a method to reduce the accuracy error should be implemented. A possible solution should be the adoption of another curve fitting or a modification of the original geometrical model that correlates the elongation of the sensor with the angle measured. This could be obtained experimentally by identifying a corrective parameter for the model, which could allow an improvement in accuracy. The disadvantage in such a case would be a more complicated model with higher computational costs.

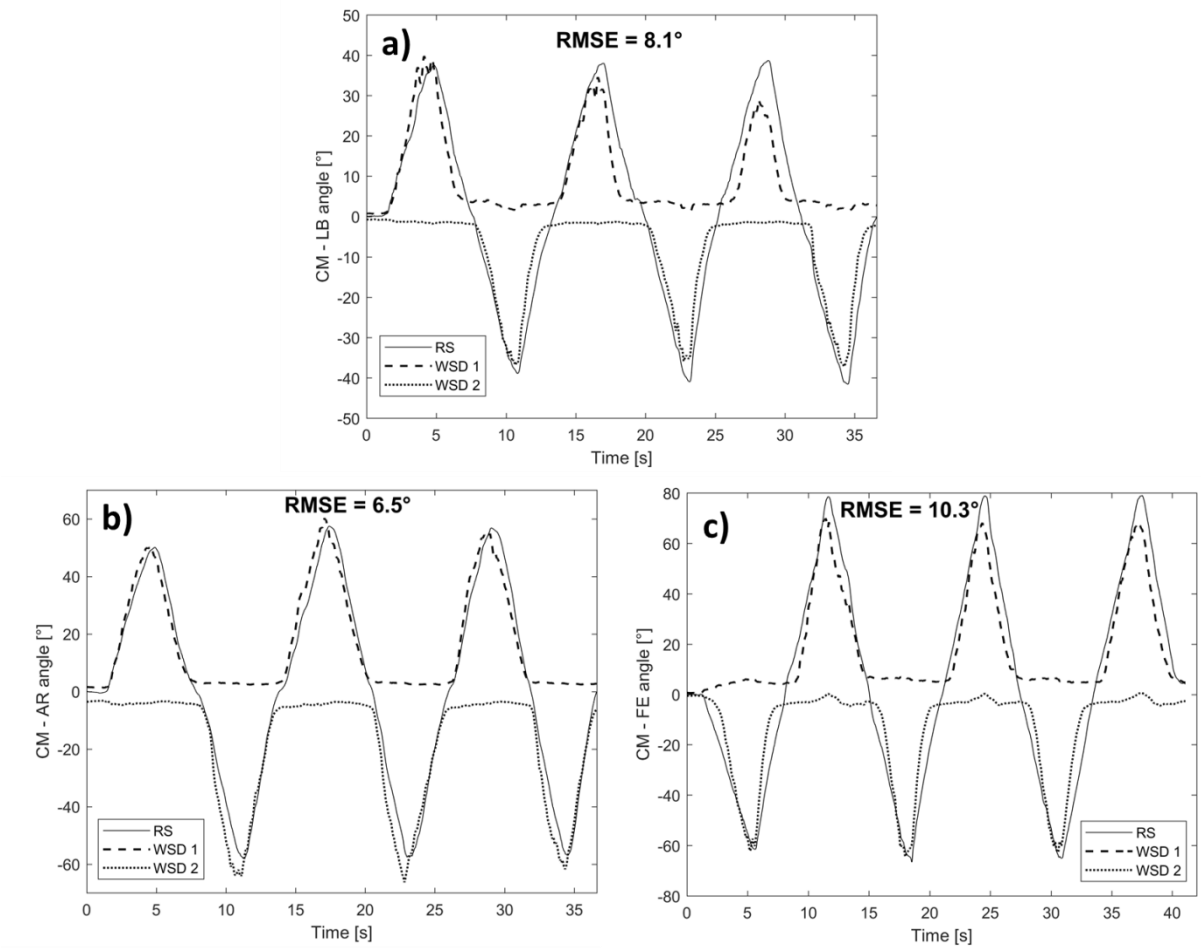

Figure 5.8 Some examples of measurements from both systems during the CM execution for (a) lateral bending, (b) axial rotation, and (c) flexion/extension.

In addition, the ROM data for all movements obtained from WSD system were positive correlated (r_s > 0.77 and p < 0.05) with those measured by RS. According to [229], Spearman's coefficient values were considered excellent if r_s > 0.90, good for r_s > 0.75, moderate for r_s > 0.50. According to the results, the correlation was statistically significant (r_s > 0.77) and the results of Mann-Whitney test underline no significant difference (p > 0.10) between ROM obtained from both measurement systems (WSD and reference Vicon system),

which means that proposed device could be considered a valid device for measuring cervical ROM.

2) Repeatability

Two motion patterns for intra-subject repeatability were reported by a graphical representation (Figure 5.9). From a visual inspection, it is possible to notice that in Figure 5.9 (a) the band thickness is thin over the all movement, therefore the intra-subject repeatability can be considered acceptable. Whereas, a greater SD shown in Figure 5.9 (b) indicates a lower intra-subject repeatability, which cannot be considered acceptable. Therefore, all movements with a lower intra-subject repeatability were discarded from the assessment of sensor repeatability.

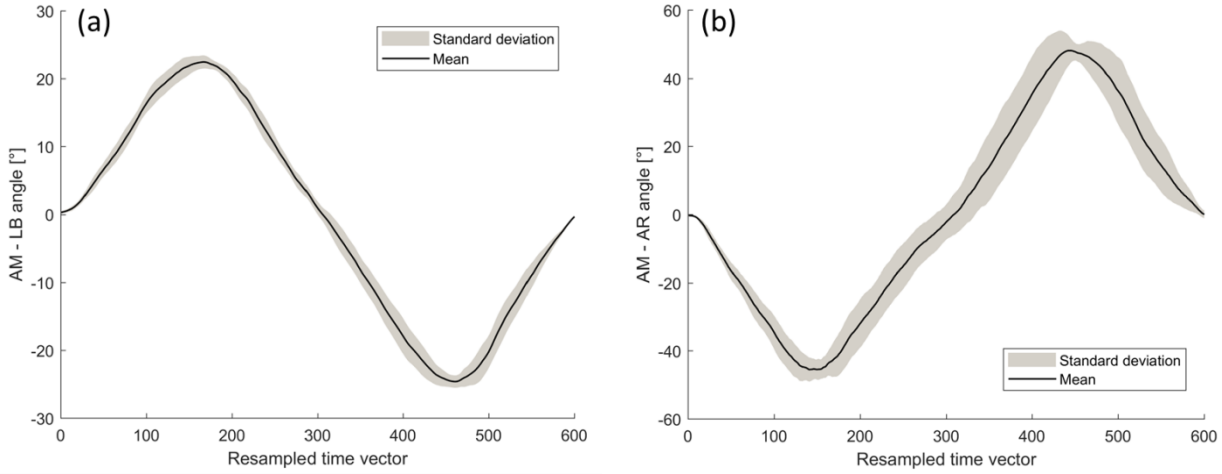

Figure 5.9 Angle pattern and its repeatability for two representative cases. Five repetitions were averaged and the mean is represented by black line, whereas the gray band corresponds to the SD. (a) LB movement performed in a repeatedly way (narrow gray band) and (b) AR movement in no repeatedly way (large gray band).

The intra-subject repeatability was evaluated for each movement task during AM and the mean and maximum SD of averaged movements are reported in Table 5.2. It is worthwhile to notice that subjects mainly executed LB and FE movements in a repeatedly way. Moreover, it is reasonable that a low value of the maximum SD corresponds to a high intra-subject repeatability. Therefore, we have defined a threshold value on the maximum SD to discriminate which tasks can be considered for assessing sensor repeatability. This value was

set at 8°, acceptable to consider good the intra-subject repeatability and not to affect the outcome measures. Movements with a maximum SD above the threshold are indicated in bold. These data indicate a lower intra-subject repeatability and therefore, these are data discarded for the assessment of sensor repeatability.

Table 5.2 Mean and Maximum SD of averaged movements for the assessment of intra-subject repeatability.

$\overline{Dev.Std.}$ *(max) [°]*	*LB* *Lateral Bending*	*AR* *Axial Rotation*	*FE* *Flexion/Extension*
Subject 1	1.45 (2.62)	**4.13 (8.27)**	**9.62 (22.79)**
Subject 2	1.96 (3.68)	4.2 (7.75)	3.91 (6.18)
Subject 3	2.56 (4.15)	**5.19 (13.89)**	**8.76 (18.25)**
Subject 4	3.63 (7.63)	**4.21 (11.44)**	**6.05 (11.06)**
Subject 5	2.92 (6.75)	2.87 (6.49)	4.58 (7.67)

The sensor repeatability was evaluated by resampling the sensor signals and superimposing the five movements repetitions (Figure 5.10). The mean and maximum SD of averaged sensor signals are reported in Table 5.3. It is important to highlight that the SD of averaged sensor signals is influenced by both the intra-subject and sensor repeatability. For this reason, the mean and maximum sensor SD values are higher than those shown in Table 5.2. However, the developed WSD shown satisfactory repeatability with maximum SD values close to 10°.

In addition, a statistical comparison between the mean SD values reported in Table 5.2 and 5.3 was performed, to evaluate if there are small differences in repeatability between proposed WSD and the RS system. A positive correlation coefficient (r_s > 0.83 and p < 0.05) was obtained, and no significant difference (p > 0.29) were found in repeatability between proposed WSD and reference Vicon system.

Therefore, the WSD data can be considered acceptable as precise measurements.

5. Biomedical application I

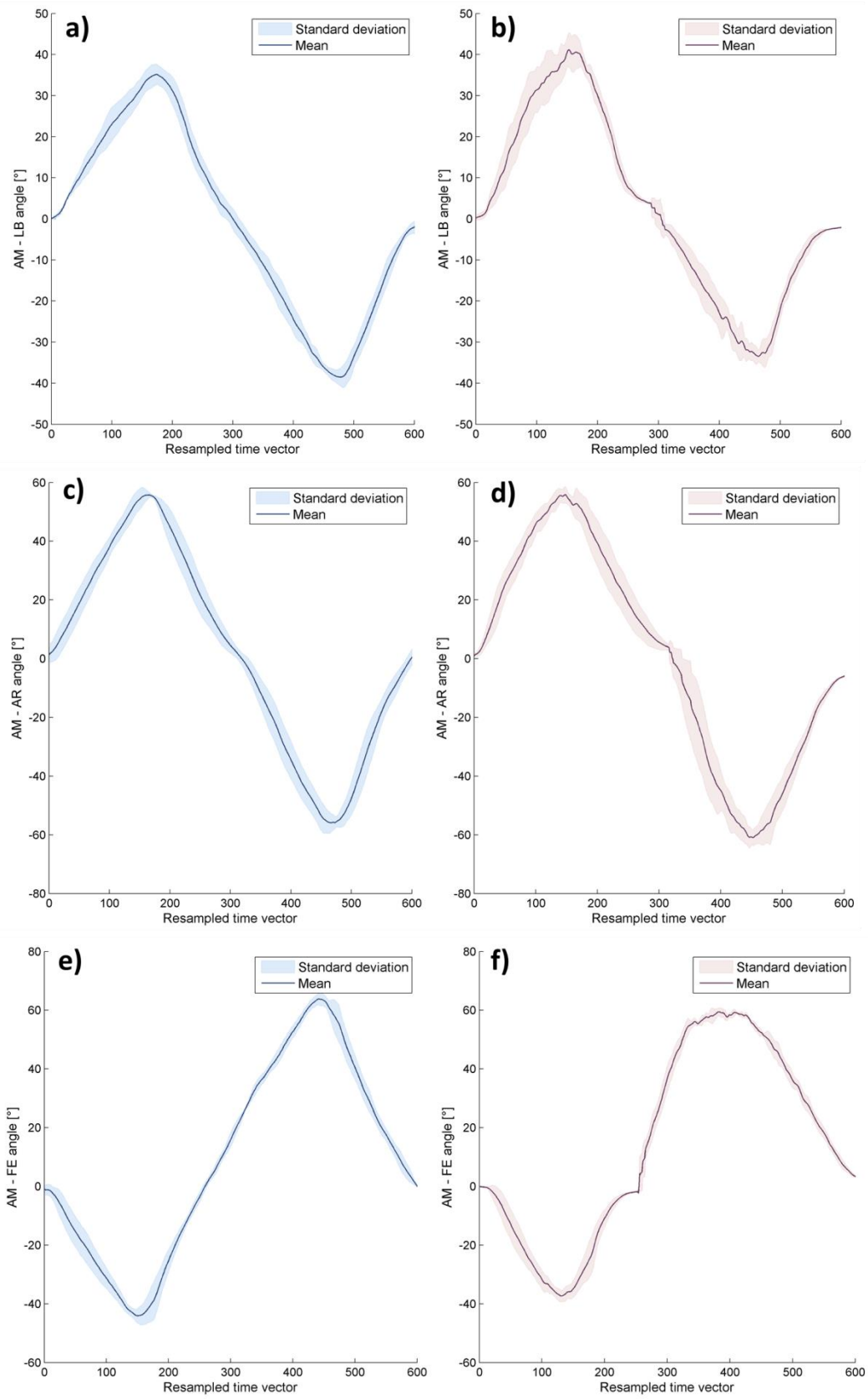

Figure 5.10 Examples of sensor repeatability assessed on LB, AR and FE task, respectively: (a), (c) and (e) illustrate the repeatability of task (according to the RS), whereas the sensor repeatability for the same tasks is seen in (b), (d) and (f).

Table 5.3 Mean and Maximum SD of averaged movements for the assessment of sensor repeatability.

$\overline{Dev.Std.}$ (max) [°]	*LB* Lateral Bending	*AR* Axial Rotation	*FE* Flexion/Extension
Subject 1	3.31 (6.12)	\	\
Subject 2	3.0 (10.26)	4.29 (12.85)	5.02 (11.66)
Subject 3	3.02 (6.85)	\	\
Subject 4	3.47 (9.23)	\	\
Subject 5	3.45 (13.1)	2.5 (6.45)	5.16 (13.59)

5.5.4 Limits of the study

Sensor accuracy and repeatability suffer from different sources of noise. The systems were attached differently, i.e. WSD uses a measuring unit fixed on two points for each neck movement, whereas RS uses four markers attached at different anatomical points on the upper body and three markers on the head. Each system can thus be influenced differently by soft tissue motion artefacts. Indeed, some errors may also come from the wearable sleeve sliding on the skin. Any skin-mounted sensor will likely suffer from soft-tissue artefacts, however, even without sliding error. Additionally, another limit to our process was due to the approximation of the neck joint radius *r*, which was not easy to quantify. It is important to underline that the sensor repeatability is also affected by the intra-subject variability.

However, the results of this study also provide evidence of the reliability of sensor placement using the chosen setup procedure. Another possible improvement of sensor performances could be obtained through a further study of different anatomical landmarks more suitable to achieve better results in terms of sensor accuracy and repeatability.

5. Biomedical application I

Considering the complete pool of presented results it is possible to confirm that WSD measurements are enough repeatable and accurate for the evaluation of single plane neck movements and good valid for the measurement of cervical ROM [230]. For this reason, it is expected to be especially useful in orthopaedics, rehabilitation and sports medicine. In this regard, to guarantee a long-term neck monitoring next study has been planned to improve the physical structure of our WSD (e.g using a neck band or turtleneck top) and to evaluate the complications related to wearability that will affect system performance. In addition, only healthy young participants were enrolled in this study. When measuring patients with neck disorders, neck deformities or shortenings of the neck may be exist. Future studies will be scheduled to characterize the system on a much larger sample size, including patients with neck disorders and elderly people.

Chapter 6

Biomedical application II: development and testing of a new cognitive technological tool for episodic memory

Studies about the potentialities of smart fabrics and sewing materials allow to design novel concepts adjustable for different aims. For instance, smart textiles can be employed to develop novel and manageable devices useful in clinical practice. These may be key elements to develop interactive platforms on which to base study and therapy protocols: fabrics intrinsic properties allow the achievement of light, soft and transportable products and the textile nature itself permits an easy integration in complex fabric prototypes.

In this Chapter, the development of a textile interactive device is described, proving the validity of the described materials in the manufacturing of efficient research instruments:

- a sensing tapestry useful for active aging exercises for elderly people, obtained in collaboration with the Clinic Neuropsychology Laboratory of Pontedera and the TIM Joint Open Laboratory (JOL WHITE) of Pisa.

This application employed conductive textiles just to perform touch detection, i.e. as human-machine interfaces, thus neglecting the pressure information.

6.1 Introduction

Coupled with a trend for low fertility rates and increased life expectancy—particularly in developed countries—the world is ageing rapidly. Today, almost 98 million Europeans (19.2% of the entire population) are aged 65 and over and will reach 150 million by 2080 (29.1% of the entire future population) [231]. Population ageing leads to increased

physiological reduction of some cognitive functions as well as physical function impairment [232]. Moreover, there will be more elderly people suffering from degenerative diseases, including dementia, impacting the ability of older adults to live safely and independently [233]. In this regard, there is a growing urgency to identify the most effective strategies to prevent cognitive decline [234]. There are currently no definitive pharmacological treatments able to improve symptoms or slow progression of dementia diseases [235]. Therefore, there is increased interest for cognitive training (CT) that is assumed to improve, or at least stabilize, performance in a given cognitive domain (i.e. near transfer effect). CT is based on the principles of neuronal plasticity and cognitive ability restoration, but also generalized effects beyond immediate training contexts are expected (i.e. far transfer effects) [236]. The most common approaches for CT use structured material for each function or cognitive process, usually administered through paper and pencil or, in recent years, computerized tools [237].

In recent years, to maximize the effect of such interventions, the interest to combine CT with a program of physical exercises is growing, in order to benefit from the synergistic impacts of the two typologies of training [238]. In this way, exercise training has led to improved executive functions, episodic memory, processing speed and other cognitive processes in older adults [239].

An important clarification concerns the typologies of the subject that, more than others, might take advantage of the aforementioned kind of intervention. CT and combined cognitive-physical training are based upon the principle of brain plasticity. For this reason, in order to exploit the treatment potential, subjects retaining a large range of cognitive capacities are considered perfect targets [240]. Therefore, several studies regarding CT and a combination of CT and physical exercise take into consideration subjects without full-blown disease. In particular, the main categories are represented by older adults and subjects suffering from mild cognitive impairment (MCI) [241][242]. MCI often represents an early stage of dementia [243]. MCI is a clinical condition characterized by objective slight deficits in one single domain (e.g. memory) or in multiple cognitive domains, which do not yet configure as overt dementia [244]. Its prevalence in the population aged 65 years or over has been estimated at 10% [245]. Between 16–41% of patients with MCI develop dementia within one year [246]. Therefore, early identification and management of MCI may help prevent further deterioration.

6. Biomedical application II

More recent studies have examined the efficacy of combined training formats such as pairing exercise and cognitive training, either in simultaneous and sequential formats [247][248][249]. For example, cognitive training followed by aerobic training in the same session produced significantly greater gains on executive functions and verbal episodic memory when compared to cognitive training alone [250]. Hiyamizu et al. [251] contrasted combined simultaneous training (strength and balance training plus cognitive tasks) with a pure physical training group and uncovered a significant advantage for the combined simultaneous training group. In [252], older adults simultaneously performed a verbal working memory test and a cardiovascular training session to improve cognitive and motor-cognitive dual task performance. Both multimodal and pure cognitive training groups showed the same degree of cognitive improvement, with the exception of a visual memory task, which improved more in the multimodal group.

Following such a research line, the main goal of the present study is to provide a tool for cognitive functions that take advantage of physical activity in the execution of the task. Specifically, this study aims to design and develop a new CT tool, called SmartTapestry, to combine physical exercise and a traditional cognitive test. In particular, the SmartTapestry tool involves the episodic memory domain, particularly vulnerable to decline in aging, while the exercise training is a physical one, which involves exercises for articulation, reinforcement and stretching of upper limbs. The characteristics of SmartTapestry will allow its utilization at home, reducing the presence of clinical staff, empowering the ecological aspect of the training and its potential frequency by reducing costs. Indeed, according to Tulving's theoretical paradigm regarding specificity of encoding [253], if patients perform the task in a more ecological and familiar environment, such as their own house, it could enhance the possibility of generalization. In addition, home-utilization could produce an intensification of session frequency, which is one of the most important aspects of cognitive rehabilitation [254].

The current study comprises two parts. The first aims at developing the SmartTapestry system, for physical and cognitive training. The second part involves evaluating the equivalence between a classical assessment instrument for episodic memory [255] and a parallel form of such exercises administered through SmartTapestry. Such equivalence will allow the use of SmartTapestry for rehabilitation purposes: a future study will determine whether SmartTapestry will improve the efficacy of training, taking advantage of the introduction of physical activity, in order to include SmartTapestry in a future rehabilitation

protocol performed at home. Before testing the efficacy of SmartTapestry as a CT tool, the present Chapter presents the instrument and demonstrates its effectiveness in stimulating the episodic memory domain by comparing scores obtained with SmartTapestry with those obtained by a standard paper-and-pencil test in a sample of 53 subjects. Additionally, since SmartTapestry was designed as an ecological tool to be used daily, the perceived usability is also evaluated.

6.2 Traditional test

The type of chosen test focuses on a specific cognitive function: episodic memory. Episodic memory loss is one of the most reported in the elderly [232]. We chose as a cognitive exercise the subtest Verbal Paired Associated (VPA) Learning Task of the Wechsler Memory Scale-Fourth Edition WMS-IV (Pearson Assessment 2009, 2010UK) [255]. The WMS-IV is an individually administered battery of tests, widely used to evaluate multiple aspects of memory in people aged 16–90. In particular, VPA is used for episodic memory assessment. The subtest comprises: (i) immediate recall subtest; (ii) delayed recall subtest; (iii) recognition subtest.

Immediate recall subtest: this subtest measures the immediate verbal memory of the associated word pairs. 14 or 10 word pairs are read to the subject (the WMS-IV provides an adult version and one for the elderly aged 65 and older). Later, the examiner reads the first word of each pair and asks the subject to recall the associated word. In the subtest, there are four versions of the same list of word pairs presented in a different order. The examiner will read these four versions and every time, after presenting each list, proceed to the recall (from here reported as *Imm1*, *Imm2*, *Imm3*, and *Imm4*). The raw score is the sum of the correct answers to the four versions.

Delayed recall subtest: this subtest is administered 20–30 minutes after the subtest Immediate recall condition. Deferred condition evaluates long-term memory for word pairs. The first word of each pair learned in the immediate condition is presented to the subject, who is asked to provide the associated word. The raw score is the sum of the correct answers.

Recognition subtest: this subtest must be given subsequent to the previous one. A list of word pairs is read to the subject, who are asked to identify each pair as one of those already

present in the previous subtest or as a new couple. The raw score is the sum of the correct answers.

6.3 SmartTapestry system

SmartTapestry is a sensorized tapestry, designed and developed in order to be used in a combined training protocol involving both physical and cognitive training.

Regarding the physical training, in elderly subjects many orthopaedic pathologies (osteoarthritis and impingement subacromiale) affect the shoulder joint, which often show a reduction in range of motion (ROM) and flexibility, particularly in flexion-extension and abduction movements [256]. Exercises for upper limbs help combat these pathologies if targeted to specific muscular reinforcement [257]. Specifically, the subject placed standing in front of the system will have to raise the upper limb to perform the exercise. This task involves flexion and rotation (internal and external) movements on the frontal plane. If the subject is placed as to have the side system, they can carry out the same exercise by performing abduction and rotation (external and internal) movements on the sagittal plane. For this purpose, SmartTapestry is 60 x 90 *cm* size so that any subject, at the front or side position, can touch any point of the system and the use of the upper limb within a medium ROM is required.

With respect to the cognitive exercise, SmartTapestry allows administration of the cognitive tasks described above with modalities that comprise an alternative with respect to traditional approaches (Figure 6.1). The elements that make up the system are the 21 Italian alphabet letters, which are the items that have to be recalled in the task, plus the 'yes' and 'no' answers used for the recognition subtest. The position of the letters in the tapestry are random and new for all subjects, and do not follow any provision already used commercially (i.e. QWERTY or alphabetical order). Each letter is 15 x 15 *cm* in size and the subject can select it with the open palm of the hand. In this way, letters can be also recognized by those who have modest presbyopia. As a result, the letters are arranged on a 4 x 6 matrix that guarantees the presence of at least 23 targets and respects the size required for the entire system (60 x 90 *cm*) and for each element (15 x 15 *cm*).

Therefore, SmartTapestry was designed with the following elements (Figure 6.2 and Figure 6.3):

- A sensitive base (60 x 90 *cm*) containing (Figure 6.2):
    - 24 sensitive elements obtained with a double sheet of conductive textile (Adhesive Conductive Fabric - ACF by Mindsets Ltd.) divided by a 1.5 *cm* thick foam layer (Figure 6.3 (a)). In correspondence with each unit, holes were driven into the foam for allowing contact of the two fabric layers in case of touch (the sensing units work as on–off switches);
    - Electronic hardware for data acquisition (Multifunction DAQ System NI USB-6218 by National Instruments), connected to the fabric patches with conductive threads sewn into the foam, and a USB connection to a laptop;

- Interchangeable layers to be placed above the sensitive base with Velcro hooks, containing the various targets of the exercises;

- A laptop with a custom LabVIEW graphic user interface to select the desired exercise (tests are administrated through the software) and acquire data from the tapestry (sequence of correct answers and total test score);

- A mobile support structure for the tapestry, able to adjust the height according to the subject's requirements.

6. Biomedical application II

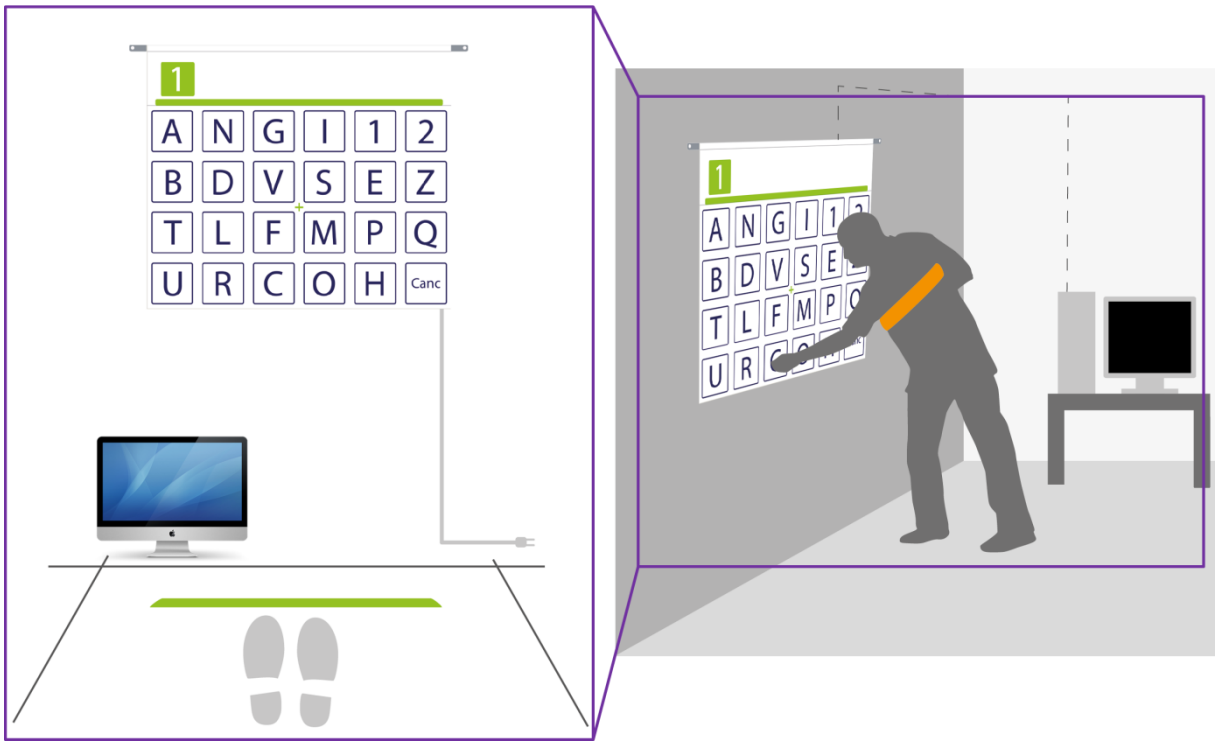

Figure 6.1 Concept of the SmartTapestry.

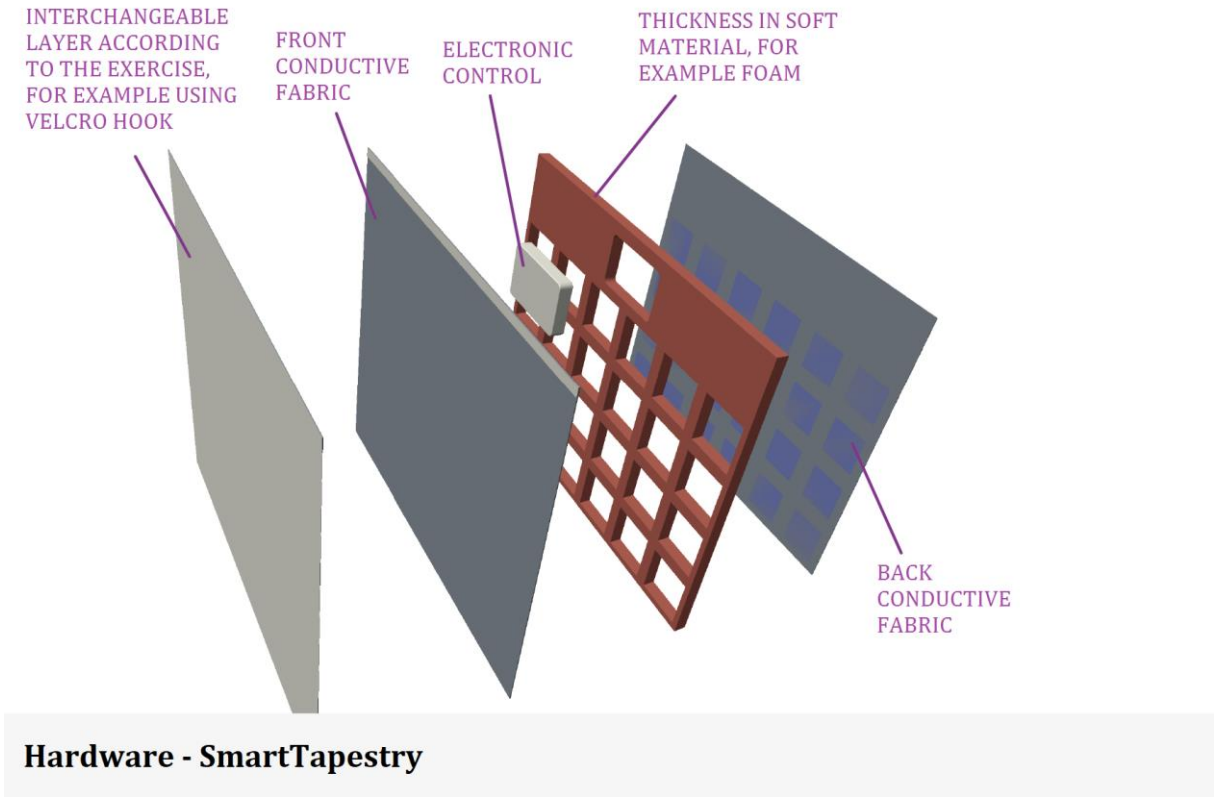

Figure 6.2 The soft layers composing the sensitive base.

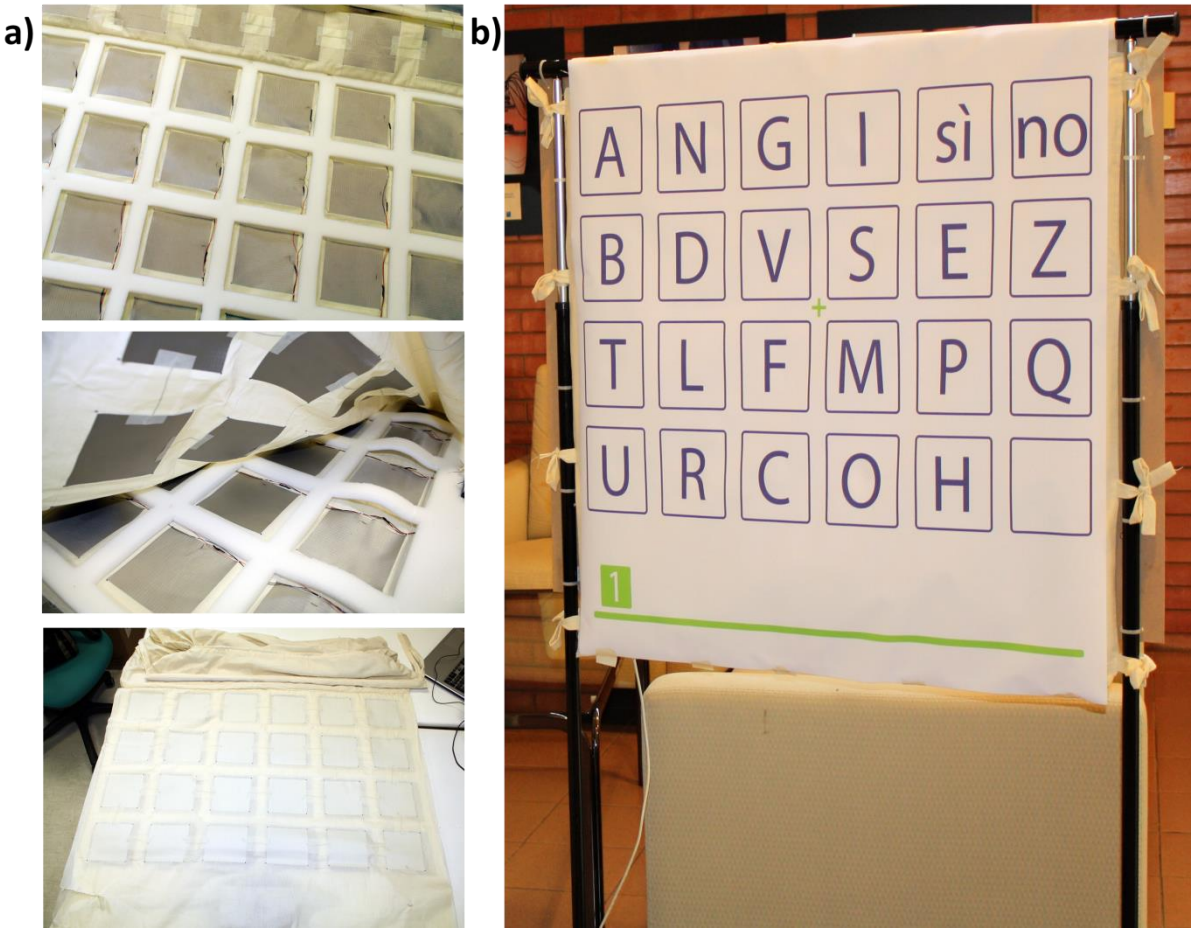

Figure 6.3 a) Development phases of the 24 sensing units in the soft base layer, and b) the SmartTapestry.

6.4 Participants

The recruitment was performed at the neuropsychological clinic of Pontedera (Italy), by means of the medical records of MCI outpatients starting from September 2014 until May 2017. The diagnosis for MCI was made according to Petersen criteria [244]; all examined subjects were also evaluated by a neurologist and underwent instrumental exams (TC, RMI). Subjects showing dementia or who were completely deficit incumbent so that they could not perform the activity were not included. After analyzing the medical records, we contacted by telephone a total of 144 subjects, among patients and their familiars, which met the general requirement criteria mentioned above (Figure 6.4).

Subsequently, further inclusion criteria of this study were verified by telephone: (i) ability to stand for one hour and a half without any help; (ii) right hand dominance; (iii) absence of hearing loss; (iv) absence of depression and other psychopathological issues; (v) absence of

other neuromotor impairment. Subjects with physical impairment were held if this impairment was able to be appropriately corrected with prosthesis (e.g. glasses or hearing aid). At the end of this preliminary screening, a total of 99 subjects confirmed inclusion criteria. 30 of them were deemed cognitively normal whereas, according to the medical records and as confirmed by telephone, the 69 remaining subjects were considered MCI (Figure 6.4).

Before starting the protocol, as a mental status exam to verify the inclusion criteria and document the MCI diagnosed, the battery of tests in the MODA [258] ('Milan Overall Dementia Assessment') was used. This retest was used during the first assessment to neutralize the risk that some MCI subjects become demented in the meantime. Then, to test the impairment in daily-life activities the 'Activities of Daily Living (ADL)' [259] and the 'Instrumental Activities of Daily Living (IADL)' [260] scales were used as another element to confirm the condition of MCI. Finally, in order to perfect the clinical judgment, neuropsychologists conducted a clinically structured interview. A total of 24 of the 69 subjects confirmed the MCI diagnosis, and the remainder were converted to dementia in the meantime. In addition, enrolled MCI subjects were classified as MCI type I (amnesic, single domain) and II (amnesic, multiple domain) =13, and MCI type III (non-amnesic, single domain) and IV (non-amnesic, multiple domain) =11, according to the diagnostic algorithm proposed by Peterson during the neuropsychology international symposium [261].

Nevertheless, one participant from the healthy cohort was excluded from the final dataset because not enough data were acquired to compute the output measures. Table 6.1 summarizes the demographic characteristics of the 53 people involved in the study: 24 people diagnosed with MCI and 29 healthy subjects (Figure 6.4).

Table 6.1 Description of Participants.

	Mean (SD) **All subjects**	**Mean (SD)** **Healthy**	**Mean (SD)** **MCI**
Men	27	14	13
Women	26	15	11
Age (years)	56.53 (21.34)	41.96 (16.91)	75.73 (4.91)
Education (years)	14.60 (3.83)	16.48 (2.82)	12.33 (3.70)

This Table reports the mean value and the Standard Deviation (SD) for the subjects involved in the study (53 participants).

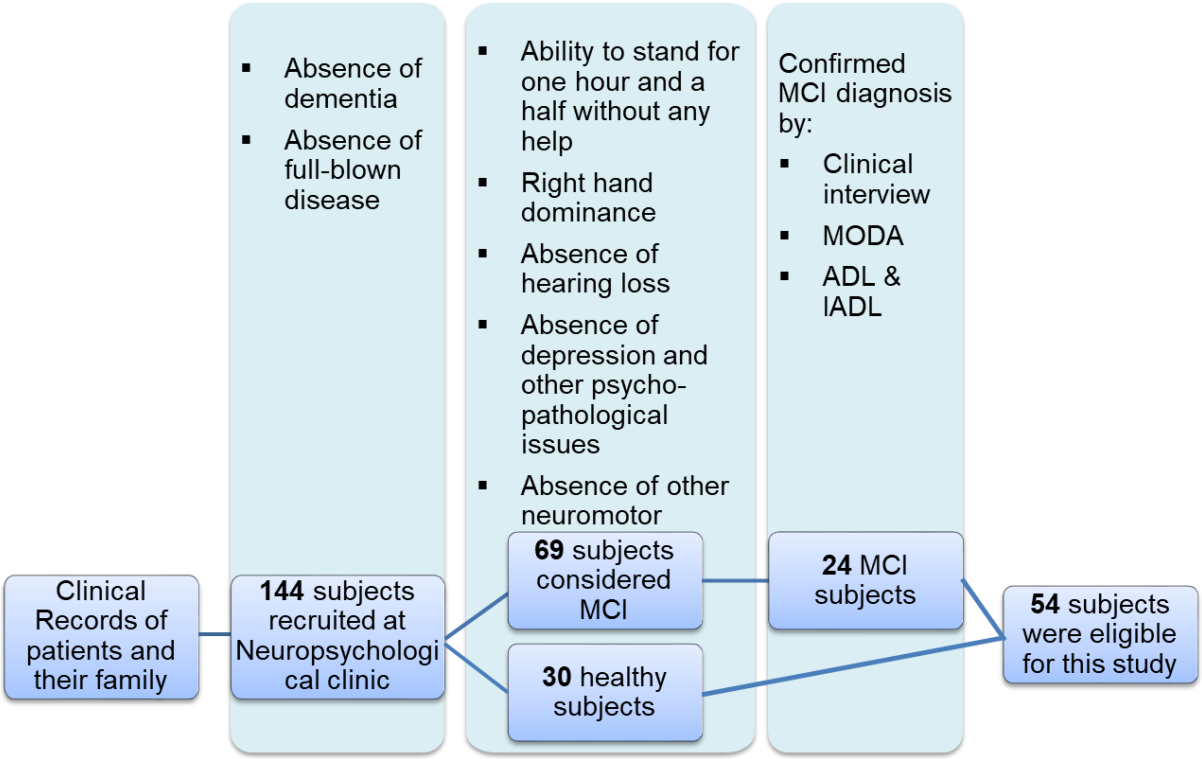

Figure 6.4 Recruitment process. A total of 144 subjects, among patients and familiars, which possibly met the general requirement were contacted by telephone. At the end of the recruitment process, the total group considered eligible for this study was 54 subjects.

6.5 Experimental protocol

Prior to testing, written informed consent was obtained from the participants. The study design and protocol, including subject privacy and sensitive data treatment, were approved by the Ethics Committee of the Scuola Superiore Sant'Anna, Pisa. All methods included in the protocol were carried out in accordance with the guidelines laid down in the Declaration of Helsinki.

All subjects performed both traditional cognitive tasks (TCT) and the parallel forms of these cognitive exercises administered through the SmartTapestry system. Each task session took approximately one hour, and was supervised by neuropsychologists and engineers in a laboratory setting. Half of the subjects performed before TCT and then SmartTapestry, half of the subjects vice versa. Each subject was randomly assigned to one of those designs.

During the traditional test, a neuropsychologist administrated the exercise as required by the traditional protocol whereas, during the SmartTapestry test, as soon as the participant was

ready, he/she pressed ‘start’ on the software module and thus the instructions were autonomously administered by SmartTapestry software. The instructions and the list of word pairs are provided by the software, while the subject has to type the remembered word by touching letters displayed on the tapestry (Figure 6.5). The data were acquired and stored by a computer.

At the end of the trial, the system usability scale (SUS) [262] was administered to participants in order to evaluate the perceived usability of the proposed system. The SUS is a survey instrument comprising ten items giving a global view of subjective assessments of usability. It is based on a 5-point Likert scale, (from ‘Strongly disagree’ to ‘Strongly agree’). It was developed according to the three usability criteria defined by the ISO 9241-11: (i) effectiveness, the ability of users to complete tasks using the system; (ii) efficiency, the resources expended by users to achieve goals; and (iii) satisfaction, the users’ subjective comfort using the system.

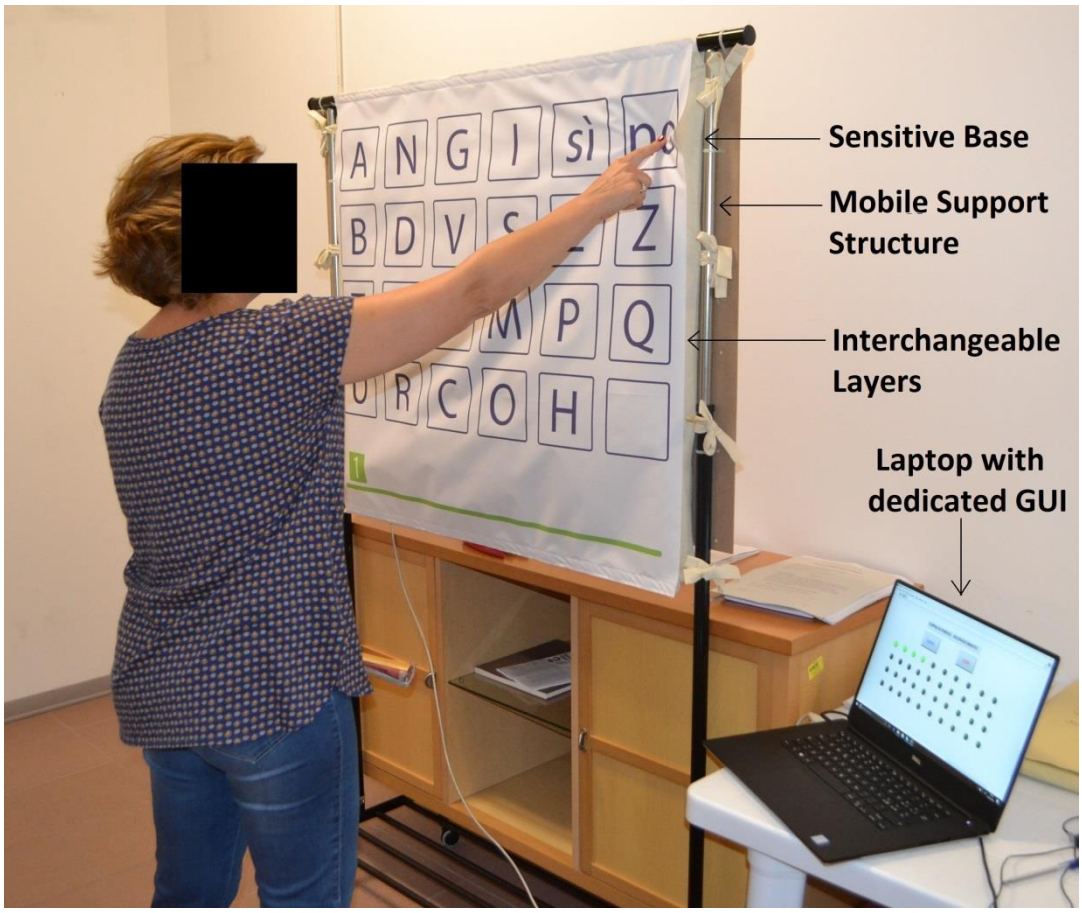

Figure 6.5 Participant performing the SmartTapestry test; on the bottom it is possible to notice the laptop with the LabVIEW graphic user interface for the test administration.

6.6 Comparison of the two tests

Raw scores of each test consisted of six signals: four immediate recall subtests, one delayed recall subtest and one recognition subtest. Considering the different numbers of associated word pairs administered to adults and elderly (14 and 10, respectively), raw scores were normalized with respect to the total number of associated word pairs. These were used for the data analysis that was performed offline using Matlab software (MathWorks Inc., Natick, MA, USA). Statistical analysis between the dataset related to the TCT and the other one related to the SmartTapestry approach was performed to reach the objective of this study. For each subtest, the normal distribution of the normalized raw scores was verified using the Kolmogorov-Smirnov normality test. Because all raw scores were not normally distributed, the Spearman (ρ) correlation coefficient was used to evaluate the relation between the different approaches on the entire sample (53 participants). In addition, to investigate similarity in the performances of the SmartTapestry test between the two cohorts (MCI vs healthy subjects) and between the two MCI groups (type I and II vs type III and IV), a Mann-Whitney u-test for non-parametric independent variables was carried out. The alpha level of significance was set to 0.05 for all statistical tests.

After completion, each SUS item's score contribution ranged from 0 to 4. For positively worded items (1, 3, 5, 7 and 9), the score contribution is the scale position minus 1. For negatively worded items (2, 4, 6, 8 and 10), it is 5 minus the scale position. To obtain the overall SUS score, the sum of the item score contributions was multiplied by 2.5. Thus, SUS scores range from 0 to 100 in 2.5-point increments. Finally, the Mann- Whitney and the Kruskal-Wallis tests were applied to SUS results in order to compare different conditions or users.

6.7 Results and discussions

The main objective of the present study was to demonstrate the effectiveness of SmartTapestry in stimulating the episodic memory domain by comparing scores obtained with SmartTapestry with those obtained by a standard paper-and-pencil test in a sample of 53 subjects (29 healthy and 24 MCI).

6. Biomedical application II

The statistics with respect to the performed performance for the entire sample in the two tests is reported in Table 6.2. Spearman coefficients between the TCT and SmartTapestry are reported together with the relevant p-value. According to [263], in neuropsychology correlation coefficients between 0.35 and 0.50 indicate good correlation, whereas correlation coefficients higher than 0.50 indicate excellent correlation. According to the results, strong positive correlations were obtained for all exercises ($p < 0.005$), which means that both instruments are substantially equivalent in the stimulation of episodic memory (Table 6.2).

Another important goal of this work was to investigate whether the two cohorts had different performance. The results of the Mann-Whitney test are also reported in Table 6.2. These results underline a significant difference ($p < 0.005$) in the performance of the SmartTapestry test between healthy and MCI subjects for all exercises, which confirms that the test is able to detect the differences in the cognitive abilities of the subjects.

Table 6.2 Spearman Correlation and Mann-Whitney Test.

	Imm1	Imm2	Imm3	Imm4	Delayed	Recog.
ρ*	0.4265	0.5233	0.6018	0.7484	0.7601	0.5247
p*	1.5E-03	5.8E-05	1.9E-06	1.2E-10	4.1E-11	5.5E-05
p**	1.9E-03	3.2E-06	3.6E-08	7.2E-09	4.7E-08	2.0E-07

*Spearman correlation coefficients (TCT/SmartTapestry)

**Mann-Whitney U independent sample tests (MCI/Healthy - SmartTapestry)

These results are also highlighted in the scatter plot of Figure 6.6 between the two tests, where the red stars represent the healthy subjects and the blue circles represent the MCI subjects. It can be clearly observed that MCI subjects have lower performance compared to healthy subjects (Table 6.3). It is also important to notice in the scatter plot that the two cohorts seem to be increasingly grouped as that the exercises are performed according with the SmartTapestry performance. We could hypothesize that this result might be due to the MCI condition itself or because MCI subjects are generally older than other experimental subjects. These findings are aligned with the most recent results in this area; indeed, both age and MCI condition lead to physiological decline of all executive functions [264].

6. Biomedical application II

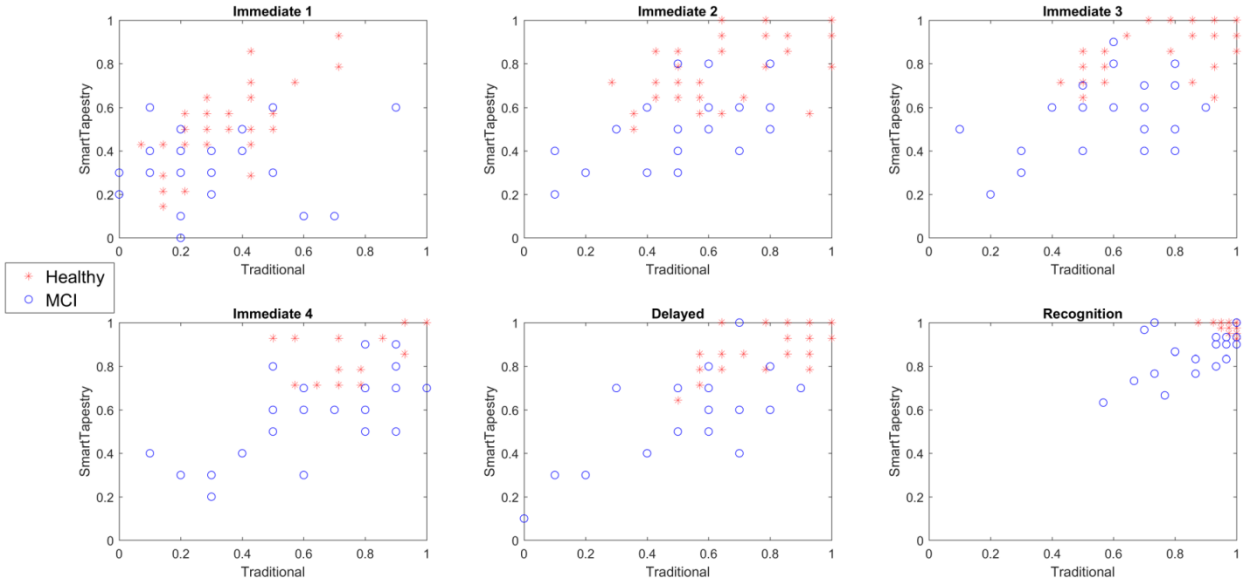

Figure 6.6 Scatter plot of normalized correct answers between traditional administration and SmartTapestry in immediate, delayed and recognition subtests. Red stars are healthy subjects the blue circles are MCI subjects.

Analyzing the differences between the two tests in the entire sample, it can be seen that the scores obtained with the SmartTapestry tool are higher to those obtained with TCT (Table 6.3 and Figure 6.7), despite the two sets of scores being significantly correlated.

Additionally, the analysis of the two cohorts separately shows that the scores obtained with the two tests follow different trends. Healthy subjects achieved higher scores with SmartTapestry compared to TCT in all subtests (Table 6.3 and Figure 6.7). These results can suggest facilitation in the memory performance may be due to the multiple nature of the mnemonic trace: the SmartTapestry task involves auditory (the auditory track repeating the list of words), visual-spatial (the position of the letters in the tapestry) and kinaesthetic information (the movements of the arms needed to press the letters in the tapestry). In fact, the subject has both to remember the associated word and press it on the tapestry, and this may help in cognitive consolidation for the added visual search strategy. In addition, this trend could be explained by the presence of a potential motivating factor. The technological nature of the device may lead the subject to enhance their attention during the training with SmartTapestry, with satisfactory results.

In contrast, MCI subjects obtained higher score in *Imm2*, *Imm3* and *Imm4* subtests administered with TCT compared to SmartTapestry (Table 6.3 and Figure 6.7). This might be

explained by a greater request, in terms of cognitive resources, during the execution of the task using SmartTapestry. In fact, SmartTapestry demands the subject to process information in two ways, both verbal and visual. Moreover, for the task accomplishment, the subject has to organize a motor plan and put in place a visual search. This result is aligned with the literature [265], which underlines that the addition of a motor task during the execution of a cognitive task causes a worse performance in elderly subjects. Contents listed might lead a subject with reduced cognitive resources, as is the case for MCI subjects, to develop weariness more quickly and perform worse in immediate memory subtests. Regarding the delayed subtest, the score obtained with SmartTapestry is higher compared to TCT (0.5667 and 0.5333, respectively). This improvement can be explained by the mechanisms of implicit memory, recruited by the motor part of the task. The output channel for the response, using SmartTapestry system, in fact, impose that the subject pushes some part of the tapestry, where letters are printed, so to form the right word. The repetition of this task could recruit neural networks involved in implicit memory. The combined effects of explicit and implicit memory allow MCI subjects to recall in the delayed condition during the SmartTapestry test, which is better than during TCT.

Concerning the *Recognition* subtest, healthy and MCI subjects showed comparable performance in the two types of administration (Table 6.3 and Figure 6.7). Such results can be explained by the nature of the task, based on similar cognitive mechanisms and on a 'yes-no' paradigm.

Table 6.3 Mean value of normalized correct answers for immediate, delayed and recognition subtests.

Mean Value		Imm1	Imm2	Imm3	Imm4	Delayed	Recognition
All subjects	**SmartTapestry**	0.4272	0.6437	0.7229	0.7606	0.7526	0.9325
	TCT	0.3081	0.5895	0.6941	0.7434	0.6916	0.9358
Healthy	**SmartTapestry**	0.5049	0.7660	0.8695	0.9212	0.9064	0.9871
	TCT	0.3251	0.6429	0.7857	0.8448	0.8227	0.9828
MCI	**SmartTapestry**	0.3333	0.4958	0.5458	0.5667	0.5667	0.8667
	TCT	0.2875	0.5250	0.5833	0.6208	0.5333	0.8792

6. Biomedical application II

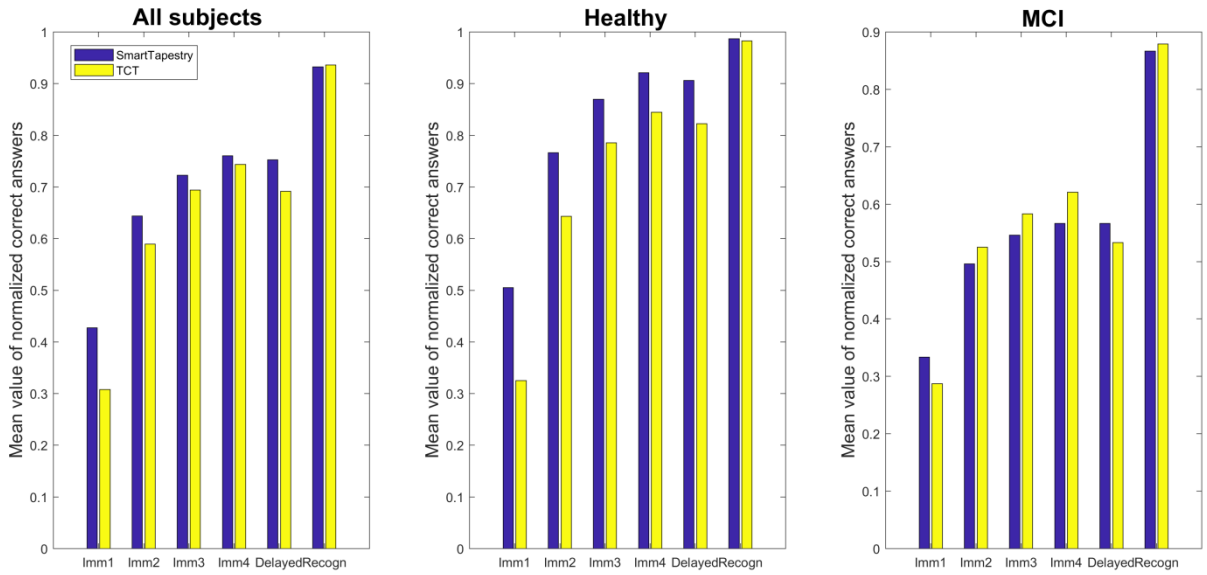

Figure 6.7 Mean value of normalized correct answers for immediate, delayed and recognition subtests in all subjects (left panel), healthy (centre panel) and MCI (right panel) subjects.

Analyzing the two groups of MCI subjects with diagnosis of type I and II and MCI subjects with diagnosis of type III and IV (Table 6.4 and Figure 6.8), it is possible to observe significant differences ($p < 0.05$) in the performance of the SmartTapestry test between amnesic and non-amnesic MCI in all the conditions with the exception of the first immediate recall task and the recognition task. These findings are in line with our expectations, in fact they reflect the amnesic MCI's (MCI I and II) consolidation process deficits as compared to non-amnesic MCI (MCI III and IV) [266]. In addition, MCI subjects with diagnosis of type III and IV achieved higher scores in all subtests compared to MCI subjects with a diagnosis of type I and II.

SmartTapestry was designed to be an ecological sensorized tool able to combine a traditional test for episodic memory with physical activity. This can lead to a set of mixed tools which can be used daily at home, reducing the presence of clinical staff, to train at the same time the brain and the body so as to improve the cognitive treatments efficacy [267]. In this framework, our CT tool has the capability to perform cognitive and physical training for the user at home, in particular for MCI subjects that are at risk of conversion to dementia. Furthermore, another important aspect is that neuropsychologists can plan personalized training which involve face-to-face and at-home treatments. Therefore, it is important to demonstrate not only the efficacy of the tool from a clinical point of view, but also the

influence of the use of our technology in real life in terms of efficacy, efficiency and usability [268].

Table 6.4 Mean value of normalized correct answers and Mann-Whitney Tests between two groups of MCI subjects.

SmartTapestry Mean Value	Imm1	Imm2	Imm3	Imm4	Delayed	Recognition
MCI Type I and II	0.30	0.4231	0.4692	0.4692	0.4692	0.8359
MCI Type III and IV	0.3727	0.5818	0.6364	0.6818	0.6818	0.9030
p*	0.2991	0.0355	0.0198	0.0063	0.0138	0.2535

*Mann-Whitney U independent sample tests (MCI type I and II vs MCI type III and IV)

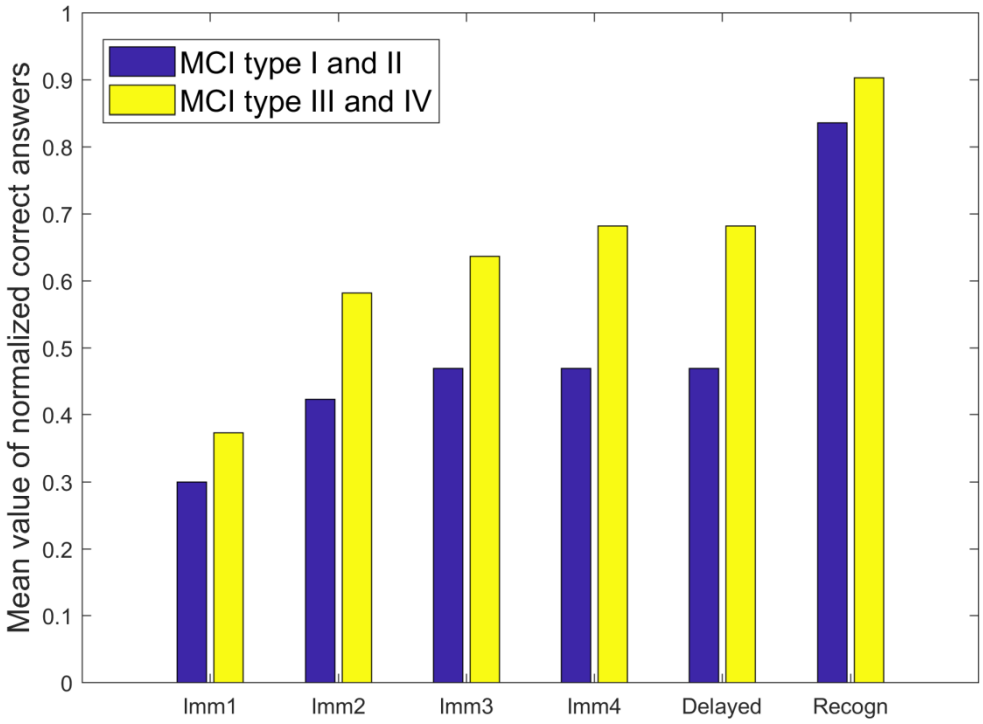

Figure 6.8 Mean value of normalized correct answers between two groups of MCI subjects for SmartTapestry test.

6. Biomedical application II

According to Bangor et al. [269], a SUS score higher than 70 indicates a usable product, and higher than 90 a very usable one. In terms of usability, the examined results show that the SmartTapestry approach is well evaluated (84.34±12.13) by participants. In particular it was found to be not usable for five volunteers (58.50±7.83), usable for 21 of them (78.33±5.44) and excellent for 27 participants (93.80±3.42).

In Table 6.5, descriptive statistics are reported and the results show that the odd-numbered items have a mean value higher than 4 and a mode value equal to 5, except for *Item1*. On the other hand, the even-numbered items have a mean value lower than 2 and a mode value equal to 1.

Regarding users' perceived satisfaction using the SmartTapestry system, the results are positive because 56.60% of the sample would like to use the SmartTapestry system frequently (*Item1*). In particular, the percentage increases to 66.67%, considering MCI participants who could gain the most benefit from the proposed system in the future.

The proposed system was also perceived as being easy to use because 43 participants gave a score of 4 to 5 to *Item3*. However, participants suffering from MCI (3.83±1.20) thought the SmartTapestry system was less easy to use then healthy ones did (4.48±0.99) (*Item3* p = 0.030). To confirm this, MCI subjects (2.38±1.44) considered that they would need the support of a technical person to be able to use this system more than healthy ones did (1.55±0.95) (*Item4* p = 0.024). This difference between MCI and healthy participants could be explained by the difference in age between the two cohorts and by the fact that MCI subjects have greater learning difficulties.

The SmartTapestry approach was perceived as efficient because 48 persons found the various functions in this system to be well integrated (*Item5*) and no participants thought there was excessive inconsistency in this system (*Item6*).

Gender was found to significantly impact overall SUS scores and this might be related to the hypothesis that women in general are more health conscious [270]. In particular, women (87.50±11.83) gave the SmartTapestry system an overall SUS score higher than men did (81.30±11.84) (p = 0.023).

However, considering only the male sample, male participants suffering from MCI (92.17±4.90) gave the SmartTapestry system an overall SUS score higher than healthy ones

did (82.86±10.96) (p = 0.021), evaluating the proposed system as being more usable because ill users tend to be more health conscious.

Regarding the impact of age, subjects aged 65–75 years (74.15±15.47) gave the SmartTapestry system an overall SUS score lower than those aged 31–55 (93.18±4.48) (p = 0.019). Indeed, age influenced the overall SUS score because elderly users typically have a less positive attitude towards technology [271].

Table 6.5 SUS results.

Item	Question	Mean	SD	Mode
Item1	I think that I would like to use SmartTapestry frequently	3.64	1.23	3
Item2	I found SmartTapestry unnecessarily complex	1.68	1.11	1
Item3	I thought the SmartTapestry tool was easy to use	4.19	1.13	5
Item4	I think that I would need the support of a technical person to be able to use SmartTapestry	1.92	1.25	1
Item5	I found that the various functions in this system were well integrated	4.58	0.72	5
Item6	I thought that there was too much inconsistency in SmartTapestry tool	1.32	0.64	1
Item7	I would image that most people would learn to use SmartTapestry very quickly	4.47	0.85	5
Item8	I found SmartTapestry very cumbersome to use	1.36	0.81	1
Item9	I felt very confident using SmartTapestry	4.49	0.85	5
Item10	I needed to learn a lot of things before I could get going with SmartTapestry	1.36	0.83	1

Considering all of the above, it is reasonable to state that SmartTapestry has a high degree of usability, underlining participants' willingness to use the SmartTapestry tools in their daily routine.

6.8 A case report

This section reports a case study about the use of the SmartTapestry tool. The main purpose of this section is to investigate the peculiarities, in terms on cognitive performances and process, bring out from a careful observation of the subject's behaviour during the use of the SmartTapestry system.

The final purpose of the entire study, in fact, is also to outline the future applications of this new CT tool with elderly people and subjects suffering MCI. For this reason, it was decided to study in details how a healthy subject and an MCI subject use the system and which supports and which difficulties he/she meet in their use. In particular, the purpose of this study is to highlight the information achievable from the use of this instrument with single subjects. The choice of case report form derives from the necessity to study in detail the functioning of the instrument with subjects which have specifics needs, strengths and weakness. In this perspective, the study has the intention to highlight the clinical hints that could be glimpsed from singles cases.

The subjects selected for the case report are one healthy elderly subject and a subjects whom is suffering from MCI. In the two following boxes are reported information about the two chosen subjects. In the case of the subject suffering from MCI also a short medical report was presented.

6. Biomedical application II

Anamnesis D. P.

The participant D. P. is a 63 year-old Caucasian woman. She attended 8 years of school and had reported to the experimenter to be in full neuropsychological and medical health. The subject reported to never have experience of psychiatric disorders, such as mood alterations or anxiety. Moreover, the subject does not believe to forget things, in a suspect way, in the last period or to go towards changing in her way to think. The subject is oriented, aware, collaborate, and with full insight. Considered all the aspects listed above, it was decided to consider the subject D. P. as the *control subject*.

Anamnesis M. R.

The participant M. R. is a 70 year-old Caucasian woman with a diagnosis of MCI. She had several cognitive and behavioural limitation based on neuropsychological assessment, neurological examination and instrumental exams (TC and echo-Doppler). Mrs. M. R. reported that since a couple of years suffer from episodic anterial-grade memory issues. These problems began in a subtle manner and got worse over time. In fact, she referred that 1 year after the memory impairment begins she had experienced an episode of topographic disorientation, coming back home from the dentist. In the meanwhile, it started also absent-minded episode. In the last 3-4 months the memory problems are getting worse and for this reason, the subject decided to turn to a neurologist. Moreover, simultaneously with the memory deterioration, M. R. started to show some behavioural changes, such as initial insomnia, negative thoughts, irritability, mild agitation and amotivational syndrome. In relation to these symptoms, the subject was treated for two months with Zoloft, Samyr, and Illumina, prescribed by the neurologist. As result of an interview about her relatives was been reported that in her father's family branch there were been two cases of Alzheimer's disease. In general, there were not referred cases of mood disorder or depression among family members.

The neurologist assessment and the instrumental exams reported a couple of newsworthy parameters: an enlargement of apical liquor system and a carotid siphons calcification. A complete neuropsychological assessment was prescribed to avoid misdiagnosis, between MCI and depression, and clarify the case. During the neuropsychological assessment the subject appears vigilant, collaborative and with full insight. The assessment consisted of a

comprehensive battery of neuropsychological tests, such as Milan Overall Dementia Assessment (MODA); Wechsler Memory Scale IV (WMS-IV); prospective memory task of Rivermead Behavioural Memory Test (RBMT); Attentional Matrix; Stroop Test; Trail Making Test A and B; Boston Naming Test (BNT); Street Test; Birmingham Object Recognition Battery; Brixton Test; Tower of London Test; Verbal Judgments Test. Based on the performance shown during the neuropsychological assessment was formulated the following clinical opinion: the subject shown a global cognitive functioning peaceable at inferior limit of normality. The study of Memory domain depict a weakening of visuospatial information treatment in all the dimension (short-term, long-term, working memory), but the global performance deposes against a true amnesia. The testing of attentional skills describes a selective impairment on dual task, in part attributed to anxiety. The deep study of executive functioning shows a planning skill inefficiency and conceptual elaboration weakness of verbal material.

6.8.1 Results and discussions

In this subsection, results of the two selected subjects on the two aforementioned cognitive tests (Verbal Paired Associated and SmartTapestry system) are reported. Therefore, in Table 6.6 are reported the results of the two test used to probe the functioning of memory domain, in particular, the episodic component of long-term memory. For the assessment of this neurocognitive skills, as previously explained, are generally used two parallel forms of the test, according to the subject age. People under 65 years old are put through on a test composed of 14 pairs of words to remember. On the other side, people over 65 years old are put through on a test composed of 10 pairs of words to remember. So to may compare the results of the two subjects, a normalization based on the maximum score was done. In this way, all the subjects have a range of possible score from 1 to 10 for the subtest: *Imm1*, *Imm2*, *Imm3*, *Imm4* and *Delayed*. And a range of possible scores from 0 to 30 for the *Recognition* subtest.

As previously explained, it is required to carry out an auditory-verbal memory task using a sensorized tapestry to deliver the response. This tapestry is thought to stimulate the use of upper limbs, in particular, to encourage the shoulder girdle mobilization during this cognitive task. In fact, as reported in Table 6.6, the clinical subject shows lower scores in all the sub-tests with SmartTapestry system, as compared to the healthy subject. Moreover, the control

subject seems to be facilitated in the tasks using the smart tools systems, indeed the results accomplished with the traditional form of the exercise are lower if compared to the results achieved with the smart system. As mentioned previously, this could be explained by the multimodal nature of the exercise [272]. In fact, the task include verbal information that the subject must remember, but also a visual support, provided by the SmartTapestry, used to emit the response. So the information undergoes to two kinds of treatment, first as verbal information, then as visual information. This multiple treatments of the mnemonic trace could be the reason why the control subjects is facilitated by the use of SmartTapestry system [272]. These results are aligned with those previously shown in Section 6.7.

On the other hand, the subject suffering from MCI obtained essentially the same results using traditional and new approach. In particular, she achieved higher score in *Imm1*, *Imm3* and *Delayed* subtests administered with SmartTapestry compared to traditional approach, and comparable score in *Imm2* and *Imm4*. Whereas, for the *Recognition* subtests, she achieved an higher score with traditional approach. This result follows the previously results obtained with a sample of 24 MCI subjects. But it also highlight as in this particular case, the clinical subject shows an improving about the majority of the performance using this new approach, as compared to the traditional test. This could be explained by the clinical history of the subject, which didn't show a true amnesia. In addition, during the neuropsychological assessment the subject appeared vigilant, collaborative and with full insight. She did not let it scare by the technological nature of the device, on the contrary, she has allowed herself to be transported more by the potential motivating factor, obtaining satisfactory results.

Also this case study confirm that the instrument is able to properly discern between a healthy subject and a subject suffering from MCI. In addition, the SmartTapestry system has proved to be useful also for people with MCI, enhancing the ability to encode, store and retrieval the information provided, at the same time, the possibility to do some exercise.

Table 6.6 Subjects' results for SmartTapestry tests.

Test Results	Clinical subject	Control subject
Verbal Paired Associated Imm1	0	1
Verbal Paired Associated Imm2	6	5
Verbal Paired Associated Imm3	4	6
Verbal Paired Associated Imm4	6	8
Verbal Paired Associated Delayed	5	5
Verbal Paired Associated Recognition	30	28
SmartTapestry system Imm1	3	4
SmartTapestry system Imm2	6	9
SmartTapestry system Imm3	6	8
SmartTapestry system Imm4	6	8
SmartTapestry system Delayed	7	6
SmartTapestry system Recognition	27	30

6.9 Concluding remarks

The aim of this work is twofold. Firstly, it aims to design an innovative “ecological” tool able to combine cognitive exercise with physical activity, in order to obtain the best benefits from the cognitive rehabilitation training and the physical exercise. The other goal of this feasibility study is to compare the traditional subtest with our SmartTapestry tool that includes physical activity.

The results suggest a good correlation between the two approaches. Such findings suggested that the instrument could be comparable in stimulating the episodic memory. Furthermore, the multimodal approach (auditive-visual-kinaesthetic) may improve subjects' performance. The high usability score underlines the participants’ willingness to use the SmartTapestry tools in their daily routine. This could be crucial for a new rehabilitation strategy and both MCI and healthy subjects could benefit from such a program.

Moreover, thanks to this design, the new cognitive tool can be customized according to elderly needs and can be easily integrated at home. In particular, in this study, we investigate the episodic memory domain, as an example; however, future improvement of the tool could include in the study other cognitive domains combined with physical exercise. Moreover, further improvement of the study should include also the analysis of upper limb movements while performing SmartTapestry test.

In addition, on the basis of this preliminary study and with the purpose to investigate the potential use of SmartTapestry as a rehabilitation tool, we believe it necessary to improve this study by analyzing the efficacy of this new CT tool within the MCI and healthy elderly populations matched by age, in order to assess how differences in cognitive performance could interfere with the task. In addition, future analyses should include the CT with different cognitive domain and exercise training, with the aim of creating a complete and efficient home rehabilitation tool.

As a conclusion, also with this application, smart textiles resulted a winning choice to develop innovative, economic and manageable devices useful in clinical practice.

Conclusions

Pressure mapping and strain detection are very often required in a huge number of practical situations regarding biomedical measurements, human motion detection, human-machine interfaces, and soft robotics. In particular, the use of sensors showing properties of flexibility and stretchability is increasing, therefore new and smart sensing solutions are widely matter of research. Smart textiles represent a valid opportunity to develop new concepts for transducers and sensors, and studies regarding their potentialities of employment deserve rising attention. In this perspective, the present thesis aimed to study the potentialities of the emerging class of textile sensors for strain and pressure detection. These sensors exhibit a wide selection of advantages as thinness, lightness, flexibility, stretchability and wearability. Such properties suggest their use in a huge number of applications, especially concerning the biomedical field.

The first study of the thesis regarded the design, development and characterization of a rectangular-shaped textile matrix sensor, assembled by sandwiching a piezoresistive fabric sheet between two outer fabric layers embedding conductive rows and columns. The location of the applied pressure can be identified by detecting the position where the change of resistances occurs between the external conductive paths. The sensor structure, its electrical circuit and characteristics were described in detail, after studying both the integration levels of the hierarchical structure and the composition of the piezoresistive fabric sheet. The readout circuit was developed considering the grounding theories for crosstalk avoidance and the electronics was compact and featured by a low powering voltage, so that the possible development of a wireless communication module can be easily envisaged to improve usability. The pressure measurement range and the calibration curve were studied by tuning circuital parameters. Repeatability, time drift, temperature dependence, SNR (signal-to-noise ratio) and dynamic response were analyzed. Novel tests were employed to consider the sensor sensitivity to stretch, shear force and surface curvature. A special analysis was taken over hysteresis and dynamic accuracy, focusing on a possible compensating solution. Results indicated that the system provides overall good quality performances with the main drawback of a limited dynamic accuracy, typical of piezoresistive sensing elements. Nevertheless, fabric

sensors are robust, cheap, easy-to-use and employable to cover large area three dimensional surfaces. In addition, this first study provided valuable insights on the design issues and performances of piezoresistive textile pressure sensors, and in particular on their strengths and limitations.

The second part of the present thesis regarded the description of a piezoresistive textile strain sensor with the analysis of its metrological properties for both static and dynamic measurement conditions and its possible application as wearable goniometer for joint angle measurements. Also for this textile sensor, the electrical circuit and sensor characteristics were described in detail, after studying both the integration levels of the hierarchical structure and the composition of the piezoresistive fabric. The main result was the introduction of a general approach that can be used for the assessment of the electro-mechanical properties of a piezoresistive conductive textile, applied as a stretch sensor. This approach is easy to follow and could be employed for other textile strain sensors for their design, characterization and optimization (e.g. the pre-stretching that increases accuracy and repeatability). The methodology could be applied to other elastic and conductive materials, with different properties, to describe their behaviour. In addition, a skin-mounted sensor for joint angle measurement was developed. The wearable goniometer made of Electrolycra is simple, light, low-cost and did not limit the joint's range of motion. The validation results on the human subject were not yet quantitative, but promising. The dynamic tests obtained using the SABIAN robot confirmed that the developed device is capable of tracking joint movements. Even though the RMSE was not negligible, the sensor signal still provided sufficient motion measurement capabilities that could be useful for specific applications.

The developed device was an example of the application of Electrolycra to monitor human joint movements. However, being intrinsically nonlinear, the signals measured from this device need some processing, in order to increase its sensing accuracy. Therefore, an improvement of the sensor performance has been necessary for the compensation of the main distortions intrinsic to this sensor, which are mainly caused by hysteresis and relaxation.

To this aim, a novel model (APL) has been proposed, able to reproduce the rate-dependent hysteresis of a piezoresistive textile (Electrolycra). The model has been derived from the power-law (PL) model, suitable for piezoelectric actuators, which also exhibit rate-dependent hysteresis, but with remarkable differences. The APL model has been validated on 13 datasets (only 5 of them have been exploited to identify the model parameters) comprising

measurements of strain and resistance, in three completely different scenarios. For the model validation also a robotic application was chosen, by using the humanoid robot iCub able to perform aperiodic movements that simulate the natural human elbow movements. The APL model provided a good hysteresis compensation performance even with a small calibration dataset. These results confirmed that an adequate processing can enhance the sensor performances in case of dynamic measurements, without a prior knowledge of the strain rate typical for a particular application, extending its general applicability. Moreover, since hysteresis is caused by the intrinsic mechanical properties of the elastic material (that requires longer recovery time) the approach can be extended to all the sensors which are based on elastomer deformations and present rate-dependent hysteresis to improve their estimation performance. Analogously to the PL model, also the APL model is suitable for implementation on digital devices, making it suitable for a real-time estimation of the textile strain, given the measurement of its electrical resistance. This allows to develop accurate strain sensors based on piezoresistive textile. The development of APL model also adds relevant results to the wearable technologies field. In particular, a correct estimation of the strain for wearable flexible sensors is of a paramount important for joint angle measurements, posture monitoring, motion patterns recognition, and so forth. For this reason, it is expected to be especially useful for real-time continuous measurement without influencing the wearer's activity.

The use of textiles allows the manufacturing of lightweight, wearable, washable, thin and stretchable sensors. The wide characterization reported here could provide precious guidelines to help researchers and users in taking advantages from all of these benefits, supporting them in choosing the best sensor design and application.

In the remaining part of the thesis, the employment of fabric sensors was investigated into two different biomedical contexts, tailoring the sensor design phases to the specific requirements.

The first biomedical application concerned the development of an innovative wearable sensor device (WSD) based on conductive textile sensors for tracking cervical head movement. Electrolycra was selected as the sensing element because it is elastic, highly conductive, low cost, light and not cumbersome, and also thanks to its features previously studied. The first result of this study was the characterization of the conductive textile to determine its electro-mechanical behaviour and its calibration curve. The second result was

the use of Electrolycra as a strain sensor combined with Kinesio Tape to develop a WSD that allowed continuous measurement without influencing the wearer's activity, following the "wear and forget" concept. Among the other characteristics, our WSD is non-invasive, easy to use, inexpensive and it offers the possibility of measurements outside of the laboratory setting. In the third phase of our investigation, the active head range of motion (ROM) was measured in a group of healthy young man and women to validate the WSD by comparison with a non-invasive optoelectronic instrument. The level of concordance for the angle patterns with the reference system (RS) was acceptable and low differences in the measured angle were observed compared to the RS. The WSD can be used with a greater confidence to assess an individual's single plane neck motion in clinical situations and in daily activities. Therefore, further research is required to evaluate the system's ability to measure neck-paired movements. The results also suggested that WSD measurements were enough repeatable and accurate for the evaluation of single plane neck movements and good valid for the measurement of cervical ROM. For this reason, it is expected to be especially useful in orthopaedics, rehabilitation and sports medicine. In this regard, to guarantee a long-term neck monitoring next study has been planned to improve the physical structure of our WSD (e.g using a neck band or turtleneck top) and to evaluate the complications related to wearability that will affect system performance.

The last biomedical application regarded the cognitive training (CT), which is defined as guided practice on a set of standard tasks designed to stimulate particular cognitive functions. Smart textiles were still involved in the project, but a different design was studied to develop an interactive interfaces relied on conductive fabrics to perform touch detection without pressure measurement. The aim of this feasibility study was twofold. Firstly, it aimed to develop a new cognitive 'ecological' tool, called SmartTapestry, which allows the administration of standardized psychometric tests with modalities that are alternative respect to tradition. The novelty of the system is that it was designed to require a commitment to the subject both on the cognitive (memory in relation to the reference standardized tests) and on that motor side (upper limb articulation movement). The second goal aimed to compare the traditional subtest with our SmartTapestry system that includes physical activity. The results of our comparison underlined that the SmartTapestry approaches could be used to stimulate episodic memory. Furthermore, the multimodal approach (auditive-visual-kinaesthetic) may improve subjects' performance. This could be crucial for a new rehabilitation strategy and both MCI and healthy subjects could benefit from such a program. Moreover, thanks to this

design, the new cognitive tool can be customized according to elderly needs and can be easily integrated at home. In this study, SmartTapestry was tested for a particular cognitive domain (episodic memory), but for the design of the device, other cognitive domains could also be easily investigated. The results of this study may be useful in designing ecological and combined cognitive-physical tools, which can be used daily at home, reducing the presence of clinical staff, to train at the same time the brain and the body so as to improve the cognitive treatments efficacy. In addition, this study also confirmed that smart textiles can be embedded in a versatile way into design items that can find space also on the market.

In conclusion, this work represents a fundamental effort in providing valuable insights on the design issues and performances of piezoresistive textile as strain or pressure sensors. Textile sensors hold great potential for measuring strain and pressure distributions in applications of modern daily lives, but their widespread acceptance was still compromised because a rigorous experimental study of their metrological properties was scarce in literature. With this thesis, a better understanding of the applications and reliability of fabric strain and pressure sensors was obtained, highlighting and partially solving the undesired effects that have to be taken into account in the processing of data. These topics are a precious instrument to help researchers and users in determining the best design and employment of their smart sensing solutions.

Furthermore, the work highlights that textile sensors have to be accurately customized for the various employments, from the point of view of both hardware and characterization. Indeed ad hoc design and tests were needed for each application, and some expertise is required to properly tailor development and metrological depiction.

Despite, only two conceivable implementations were investigated in this study, envisaged applications for fabric sensors are actually uncountable, particularly in the biomedical scenario. Their use is especially encouraged in contexts where accuracy error margins are acceptable, while flexibility, stretchability, lightness, washability and wearability are features of primary importance.

Appendix I: Actigraph assessment for measuring upper limb activity in unilateral cerebral palsy

In the context of this PhD project, another important work was carried out in collaboration with the Department of Developmental Neuroscience, IRCCS Stella Maris Foundation. This work focused on the use of inertial sensors to understand the development of bimanual upper extremity activities both in children with typical development and with neurodevelopmental disorders.

Understanding development of bimanual upper limb (UL) activities in both typical and atypical conditions in children is important for: i) tailoring rehabilitation programs, ii) monitoring progress, iii) determining outcomes and iv) evaluating effectiveness of treatment/rehabilitation. Recent technological advances, such as wearable sensors, offer possibilities to perform standard medical monitoring. Body-worn motion sensors, mainly accelerometers, have shown very promising results but, so far, these studies have mainly focused on adults. In this framework, a systematic review was firstly performed to report the evidence of upper limb (UL) activity of both typically developing (TD) children and children with neurodevelopmental disorders (NDDs) that are reliably reported and comparable, using a combination of multiple wearable inertial sensors, both in laboratory and natural settings.

Articles were selected from three research databases (PubMed, Web of Science and EBSCO). Included studies reported data on children aged 0-20 years old simultaneously wearing at least two inertial sensors on upper extremities. The collected and reported data were relevant in order to describe the amount of physical activity performed by the two UL separately. A total of 21 articles were selected: 11 including TD, and 10 regarding NDDs (Figure I.1). For each article, a review of both clinical and technical data was performed. To summarize the main findings obtained from the systematic review, this Appendix reports both clinical and technical data extraction in Table I.3, I.4, I.5, I.6, I.7, and I.8. We considered inertial sensors used for following aims: (i) to establish activity intensity cut-points; (ii) to investigate validity and reliability of specified markers, placement and/or number of inertial

sensors; (iii) to evaluate duration and intensity of natural UL movements, defined motor tasks and tremor; and (iv) to assess efficacy of certain rehabilitation protocols.

Our conclusions were that inertial sensors are able to detect differences in use between both hands and that all reviewed studies support use of accelerometers as an objective outcome measure, appropriate in assessing UL activity in young children with NDDs and determining intervention effectiveness. Amongst the different inertial sensors, the triaxial accelerometer is the most commonly used in the articles, and it seems to be the most suitable and reliable to monitor and to collect consistent data about body movement. In addition, use of inertial sensors exhibits several positive aspects if compared to traditional clinical assessments. Firstly, clinical assessments need to be administered by trained therapists and therefore outcomes can be easily influenced by level of training and experience. Moreover, subjects have to visit the clinic every time they want to check progress, which not only makes the whole process very time consuming but also raises the burden on healthcare costs. Consequently, wrist actigraphy could be introduced as a more affordable and accessible follow-up strategy for a wide number of distant healthcare centres. Evaluation of differences between dominant and non-dominant UL measured by inertial sensors could play an important role as criteria for evaluating age-appropriate development in neurological functions both in TD children and children with NDDs. Therefore, the accelerometer could be introduced as a reliable assessment tool and as a quantitative evaluation method for developmental disorders. This information could be useful in planning UL rehabilitation strategies.

On the basis of our conclusion obtained from the analysis of reviewed articles, an experimental study was carried out to determine the validity of Actigraph GT3X+ to measure asymmetry in use of the two ULs during the Assisting Hand Assessment (AHA) in patients aged 3-25 years with unilateral cerebral palsy (UCP) compared to age-matched TD subjects. In the UCP the quantitatively measurement of the asymmetry in the use of ULs can overcome the limitation of many outcome measures which are dependent on the experience of therapists. 50 UCP (mean age 9.93±5.23) and 50 TD (mean age 10.14±5.19) subjects were assessed with AHA while wearing Actigraphs on their wrists. The mean activity of each hand (MA_{DH} and MA_{NDH}, dominant and non dominant, respectively) and the asymmetry index (AI) were calculated. Following sections report the study design and results obtained.

Appendix I

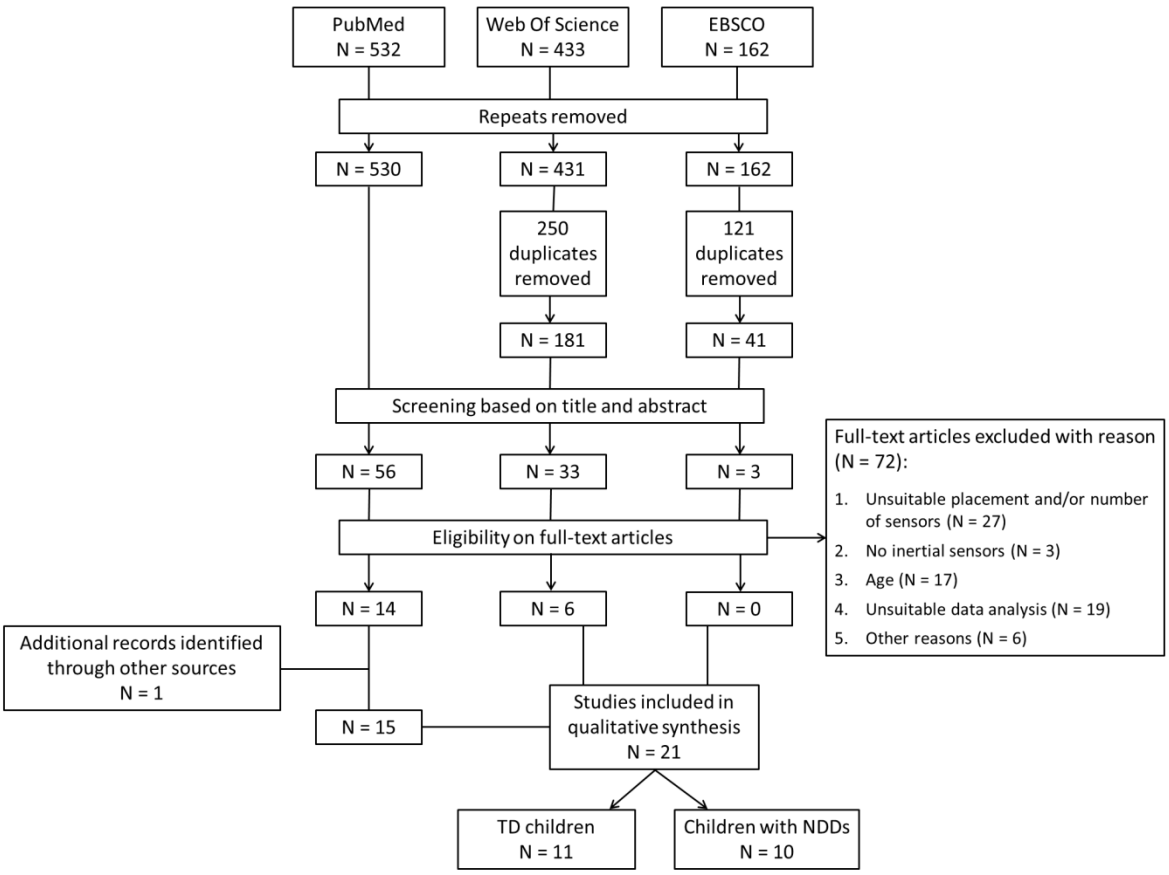

Figure I.1 Flowchart of selection of included articles.

Introduction

Cerebral palsy (CP) is the most common cause of chronic childhood physical disability in industrialised societies. The incidence is between 2 and 3 per 1000 live births and increases to 40–100 per 1000 live births among very premature and very low birth-weight infants [273]. Unilateral Cerebral Palsy (UCP), where the motor impairment impacts one side of the body, constitutes the most frequent form of CP, comprising 30-40% of children with CP [274][275]. Recent estimations of incidence and prevalence of CP have shown a significant increase in UCP in Europe [276]. In children with UCP, the presence of abnormal movement patterns at the impaired upper limb (UL) has been shown to be associated with lower levels of unimanual capacity and bimanual performance impeding activities of daily life [277].

UL function is important for performing activities of daily living, as self-care, work, leisure, and household activities. These activities include both global and fine-motor movements and involve the cooperation between the ULs, where one of the hand conducts the

action and the contralateral hand assists in completing the motor task, playing a secondary role. For this reason, the two hands are commonly called “dominant” and “non-dominant”, respectively with optimization of the bilateral collaboration between the two sides, referred to as “handedness” [278].

The assessment of UL (hand and arm) function and performance and handedness is important in both clinical practice and research. Clinicians interested in the evaluation and treatment of the upper extremity of children with UCP can choose from a wide range of assessment tools and classification systems. In systematic reviews of existing clinical tools [279][280] the best measure of unimanual capacity was the Melbourne Assessment of Unilateral Upper Limb Function (MUUL, upgraded to MA2) [281][282]; although the Shriners Hospital Upper Extremity Evaluation (SHUEE) [283], and the Quality of Upper Extremity Skills Test (QUEST) [284] can also be utilised. The best performance-based measure of bimanual upper limb activity in children with UCP is the Assisting Hand Assessment (AHA) [285]. The ABILHAND-Kids [286], a parent-report, performance-based questionnaire with excellent clinical utility and psychometric properties, has also been recommended.

A major limitation of many UL measures is that they only provide a subjective description of UL performance, where the rater visually scores the range, quality of movement, capacity and performance during execution of tasks. These assessments are therefore highly dependent on the examiner’s experience. There are few tests which require a certificated training course for assessors (e.g. AHA), which highlights the potential bias due to rater experience.

Recently with the advent of technology, some innovative devices have been developed to quantitatively measure different parameters integrated into the clinical assessment conducted with traditional tools [287]. These technology assessments included energy cost associated to human motor activity [288], the classification of specific features of motor activity [289], kinematic movement analysis integrated with physiological sensors [290], the identification of circadian motor asymmetry [291] and monitoring of motor activities by quantification of performance indexes and variables [292][293].

There is increased use commercial devices, such as wearable sensors, including accelerometers which can be worn as bracelets (e.g. IMUs, ETHOS, Actigraphs). This differential approach, based on two symmetrically located sensors, has been used for the study of unbalanced conditions: such handedness assessment in healthy [294] or unhealthy subjects

[295] (e.g upper limb mobility of post-stroke patients). Most studies adopt a multiple sensor arrangement with accelerometers placed on both wrists [296][297][298].

There is increased use of technological devices to record and provide raw data that can be further evaluated, however these devices need validation. In the validation process, the selected tool should be tested for its suitability and applicability for the purpose. Technology measures can provide quantitative data, however they are often designed for "standardized applications", which means that the quantity and quality of data may be related to the methodology of use. An advantage of wearable sensors data capture is that the subject is free to behave in the most natural and spontaneous way.

The primary purpose of this study was to examine the validity of accelerometers, such as the Actigraph GT3X+, worn on the both wrists, to measure asymmetry in use of the two ULs during the AHA in children and youth aged 3-25 years old with UCP compared to age-matched typically developing (TD) subjects. The hypothesis to be tested is that triaxial accelerometers (Actigraph GT3X+), in a standardized setting, can discriminate the differences in the use of the two upper limbs in UCP subjects compared to TD and detect asymmetry in UCP group related to clinical outcome measures (Assisting Hand Assessment scores and Manual Ability Classification System).

Study participants and settings

Data were collected at the Stella Maris Research Centre, Pisa in Italy and at the Queensland Cerebral Palsy and Rehabilitation Research Centre in Brisbane, Australia. Potential participants were identified from a database of children with hemiplegia at the Department of Developmental Neuroscience of the IRCCS Stella Maris (Pisa, Italy) for the UCP children and from a clinical register at the Queensland Cerebral Palsy and Rehabilitation Research Centre (Brisbane, Australia). A convenience sample of TD were identified as volunteers.

Eligible children and their parents were then invited to participate in the study trial and informed consent to participate was obtained from the child and/or by her/his parents prior to begin the assessment. Ethics approval was obtained from the various relevant ethics committees at participating hospitals and universities in Italy by Tuscany Paediatric Ethics

Committee (78/2016) and in Australia at the Child Health Queensland Ethics in Human Research as part of the PREDICT study (NHMRC 465128). The study has been registered at the www.clinicaltrials.gov (NCT03054441).

Participants of the CP group were selected based on the following inclusion criteria:

(i) diagnosis of UCP confirmed by a medical physician;
(ii) aged between 3 and 25 years old at study assessment;
(iii) located in Italy or Queensland (Australia).

Exclusion criteria were:

(i) medical complications that would interfere with study participation (e.g., uncontrolled seizures, epilepsy);
(ii) predominantly dystonia or athetoid movement patterns;
(iii) insufficient cognitive level to follow instructions;
(iv) other progressive neurological disorders;
(v) marked visual or hearing impairment.

Participants of the healthy group were selected based on the following inclusion criteria:

(i) age between 3 and 25 years old at study assessment;
(ii) no clinical documented disorders;
(iii) right-hand dominance;
(iv) located in Italy or Queensland (Australia).

Materials

Actigraphs: Each participant wore an activity monitor (wGT3X-BT Monitor, ActiGraph, Florida, FL, model 7164; 4.6*cm* x 3.3*cm* x 1.5*cm*, 19*g*) on each wrist. The accelerometers were fastened to the wrist using custom-made Velcro wristbands. The Actigraph GT3X+® monitor was selected for this study as it has been identified as a reliable instrument for measuring movement intensity [299][300]. The wrist was identified as potentially viable location for wearing the Actigraph GT3X+® monitor when assessing use of the upper limb in children with UCP.

Appendix I

AHA: The Assisting Hand Assessment (β-version 5.0) measures and describes the effectiveness with which a child with unilateral disability makes use of his impaired (assisting) hand during bimanual activities [285]. The AHA is scored from video recordings (lasting about 20 minutes) of the play activity, subsequently scored based on 20 predefined items using a four-point rating scale. There are different versions of the AHA, which are comparable with each other, allowing the comparisons amongst subjects of different ages and the detection of potential changes over time in the same subject [301]. Children aged 5-12 years old are tested with the School-Kids AHA, using a board game [302]. There are two different themes for the board games: "the Captive in the Fortress Game" and "the Alien Game". In both versions, children have a mission to complete, which involves performing different tasks during the course of the game. On each board there is a path with several steps, linked to a specific card with the instruction about how to reach the next step. For children younger than 5 years old, or if greater than 5 years but are not interested in board game due to their cognitive level, toys from the AHA kit can be used as a free play session. For adolescent participants, the Ad-AHA board game "Go with the Ice Floe" is used. UCP and TD participants undertook different versions of the AHA assessment, depending on their age and on their cognitive ability.

The **Edinburgh Handedness Inventory (EHI)** is a simple and brief quantitative method of assessing of handedness, composed by 10 items (writing, drawing, throwing, scissors, toothbrush, knife without a fork, spoon, broom, striking a match, open the lid of a box) [303]. Handedness is calculated based on the activities mainly done with right or left hand: it is the ratio between the difference of the two values divided by their sum, expressed in percentage. It can range from -100 (left-handed) to +100 (right-handed). Participants of TD group have been tested with EHI.

The **Manual Ability Classification System (MACS)** classifies how children with CP use their hands to handle objects in daily activities. The MACS describes five levels based on the children's self-initiated ability to handle objects and their need for assistance or adaption to perform manual activities in everyday life. It is suitable for children between 4 and 18 years [304].

Appendix I

Methods

This trial was conducted in clinical environment, in a quiet room during a play session. Each child wore two wearable accelerometers (Actigraph GT3X+), that had been initialized and embedded on Velcro-strap bracelets on both wrists during performance of the AHA test using the age-appropriate version: Kids-AHA for children between 18 months and 12 years (free play for children aged less than 5 years, alien game or fortress game for children aged between 5 and 12 years) or Ad-AHA board game "Go with the Ice Floe" for adolescents aged 12 years or more.

The AHA assessment was video recorded, as described in the manual, and the start and end times of the test were registered. In addition, the MACS levels of UCP participants were rated by therapists together with participant's family. The EHI Test was performed as a structured interview to determine the handedness/laterality of each TD participant and it was scored with the online software (http://zhanglab.wdfiles.com/local--files/survey/handedness.html). The AHA was scored by a certified AHA rater from the video recording and expressed in AHA units and EHI. Acceleration data were recorded in 3 axes at 80 *Hz* (stored locally in the device), downloaded using ActiLife 6 software (Actigraph, Pensacola, FL), down-loaded to 1 *Hz* and converted to activity counts within the ActiLife 6 software. The activity counts provide an index of the intensity of physical activity at a given time point: the higher the counts, the greater the intensity [305]. In addition, the activity counts across three axes were combined using a Vector Magnitude.

Movement of each upper limbs during the AHA was quantified by the mean activity count. Mean activity counts were defined as the mean of activity counts per second over the entire monitoring period. The Mean Activity was extracted separately for the dominant hand (MA_{DH}) and non-dominant hand (MA_{NDH}), regarding the values of Vector Magnitude. To quantify the dominant hand movement relative to the non-dominant hand movement during AHA, an asymmetry index was computed. The asymmetry index (AI) was calculated processing the mean activity of each UL obtained by the accelerometers data of the AHA collection following the Edinburgh Inventory formula:

$$AI = \frac{MA_{DH} - MA_{NDH}}{MA_{DH} + MA_{NDH}} * 100$$

Appendix I

The AI value of 0 indicates both ULs contributed equally to activity during the AHA assessment, while positive or negative values indicate greater contributions from dominant or non-dominant UL compared to the contralateral limb, respectively. Clinical (AHA unit scores and MACS levels) and Actigraph (MA_{DH}, MA_{NDH} and AI) data were analyzed using the Statistical Package for Social Sciences (SPSS, version 20.0). Median and 95% confidence intervals (CI) were calculated and reported. Age and sex measures for both groups were calculated to check for differences between groups by means of Mann–Whitney U independent sample tests.

Initially, intra group differences (for TD and for UCP) between the MA_{DH} and the MA_{NDH} were evaluated by means of Wilcoxon matched-pairs signed rank test. Between-group differences (UCP vs TD) for all actigraphic parameters (MA_{DH}, MA_{NDH} and AI) were evaluated using the Mann–Whitney U independent sample tests. For the MACS level of UCP group, the three groups (MACS I, II and III) were compared using the Kruskall–Wallis. Two sided p-values <0.05 were regarded statistically significant and post hoc analyses were made by Mann Whitney U post hoc tests with p-values <0.017. Finally, in the UCP group, Spearman ρ correlation has been used to examine the relationship between the MA_{DH}, the MA_{NDH} and the AI with AHA scores, respectively.

Results and discussions

Participants

A total sample of 106 children (55 UCP and 51 TD) were evaluated and 100 met the full inclusion criteria. The reasons of exclusion were:

(i) Movement disorder associated with CP (n=2);
(ii) Insufficient cognitive levels to comply with the instructions (n=3);
(iii) Left-hand dominance for a TD subject (n=1).

The UCP group consisted of 50 subjects with CP (mean age 9.93±5.23 years, median 8.90, IQR 8.86, range 3-25) diagnosed as hemiplegia according to Hagberg's classification [306]. Gender and affected side were distributed as follows: male = 30, female = 20; and affected side was right = 33 and left = 17. Children were classified on the MACS level I=16, MACS II=23 and MACS III=11 [304].

Appendix I

The TD group consisted of 50 subjects (mean age 10.14±5.19 years, median 8.90, IQR 5.08, range 3-24.91, 30 Male, 20 Female). All TD presented right hand handedness, as confirmed by the EHI scores (>0.8). No statistically significant differences were found between the two groups for age and sex.

Intra and between groups comparisons of UCP and TD: Mean activity of dominant hand (MA_{DH}), Mean activity of non dominant hand (MA_{NDH}) and Asymmetry index (AI) (Table I.1)

To our knowledge this is the first study aimed to evaluate the validity of accelerometers (Actigraph GT3X+) for detecting the asymmetry in the use of the two ULs in children with UCP. The semi-structured setting of the AHA allowed a consistent environment, in which the spontaneous use of the two ULs can be detected both in TD and UCP subjects. The use of the Actigraphs for each UL was the only additional request respect to the traditional assessment with the AHA. Performing the AHA wearing the two Actigraphs did not interfere with subjects' play and the Actigraphs were well accepted due to their resemblance to a digital watch.

Within each group (UCP and TD) the MA_{DH} was significantly higher than the MA_{NDH} ($p<0.000001$ and $p<0.000001$, respectively). This is the most important result, which shows that the Actigraphs were able to quantify the differences in the mean activity between the two hands (DH and NDH) in both groups (TD and UCP) showing that the DH had greater activity than NDH. The DH, in fact, also in TD, had a more active role during bimanual activities than the NDH which acted as support and for stabilization with an expected lower quantity of movement

For the between-groups comparisons, the MA_{DH} was significantly higher in the UCP group than the TD group ($p=0.001$) while the MA_{NDH} was significantly lower in UCP than in TD group ($p<0.000001$) (Figure I.2). This finding is in contrast with other studies [308][309][310], where it is reported that the non-paretic hand of children with hemiplegia was significantly impaired, although to a lesser extent than the paretic hand of children with UCP, with respect to the dominant hand of the TD group. As the actigraphic data measures the quantity of movement, the higher activity demonstrates the higher movements in UCP subject utilized in their DH in order to support the activity of impaired hand.

Appendix I

For the UCP group, these data confirm that children with UCP have develop their handedness on the less affected side [311]. The values of MA_{DH} and of MA_{NDH} found some outliers in UCP group. In particular, for the MA_{DH} there was the subject #38 who had a very high value and it could be related to the particular active behaviour of the child during the assessment, while subjects #3 and #22 are were young adults who were very quiet and they moved their non-affected arms few times. The three outliers (#48, #49 and #50) with higher values of MA_{NDH} were the subjects with higher values of AHA.

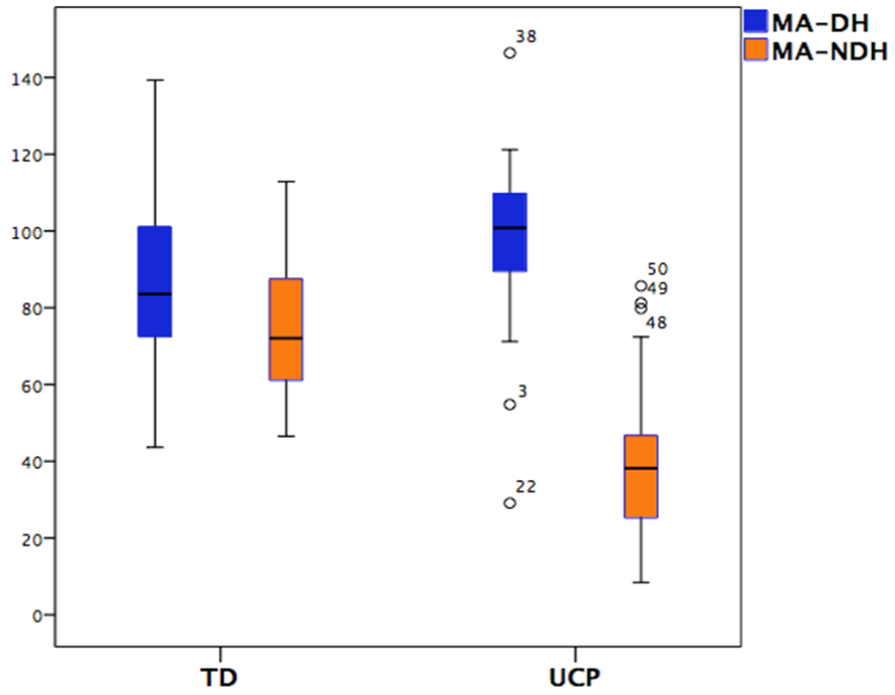

Figure I.2 Mean activity of DH and NDH in TD and UCP groups.

In addition, the values of AI of UCP were significantly higher than those of TD group ($p<0.000001$) (Figure I.3). In TD the asymmetry index was very low demonstrating a high cooperation between the two hands and similar amount of activity in contrast to the significantly higher values of asymmetry in UCP. As manual activities typically require the co-operation of both hands, and also tend to be specialized for different functions [307]. For instance, when we remove the lid from a jar or we button up a shirt, the NDH holds the object in a stable position while the DH acts upon it. The NDH therefore plays a postural role in stabilizing the object and at the same time provides a spatial reference frame into which the DH manipulates the object. While the NDH offers stability, it does not however mean that the hand is immobile. On the contrary, the NDH ensures a static or dynamic stabilization. For

instance, in handwriting, the pen cannot be dexterously manipulated by the DH if the page is not stabilized and periodically re-positioned by the NDH so that the position and orientation of the page always remain appropriate to the DH action. Based on these previous findings, our results confirm that in TD, the NDH has lower values than the DH.

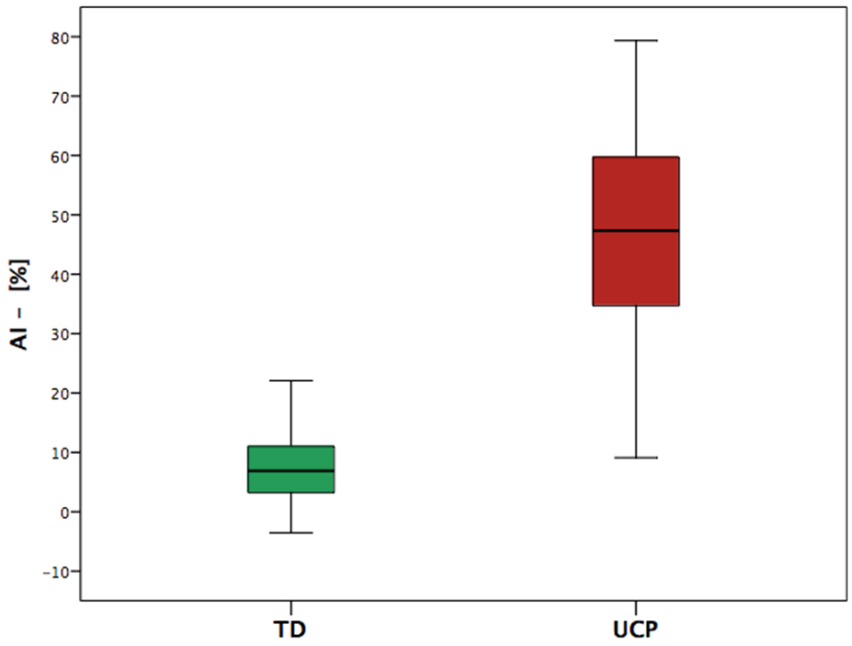

Figure I.3 Asymmetry index in TD and UCP groups.

Table I.1 Mean activity of DH and NDH in TD and UCP groups.

MEAN	UCP mean [CI 95%]	TD mean [CI 95%]	p*
MA_{DH}	97.71 [92.32-103.09]	86.60 [81.1-92.09]	0.001
MA_{NDH}	38.8 [33.65-43.95]	74.72 [70.1-79.33]	<1.0E-06
p**	<1.0E-06	<1.0E-06	
AI	45.88 [40.75-51.02]	7.27 [5.47-9.6]	<1.0E-06

*Mann-Whitney U independent sample tests

**Wilcoxon matched-pairs signed rank test

Relationship among MACS levels in UCP group (Table I.2)

Another important finding were the differences in Actigraph data according to the MACS levels. The MACS classifies how children with CP use their hands to handle objects in daily activities and it is expected that it is highly correlated to the AHA performance, which evaluates the spontaneous use of the assisting hand (affected hand) during a semi-structured play session requiring bimanual handling. There was a significant difference among the MACS levels (I, II and III) on both clinical (AHA, $p<0.000001$) (Figure I.4) and the Actigraph data (MA_{DH}, MA_{NDH} and AI; $p = 0.004$, 0.001 and <0.000001, respectively). The AHA unit values were significantly higher for MACS I than MACS II ($p<0.000001$) and MACS III ($p<0.000001$) and also between MACS II and MACS III ($p<0.000001$). In the UCP group there were a few outliers, including case #13 and #31 whom had lower values than expected for their MACS level I and III, respectively. In contrast cases #5 and #40 had higher values than expected for their MACS level II. These discrepancies could be related to a lower or higher performance during the assessment as AHA with respect to the use of their hands during daily activities.

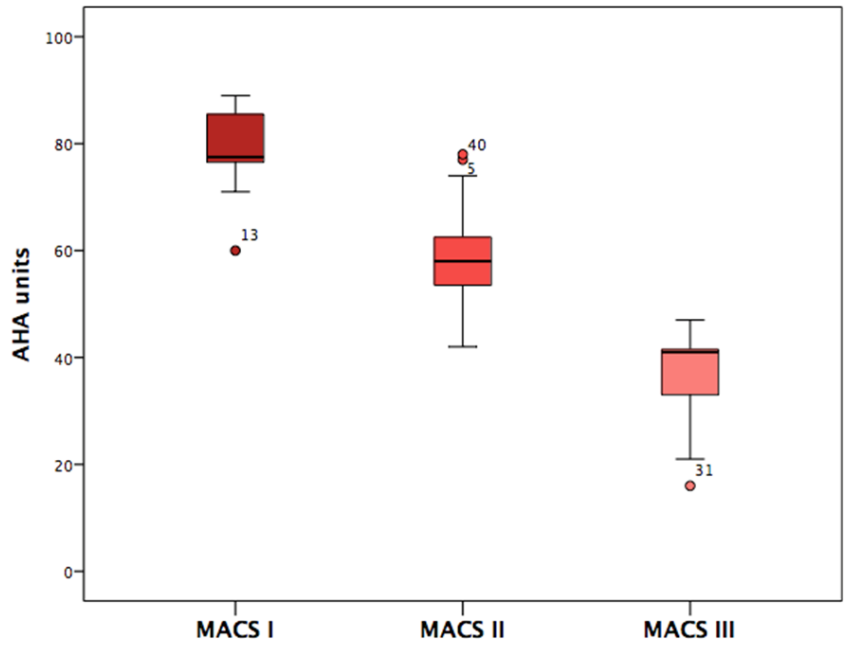

Figure I.4 AHA scores of UCP children grouped by MACS levels.

Further analysis of the mean activity of each hand separately in relation to MACS levels found a significant difference between hands.

Appendix I

The MA_{DH} values were significantly lower in the MACS I and in the MACS III than the MACS II (p=0.004 and p=0.012, respectively) and similar between MACS I and MACS III (p=0.251) (Figure I.5).

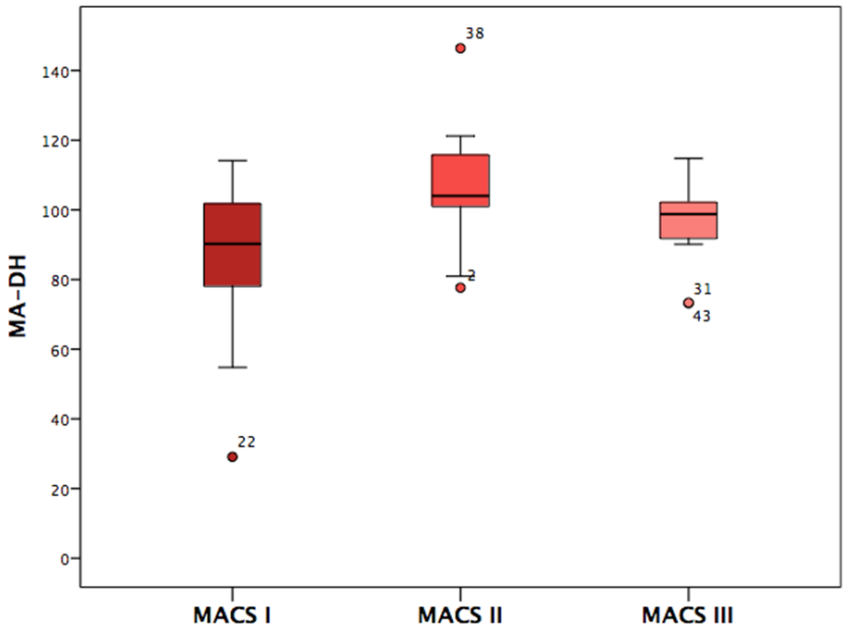

Figure I.5 Mean activity of DH of UCP children grouped by MACS levels.

The MA_{NDH} values were significantly higher in the MACS I and in the MACS II than the MACS III (p<0.000001 and p=0.001, respectively) while the values were similar between MACS I and MACS II (p=0.168) (Figure I.6).

This finding could be related to the crucial difference between MACS II and MACS III. Children classified as MACS II can achieve the required tasks using alternative ways of performance with both hands and also extra activity of the DH for have success in bimanual tasks that can determine higher values of MA_{DH}. This usually does not occur in MACS III who require environmental support to achieve their goals.

When comparing MACS levels with AI, the data confirmed that there were significant differences among levels with a significant increase in the AI so that the UCP children at MACS level III have the highest level of asymmetry between limbs. In particular, the AI values were significantly lower in the MACS I and the MACS II than the MACS III (p<0.000001 and p=0.004) and also in the MACS I with respect to MACS II (p=0.001) (Figure I.7).

Appendix I

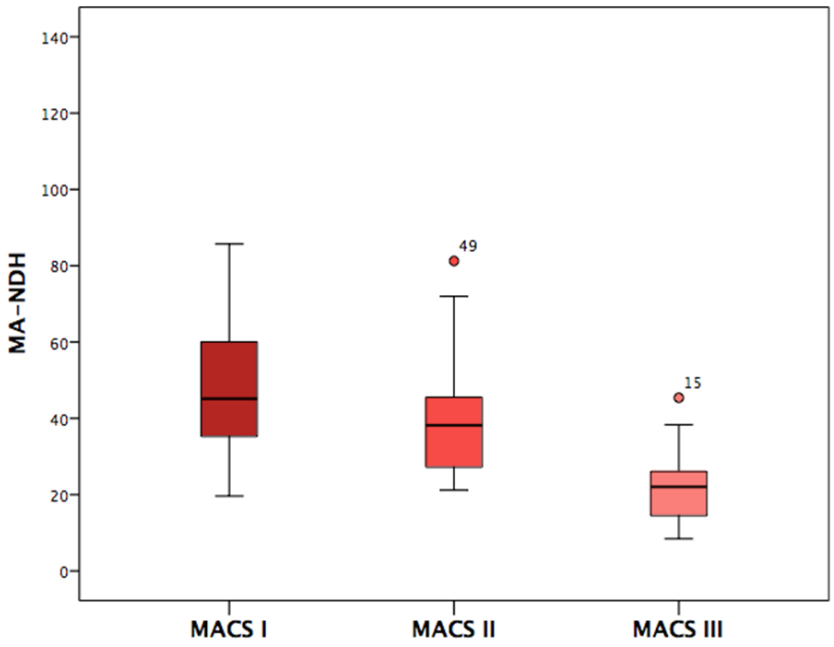

Figure I.6 Mean activity of NDH of UCP children grouped by MACS levels.

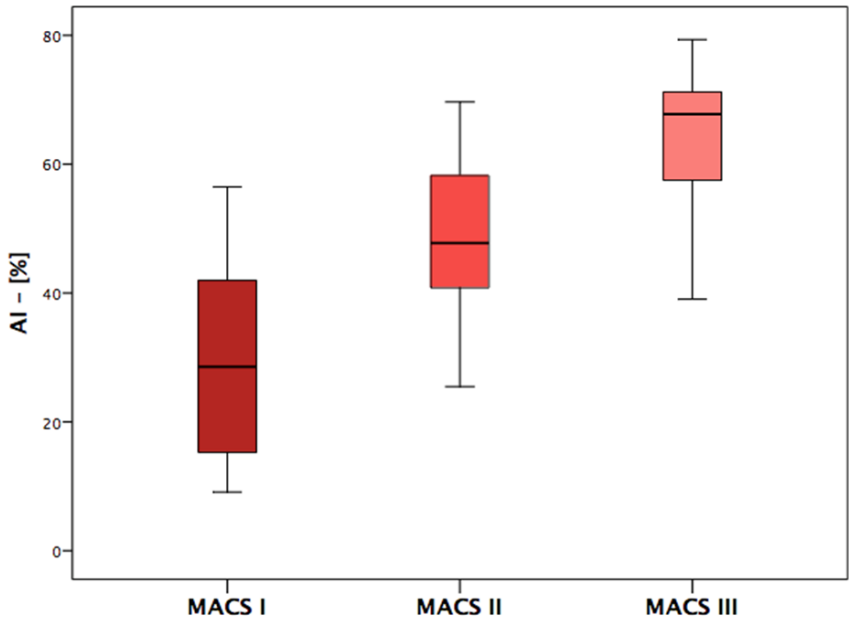

Figure I.7 Asymmetry index of UCP children grouped by MACS levels.

Table I.2 Clinical and Actigraph data according to the MACS levels of the UCP group.

UCP	MACS I (n. 16)	MACS II (n. 23)	MACS III (n. 11)	p*	p** I vs II	p** I vs III	p** II vs III
MA_{DH}	86.90 ± 22.22	106.29 ± 15.01	95.47 ± 12.61	0.004	0.004	0.251	0.012
MA_{NDH}	48.33 ± 19.25	39.9 ± 14.91	22.62 ± 11.18	0.001	0.168	<1.0E-06	0.001
AI	29.89 ± 16.37	48.7 ± 11.21	63.25 ± 12.60	<1.0E-06	0.001	<1.0E-06	0.004
AHA score	79.06 ± 7.59	58.7 ± 9.42	36.45 ± 10.38	<1.0E-06	<1.0E-06	<1.0E-06	<1.0E-06

*Kruskall-Wallis

**post-hoc analysis by Mann-Whitney U independent sample tests

Relationship between AHA in UCP group

All the findings in UCP children were confirmed by the strong correlation between AHA unit scores and all the quantitative actigraphic parameters (MA_{DH} and MA_{NDH} and AI).

Clinical scores on the AHA of UCP group ranged from a minimum of 16 to a maximum of 89 AHA units (logits). There was a significant negative correlation between AHA unit scores and the MA_{DH} values (Spearman' ρ= -0.285, p=0.045) (Figure I.8) and the AI (Spearman' ρ = -0.819, p<0.000001) (Figure I.9) while it was significantly positive between AHA unit scores and the MA_{NDH} (Spearman' ρ = 0.668, p<0.000001) (Figure I.8).

As expected, higher AHA score were related to a good symmetry of upper limbs use (and therefore low AI values) and the lower activity of DH with higher values of NDH.

Concluding remarks

This study confirmed that accelerometry is a valid tool, able to measure the amount of movement of the two ULs to quantify comparisons between limbs. This study confirmed construct validity between the Actigraph and MACS levels and severity of bimanual coordination on the AHA.

Appendix I

Our work confirms validity of the Triaxial Accelerometer approach with Actigraphs, to the traditional evaluation without require time or effort to the child. Our data confirms the relationship between wearable sensors such as the Actigraph as clinical assessments and added other quantitative data to clinical scores. The clinical implications confirm that quantitative data provide a more detailed description of upper limb activity and symmetry, with the opportunity to have a sensitive tool for detect spontaneous and intervention-induced changes. Future perspectives, may confirm that accelerometry could become a reliable and not invasive assessment tool for systematically measuring the UL activity, addressing further studies of the bimanual activities and handedness in clinical situations. Use of wearable sensors for planning UL activity strategies in interventions, may enable customization in relation to subjects' rehabilitative needs with a sensitive tool to detect spontaneous and intervention-induced changes. Our ongoing work is the data collection by actigraphy of daily life activities for testing the hypothesis that the accelerometry could be a reliable tool also in real-world conditions, encompassing potential differences between the experimental situation and recording the real-life spontaneous upper limb use.

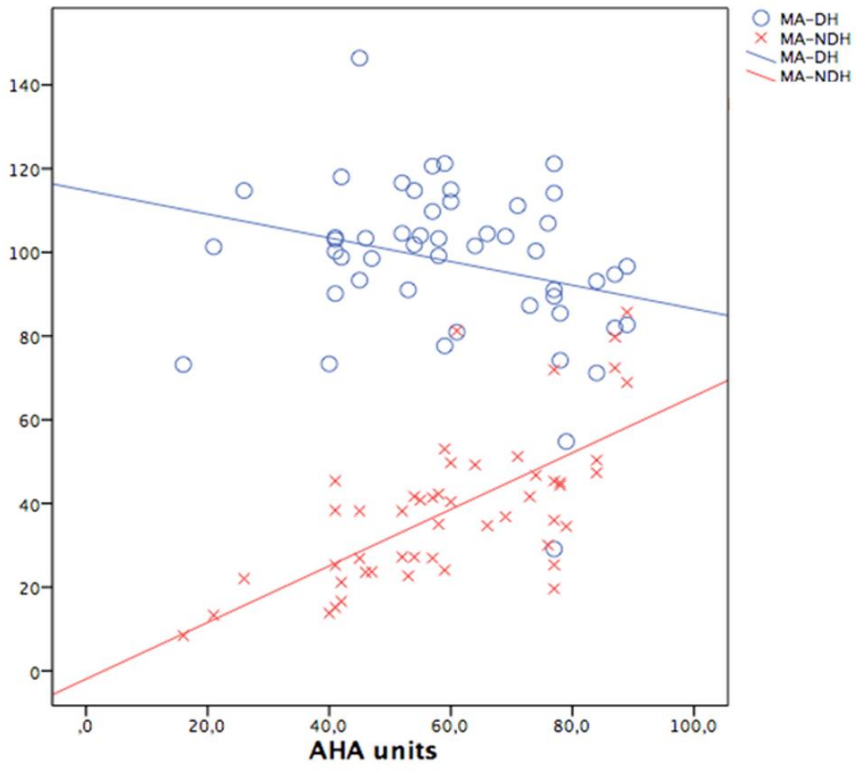

Figure I.8 Correlation between mean activity of DH and NDH and AHA scores in UCP group.

Appendix I

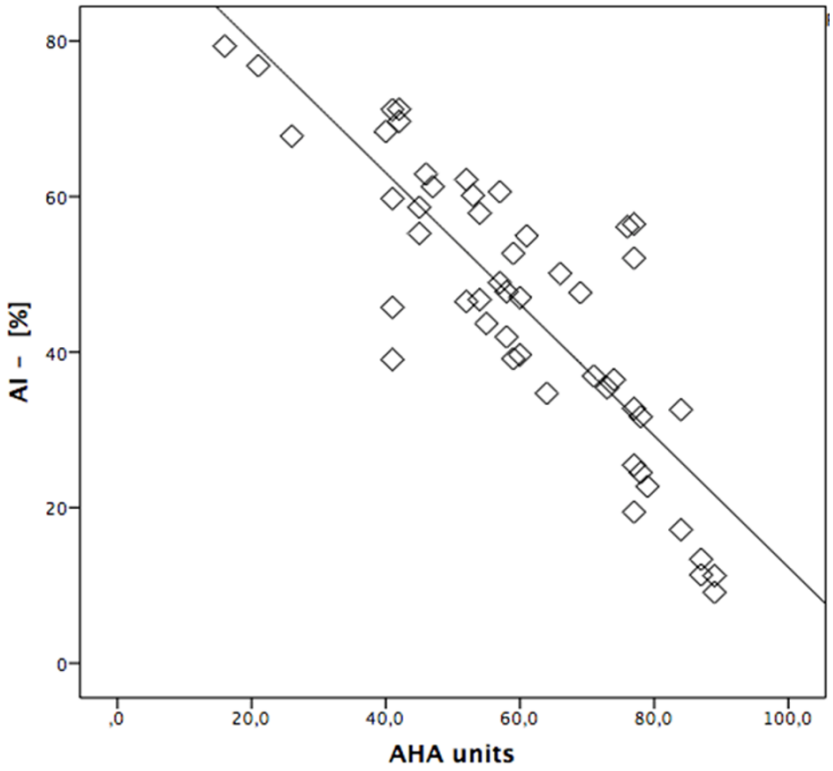

Figure I.9 Correlation between asymmetry index and AHA scores in UCP group.

Table I.3: Study Data in Typically Developing Children.

Author	Study type	Aims	Setting	Sample Size	Mean Age (yrs)	Inclusion Criteria	Exclusion Criteria	Reference Standard
[312] Birmingham A. T. et al. ***(1985)***	Survey	To evaluate the variation of tremor frequency and amplitude in relation to the age	Laboratory	109	n=22 (7-9), n=28 (9-11), n=24 (11-13), n=22 (13-15), n=13 (16-18)	To be attending specific schools or fit classes	NA	NA
[313] Avi Sadeh et al. ***(1994)*** **[STUDY 1]**	Lab-based validation and calibration study	To develop a new sleep-wake scoring algorithm	Laboratory	16	13.8±1.9	Volunteers	NA	NA
[314] Deutsch K. M. et al. ***(2006)***	Observational study	To investigate the mechanical and neural components of postural finger tremor	Laboratory	39	n=20 (6.4±3), n=19 (10.5±0.3), n= 21 (20.8±1.4)	Volunteers	Neurological disorders, influencing tremor	NA
[315] Graves L.E.S. et al. ***(2008)***	Observational study	To examine the contribution of the upper limb and total body movement to adolescents' energy expenditure whilst playing videogames	Laboratory	13	11-17	Good health picture	NA	NA

Appendix I

[316] Davila E. M. ***(2011)***	Observational study	To evaluate the influence of wearing AMs on the D vs ND wrists on measurements of free living PA	Laboratory + outpatient	20	12-17	1) volunteer participants from Bozeman, Montana, 2) 12-17 yrs	NA	NA
[317] Phillips L. R. S. et al. ***(2012)***	Lab-based validation and calibration study	To develop physical activity intensity cut-points for use with GENEA accelerometer	Laboratory	44	10.9 ± 1.9	NA	NA	NA
[318] MacArthur B. et al. ***(2014)***	2x2 mixed design with random allocation.	To measure percentage of time engaged in MVPA and estimated EE with accelerometry in playing AVG vs unstructured OP	ELC playground, ELC room	16 (8 OP vs. 8 AVG)	OP= 6.6±0.7, AVG= 6.3±0.9	1) good health, 2) healthy weight (BMI percentile= 5-85), 3) no limit for physical activity.	Grass allergies. Skin sensitivity to light. Failure to complete all session within a 3-week period.	NA
[319] Lemmens R. J. M. et al. ***(2015)***	Cross sectional study	To evaluate the reliability of arm-hand tasks accelerometer records	Laboratory	32	n=16 children (8.5±1.7), n=16 (14.6±1.5)	Volunteers	Motor problems with arm, hand or shoulder	NA
[320] Kaneko M. et al. ***(2015)***	Observational Study	To quantify age-appropriate developmental changes of SNS	Laboratory	233	4-12	Student at the Fukuoka Municipal Elementary School	NA	NA
[321] Dadashi F. et al. ***(2015)***	Observational study	To characterise front-crawl swimming skills	Outdoor pool	9	16.0 ±1.8	Recreational swimmers	NA	NA

Appendix I

[GROUP 2]								
[322] Mackintosh K.A. et al. *(2016)*	Observational study	To validate and compare ANNs	Laboratory, semi-structured setting	27	10.8 ±1.0	Volunteers recruited via a local primary school. The children attended the the laboratory only if: 1) rested state, 2) at least 2h postprandial, 3) strenous exercise and coffeine avoided in the previous 24h	NA	NA

ANNs: Artificial Neural Networks, AVG : Active Videogames, EE: Energy Expenditure, ELC: Early Learning Center, OP: Outdoor Play, NA: not available

Table I.4: Study Data in Children with Neurodevelopmental Disorders.

Author	Study type	Aims	Setting	Sample Size	Disease	Mean Age (yrs)	Inclusion Criteria	Exclusion Criteria	Reference Standard
[323] Floyd A. G. et al. ***(2007)***	Multy-centered study	To analyze the UL motor physiology	Laboratory	15	NP-C	25 ± 10	1) => 12 years of age, 2) confirmed diagnosis of NP-C by abnormal cholesterol esterification and abnormal filipin staining	1) concurrent enrolment in other clinical trials, 2) drugs or diet supplements, interfering with digestive absorption of study medication, 3) significant history of gastrointestinal disorders, HIV or hepatitis, 4) not comply with study procedures	EDSS
[324] Gordon A. M. et al. ***(2007)***	Single-blinded randomized control study	To examine the efficacy of the HABIT	Summer camp	20 (10 HABIT vs 10 CG)	UCP	total sample = 9.6±6.0, HABIT = 4.5-13.7, CG= 3.9-10.6	1) ability to extend the wrist>20° and the fingers at the metacarpophalangeal joints>10° from full flexion, 2) JTHF: >50% difference between the involved and the non-involved hand, 3) ability to lift the involved arm>6 inches, 4) BBIT= mean score +/-<1DS	1) health problems unassociated with CP, 2) current/untreated seizures, 3) visual problems interfering with the intervention or testing, 4) MAS> 3.5, 5) orthopaedic surgery on the involved upper extremity, 6) dorsal rhizotomy, 7) botox therapy in the UL in the prior 6 months or within the period of study, 8) intrathecal baclofen.	AHA, BOT-2, CFUS, JTHF

Appendix I

[325] Strohrmann C. et al. *(2013)*	Longitudinal study	i) to monitor children activities in daily life, ii) to evaluate the use of body worn sensors for motor assessment in children	Laboratory	4	CP (2), acquired stroke (2)	10.5 ± 2,12	1) neurological diagnosis leading to stationary stay, 2) age= 5-18 years, 3) cognitive ability to understand the aim of the tasks	NA	Motor Capacity Assessment
[326] Zoccolillo L. et al. *(2015)*	cross-sectional experimental quantitative study*	i) to monitor physical activity during VGT vs conventional therapy, ii) to quantify if VGT enhances number of movements	Outpatient + inpatient	8	UCP	6,6 ± 1,4	1) UCP, 2) 4-14 yrs, 3) GMFCS: I-IV, 4) any Xbox with Kinect at home.	1) IQ<35, 2) severe comorbidities, 3) incapacity to stand, even with an external support.	QUEST, ABILHAND-kids

Appendix I

[327] Sokal B. et al. ***(2015)***	Cross sectional, observational design	i) to evaluate the UL activity, ii) to compare the use of the affected arm between children and adult with hemiplegia	Not reported	28	UCP	3.9 ± 1.7	NA	1) serious or recurring medical complications, 2) spasticity medication within the last 3 months, 3) previous paediatric CIMT, 4) fixed contractures in the affected-arm, 5) invalid accelerometer records (insufficient time, only 1 wrist, unrealistic records, malfunction)	PMAL-R, PAFT
[328] Bergamini E. ***(2014)***	Three experimental sessions	i) to identify a biomechanical performance indicators of wheelchair propulsion, ii) develop and assess the efficacy of a specific training program	Basketball court	12 (6 EG vs 6 CG)	paraplegia (4), myelomeningocele (3), poliomyelitis (2), spastic diplegia (1), below-knee amputation (1), knee arthroprothesis (1)	total sample = 17.1 ± 2.7, EG= 13-20, CG= 12-20	At least two years of previous wheelchair basketball experience.	Medical contraindications	NA

Appendix I

[329] Kaneko M. et al. ***(2016)***	Observational study	i) to establish a quantitative evaluation system of soft neurological signs	Laboratory	33	ADHD	7-11	1) patients of the Kurume University Hospital, 2) positive DSM-IV criteria for ADHD diagnosis, 3) WISC-III>70	NA	NA
[330] Le Moing A.G. et al. ***(2016)***	Observational study	i) to highlight the feasibility of quantifying the range of upper limb movements	Laboratory	7	DMD	18.5+/-5.5	1) patients of the Institute of Myology, 2) age> 10 years old, 3) non-ambulant, 4) able to sit for at least 3 hours in the wheelchair	1) cognitive impairment, 2) occurrence of neurological/inflammatory/infectious/endocrine/acute orthopaedic disease in the precious month, 3) scheduled surgery within 3 weeks of inclusion date, 4) surgery of the upper limbs in the previous three months	MyoSet (MyoPinch, MyoGrip and MyoPlate), BBT, Minnesota Test

Appendix I

[331] O'Neil M.E. et al. *(2016)*	Observational study	i) to evaluate the inter-instrument reliability and concurrent validity of 3 accelerometer-based motion sensors for measuring PA intensity	Clinical standardized setting	57	CP: hemiplegia (29), diplegia (26), quadriplegia (3)	12.5±3.3	1) GMFCS= I-III, 2) ambulatory children, 3) 6-20 years old, 4) able to follow instructions and protocol directions, 5) able to wear 3 pairs of accelerometers and 1 portable indirect calorimeter.	1) recent musculoskeletal injuries, limiting their PA levels, 2) orthopaedic surgery within the precious 6 months, 3) botulinum toxin or phenol injections within the previous three months, 4) previous unstable medical conditions limiting PA levels, 5) unstable emotional or behavioural status.	NA
[332] Coker-Bolt P. et al. *(2016)*	Prospective pre-test/post-test study	To determine the feasibility and use accelerometers before, during and after a CIMT program	Outpatient + Laboratory	12	UCP	4.9 ±1.33	1) UCP, 2) able to use the affected UL as a gross assist during play and self-care activities, 3) no significant developmental delays, 4) ambulatory, 5) no additional health impairments	1) significant intellectual disabilities, 2) seizure disorders, 3) botulinum toxin injections in the previous 6 months	MA2

ADHD: Attention Deficit Hyperactivity Disorder, AHA: Assisting Hand Assessment, BOT-2: Bruininks–Oseretsky Test of Motor Proficiency, CFUS: Caregiver Functional Use Survey, CG: Control Group, CIMT: Constraint-Induced Movement Therapy, DMD: Duchenne Muscular Dystrophia, EDSS: Extended Disability Status Scale, EG: Experimental Group, IQ: Intelligence Quotient, JTHF: Jebsen–Taylor Test of Hand Function, MA2: Melbourne Unilateral Upper Limb Assessment – 2, MAS: Modified Ashworth Score, NP – C: Nieman Pick C, PAFT: Pediatric Arm Function Test, PMAL-R: Pediatric Motor Activity Log – Revised, QUEST: Quality of Upper Extremity Skills Test, UL: upper limb VGT: Video-Game based Therapy.

Table I.5: Technical Data for collection phase in Typically Developing Children.

Author	Sensors Number	Sensors Type & Make	Placement	Wear time	Sample frequency
[312] Birmingham A. T. et al. ***(1985)***	2	Accelerometers (Bruel and Kjaer type 4367).	Terminal phalanx of each middle finger	3 min for each hand	5-second epoch
[313] Avi Sadeh et al. ***(1994) [Study 1]***	2	Actigraphs (AMA-32, Ambulatory Monitoring, Inc., Ardsley, NY).	Each wrists	2 nights (about 7 hours to night)	1-minute epochs.
[314] Deutsch K. M. et al. ***(2006)***	2	Uniaxial wireless accelerometers (Coulbourn T45-10, calibrated on each day of testing).	Dorsal surface of the tip of the distal segment of each index finger.	three 10-s consecutive trials, about 5 s breaks between trials.	200 Hz
[315] Graves L.E.S. et al. (2008)	6	1) Actiheart (Cambridge Neurotechnology Cambridge, UK), 2) 4 uniaxial ActiGraph accelerometers (GT1M, Fort Walton Beach, FL, USA)	1) on the skin at the base of the sternum, 2) on the midaxillary line of the right and left hip and on each forearm proximally from the wrist joint .	60 min	2) 30 Hz
[316] Davila E. M. ***(2011)***	2	Actical triaxial AMs (Respironics Co., Inc., Bend, OR, USA).	Dorsal side of each wrist	Full seven days (24 hrs/day).	15-second epoch
[317] Phillips L. R. S. et al. ***(2012)***	3 + 1	Triaxial wireless accelerometers GeneActive (Unilever Discover, Colworth, UK) + ActiGraph GT1M (Actigraph, Pensacola, FL, USA).	Each wrist and + right hip (ActiGraph GT1M worn adjacent to the hip mounted GENEA)	Activities: 5 min; Lying supine: 10 min.	GENEA: 80 Hz, ActiGraph GT1M: 1 s epochs.

[318] MacArthur B. et al. *(2014)*	3	Actical accelerometers (Actical, Philips Respironics Co. Inc., Bend, OR).	Each wrist + hip	20 minutes	15-second epoch
[319] Lemmens R. J. M. et al. *(2015)*	7	Sensor devices, composed by a triaxial accelerometer, triaxial gyroscope, triaxial magnetometer (SHIMMER Research, Dublin, Ireland).	Chest + Dominant and non-dominant arm-hand: on the dorsal side of the hand, of the wrist and on the upper arm	Not specified.	128 Hz
[320] Kaneko M. et al. (2015)	4	wearable sensors composed of three-axis acceleration and three-axis angular velocity sensors (WAA-006, WAA-010, ATR-Promotions, Kyoto, Japan)	both hands and elbows	four motor tasks: 10 s for each task	100 Hz
[321] Dadashi F. et al. (2016)	3	waterproofed IMUs (Physilog III, BioAGM, CH, 3D accelerometer, 3D gyroscope).	2 IMUs placed on the dorsal side and distal end of the forearms, one on the sacrum.	Not specified.	500 Hz
[322] Mackintosh K.A. et al. (2016)	9	triaxial accelerometer (Actigraph wGT3X+, Florida, USA)	on the lateral plane of each ankle, knee, hip, wrist, and centre of the chest.	30 minutes	100 Hz

IMU: Inertial Measurement Unit, Hz: Herz

Table I.6: Technical Data for analysis phase in Typically Developing Children.

Author	Accelerometer data comparison	Differences between the two hands	Data cleaning	Threshold to assess the intensity of arm movement
[312] Birmingham A. T. et al. *(1985)*	RMS of tremor amplitude, dominant peak and its frequency.	For rest tremor, amplitude in the dominant hand was significantly lower in adolescence and early adult life than in childhood, for the non-dominant hand the statistically significant difference was sustained to later life. For work tremor, dominant hand frequency declined significantly with age, both hands continue to decline in adulthood.	Frequency analysis of the tremor waveform was filtered to remove frequencies above 50 Hz to prevent alias contamination	NA
[313] Avi Sadeh et al. *(1994) [Study 1]*	Accelerometric data matched with PSG scoring performed to develop the scoring algorithm: PS probability of sleep	The mean activity level of the dominant wrist was significantly higher than that of the nondominant wrist during PSG-determined sleep (6.84 vs. 6.16), as well as during wakefulness (25.8 vs. 22.3).	NA	NA
[314] Deutsch K. M. et al. *(2006)*	The peak frequency within two frequency bands (5-15 Hz and 15-30 Hz) and the proportion of power exhibited at the peak frequency determined (based on power spectral density calculated using Welch's averaged periodogram method).	The peak frequency of the finger of the dominant hand (21.4 Hz) was higher than nondominant hand (20.7 Hz) in the 15-30 Hz frequency band. No significant differences in proportion of power exhibited at peak frequency within the 5-15 Hz of postural tremor as a function of age, hand dominance or hand configuration. Postural tremor of nondominant hand was significantly more regular than dominant hand.	Band-pass filtered (1– 50 Hz)	NA

[315] Graves L.E.S. et al. (2008)	Means and standard deviations of activity counts (counts/min)	Activity of the dominant limb was significantly greater than non-dominant during tennis and bowling ($P < 0.001$) and non-dominant limb activity was significantly greater during boxing than bowling or tennis ($P < 0.001$). Activity counts from the left wrist for tennis and boxing ($r = 0.710$ and 0.744, $P \cdot 0.01$) and the right wrist for boxing ($r = 0.586$, $P < 0.05$) were significantly correlated with EE.	Band pass filtering (0.21 – 2.28 Hz)	NA
[316] Davila E. M. *(2011)*	Data Trasformation: AEE, Time. Data Summarization Characteristics: Bouts Duration, Intensity Thresholds.	No statistical differences between outcome variables for any bout duration (1, 5, 10 minutes) within L and MV intensity categories between AMs (D versus ND, LW versus RW) or model (1R versus 2R). Dominant and RW AMs were no-significantly higher than ND and LW, respectively, within MVPA intensity. In contrast, ND and LW AMs were non-significantly higher than D and RW within L intensity PA. Identical results within gender.	Quantity control checks were performed to identify periods on non-wear.	Light (AEE < 0.05 kcals/kg/min), moderate (0.05 < AEE < 0.09 kcals/kg/min), vigorous (AEE ≥ 0.10 kcals/kg/min).
[317] Phillips L. R. S. et al. *(2012)*	VM with gravity-substracted.	Both sides demonstrated good criterion validity (right: r=0.9, left: r=0.91) and good concurrent validity (right: r=0.83, left: r=0.845). ROC analysis proved GENEA monitors able to successfully discriminate among all intensity levels.	NA	Sedentary (< 1.5 METs), light (1.5-2.99 METs), moderate (3-5.99 METs) and vigorous (≥ 6 METs). The accelerometer counts for activities were coded into binary indicator variables (0 or 1) based on intensity.

[318] MacArthur B. et al. *(2014)*	Percentage of time in MVPA calculated by summing the number of 15-second intervals in which the activity counts were ≥ 574 counts/15 seconds.	The accelerometers placed on the wrists did not find differences in the conditions in percentage MVPA (right: 48.8±29.5%, left: 47.6±28.8%).	NA	MVPA: activity counts ≥ 574 counts/15 seconds.
[319] Lemmens R. J. M. et al. *(2015)*	ICC parameter (based on VM).	Within-subject reliability calculated for the 2 arm hands separately, median ICCs ranged between 0.68-0.92. Between subject reliability for the 2 arm hands separately, median ICCs ranged between 0.61-0.90.	Zero time-phase, low-pass filtered (1.28 Hz)	NA
[320] Kaneko M. et al. (2015)	Postural stability of the hands and elbows, rotational speed, mirror movement, two parameters of bimanual symmetry, compliance	All indices had a tendency to increase with age.	Low-pass filter (6 Hz)	NA
[321] Dadashi F. et al. (2016)	Average propulsive phases of right and left arms, pull and push phases (Δpull, Δpush), sum of aerial recovery and entry catch phases (ΔNProp), index of coordination (IdC).	By increasing the velocity, the duration of arm under-water phases (Δpull + Δpush) and accordingly IdC did not change significantly. G2 group used 2,8% lower catch-up pattern (P<0,01) by increasing the arm under-water phases (P<0.016) and using 6.5 more arm stroke (P<0.001). No changes in the stroke length and cycle velocity variation were observed (P > 0.22).	NA	NA

Appendix I

[322] Mackintosh K.A. et al. (2016)	Mean and variance of the accelerometer counts in each 15 s window. These extracted features were used as inputs into the ANNs, a specific type of machine learning model. RMSE.	The ANNs for left and right wrist accelerometers had a lower correlations with predicted EE. No significant differences in RMSE analysis. Despite significant advantages in terms of compliance, they could lead to potentially marginal losses in EE prediction accuracy.	NA	1,4% of collected data were removed when EE < 0,5 MET (measured with MetaMax 3B)

AEE: Activity Energy Expenditure, AM: Activity Monitors, ICC: Intraclass Correlation Coefficient, IMU: Inertial Measurement Unit, MET: Molecular Electronic Transducers, PSG: Polysomnography, RMS: Root Mean Square, RMSE: Root Mean Square Error, ROC: Receiver Operating Characteristic, VM: Vector Magnitudes.

Table I.7: Technical Data for collection phase in Children with Neurodevelopmental Disorders.

Author	Sensors Number	Sensors Type & Make	Placement	Wear Time	Sample frequency
[323] Floyd A. G. et al. ***(2007)***	2	Piezoresistive uniaxial accelerometers with linear sensitivities of 4.5 mV/g in the biological tremor range (0-25 Hz)	Over the dorsum of both hands	Multiple recording and total recording time lasted 1-2 h	300 Hz
[324] Gordon A. M. et al. ***(2007)***	2	Accelerometers (Manufacturing Technology Inc. Fort Walton Beach, FL, model 7164)	Each wrist	During the AHA test session	10 Hz
[325] Strohrmann C. et al. ***(2013)***	10	ETH Orientation Sensor (ETHOS)= IMU composed by a 3D accelerometer, a 3D gyroscope and a 3D digital compass. Not commercially available.	Upper (wrists and upper arms) and lower extremities (upper legs and feet) and the trunk.	1h, once per week over a course of four weeks.	100 Hz
[326] Zoccolillo L. et al. ***(2015)***	5	Wireless triaxial accelerometers (Trigno, Delsys®).	Posterior part of forearms, of shanks and of lower trunk in correspondence of the centre of mass (L2-L3).	During 5 continuous minutes of video-game based therapy and 5 minutes of CT.	Not specified
[327] Sokal B. et al. ***(2015)***	2	Biaxial wireless accelerometers (Model 71256, Actigraph, Pensacola, FL)	Dorsal side of both wrists just above the styloid process	During waking hours for at least 9 hours daily for 3 consecutive days after the testing session.	10 Hz, integrated over a user-specified epoch (2 s).
[328] Bergamini E. ***(2014)***	3	IMUs (Opal, APDM Inc., Portland, Oregon, USA).	Both wrists and backrest of the wheelchair.	Time was manually recorded. Total time not reported.	128 Hz

Appendix I

[329] Kaneko M. et al. (2016)	4	Acceleration and angular velocity sensors (WAA-006, WAA-010, ATR-Promotions, Kyoto, Japan)	Both hands and elbows	two motor tasks (imitative motor task and a maximal-effort motor task): 10 s for each task	100 Hz
[330] Le Moing A.-G. et al. (2016)	2	Watch-like devices contained a three-axis accelerometer, a three-axis gyroscope, and a three-axis magnetometer	On each wrist	at least 30 minutes to complete all the tasks, without concerning potential resting period	NA
[331] O'Neill M.E. et al. (2016)	6	1) StepWatch activity monitor (uniaxial), 2) Actigraph GT3X (triaxial), 3) BodyMedia SenseWear Pro Armband (triaxial).	1) superior to the left/right malleolus, 2) on a waist elastic belt superior to the right/left iliac crest, 3) dorsal side of each upper arm at the midbelly of the triceps muscle	During each data collection, lasting 2-2,5 hours	1 s for ActiGraph, 3 s for StepWatch, and 60 s for SenseWear.
[332] Coker-Bolt P. et al. (2017)	2	Triaxial Actigraph GT9X Link (Actigraph, Pensacola, FL)	on each wrist	6 hours a day before and after the CIMT program (tot: 12 hours)	30 Hz

Table I.8: Technical Data for analysis phase in Children with Neurodevelopmental Disorders.

Author	Accelerometer data comparison	Differences between the two hands	Data cleaning	Threshold to assess the intensity of arm movement
[323] Floyd A. G. et al. ***(2007)***	Side-to-side relationship of tremor amplitude, peak tremor frequencies and amplitude variability.	Action tremor amplitudes were relatively symmetric between the dominant and non-dominant hands, postural tremor was not symmetric bilaterally (3 of 8 patients were unilateral), amplitudes of bilateral cases correlated within subjects.	In the FTN trials only, frequencies below 2 Hz were excluded	NA
[324] Gordon A. M. et al. ***(2007)***	Percentage of hand use (activity counts)	The percentage of use of involved extremity remain the same in controls, 70% of the task performance, while increased from 62.6 to 77.8% for the children who received HABIT (not correlate with the change in AHA scores). Use of the non-involved extremity remained the same across testing sessions in both groups.	NA	NA
[325] Strohrmann C. et al. ***(2013)***	TIME, mean value of MI, MIV, DF, SM, ARE, RANG, ArmSync, gait parameters (all based on VM).	MIV is larger for the unaffected hand, the energy associated to the dominant frequency of the affected hand vs. unaffected hand was much lower, the SM parameter of the unaffected side vs. affected side was twofold.	Low-pass filtered (45 Hz)	NA
[326] Zoccolillo L. et al. ***(2015)***	RMS of acceleration.	Hemiparetic side was moved less than healthy side. In VGT the paretic side was moved -20±13% less than the other side, while this difference was not significant in CT (-10±28%).	Low-pass filtered (20 Hz) and after the mean substraction for removing the contribution of gravity acceleration.	NA

[327] Sokal B. et al. *(2015)*	Duration SV, duration ratio SV, intensity SV, intensity ratio SV.	Partecipants moved their more-affected arm for 55.7% and their less-affected arm for 64.9%, ratio 0.86. The intensity of more-affected arm was 41.3 counts/s and for less-affected arm was 60.5, ratio 0.71.	Segments when partecipants appeared to have removed the accelerometers were removed.	Raw values for each 2 s recording epoch were dichotomized around a low threshold (i.e., 2) with above-threshold values set to a positive costant and at- or below-threshold values set to zero.
[328] Bergamini E. *(2014)*	Symmetry index, a peak of the acceleration magnitude and CV (all based on VM).	Symmetry index: - CG: ES2 (48.92%) and ES3 (47.86%), - EG: ES2 (47.77%) and ES3 (48.62%). These values indicate good symmetry.	Low-pass filtered (12 Hz)	NA
[329] Kaneko M. et al. (2016)	Rotational speed, mirror movement, postural stability of rotating elbow, temporal change of rotational size in each index, bimanual symmetry, compliance.	All scores of ADHD children was lower than TD children. In bimanual symmetry the score of ADHD children increased with age and was significantly different to TD aged 8 and 10 years old. The variability of children's score in compliance and temporal change of rotational size in ADHD vs. TD was larger.	low-pass filter (6 Hz)	NA
[330] Le Moing A.-G. et al. (2016)	Norm of the angular velocity, ratio of the vertical component of the acceleration, model-based computed power, elevation rate	Not find any side effect between the dominant and non-dominant hands. Patients performed better with their dominant side but this was not statistically significant, due to the small size of the population and the advanced stage of the disease.	NA	NA

[331] O'Neill M.E. et al. (2016)	Median (IQR) evaluated and compared between right and left side for each parameter and each device, ICC, CIs	Each accelerometer is stable in data collection on both sides, indicating that movement asymmetries may not influence PA measures. Because all 3 accelerometer models exhibited excellent inter-instrument reliability for measuring PA in a variety of real-world activities in TD, it may be appropriate also for CP to wear accelerometers on the right side.	NA	NA
[332] Coker-Bolt P. et al. (2017)	Active duration, mean activity count, use ratio and magnitude ratio (all based on VM, down-sampled to 1 Hz).	Significant increase in the duration and mean actvity count of affected upper limb use during each camp day and in three of five days in comparison to pre-test data, respectively. No significant changes in all scores pre- vs. post-CIMT.	NA	Upper limb activity when the vector sum activity count > 0.

ARE: Average Rotation Energy, ArmSync: Synchrony of Arm Movement, CIs: Confidence Intervals, CT: Conventional Therapy, CV: Intercycle Variability, DF: Dominant Frequency, FTN: finger – to – nose, IQR: Interquartile Range, MI: Movement Intensity, MIV: Movement Intensity Variation, RANG: Range of Angular Velocity, SM: Smoothness of Movement, SV: Summary Variable, TIME: Task Completion Time.

Appendix II: Publications list

Candidate's publications in the thesis framework

In peer-reviewed journals:

- Baldoli, I., **Maselli, M.**, Cecchi, F., & Laschi, C. (2017). Development and characterization of a multilayer matrix textile sensor for interface pressure measurements. *Smart Materials and Structures*, 26(10), 104011.
- Grassi, A., Cecchi, F., **Maselli, M.,** Röling, M., Laschi, C., & Cianchetti, M. (2017). Warp-knitted textile as a strain sensor: Characterization procedure and application in a comfortable wearable goniometer. *IEEE Sensors Journal*, 17(18), 5927-5936.
- **Maselli, M.,** Mussi, E., Cecchi, F., Manti, M., Tropea, P., & Laschi, C. (2018). A wearable sensing device for monitoring single planes neck movements: assessment of its performance. *IEEE Sensors Journal,* 18(15), 6327-6336.
- Oliveri, A., **Maselli, M.**, Lodi, M., Storace, M., & Cianchetti, M. Model-based compensation of rate-dependent hysteresis in a piezoresistive strain sensor. *Transactions on Industrial Electronics*. doi:10.1109/TIE.2018.2884204.
- **Maselli, M.**, Fiorini, L., Cecchi, F., Castro, E., Esposito, R., ... & Laschi, C. Can Physical and Cognitive Training based on Episodic Memory be Combined in a New Protocol for Daily Training? Resubmitted to *Aging clinical and Experimental research* after major revision.
- Fiorini, L., **Maselli, M.**, Esposito, R., Castro, E., Mancioppi, G., ... & Cavallo, F. Foot Inertial Sensing for Combined Cognitive-Motor Exercise of the Sustained Attention Domain. Resubmitted to *Transactions on Biomedical Engineering* after major revision.
- Braito, I.*, **Maselli, M.***, Sgandurra, G., Inguaggiato, E., Beani, E., Cecchi, F., ... & Boyd, R. (2018). Assessment of upper limb use in children with typical development and neurodevelopmental disorders by inertial sensors: a systematic review. *Journal of neuroengineering and rehabilitation*, 15(1), 94.

- Sgandurra, G., Cecchi, F., Beani, E., Mannari, I., **Maselli, M.,** Falotico, F. P., ... & Klingels, K. (2018). Tele-UPCAT: study protocol of a randomised controlled trial of a home-based Tele-monitored UPper limb Children Action observation Training for participants with unilateral cerebral palsy. *BMJ open*, 8(5), e017819.
- Beani, E., **Maselli, M.**, Sicola, E., Perazza, S., Cecchi, F., …& Sgandurra. G. Actigraph assessment for measuring upper limb activity in Unilateral Cerebral Palsy. Submitted to *Journal of NeuroEngineering and Rehabilitation*.
- Sgandurra, G., …, **Maselli, M.**, et al. (2018). Early intervention at home in infants with congenital brain lesion with CareToy revised: a RCT protocol. *BMC pediatrics*, 18(1), 295.

In conference proceedings:

- **Maselli, M.**, Fiorini, L., Castro, E., Baldoli, I., Tocchini, S., Sportiello, M. T., ... & Laschi, C. (2017, July). Development and testing of a new cognitive technological tool for episodic memory: A feasibility study. In *Engineering in Medicine and Biology Society (EMBC), 2017 39th Annual International Conference of the IEEE* (pp. 893-896). IEEE.
- Fiorini, L., **Maselli, M.**, Castro, E., Tocchini, S., Sportiello, M. T., Laschi, C., ... & Cavallo, F. (2017, July). Feasibility study on the assessment of auditory sustained attention through walking motor parameters in mild cognitive impairments and healthy subjects. In *Engineering in Medicine and Biology Society (EMBC), 2017 39th Annual International Conference of the IEEE* (pp. 897-900). IEEE.
- Baldoli, I., **Maselli, M.**, Manti, M., Surace, E., Cianchetti, M., & Laschi, C. (2017, July). A pressure-sensitive palatograph for speech analysis. In *Engineering in Medicine and Biology Society (EMBC), 2017 39th Annual International Conference of the IEEE* (pp. 4431-4434). IEEE. **Oral presentation**.
- Mancioppi, G., Castro, E., Fiorini, L., **Maselli, M.**, Laschi, C., Cecchi, F., Cavallo, F. (2018). The use of smart tools for combined training of people with MCI: a case report. In *ForItAAL 2018*, in press.
- Sgandurra, G., **Maselli, M.**, Beani, E., Baldoli, I., Braito, I., Cecchi, F., ... & Cioni, G. (2017). Bimanual upper limb activity in children with typical development and

unilateral cerebral palsy: validation of a triaxial accelerometer approach. *Dev Med Child Neurol*, 59(3), 23.

- Sgandurra, G., Braito, I., **Maselli, M.**, Beani, E., et al. (2017) Asymmetry of upper limb activity in children with unilateral cerebral palsy: validation of a triaxial accelerometer approach. *Dev Med Child Neurol*, 59 (Supll 2): 35.

References

[1] Yamada, T., Hayamizu, Y., Yamamoto, Y., Yomogida, Y., Izadi-Najafabadi, A., Futaba, D. N., & Hata, K. (2011). A stretchable carbon nanotube strain sensor for human-motion detection. *Nature nanotechnology*, 6(5), 296.

[2] Pang, C., Lee, G. Y., Kim, T. I., Kim, S. M., Kim, H. N., Ahn, S. H., & Suh, K. Y. (2012). A flexible and highly sensitive strain-gauge sensor using reversible interlocking of nanofibres. *Nature materials*, 11(9), 795.

[3] Kim, D. H., Ghaffari, R., Lu, N., & Rogers, J. A. (2012). Flexible and stretchable electronics for biointegrated devices. *Annual review of biomedical engineering*, 14, 113-128.

[4] Levi, A., Piovanelli, M., Furlan, S., Mazzolai, B., & Beccai, L. (2013). Soft, transparent, electronic skin for distributed and multiple pressure sensing. *Sensors*, 13(5), 6578-6604.

[5] Nag, A., Mukhopadhyay, S. C., & Kosel, J. (2017). Wearable flexible sensors: A review. *IEEE Sensors Journal*, 17(13), 3949-3960.

[6] Pang, C., Lee, C., & Suh, K. Y. (2013). Recent advances in flexible sensors for wearable and implantable devices. *Journal of Applied Polymer Science*, 130(3), 1429-1441.

[7] Nuwaysir, E. F., Huang, W., Albert, T. J., Singh, J., Nuwaysir, K., Pitas, A., ... & McCormick, M. (2002). Gene expression analysis using oligonucleotide arrays produced by maskless photolithography. *Genome research*, 12(11), 1749-1755.

[8] Locher, I., & Tröster, G. (2007). Screen-printed textile transmission lines. *Textile Research Journal*, 77(11), 837-842.

[9] Wang, C. T., Huang, K. Y., Lin, D. T., Liao, W. C., Lin, H. W., & Hu, Y. C. (2010). A flexible proximity sensor fully fabricated by inkjet printing. *Sensors*, 10(5), 5054-5062.

[10] Birnbaum, A. J., Kim, H., Charipar, N. A., & Piqué, A. (2010). Laser printing of multi-layered polymer/metal heterostructures for electronic and MEMS devices. *Applied Physics A*, 99(4), 711-716.

[11] Girão, P. S., Ramos, P. M. P., Postolache, O., & Pereira, J. M. D. (2013). Tactile sensors for robotic applications. *Measurement*, 46(3), 1257-1271.

[12] Puangmali, P., Althoefer, K., Seneviratne, L. D., Murphy, D., & Dasgupta, P. (2008). State-of-the-art in force and tactile sensing for minimally invasive surgery. *IEEE Sensors Journal*, 8(4), 371-381.

[13] "Intuitive surgical, inc. - da vinci surgical system." http://www.intuitivesurgical.com/ (Accessed on 07/30/2018).

[14] Tomanova, M., Lippert-Grüner, M., & Lhotska, L. (2015). Specific rehabilitation exercise for the treatment of patients with chronic low back pain. *Journal of physical therapy science*, 27(8), 2413-2417.

[15] Kim, K., Kim, Y. M., & Kang, D. Y. (2015). Repetitive sit-to-stand training with the step-foot position on the non-paretic side, and its effects on the balance and foot pressure of chronic stroke subjects. *Journal of physical therapy science*, 27(8), 2621-2624.

[16] "Pressure and force measurement applications | tekscan." https://www.tekscan.com/applications (Accessed on 07/30/2018).

[17] Crea, S., Donati, M., De Rossi, S. M. M., Oddo, C. M., & Vitiello, N. (2014). A wireless flexible sensorized insole for gait analysis. *Sensors*, 14(1), 1073-1093.

[18] Weinstein, U., Kinrot, O., Bernstein, A., & Slovin, Z. (2006*). U.S. Patent Application No. 11/193,309*.

[19] Baldoli, I., Maselli, M., Manti, M., Surace, E., Cianchetti, M., & Laschi, C. (2017, July). A pressure-sensitive palatograph for speech analysis. In *Engineering in Medicine and Biology Society (EMBC), 2017 39th Annual International Conference of the IEEE* (pp. 4431-4434). IEEE.

[20] Peterson, M. J., Gravenstein, N., Schwab, W. K., van Oostrom, J. H., & Caruso, L. J. (2013). Patient repositioning and pressure ulcer risk-Monitoring interface pressures of at-risk patients. *Journal of Rehabilitation Research & Development*, 50(4).

[21] "Pps | tactile sensors and pressure mapping solutions." http://www.pressureprofile.com/ (Accessed on 07/30/2018).

[22] "Tactile surface pressure indicating sensors | contact force measurement | surface pressure mapping | pressure measurement | compression force | nip impression | pressure sensor| pressure sensitive sensors | pressure interface | tactile sensor." http://www.sensorprod.com/index.php (Accessed on 07/30/2018).

[23] Baldoli, I., Tognarelli, S., Vangi, F., Panizza, D., Scaramuzzo, R. T., Cuttano, A., ... & Menciassi, A. (2017). An active simulator for neonatal intubation: Design, development and assessment. *Medical engineering & physics*, 39, 57-65.

[24] Liu, R., Kwok, Y. L., Li, Y., Lao, T. T., Zhang, X., & Dai, X. Q. (2005). Objective evaluation of skin pressure distribution of graduated elastic compression stockings. *Dermatologic Surgery*, 31(6), 615-624.

[25] Doan, B., Kwon, Y. H., Newton, R., Shim, J., Popper, E. V. A., Rogers, R., ... & Kraemer, W. (2003). Evaluation of a lower-body compression garment. *Journal of sports sciences*, 21(8), 601-610.

[26] Kahle, J. T., & Highsmith, M. J. (2013). Transfemoral sockets with vacuum-assisted suspension comparison of hip kinematics, socket position, contact pressure, and preference: ischial containment versus brimless. *J Rehabil Res Dev*, 50(9), 1241-52.

[27] Giles, J. W., Puskas, G. J., Welsh, M. F., Johnson, J. A., & Athwal, G. S. (2013). Suture anchor fixation of bony Bankart fractures: Comparison of single-point with double-point "suture bridge" technique. *The American journal of sports medicine*, 41(11), 2624-2631.

[28] Mukhopadhyay, S. C. (2015). Wearable sensors for human activity monitoring: A review. *IEEE sensors journal*, 15(3), 1321-1330.

[29] Patel, S., Park, H., Bonato, P., Chan, L., & Rodgers, M. (2012). A review of wearable sensors and systems with application in rehabilitation. *Journal of neuroengineering and rehabilitation*, 9(1), 21.

[30] Gioberto, G., & Dunne, L. E. (2013). Overlock-stitched stretch sensors: characterization and effect of fabric property. *Journal of Textile and Apparel, Technology and Management*, 8(3).

[31] Rodgers, M. M., Pai, V. M., & Conroy, R. S. (2015). Recent advances in wearable sensors for health monitoring. *IEEE Sensors Journal*, 15(6), 3119-3126.

[32] Veltink, P. H., & De Rossi, D. (2010). Wearable technology for biomechanics: e-textile or micromechanical sensors?[conversations in bme]. *IEEE engineering in medicine and biology magazine*, 29(3), 37-43.

[33] Amjadi, M., Kyung, K. U., Park, I., & Sitti, M. (2016). Stretchable, skin-mountable, and wearable strain sensors and their potential applications: a review. *Advanced Functional Materials*, 26(11), 1678-1698.

[34] Bingger, P., Zens, M., & Woias, P. (2012). Highly flexible capacitive strain gauge for continuous long-term blood pressure monitoring. *Biomedical microdevices*, 14(3), 573-581.

[35] Lu, N., Lu, C., Yang, S., & Rogers, J. (2012). Highly sensitive skin-mountable strain gauges based entirely on elastomers. *Advanced Functional Materials*, 22(19), 4044-4050.

[36] Wang, Y., Wang, L., Yang, T., Li, X., Zang, X., Zhu, M., ... & Zhu, H. (2014). Wearable and highly sensitive graphene strain sensors for human motion monitoring. *Advanced Functional Materials*, 24(29), 4666-4670.

[37] Hwang, B. U., Lee, J. H., Trung, T. Q., Roh, E., Kim, D. I., Kim, S. W., & Lee, N. E. (2015). Transparent stretchable self-powered patchable sensor platform with ultrasensitive recognition of human activities. *ACS nano*, 9(9), 8801-8810.

[38] Gong, S., Lai, D. T., Su, B., Si, K. J., Ma, Z., Yap, L. W., ... & Cheng, W. (2015). Highly Stretchy Black Gold E-Skin Nanopatches as Highly Sensitive Wearable Biomedical Sensors. *Advanced Electronic Materials*, 1(4), 1400063.

[39] Yao, S., & Zhu, Y. (2014). Wearable multifunctional sensors using printed stretchable conductors made of silver nanowires. *Nanoscale*, 6(4), 2345-2352.

[40] Li, M., Li, H., Zhong, W., Zhao, Q., & Wang, D. (2014). Stretchable conductive polypyrrole/polyurethane (PPy/PU) strain sensor with netlike microcracks for human breath detection. *ACS applied materials & interfaces*, 6(2), 1313-1319.

[41] Amjadi, M., Pichitpajongkit, A., Lee, S., Ryu, S., & Park, I. (2014). Highly stretchable and sensitive strain sensor based on silver nanowire–elastomer nanocomposite. *ACS nano*, 8(5), 5154-5163.

[42] Ryu, S., Lee, P., Chou, J. B., Xu, R., Zhao, R., Hart, A. J., & Kim, S. G. (2015). Extremely elastic wearable carbon nanotube fiber strain sensor for monitoring of human motion. *ACS nano*, 9(6), 5929-5936.

[43] Mengüç, Y., Park, Y. L., Martinez-Villalpando, E., Aubin, P., Zisook, M., Stirling, L., ... & Walsh, C. J. (2013, May). Soft wearable motion sensing suit for lower limb biomechanics measurements. In *Robotics and Automation (ICRA), 2013 IEEE International Conference* on (pp. 5309-5316). IEEE.

[44] Mengüç, Y., Park, Y. L., Pei, H., Vogt, D., Aubin, P. M., Winchell, E., ... & Walsh, C. J. (2014). Wearable soft sensing suit for human gait measurement. *The International Journal of Robotics Research*, 33(14), 1748-1764.

[45] Tognetti, A., Lorussi, F., Dalle Mura, G., Carbonaro, N., Pacelli, M., Paradiso, R., & De Rossi, D. (2014). New generation of wearable goniometers for motion capture systems. *Journal of neuroengineering and rehabilitation*, 11(1), 56.

[46] Shyr, T. W., Shie, J. W., Jiang, C. H., & Li, J. J. (2014). A textile-based wearable sensing device designed for monitoring the flexion angle of elbow and knee movements. *Sensors*, 14(3), 4050-4059.

[47] Window, A. L., Holister, G. S., et al., *Strain gauge technology*. Applied science publishers, 1982.

[48] Xu, Y., Jiang, F., Newbern, S., Huang, A., Ho, C. M., & Tai, Y. C. (2003). Flexible shear-stress sensor skin and its application to unmanned aerial vehicles. *Sensors and Actuators A: Physical*, 105(3), 321-329.

[49] Choi, W. C. (2010). Polymer micromachined flexible tactile sensor for three-axial loads detection. *Transactions on electrical and electronic materials*, 11(3), 130-133.

[50] Muth, J. T., Vogt, D. M., Truby, R. L., Mengüç, Y., Kolesky, D. B., Wood, R. J., & Lewis, J. A. (2014). Embedded 3D printing of strain sensors within highly stretchable elastomers. *Advanced Materials*, 26(36), 6307-6312.

[51] Elgeneidy, K., Neumann, G., Jackson, M., & Lohse, N. (2018). Directly Printable Flexible Strain Sensors for Bending and Contact Feedback of Soft Actuators. *Frontiers in Robotics and AI*, 5, 2.

[52] Schmidt, P. A., Maël, E., & Würtz, R. P. (2006). A sensor for dynamic tactile information with applications in human–robot interaction and object exploration. *Robotics and Autonomous Systems*, 54(12), 1005-1014.

[53] Pritchard, E., Mahfouz, M., Evans, B., Eliza, S., & Haider, M. (2008, October). Flexible capacitive sensors for high resolution pressure measurement. In *Sensors, 2008 IEEE* (pp. 1484-1487). IEEE.

[54] Cannata, G., Maggiali, M., Metta, G., & Sandini, G. (2008, August). An embedded artificial skin for humanoid robots. In *Multisensor Fusion and Integration for Intelligent Systems, 2008. MFI 2008. IEEE International Conference* on (pp. 434-438). IEEE.

[55] Hasegawa, Y., Shikida, M., Ogura, D., Suzuki, Y., & Sato, K. (2008). Fabrication of a wearable fabric tactile sensor produced by artificial hollow fiber. *Journal of micromechanics and microengineering*, 18(8), 085014.

[56] Polygerinos, P., Correll, N., Morin, S. A., Mosadegh, B., Onal, C. D., Petersen, K., ... & Shepherd, R. F. (2017). Soft robotics: Review of fluid-driven intrinsically soft devices; manufacturing, sensing, control, and applications in human-robot interaction. *Advanced Engineering Materials*, 19(12), 1700016.

[57] Keplinger, C., Sun, J. Y., Foo, C. C., Rothemund, P., Whitesides, G. M., & Suo, Z. (2013). Stretchable, transparent, ionic conductors. *Science*, 341(6149), 984-987.

[58] Cai, L., Song, L., Luan, P., Zhang, Q., Zhang, N., Gao, Q., ... & Zhou, W. (2013). Super-stretchable, transparent carbon nanotube-based capacitive strain sensors for human motion detection. *Scientific reports*, 3, 3048.

[59] Li, S., Peele, B. N., Larson, C. M., Zhao, H., & Shepherd, R. F. (2016). A stretchable multicolor display and touch interface using photopatterning and transfer printing. *Advanced Materials*, 28(44), 9770-9775.

[60] Wissler, M., & Mazza, E. (2007). Mechanical behavior of an acrylic elastomer used in dielectric elastomer actuators. *Sensors and Actuators A: Physical*, 134(2), 494-504.

[61] Mannsfeld, S. C., Tee, B. C., Stoltenberg, R. M., Chen, C. V. H., Barman, S., Muir, B. V., ... & Bao, Z. (2010). Highly sensitive flexible pressure sensors with microstructured rubber dielectric layers. *Nature materials*, 9(10), 859.

[62] Park, G., Rosing, T., Todd, M. D., Farrar, C. R., & Hodgkiss, W. (2008). Energy harvesting for structural health monitoring sensor networks. *Journal of Infrastructure Systems*, 14(1), 64-79.

[63] Motoo, K., Arai, F., & Fukuda, T. (2007). Piezoelectric vibration-type tactile sensor using elasticity and viscosity change of structure. *IEEE Sensors Journal*, 7(7), 1044-1051.

[64] Hosoda, K., Tada, Y., & Asada, M. (2006). Anthropomorphic robotic soft fingertip with randomly distributed receptors. *Robotics and Autonomous Systems*, 54(2), 104-109.

[65] Takamuku, S., Gomez, G., Hosoda, K., & Pfeifer, R. (2007, July). Haptic discrimination of material properties by a robotic hand. In *Development and Learning, 2007. ICDL 2007. IEEE 6th International Conference* on (pp. 1-6). IEEE.

[66] Zhou, J., Fei, P., Gu, Y., Mai, W., Gao, Y., Yang, R., ... & Wang, Z. L. (2008). Piezoelectric-potential-controlled polarity-reversible Schottky diodes and switches of ZnO wires. *Nano letters*, 8(11), 3973-3977.

[67] Fixter, L., & Williamson, C. (2006). State of the Art Review–Structural Health Monitoring. *Smart Materials, Surfaces, and Structures Network (Smart. Mat) Report*.

[68] Kumar, S., & Singh, R. N. (1996). Crack propagation in piezoelectric materials under combined mechanical and electrical loadings. *Acta materialia*, 44(1), 173-200.

[69] Gullapalli, H., Vemuru, V. S., Kumar, A., Botello-Mendez, A., Vajtai, R., Terrones, M., ... & Ajayan, P. M. (2010). Flexible piezoelectric ZnO–paper nanocomposite strain sensor. *small*, 6(15), 1641-1646.

[70] Lee, C. S., Joo, J., Han, S., & Koh, S. K. (2004). Multifunctional transducer using poly (vinylidene fluoride) active layerand highly conducting poly (3, 4-ethylenedioxythiophene) electrode: Actuator and generator. *Applied physics letters*, 85(10), 1841-1843.

[71] Sareh, S., Noh, Y., Li, M., Ranzani, T., Liu, H., & Althoefer, K. (2015). Macrobend optical sensing for pose measurement in soft robot arms. *Smart Materials and Structures*, 24(12), 125024.

[72] Kiesel, S., Peters, K., Hassan, T., & Kowalsky, M. (2007). Behaviour of intrinsic polymer optical fibre sensor for large-strain applications. *Measurement Science and Technology*, 18(10), 3144.

[73] Dobrzynski, M. K., Pericet-Camara, R., & Floreano, D. (2011, September). Contactless deflection sensor for soft robots. In *Intelligent Robots and Systems (IROS), 2011 IEEE/RSJ International Conference on* (pp. 1913-1918). IEEE.

[74] Heo, J. S., Kim, J. Y., & Lee, J. J. (2008, November). Tactile sensors using the distributed optical fiber sensors. In *Sensing Technology, 2008. ICST 2008. 3rd International Conference on* (pp. 486-490). IEEE.

[75] Yamada, Y., Morizono, T., Umetani, Y., & Takahashi, H. (2005). Highly soft viscoelastic robot skin with a contact object-location-sensing capability. *IEEE Transactions on Industrial electronics*, 52(4), 960-968.

[76] Xiong, Z., Peng, G. D., Wu, B., & Chu, P. L. (1999). Highly tunable Bragg gratings in single-mode polymer optical fibers. *IEEE Photonics technology letters*, 11(3), 352-354.

[77] Kuang, K. S. C., Quek, S. T., & Maalej, M. (2004). Assessment of an extrinsic polymer-based optical fibre sensor for structural health monitoring. *Measurement Science and Technology*, 15(10), 2133.

[78] Chen, X., Yang, S., Hasegawa, M., Kawabe, K., & Motojima, S. (2005). Tactile microsensor elements prepared from arrayed superelastic carbon microcoils. *Applied Physics Letters*, 87(5), 054101.

[79] Ozel, S., Keskin, N. A., Khea, D., & Onal, C. D. (2015). A precise embedded curvature sensor module for soft-bodied robots. *Sensors and Actuators A: Physical*, 236, 349-356.

[80] Luo, M., Pan, Y., Skorina, E. H., Tao, W., Chen, F., Ozel, S., & Onal, C. D. (2015). Slithering towards autonomy: a self-contained soft robotic snake platform with integrated curvature sensing. *Bioinspiration & biomimetics*, 10(5), 055001.

[81] Ozel, S., Skorina, E. H., Luo, M., Tao, W., Chen, F., Pan, Y., & Onal, C. D. (2016, May). A composite soft bending actuation module with integrated curvature sensing. In *Robotics and Automation (ICRA), 2016 IEEE International Conference on* (pp. 4963-4968). IEEE.

[82] Weiß, K., & Worn, H. (2005, July). The working principle of resistive tactile sensor cells. In *Mechatronics and Automation, 2005 IEEE International Conference* (Vol. 1, pp. 471-476). IEEE.

[83] Beccai, L., Roccella, S., Ascari, L., Valdastri, P., Sieber, A., Carrozza, M. C., & Dario, P. (2008). Development and experimental analysis of a soft compliant tactile microsensor for anthropomorphic artificial hand. *IEEE/Asme Transactions on Mechatronics*, 13(2), 158-168.

[84] Dao, D. V., Sugiyama, S., & Hirai, S. (2009, May). Analysis of sliding of a soft fingertip embedded with a novel micro force/moment sensor: Simulation, experiment, and application. In *Robotics and Automation, 2009. ICRA'09. IEEE International Conference on* (pp. 889-894). IEEE.

[85] Flandin, L., Hiltner, A., & Baer, E. (2001). Interrelationships between electrical and mechanical properties of a carbon black-filled ethylene–octene elastomer. *Polymer*, 42(2), 827-838.

[86] Rosset, S., & Shea, H. R. (2013). Flexible and stretchable electrodes for dielectric elastomer actuators. *Applied Physics A*, 110(2), 281-307.

[87] Araby, S., Zhang, L., Kuan, H. C., Dai, J. B., Majewski, P., & Ma, J. (2013). A novel approach to electrically and thermally conductive elastomers using graphene. *Polymer*, 54(14), 3663-3670.

[88] Bae, S. H., Lee, Y., Sharma, B. K., Lee, H. J., Kim, J. H., & Ahn, J. H. (2013). Graphene-based transparent strain sensor. *Carbon*, 51, 236-242.

[89] Lee, C., Jug, L., & Meng, E. (2013). High strain biocompatible polydimethylsiloxane-based conductive graphene and multiwalled carbon nanotube nanocomposite strain sensors. *Applied Physics Letters*, 102(18), 183511.

[90] Han, C. J., Chiang, H. P., & Cheng, Y. C. (2018). Using Micro-Molding and Stamping to Fabricate Conductive Polydimethylsiloxane-Based Flexible High-Sensitivity Strain Gauges. *Sensors*, 18(2), 618.

[91] Yang, Y. J., Cheng, M. Y., Shih, S. C., Huang, X. H., Tsao, C. M., Chang, F. Y., & Fan, K. C. (2010). A 32× 32 temperature and tactile sensing array using PI-copper films. *The International Journal of Advanced Manufacturing Technology*, 46(9-12), 945-956.

[92] Cheng, M. Y., Tsao, C. M., & Yang, Y. J. (2010, June). An anthropomorphic robotic skin using highly twistable tactile sensing array. *In Industrial Electronics and Applications (ICIEA), 2010 the 5th IEEE Conference on* (pp. 650-655). IEEE.

[93] Chang, N. K., Su, C. C., & Chang, S. H. (2008). Fabrication of single-walled carbon nanotube flexible strain sensors with high sensitivity. *Applied Physics Letters*, 92(6), 063501.

[94] Park, Y. L., Majidi, C., Kramer, R., Bérard, P., & Wood, R. J. (2010). Hyperelastic pressure sensing with a liquid-embedded elastomer. *Journal of Micromechanics and Microengineering*, 20(12), 125029.

[95] Park, Y. L., Chen, B. R., & Wood, R. J. (2012). Design and fabrication of soft artificial skin using embedded microchannels and liquid conductors. *IEEE Sensors Journal*, 12(8), 2711-2718.

[96] Vogt, D. M., Park, Y. L., & Wood, R. J. (2013). Design and characterization of a soft multi-axis force sensor using embedded microfluidic channels. *IEEE Sensors Journal*, 13(10), 4056-4064.

[97] White, E. L., Case, J. C., & Kramer, R. K. (2017). Multi-mode strain and curvature sensors for soft robotic applications. *Sensors and Actuators A: Physical*, 253, 188-197.

[98] Mohammed, M. G., & Kramer, R. (2017). All-Printed Flexible and Stretchable Electronics. *Advanced Materials*, 29(19), 1604965.

[99] Liu, C. (2007). Recent developments in polymer MEMS. *Advanced Materials*, 19(22), 3783-3790.

[100] Tsao, L. C., Chang, D. R., Shih, W. P., & Fan, K. C. (2008). Fabrication and characterization of electro-active polymer for flexible tactile sensing array. In *Key Engineering Materials* (Vol. 381, pp. 391-394). Trans Tech Publications.

[101] Li, Y., Cheng, X. Y., Leung, M. Y., Tsang, J., Tao, X. M., & Yuen, M. C. W. (2005). A flexible strain sensor from polypyrrole-coated fabrics. *Synthetic metals*, 155(1), 89-94.

[102] Li, Z., Ma, G., Ge, R., Qin, F., Dong, X., Meng, W., ... & Li, K. (2016). Free-standing conducting polymer films for high-performance energy devices. *Angewandte Chemie*, 128(3), 991-994.

[103] Teng, C., Lu, X., Zhu, Y., Wan, M., & Jiang, L. (2013). Polymer in situ embedding for highly flexible, stretchable and water stable PEDOT: PSS composite conductors. *Rsc Advances*, 3(20), 7219-7223.

[104] Lee, Y. Y., Kang, H. Y., Gwon, S. H., Choi, G. M., Lim, S. M., Sun, J. Y., & Joo, Y. C. (2016). A Strain-Insensitive Stretchable Electronic Conductor: PEDOT: PSS/Acrylamide Organogels. *Advanced Materials*, 28(8), 1636-1643.

[105] Zhao, S., Li, J., Cao, D., Zhang, G., Li, J., Li, K., ... & Wong, C. P. (2017). Recent advancements in flexible and stretchable electrodes for electromechanical sensors: strategies, materials, and features. *ACS applied materials & interfaces*, 9(14), 12147-12164.

[106] Brady, S., Lau, K. T., Megill, W., Wallace, G. G., & Diamond, D. (2005). The development and characterisation of conducting polymeric-based sensing devices. *Synthetic metals*, 154(1-3), 25-28.

[107] Papakostas, T. V., Lima, J., & Lowe, M. (2002). A large area force sensor for smart skin applications. In *Sensors, 2002. Proceedings of IEEE* (Vol. 2, pp. 1620-1624). IEEE.

[108] Maheshwari, V., & Saraf, R. F. (2006). High-resolution thin-film device to sense texture by touch. *Science*, 312(5779), 1501-1504.

[109] Tiwana, M. I., Redmond, S. J., & Lovell, N. H. (2012). A review of tactile sensing technologies with applications in biomedical engineering. *Sensors and Actuators A: physical*, 179, 17-31.

[110] D'Alessio, T. (1999). Measurement errors in the scanning of piezoresistive sensors arrays. *Sensors and Actuators A: Physical*, 72(1), 71-76.

[111] Castano, L. M., & Flatau, A. B. (2014). Smart fabric sensors and e-textile technologies: a review. *Smart Materials and Structures*, 23(5), 053001.

[112] Stoppa, M., & Chiolerio, A. (2014). Wearable electronics and smart textiles: a critical review. Sensors, 14(7), 11957-11992.

[113] Cherenack, K., & van Pieterson, L. (2012). Smart textiles: challenges and opportunities. *Journal of Applied Physics*, 112(9), 091301.

[114] Axisa, F., Schmitt, P. M., Gehin, C., Delhomme, G., McAdams, E., & Dittmar, A. (2005). Flexible technologies and smart clothing for citizen medicine, home healthcare, and disease prevention. *IEEE Transactions on information technology in biomedicine*, 9(3), 325-336.

[115] Holland, S. A. (2013). Conductive Textiles and their use in Combat Wound Detection, Sensing, and Localization Applications.

[116] Simon, C., Potter, E., Potter, E., McCabe, M., & Baggerman, C. (2010). Smart fabrics technology development. *NASA Innovation Fund Project, NASA Johnson Space Center Report.*

[117] Roh, J. S., Mann, Y., Freed, A., Wessel, D., Berkeley, U. C., Freed, A., ... & Wessel, D. (2011, June). Robust and Reliable Fabric, Piezoresistive Multitouch Sensing Surfaces for Musical Controllers. In *NIME* (pp. 393-398).

[118] Holleczek, T., Rüegg, A., Harms, H., & Tröster, G. (2010, November). Textile pressure sensors for sports applications. In *Sensors, 2010 IEEE* (pp. 732-737). IEEE.

[119] Farboodmanesh, S., Chen, J., Mead, J. L., White, K. D., Yesilalan, H. E., Laoulache, R., & Warner, S. B. (2005). Effect of coating thickness and penetration on shear behavior of coated fabrics. *Journal of Elastomers & Plastics*, 37(3), 197-227.

[120] Hu, J., Meng, H., Li, G., & Ibekwe, S. I. (2012). A review of stimuli-responsive polymers for smart textile applications. *Smart Materials and Structures*, 21(5), 053001.

[121] Skrifvars, M., Rehnby, W., & Gustafsson, M. (2008). Coating of textile fabrics with conductive polymers for smart textile applications.

[122] "Eeonyx-function follows form." http://eeonyx.com/ (Accessed on 18/08/2018).

[123] "Mindsets online." http://www.mindsetsonline.co.uk/Site/Home (Accessed on 18/08/2018).

[124] Bera, T. K., Mohamadou, Y., Lee, K., Wi, H., Oh, T. I., Woo, E. J., ... & Seo, J. K. (2014). Electrical impedance spectroscopy for electro-mechanical characterization of conductive fabrics. *Sensors*, 14(6), 9738-9754.

[125] Cianchetti, M., Renda, F., Licofonte, A., & Laschi, C. (2012, June). Sensorization of continuum soft robots for reconstructing their spatial configuration. In *Biomedical Robotics and Biomechatronics (BioRob), 2012 4th IEEE RAS & EMBS International Conference on* (pp. 634-639). IEEE.

[126] De Rossi, D., Carpi, F., Lorussi, F., Mazzoldi, A., Paradiso, R., Scilingo, E. P., & Tognetti, A. (2003). Electroactive fabrics and wearable biomonitoring devices. *AUTEX Research Journal*, 3(4), 180-185.

[127] Ouyang, Y., & Chappell, W. J. (2008). High frequency properties of electro-textiles for wearable antenna applications. *IEEE Transactions on Antennas and Propagation*, 56(2), 381-389.

[128] Kim, S. H., Jang, S. H., Byun, S. W., Lee, J. Y., Joo, J. S., Jeong, S. H., & Park, M. J. (2003). Electrical properties and EMI shielding characteristics of polypyrrole–nylon 6 composite fabrics. *Journal of Applied Polymer Science*, 87(12), 1969-1974.

[129] Bryant, Y. G., & Colvin, D. P. (1994). *U.S. Patent No*. 5,366,801. Washington, DC: U.S. Patent and Trademark Office.

[130] Pacelli, M., Loriga, G., Taccini, N., & Paradiso, R. (2006, September). Sensing fabrics for monitoring physiological and biomechanical variables: E-textile solutions. In *Medical Devices and Biosensors, 2006. 3rd IEEE/EMBS International Summer School on* (pp. 1-4). IEEE.

[131] Hwang, L. S., Ko, J. M., Rhee, H. W., & Kim, C. Y. (1993). A polymer humidity sensor. *Synthetic metals*, 57(1), 3671-3676.

[132] El-Sherif, M. A., Yuan, J., & MacDiarmid, A. (2000). Fiber optic sensors and smart fabrics. *Journal of intelligent material systems and structures*, 11(5), 407-414.

[133] Stylios, G. K., & Wan, T. (2007). Shape memory training for smart fabrics. *Transactions of the Institute of Measurement and Control*, 29(3-4), 321-336.

[134] Torsi, L., Pezzuto, M., Siciliano, P., Rella, R., Sabbatini, L., Valli, L., & Zambonin, P. G. (1998). Conducting polymers doped with metallic inclusions: New materials for gas sensors. *Sensors and Actuators B: Chemical*, 48(1-3), 362-367.

[135] Lorussi, F., Scilingo, E. P., Tesconi, M., Tognetti, A., & De Rossi, D. (2005). Strain sensing fabric for hand posture and gesture monitoring. *IEEE transactions on information technology in biomedicine*, 9(3), 372-381.

[136] Rundqvist, K., Hernández, N., Syrén, F., Lund, A., & Nierstrasz, V. (2015). Textile sensor for human motion detection in healthcare applications. In *9. Aachen-Dresden International Textile Conference 2015*.

[137] "Eleksen group plc: Company profile - bloomberg." http://www.bloomberg.com/profiles/companies/ELG:LN-eleksen-group-plc (Accessed on 18/08/2018).

[138] Lucarotti, C., Totaro, M., Sadeghi, A., Mazzolai, B., & Beccai, L. (2015). Revealing bending and force in a soft body through a plant root inspired approach. *Scientific reports*, 5, 8788.

[139] Sergio, M., Manaresi, N., Campi, F., Canegallo, R., Tartagni, M., & Guerrieri, R. (2003). A dynamically reconfigurable monolithic CMOS pressure sensor for smart fabric. *IEEE Journal of solid-state circuits*, 38(6), 966-975.

[140] Meyer, J., Arnrich, B., Schumm, J., & Troster, G. (2010). Design and modeling of a textile pressure sensor for sitting posture classification. *IEEE Sensors Journal*, 10(8), 1391-1398.

[141] "Home page - plug and wear." http://www.plugandwear.com/ (Accessed on 20/08/2018).

[142] Cho, G., Jeong, K., Paik, M. J., Kwun, Y., & Sung, M. (2011). Performance evaluation of textile-based electrodes and motion sensors for smart clothing. *IEEE Sensors Journal*, 11(12), 3183-3193.

[143] Huang, C. T., Shen, C. L., Tang, C. F., & Chang, S. H. (2008). A wearable yarn-based piezo-resistive sensor. *Sensors and Actuators A: Physical*, 141(2), 396-403.

[144] Huang, C. T., Tang, C. F., Lee, M. C., & Chang, S. H. (2008). Parametric design of yarn-based piezoresistive sensors for smart textiles. *Sensors and Actuators A: Physical*, 148(1), 10-15.

[145] Sawhney, A., Agrawal, A., Patra, P., & Calvert, P. (2006). Piezoresistive sensors on textiles by inkjet printing and electroless plating. *MRS Online Proceedings Library Archive*, 920.

[146] Kim, K. J., Chang, Y. M., Yoon, S., & Kim, H. J. (2009). A novel piezoelectric PVDF film-based physiological sensing belt for a complementary respiration and heartbeat monitoring system. *Integrated Ferroelectrics*, 107(1), 53-68.

[147] Carpi, F., De Rossi, D., Kornbluh, R., Pelrine, R. E., & Sommer-Larsen, P. (Eds.). (2011). *Dielectric elastomers as electromechanical transducers:*

Fundamentals, materials, devices, models and applications of an emerging electroactive polymer technology. Elsevier.

[148] Scilingo, E. P., Lorussi, F., Mazzoldi, A., & De Rossi, D. (2003). Strain-sensing fabrics for wearable kinaesthetic-like systems. *IEEE sensors journal*, 3(4), 460-467.

[149] Daoud, W. A., Xin, J. H., & Szeto, Y. S. (2005). Polyethylenedioxythiophene coatings for humidity, temperature and strain sensing polyamide fibers. *Sensors and Actuators B: Chemical*, 109(2), 329-333.

[150] Lipomi, D. J., Lee, J. A., Vosgueritchian, M., Tee, B. C. K., Bolander, J. A., & Bao, Z. (2012). Electronic properties of transparent conductive films of PEDOT: PSS on stretchable substrates. *Chemistry of Materials*, 24(2), 373-382.

[151] Molina, J., Esteves, M. F., Fernández, J., Bonastre, J., & Cases, F. (2011). Polyaniline coated conducting fabrics. Chemical and electrochemical characterization. *European Polymer Journal*, 47(10), 2003-2015.

[152] Kim, H. K., Kim, M. S., Chun, S. Y., Park, Y. H., Jeon, B. S., Lee, J. Y., ... & Kim, S. H. (2003). Characteristics of electrically conducting polymer-coated textiles. *Mol. Cryst. Liq. Cryst.*, 405(1), 161-169.

[153] Castano, L. M., Winkelmann, A. E., & Flatau, A. B. (2009, March). A first approach to foot motion monitoring using conductive polymer sensors. In *Sensors and Smart Structures Technologies for Civil, Mechanical, and Aerospace Systems 2009* (Vol. 7292, p. 72922O). International Society for Optics and Photonics.

[154] Salerno, M., Mazzocchi, T., Ranzani, T., Mulana, F., Dario, P., & Menciassi, A. (2013, November). Safety systems in magnetically driven wireless capsule endoscopy. In *Intelligent Robots and Systems (IROS), 2013 IEEE/RSJ International Conference on* (pp. 3090-3095). IEEE.

[155] Shimojo, M., Namiki, A., Ishikawa, M., Makino, R., & Mabuchi, K. (2004). A tactile sensor sheet using pressure conductive rubber with electrical-wires stitched method. *IEEE Sensors journal*, 4(5), 589-596.

[156] Robertson, B. E., & Walkden, A. J. (1985). Tactile sensor system for robotics. *Measurement and Control*, 18(7), 262-265.

[157] Hillis, W. D. (1982). A high-resolution imaging touch sensor. *The International Journal of Robotics Research*, 1(2), 33-44.

[158] Del Prete, Z., Monteleone, L., & Steindler, R. (2001) A novel pressure array sensor based on contact resistance variation: metrological properties. *Rev. Sci. Instrum.* 72, 1548–53.

[159] Hyndman, R. J., & Koehler, A. B. (2006). Another look at measures of forecast accuracy. *International journal of forecasting*, 22(4), 679-688.

[160] Komi, E. R., Roberts, J. R., & Rothberg, S. J. (2007). Evaluation of thin, flexible sensors for time-resolved grip force measurement. *Proceedings of the Institution of Mechanical Engineers, Part C: Journal of Mechanical Engineering Science*, 221(12), 1687-1699.

[161] Smith, S. W. (1997) The Scientist And Engineer's Guide To Digital Signal Processing. (San Diego, CA: California Technical Pub).

[162] Rosenberg, I., & Perlin, K. (2009). The UnMousePad: an interpolating multi-touch force-sensing input pad. *ACM Transactions on Graphics (TOG)*, 28(3), 65.

[163] Chuan, Y., & Chen, L. (2011). The compensation for hysteresis of silicon piezoresistive pressure sensor. *IEEE Sensors Journal*, 11(9), 2016-2021.

[164] Hall, R. S., Desmoulin, G. T., & Milner, T. E. (2008). A technique for conditioning and calibrating force-sensing resistors for repeatable and reliable measurement of compressive force. *Journal of biomechanics*, 41(16), 3492-3495.

[165] http://marktek-inc.com/doc/EeonTexTDSF1.pdf (Accessed on 23/08/2018)

[166] Baldoli, I. et. al. (2016). Pressure mapping with textile sensors for compression therapy monitoring. *Proc. Inst. Mech. Eng. H*, 230, 795–808.

[167] Atalay, O., Kennon, W. R., & Husain, M. D. (2013). Textile-based weft knitted strain sensors: effect of fabric parameters on sensor properties. *Sensors*, 13, 11114–27.

[168] Pantelopoulos, A., & Bourbakis, N. G. (2010). A survey on wearable sensor-based systems for health monitoring and prognosis. *IEEE Trans. Syst., Man, and Cybern. C*, 40, 1–12.

[169] Ferguson-Pell, M., & Cardi, M. D. (1993). Prototype development and comparative evaluation of wheelchair pressure mapping system. *Assistive Technology*, 5(2), 78-91.

[170] Baldoli, I., Maselli, M., Cecchi, F., & Laschi, C. (2017). Development and characterization of a multilayer matrix textile sensor for interface pressure measurements. *Smart Materials and Structures*, 26(10), 104011.

[171] Lorussi, F., Rocchia, W., Scilingo, E. P., Tognetti, A., & De Rossi, D. (2004). Wearable, redundant fabric-based sensor arrays for reconstruction of body segment posture. *IEEE sensors Journal*, 4(6), 807-818.

[172] Neumann, J. J., Greve, D. W., & Oppenheim, I. J. (2004, July). Comparison of piezoresistive and capacitive ultrasonic transducers. In *Smart Structures and Materials 2004: Sensors and Smart Structures Technologies for Civil, Mechanical, and Aerospace Systems* (Vol. 5391, pp. 230-239). International Society for Optics and Photonics.

[173] Sergio, M., Manaresi, N., Nicolini, M., Gennaretti, D., Tartagni, M., & Guerrieri, R. (2004). A textile-based capacitive pressure sensor. *Sensor Letters*, 2(2), 153-160.

[174] Hardy, V. G. (2008). Design and construction of smart structures for technical textiles (Doctoral dissertation, University of Leeds).

[175] Mattmann, C., Kirstein, T., & Tröster, G. (2005, September). A method to measure elongations of clothing. In *Proc. 1st International Scientific Conference Ambience* (Vol. 5).

[176] Cochrane, C., Koncar, V., Lewandowski, M., & Dufour, C. (2007). Design and development of a flexible strain sensor for textile structures based on a conductive polymer composite. *Sensors*, 7(4), 473-492.

[177] Mattmann, C., Clemens, F., & Tröster, G. (2008). Sensor for measuring strain in textile. *Sensors*, 8(6), 3719-3732.

[178] Gibbs, P., & Asada, H. H. (2004, April). Wearable conductive fiber sensors for measuring joint movements. In *Robotics and Automation, 2004. Proceedings. ICRA'04. 2004 IEEE International Conference on* (Vol. 5, pp. 4753-4758). IEEE.

[179] Guo, L., Berglin, L., & Mattila, H. (2010). Textile strain sensors characterization-sensitivity, linearity, stability and hysteresis. *Nordic Textile Journal*, (2), 51-63.

[180] Shyr, T. W., Shie, J. W., & Jhuang, Y. E. (2011). The effect of tensile hysteresis and contact resistance on the performance of strain-resistant elastic-conductive webbing. *Sensors*, 11(2), 1693-1705.

[181] Muscolo, G. G., Recchiuto, C. T., Hashimoto, K., Dario, P., & Takanishi, A. (2012). Towards an improvement of the SABIAN humanoid robot: From design to optimization. *Journal of Mechanical Engineering and Automation*, 2(4), 80-84.

[182] Lim, C. K., Luo, Z., Chen, I. M., & Yeo, S. H. (2011). A low cost wearable optical-based goniometer for human joint monitoring. *Frontiers of Mechanical Engineering*, 6(1), 13-22.

[183] Nakamoto, H., Ootaka, H., Tada, M., Hirata, I., Kobayashi, F., & Kojima, F. (2016). Stretchable strain sensor with anisotropy and application for joint angle measurement. *IEEE Sensors Journal*, 16(10), 3572-3579.

[184] Atalay, O., Kennon, W. R., & Demirok, E. (2015). Weft-knitted strain sensor for monitoring respiratory rate and its electro-mechanical modeling. *IEEE Sensors Journal*, 15(1), 110-122.

[185] Fraden, J. (2004). Handbook of modern sensors: physics, designs, and applications. Springer Science & Business Media.

[186] Wang, L., Han, Y., Wu, C., & Huang, Y. (2013). A solution to reduce the time dependence of the output resistance of a viscoelastic and piezoresistive element. *Smart Materials and Structures*, 22(7), 075021.

[187] Atalay, O., & Kennon, W. R. (2014). Knitted strain sensors: Impact of design parameters on sensing properties. *Sensors*, 14(3), 4712-4730.

[188] Sunny, M. R., & Kapania, R. K. (2010). A Hysteresis Compensator Based on a Modified Dynamic Preisach Model for Conductive Polymer Nanocomposites. In *IUTAM Symposium on Multi-Functional Material Structures and Systems* (pp. 87-94). Springer, Dordrecht.

[189] Lee, H., Cho, H., Kim, S. J., Kim, Y., & Kim, J. (2018). Dispenser printing of piezo-resistive nanocomposite on woven elastic fabric and hysteresis compensation for skin-mountable stretch sensing. *Smart Materials and Structures*, 27(2), 025017.

[190] Biggio, M., Oliveri, A., Stellino, F., Parodi, M., & Storace, M. (2015). A circuit model of hysteresis and creep. *IEEE Transactions on Circuits and Systems II: Express Briefs*, 62(5), 501-505.

[191] Devasia, S., Eleftheriou, E., & Moheimani, S. R. (2007). A survey of control issues in nanopositioning. *IEEE Transactions on Control Systems Technology*, 15(5), 802-823.

[192] Sun, Z., Song, B., Xi, N., Yang, R., Hao, L., Yang, Y., & Chen, L. (2017). Asymmetric hysteresis modeling and compensation approach for nanomanipulation system motion control considering working-range effect. *IEEE Transactions on Industrial Electronics*, 64(7), 5513-5523.

[193] Grassi, A., Cecchi, F., Maselli, M., Röling, M., Laschi, C., & Cianchetti, M. (2017). Warp-knitted textile as a strain sensor: Characterization procedure and application in a comfortable wearable goniometer. *IEEE Sensors Journal*, 17(18), 5927-5936.

[194] Oliveri, A., Lodi, M., Parodi, M., Stellino, F., & Storace, M. (2017). Model reduction for optimized online compensation of hysteresis and creep in piezoelectric actuators. *IEEE Transactions on Circuits and Systems II: Express Briefs*.

[195] Metta, G., Natale, L., Nori, F., Sandini, G., Vernon, D., Fadiga, L., ... & Bernardino, A. (2010). The iCub humanoid robot: An open-systems platform for research in cognitive development. *Neural Networks*, 23(8-9), 1125-1134.

[196] Tsagarakis, N. G., Metta, G., Sandini, G., Vernon, D., Beira, R., Becchi, F., ... & Caldwell, D. G. (2007). iCub: the design and realization of an open humanoid platform for cognitive and neuroscience research. *Advanced Robotics*, 21(10), 1151-1175.

[197] Oliveri, A., Lodi, M., Stellino, F., & Storace, M. (2018, May). Modeling and compensation of hysteresis and creep: The HysTool toolbox. In *Circuits and Systems (ISCAS), 2018 IEEE International Symposium on* (pp. 1-5). IEEE.

[198] Oliveri, A., Stellino, F., Caluori, G., Parodi, M., & Storace, M. (2016). Open-loop compensation of hysteresis and creep through a power-law circuit model. *IEEE Transactions on Circuits and Systems I: Regular Papers*, 63(3), 413-422.

[199] Snodgrass, S. J., Cleland, J. A., Haskins, R., & Rivett, D. A. (2014). The clinical utility of cervical range of motion in diagnosis, prognosis, and evaluating the effects of manipulation: a systematic review. *Physiotherapy*, 100(4), 290-304.

[200] Dall'Alba, P. T., Sterling, M. M., Treleaven, J. M., Edwards, S. L., & Jull, G. A. (2001). Cervical range of motion discriminates between asymptomatic persons and those with whiplash. *Spine*, 26(19), 2090-2094.

[201] Strimpakos, N. (2011). The assessment of the cervical spine. Part 1: range of motion and proprioception. *Journal of bodywork and movement therapies*, 15(1), 114-124.

[202] Ferrario, V. F., Sforza, C., Serrao, G., Grassi, G., & Mossi, E. (2002). Active range of motion of the head and cervical spine: a three-dimensional investigation in healthy young adults. *Journal of orthopaedic research*, 20(1), 122-129.

[203] Sforza, C., Grassi, G., Fragnito, N., Turci, M., & Ferrario, V. F. (2002). Three-dimensional analysis of active head and cervical spine range of motion: effect of age in healthy male subjects. *Clinical Biomechanics*, 17(8), 611-614.

[204] Gelalis, I. D., DeFrate, L. E., Stafilas, K. S., Pakos, E. E., Kang, J. D., & Gilbertson, L. G. (2009). Three-dimensional analysis of cervical spine motion: reliability of a computer assisted magnetic tracking device compared to inclinometer. *European Spine Journal*, 18(2), 276-281.

[205] Koerhuis, C. L., Winters, J. C., Van der Helm, F. C. T., & Hof, A. L. (2003). Neck mobility measurement by means of the 'Flock of Birds' electromagnetic tracking system. *Clinical Biomechanics*, 18(1), 14-18.

[206] Wang, S. F., Teng, C. C., & Lin, K. H. (2005). Measurement of cervical range of motion pattern during cyclic neck movement by an ultrasound-based motion system. *Manual therapy*, 10(1), 68-72.

[207] Song, H., Zhai, X., Gao, Z., Lu, T., Tian, Q., Li, H., & He, X. (2018). Reliability and validity of a Coda Motion 3-D Analysis system for measuring cervical range of motion in healthy subjects. *Journal of Electromyography and Kinesiology*, 38, 56-66.

[208] Feipel, V., Rondelet, B., Le Pallec, J. P., & Rooze, M. (1999). Normal global motion of the cervical spine:: an electrogoniometric study. *Clinical Biomechanics*, 14(7), 462-470.

[209] Christensen, H. W., & Nilsson, N. (1998). Natural variation of cervical range of motion: a one-way repeated-measures design. *Journal of manipulative and physiological therapeutics*, 21(6), 383-387.

[210] Christensen, H. W. (1999). Precision and accuracy of an electrogoniometer. *Journal of manipulative and physiological therapeutics*, 22(1), 10-14.

[211] Salian, S. C., & Tiwari, A. (2018). Intra-and Inter-reliability of Cervical Goniometer Used to Measure Cervical Range of Motion in Young Adults. In *Ergonomics in Caring for People* (pp. 223-232). Springer, Singapore.

[212] Stenneberg, M. S., Busstra, H., Eskes, M., van Trijffel, E., Cattrysse, E., Scholten-Peeters, G. G., & de Bie, R. A. (2018). Concurrent validity and interrater reliability of a new smartphone application to assess 3D active cervical range of motion in patients with neck pain. *Musculoskeletal Science and Practice*, 34, 59-65.

[213] Duc, C., Salvia, P., Lubansu, A., Feipel, V., & Aminian, K. (2014). A wearable inertial system to assess the cervical spine mobility: comparison with an

optoelectronic-based motion capture evaluation. *Medical engineering & physics*, 36(1), 49-56.

[214] Jasiewicz, J. M., Treleaven, J., Condie, P., & Jull, G. (2007). Wireless orientation sensors: their suitability to measure head movement for neck pain assessment. *Manual therapy*, 12(4), 380-385.

[215] Inokuchi, H., Tojima, M., Mano, H., Ishikawa, Y., Ogata, N., & Haga, N. (2015). Neck range of motion measurements using a new three-dimensional motion analysis system: validity and repeatability. *European Spine Journal*, 24(12), 2807-2815.

[216] Lorussi, F., Carbonaro, N., De Rossi, D., & Tognetti, A. (2017). Strain-and Angular-Sensing Fabrics for Human Motion Analysis in Daily Life. In *Smart Textiles* (pp. 49-70). Springer, Cham.

[217] Cheng, J., Amft, O., & Lukowicz, P. (2010, May). Active capacitive sensing: Exploring a new wearable sensing modality for activity recognition. In *International conference on pervasive computing* (pp. 319-336). Springer, Berlin, Heidelberg.

[218] Dunne, L. E., Brady, S., Smyth, B., & Diamond, D. (2005). Initial development and testing of a novel foam-based pressure sensor for wearable sensing. *Journal of NeuroEngineering and Rehabilitation*, 2(1), 4.

[219] Chen, S., Liu, S., Wang, P., Liu, H., & Liu, L. (2018). Highly stretchable fiber-shaped e-textiles for strain/pressure sensing, full-range human motions detection, health monitoring, and 2D force mapping. *Journal of Materials Science*, 53(4), 2995-3005.

[220] Meghdari, A., & Bahrami, A. H. (2004). A biomechanical model to analyze normal, degenerated, and fused cervical spines using IAR's concept. *IRANIAN JOURNAL OF SCIENCE AND TECHNOLOGY*, 28(B4), 423-433.

[221] Zatsiorsky, V. M., & Zaciorskij, V. M. (2002). *Kinetics of human motion*. Human Kinetics.

[222] Lim, C. K., Chen, I. M., Luo, Z., & Yeo, S. H. (2010, June). A low cost wearable wireless sensing system for upper limb home rehabilitation. In *Robotics Automation and Mechatronics (RAM), 2010 IEEE Conference on* (pp. 1-8). IEEE.

[223] Leardini, A., Biagi, F., Merlo, A., Belvedere, C., & Benedetti, M. G. (2011). Multi-segment trunk kinematics during locomotion and elementary exercises. *Clinical Biomechanics*, 26(6), 562-571.

[224] "Kinesiotaping Web Site." https://kinesiotaping.com/about/what-is-kinesio-tape (Accessed on 13/09/2018).

[225] "BuildItSolar Web Site." http://www.builditsolar.com/References/Glazing/physicalpropertiesAcrylic.pdf (Accessed on 13/09/2018).

[226] "MatWeb Web Site." http://www.matweb.com/index.aspx (Accessed on 13/09/2018).

[227] Anderst, W. J., Donaldson III, W. F., Lee, J. Y., & Kang, J. D. (2015). Cervical motion segment contributions to head motion during flexion\extension, lateral bending, and axial rotation. *The Spine Journal*, 15(12), 2538-2543.

[228] Preis, S. R., Massaro, J. M., Hoffmann, U., D'Agostino Sr, R. B., Levy, D., Robins, S. J., ... & Fox, C. S. (2010). Neck circumference as a novel measure of cardiometabolic risk: the Framingham Heart study. *The journal of clinical endocrinology & metabolism*, 95(8), 3701-3710.

[229] L. G. Portney and M. P. Watkins. (2000) *Foundations of Clinical Research: Applications to Practice*. Englewood Cliffs, NJ, USA: Prentice-Hall.

[230] Maselli, M., Mussi, E., Cecchi, F., Manti, M., Tropea, P., & Laschi, C. (2018). A wearable sensing device for monitoring single planes neck movements: Assessment of its performance. *IEEE Sens*. J, 18, 6327-6336.

[231] "Eurostat. Population structure and ageing – Statistics Explained." http://ec.europa.eu/eurostat/statistics-explained/index.php/Population_structure_and_ageing. (Accessed on 17/09/2018).

[232] Harada, C. N., Love, M. C. N., & Triebel, K. L. (2013). Normal cognitive aging. *Clinics in geriatric medicine*, 29(4), 737-752.

[233] Lee, T. M., Chan, F. H., Chu, L. W., Kwok, T. C. Y., Lam, L. C. W., Tam, H. M. K., & Woo, J. (2017). Auditory-based cognitive training programme for attention and memory in older people at risk of progressive cognitive decline: a randomised controlled trial. *Hong Kong Med J*, 23(3 Supplement 2).

[234] Gregory, M. A., Gill, D. P., Shellington, E. M., Liu-Ambrose, T., Shigematsu, R., Zou, G., ... & Petrella, R. J. (2016). Group-based exercise and cognitive-physical training in older adults with self-reported cognitive complaints: The Multiple-Modality, Mind-Motor (M4) study protocol. *BMC geriatrics*, 16(1), 17.

[235] Alzheimer's Association. (2017). 2017 Alzheimer's disease facts and figures. *Alzheimer's & Dementia*, 13(4), 325-373.

[236] Kallio, E. L., Öhman, H., Kautiainen, H., Hietanen, M., & Pitkälä, K. (2017). Cognitive training interventions for patients with Alzheimer's disease: A systematic review. *Journal of Alzheimer's Disease*, 56(4), 1349-1372.

[237] Lampit, A., Hallock, H., & Valenzuela, M. (2014). Computerized cognitive training in cognitively healthy older adults: a systematic review and meta-analysis of effect modifiers. *PLoS medicine*, 11(11), e1001756.

[238] Bherer, L., Erickson, K. I., & Liu-Ambrose, T. (2013). A review of the effects of physical activity and exercise on cognitive and brain functions in older adults. *Journal of aging research*, 2013.

[239] Nouchi, R., Taki, Y., Takeuchi, H., Sekiguchi, A., Hashizume, H., Nozawa, T., ... & Kawashima, R. (2014). Four weeks of combination exercise training improved executive functions, episodic memory, and processing speed in healthy elderly people: evidence from a randomized controlled trial. *Age*, 36(2), 787-799.

[240] Belleville, S. (2008). Cognitive training for persons with mild cognitive impairment. *International Psychogeriatrics*, 20(1), 57-66.

[241] Forte, R., Boreham, C. A., Leite, J. C., De Vito, G., Brennan, L., Gibney, E. R., & Pesce, C. (2013). Enhancing cognitive functioning in the elderly: multicomponent vs resistance training. *Clinical interventions in aging*, 8, 19.

[242] Suzuki, T., Shimada, H., Makizako, H., Doi, T., Yoshida, D., Tsutsumimoto, K., ... & Park, H. (2012). Effects of multicomponent exercise on cognitive function in older adults with amnestic mild cognitive impairment: a randomized controlled trial. *BMC neurology*, 12(1), 128.

[243] Petersen, R. C., Parisi, J. E., Dickson, D. W., Johnson, K. A., Knopman, D. S., Boeve, B. F., ... & Braak, H. (2006). Neuropathologic features of amnestic mild cognitive impairment. *Archives of neurology*, 63(5), 665-672.

[244] Petersen, R. C. (2004). Mild cognitive impairment as a diagnostic entity. *Journal of internal medicine*, 256(3), 183-194.

[245] Stephan, B. C., Matthews, F. E., McKeith, I. G., Bond, J., Brayne, C., & Medical Research Council Cognitive Function and Aging Study. (2007). Early cognitive change in the general population: how do different definitions work?. *Journal of the American Geriatrics Society*, 55(10), 1534-1540.

[246] Amieva, H., Jacqmin-Gadda, H., Orgogozo, J. M., Le Carret, N., Helmer, C., Letenneur, L., ... & Dartigues, J. F. (2005). The 9 year cognitive decline before

dementia of the Alzheimer type: a prospective population-based study. *Brain*, 128(5), 1093-1101.

[247] Zhu, X., Yin, S., Lang, M., He, R., & Li, J. (2016). The more the better? A meta-analysis on effects of combined cognitive and physical intervention on cognition in healthy older adults. *Ageing research reviews*, 31, 67-79.

[248] Lai, L., Bruce, H., Bherer, L., Lussier, M., & Li, K. Z. (2017). Comparing the transfer effects of simultaneously and sequentially combined aerobic exercise and cognitive training in older adults. *Journal of Cognitive Enhancement*, 1(4), 478-490.

[249] Fraser, S. A., Li, K. Z. H., Berryman, N., Desjardins-Crépeau, L., Lussier, M., Vadaga, K., ... & Bherer, L. (2017). Does combined physical and cognitive training improve dual-task balance and gait outcomes in sedentary older adults?. *Frontiers in human neuroscience*, 10, 688.

[250] Rahe, J., Petrelli, A., Kaesberg, S., Fink, G. R., Kessler, J., & Kalbe, E. (2015). Effects of cognitive training with additional physical activity compared to pure cognitive training in healthy older adults. *Clinical interventions in aging*, 10, 297.

[251] Hiyamizu, M., Morioka, S., Shomoto, K., & Shimada, T. (2012). Effects of dual task balance training on dual task performance in elderly people: a randomized controlled trial. *Clinical rehabilitation*, 26(1), 58-67.

[252] Theill, N., Schumacher, V., Adelsberger, R., Martin, M., & Jäncke, L. (2013). Effects of simultaneously performed cognitive and physical training in older adults. *BMC neuroscience*, 14(1), 103.

[253] Tulving, E., & Thomson, D. M. (1973). Encoding specificity and retrieval processes in episodic memory. *Psychological review*, 80(5), 352.

[254] Bozoki, A., Radovanovic, M., Winn, B., Heeter, C., & Anthony, J. C. (2013). Effects of a computer-based cognitive exercise program on age-related cognitive decline. *Archives of Gerontology and Geriatrics*, 57(1), 1-7.

[255] Hartman, D. E. (2009). Wechsler Adult Intelligence Scale IV (WAIS IV): return of the gold standard. *Applied neuropsychology*, 16(1), 85-87.

[256] Guo, J. J., Wu, K., Guan, H., Zhang, L., Ji, C., Yang, H., & Tang, T. (2016). Three-year follow-up of conservative treatments of shoulder osteoarthritis in older patients. *Orthopedics*.

[257] Whitehurst, M. A., Johnson, B. L., Parker, C. M., Brown, L. E., & Ford, A. M. (2005). The benefits of a functional exercise circuit for older adults. *Journal of strength and conditioning research*, 19(3), 647.

[258] Brazzelli, M., Capitani, E., Della Sala, S., Spinnler, H., & Zuffi, M. (1994). *MODA Milan Overall Dementia Assessment: manuale*. OS.

[259] Katz, S., Downs, T. D., Cash, H. R., & Grotz, R. C. (1970). Progress in development of the index of ADL. *The gerontologist*, 10(1_Part_1), 20-30.

[260] Graf, C. (2009). The Lawton instrumental activities of daily living (IADL) scale. *Medsurg Nurs*, 18(5), 315-6.

[261] Petersen, R. C., & Morris, J. C. (2005). Mild cognitive impairment as a clinical entity and treatment target. *Archives of neurology*, 62(7), 1160-1163.

[262] Brooke, J. (1996). SUS-A quick and dirty usability scale. *Usability evaluation in industry*, 189(194), 4-7.

[263] Muñiz, J. (2009, July). The role of EFPA in setting standards for tests and test use. In *11th European Congress of Psychology, Oslo, Norway*.

[264] Buczylowska, D., & Petermann, F. (2016). Age-related differences and heterogeneity in executive functions: analysis of NAB executive functions module scores. *Archives of Clinical Neuropsychology*, 31(3), 254-262.

[265] Brustio, P. R., Magistro, D., Zecca, M., Rabaglietti, E., & Liubicich, M. E. (2017). Age-related decrements in dual-task performance: Comparison of different mobility and cognitive tasks. A cross sectional study. *PloS one*, 12(7), e0181698.

[266] De Simone, M. S., Perri, R., Fadda, L., De Tollis, M., Turchetta, C. S., Caltagirone, C., & Carlesimo, G. A. (2017). Different deficit patterns on word lists and short stories predict conversion to Alzheimer's disease in patients with amnestic mild cognitive impairment. *Journal of neurology*, 264(11), 2258-2267.

[267] Law, L. L., Barnett, F., Yau, M. K., & Gray, M. A. (2014). Effects of combined cognitive and exercise interventions on cognition in older adults with and without cognitive impairment: a systematic review. *Ageing research reviews*, 15, 61-75.

[268] Barnard, Y., Bradley, M. D., Hodgson, F., & Lloyd, A. D. (2013). Learning to use new technologies by older adults: Perceived difficulties, experimentation behaviour and usability. *Computers in Human Behavior*, 29(4), 1715-1724.

[269] Bangor, A., Kortum, P. T., & Miller, J. T. (2008). An empirical evaluation of the system usability scale. *Intl. Journal of Human–Computer Interaction*, 24(6), 574-594.

[270] Krieger, N. (2003). Genders, sexes, and health: what are the connections—and why does it matter?. *International journal of epidemiology*, 32(4), 652-657.

[271] Giuliani, M. V., Scopelliti, M., & Fornara, F. (2005, August). Elderly people at home: technological help in everyday activities. In *Robot and Human Interactive Communication, 2005. ROMAN 2005. IEEE International Workshop on* (pp. 365-370). IEEE.

[272] Shams, L., & Seitz, A. R. (2008). Benefits of multisensory learning. *Trends in cognitive sciences*, 12(11), 411-417.

[273] Stavsky, M., Mor, O., Mastrolia, S. A., Greenbaum, S., Than, N. G., & Erez, O. (2017). Cerebral Palsy—Trends in epidemiology and Recent Development in Prenatal Mechanisms of Disease, Treatment, and Prevention. *Frontiers in pediatrics*, 5, 21.

[274] Cioni, G., Sgandurra, G., Muzzini, S., Paolicelli, P. B., & Ferrari, A. (2010). Forms of hemiplegia. In *The Spastic Forms of Cerebral Palsy* (pp. 331-356). Springer, Milano.

[275] Novak, I., Morgan, C., Adde, L., Blackman, J., Boyd, R. N., Brunstrom-Hernandez, J., ... & De Vries, L. S. (2017). Early, accurate diagnosis and early intervention in cerebral palsy: advances in diagnosis and treatment. *JAMA pediatrics*, 171(9), 897-907.

[276] Andersen, G. L., Romundstad, P., CRUZ, J. D. L., Himmelmann, K., Sellier, E., Cans, C., ... & Vik, T. (2011). Cerebral palsy among children born moderately preterm or at moderately low birthweight between 1980 and 1998: a European register-based study. *Developmental Medicine & Child Neurology*, 53(10), 913-919.

[277] Mailleux, L., Jaspers, E., Ortibus, E., Simon-Martinez, C., Desloovere, K., Molenaers, G., ... & Feys, H. (2017). Clinical assessment and three-dimensional movement analysis: an integrated approach for upper limb evaluation in children with unilateral cerebral palsy. *PloS one*, 12(7), e0180196.

[278] Duruöz, M. T. (Ed.). (2014). *Hand function: a practical guide to assessment*. Springer Science & Business Media.

[279] Gilmore, R., Sakzewski, L., & Boyd, R. (2010). Upper limb activity measures for 5-to 16-year-old children with congenital hemiplegia: a systematic review. *Developmental Medicine & Child Neurology*, 52(1), 14-21.

[280] Klingels, K., Jaspers, E., Van de Winckel, A., De Cock, P., Molenaers, G., & Feys, H. (2010). A systematic review of arm activity measures for children with hemiplegic cerebral palsy. *Clinical rehabilitation*, 24(10), 887-900.

[281] Gerber, C. N., Plebani, A., & Labruyère, R. (2017). Translation, reliability, and clinical utility of the Melbourne Assessment 2. *Disability and rehabilitation*, 1-9.

[282] Randall, M., Carlin, J. B., Chondros, P., & Reddihough, D. (2001). Reliability of the Melbourne assessment of unilateral upper limb function. *Developmental medicine and child neurology*, 43(11), 761-767.

[283] Davids, J. R., Peace, L. C., Wagner, L. V., Gidewall, M. A., Blackhurst, D. W., & Roberson, W. M. (2006). Validation of the Shriners Hospital for Children Upper Extremity Evaluation (SHUEE) for children with hemiplegic cerebral palsy. *JBJS*, 88(2), 326-333.

[284] Thorley, M., Lannin, N., Cusick, A., Novak, I., & Boyd, R. (2012). Construct validity of the Quality of Upper Extremity Skills Test for children with cerebral palsy. *Developmental Medicine & Child Neurology*, 54(11), 1037-1043.

[285] Krumlinde-Sundholm, L., Holmefur, M., Kottorp, A., & Eliasson, A. C. (2007). The Assisting Hand Assessment: current evidence of validity, reliability, and responsiveness to change. *Developmental Medicine & Child Neurology*, 49(4), 259-264.

[286] Arnould, C., Penta, M., Renders, A., & Thonnard, J. L. (2004). ABILHAND-Kids A measure of manual ability in children with cerebral palsy. *Neurology*, 63(6), 1045-1052.

[287] Rabuffetti, M., Meriggi, P., Pagliari, C., Bartolomeo, P., & Ferrarin, M. (2016). Differential actigraphy for monitoring asymmetry in upper limb motor activities. *Physiological measurement*, 37(10), 1798.

[288] Strath, S. J., Kate, R. J., Keenan, K. G., Welch, W. A., & Swartz, A. M. (2015). Ngram time series model to predict activity type and energy cost from wrist, hip and ankle accelerometers: implications of age. *Physiological measurement*, 36(11), 2335.

[289] Ellis, K., Kerr, J., Godbole, S., Lanckriet, G., Wing, D., & Marshall, S. (2014). A random forest classifier for the prediction of energy expenditure and type of physical activity from wrist and hip accelerometers. *Physiological measurement*, 35(11), 2191.

[290] Lugade, V., Fortune, E., Morrow, M., & Kaufman, K. (2014). Validity of using tri-axial accelerometers to measure human movement—Part I: Posture and movement detection. *Medical engineering & physics*, 36(2), 169-176.

[291] Natale, V. (2002). Circadian motor asymmetries in humans. *Neuroscience Letters*, 320(1-2), 102-104.

[292] Atallah, L., Wiik, A., Lo, B., Cobb, J. P., Amis, A. A., & Yang, G. Z. (2014). Gait asymmetry detection in older adults using a light ear-worn sensor. *Physiological measurement*, 35(5), N29.

[293] Brodie, M. A., Beijer, T. R., Canning, C. G., & Lord, S. R. (2015). Head and pelvis stride-to-stride oscillations in gait: validation and interpretation of measurements from wearable accelerometers. *Physiological measurement*, 36(5), 857.

[294] Nagels, G., Mariën, P., Pickut, B. A., Timmermans, L., & De Deyn, P. P. (1996). Actigraphic evaluation of handedness. *Clinical Neurophysiology*, 101(3), 226-232.

[295] Rinehart, J. K., Singleton, R. D., Adair, J. C., Sadek, J. R., & Haaland, K. Y. (2009). Arm use after left or right hemiparesis is influenced by hand preference. *Stroke*, 40(2), 545-550.

[296] de Niet, M., Bussmann, J. B., Ribbers, G. M., & Stam, H. J. (2007). The stroke upper-limb activity monitor: its sensitivity to measure hemiplegic upper-limb activity during daily life. *Archives of physical medicine and rehabilitation*, 88(9), 1121-1126.

[297] Gebruers, N., Truijen, S., Engelborghs, S., Nagels, G., Brouns, R., & De Deyn, P. P. (2008). Actigraphic measurement of motor deficits in acute ischemic stroke. *Cerebrovascular Diseases*, 26(5), 533-540.

[298] Gubbi, J., Rao, A. S., Fang, K., Yan, B., & Palaniswami, M. (2013). Motor recovery monitoring using acceleration measurements in post acute stroke patients. *Biomedical engineering online*, 12(1), 33.

[299] Clanchy, K. M., Tweedy, S. M., & Boyd, R. (2011). Measurement of habitual physical activity performance in adolescents with cerebral palsy: a systematic review. *Developmental Medicine & Child Neurology*, 53(6), 499-505.

[300] Mitchell, L. E., Ziviani, J., & Boyd, R. N. (2015). Variability in measuring physical activity in children with cerebral palsy. *Medicine and science in sports and exercise*, 47(1), 194-200.

[301] Holmefur, M., Aarts, P., Hoare, B., & Krumlinde-Sundholm, L. (2009). Test-retest and alternate forms reliability of the assisting hand assessment. *Journal of rehabilitation medicine*, 41(11), 886-891.

[302] Holmefur, M. M., & Krumlinde-Sundholm, L. (2016). Psychometric properties of a revised version of the Assisting Hand Assessment (Kids-AHA 5.0). *Developmental Medicine & Child Neurology*, 58(6), 618-624.

[303] Oldfield, R. C. (1971). The assessment and analysis of handedness: the Edinburgh inventory. *Neuropsychologia*, 9(1), 97-113.

[304] Eliasson, A. C., Krumlinde-Sundholm, L., Rösblad, B., Beckung, E., Arner, M., Öhrvall, A. M., & Rosenbaum, P. (2006). The Manual Ability Classification System (MACS) for children with cerebral palsy: scale development and evidence of validity and reliability. *Developmental medicine and child neurology*, 48(7), 549-554.

[305] O'Dwyer, M., Fairclough, S. J., Ridgers, N. D., Knowles, Z. R., Foweather, L., & Stratton, G. (2014). Patterns of objectively measured moderate-to-vigorous physical activity in preschool children. *Journal of Physical Activity and Health*, 11(6), 1233-1238.

[306] Hagberg, B., Hagberg, G., & Olow, I. (1993). The changing panorama of cerebral palsy in Sweden. VI. Prevalence and origin during the birth year period 1983–1986. *Acta Paediatrica*, 82(4), 387-393.

[307] Guiard, Y. (1987). Asymmetric division of labor in human skilled bimanual action: The kinematic chain as a model. *Journal of motor behavior*, 19(4), 486-517.

[308] Cooper, J., Majnemer, A., Rosenblatt, B., & Birnbaum, R. (1995). The determination of sensory deficits in children with hemiplegic cerebral palsy. *Journal of Child Neurology*, 10(4), 300-309.

[309] Duque, J., Thonnard, J. L., Vandermeeren, Y., Sébire, G., Cosnard, G., & Olivier, E. (2003). Correlation between impaired dexterity and corticospinal tract dysgenesis in congenital hemiplegia. *Brain*, 126(3), 732-747.

[310] Rich, T. L., Menk, J. S., Rudser, K. D., Feyma, T., & Gillick, B. T. (2017). Less-Affected Hand Function in Children With Hemiparetic Unilateral Cerebral Palsy: A Comparison Study With Typically Developing Peers. *Neurorehabilitation and neural repair*, 31(10-11), 965-976.

[311] Arnould, C., Penta, M., & Thonnard, J. L. (2008). Hand impairments and their relationship with manual ability in children with cerebral palsy. *Journal of Rehabilitation Medicine*, 39(9), 708-714.

[312] Birmingham, A. T., Wharrad, H. J., & Williams, E. J. (1985). The variation of finger tremor with age in man. *Journal of Neurology, Neurosurgery & Psychiatry*, 48(8), 788-798.

[313] Sadeh, A., Sharkey, M., & Carskadon, M. A. (1994). Activity-based sleep-wake identification: an empirical test of methodological issues. *Sleep*, 17(3), 201-207.

[314] Deutsch, K. M., & Newell, K. M. (2006). Age-related changes in the frequency profile of children's finger tremor. *Neuroscience letters*, 404(1-2), 191-195.

[315] Graves, L. E., Ridgers, N. D., & Stratton, G. (2008). The contribution of upper limb and total body movement to adolescents' energy expenditure whilst playing Nintendo Wii. *European journal of applied physiology*, 104(4), 617.

[316] Davila, E. M. (2011). *A comparison of bilaterally wrist-worn accelerometers on measures of free-living physical activity in adolescents* (Doctoral dissertation, Montana State University-Bozeman, College of Education, Health & Human Development).

[317] Phillips, L. R., Parfitt, G., & Rowlands, A. V. (2013). Calibration of the GENEA accelerometer for assessment of physical activity intensity in children. *Journal of science and medicine in sport*, 16(2), 124-128.

[318] MacArthur, B., Coe, D., Sweet, A., & Raynor, H. (2014). Active videogaming compared to unstructured, outdoor play in young children: Percent time in moderate-to vigorous-intensity physical activity and estimated energy expenditure. *Games for health journal*, 3(6), 388-394.

[319] Lemmens, R. J., Seelen, H. A., Timmermans, A. A., Schnackers, M. L., Eerden, A., Smeets, R. J., & Janssen-Potten, Y. J. (2015). To What Extent Can Arm–Hand Skill Performance—of Both Healthy Adults and Children—Be Recorded Reliably Using Multiple Bodily Worn Sensor Devices?. *IEEE Transactions on Neural Systems and Rehabilitation Engineering*, 23(4), 581-590.

[320] Kaneko, M., Yamashita, Y., Inomoto, O., & Iramina, K. (2015). Soft neurological signs in childhood by measurement of arm movements using acceleration and angular velocity sensors. *Sensors*, 15(10), 25793-25808.

[321] Dadashi, F., Millet, G. P., & Aminian, K. (2016). Front-crawl stroke descriptors variability assessment for skill characterisation. *Journal of sports sciences*, 34(15), 1405-1412.

[322] Mackintosh, K. A., Montoye, A. H. K., Pfeiffer, K. A., & McNarry, M. A. (2016). Investigating optimal accelerometer placement for energy expenditure prediction in children using a machine learning approach. *Physiological measurement*, 37(10), 1728.

[323] Floyd, A. G., Yu, Q. P., Piboolnurak, P., Wraith, E., Patterson, M. C., & Pullman, S. L. (2007). Kinematic analysis of motor dysfunction in Niemann-Pick type C. *Clinical neurophysiology*, 118(5), 1010-1018.

[324] Gordon, A. M., Schneider, J. A., Chinnan, A., & Charles, J. R. (2007). Efficacy of a hand–arm bimanual intensive therapy (HABIT) in children with hemiplegic cerebral palsy: a randomized control trial. *Developmental Medicine & Child Neurology*, 49(11), 830-838.

[325] Strohrmann, C., Labruyère, R., Gerber, C. N., van Hedel, H. J., Arnrich, B., & Tröster, G. (2013). Monitoring motor capacity changes of children during rehabilitation using body-worn sensors. *Journal of neuroengineering and rehabilitation*, 10(1), 83.

[326] Zoccolillo, L., Morelli, D., Cincotti, F., Muzzioli, L., Gobbetti, T., Paolucci, S., & Iosa, M. (2015). Video-game based therapy performed by children with cerebral palsy: a cross-over randomized controlled trial and a cross-sectional quantitative measure of physical activity. *Eur J Phys Rehabil Med*, 51(6), 669-76.

[327] Sokal, B., Uswatte, G., Vogtle, L., Byrom, E., & Barman, J. (2015). Everyday movement and use of the arms: Relationship in children with hemiparesis differs from adults. *Journal of pediatric rehabilitation medicine*, 8(3), 197-206.

[328] Bergamini, E., Morelli, F., Marchetti, F., Vannozzi, G., Polidori, L., Paradisi, F., ... & Delussu, A. S. (2015). Wheelchair propulsion biomechanics in junior basketball players: A method for the evaluation of the efficacy of a specific training program. *BioMed research international*, 2015.

[329] Kaneko, M., Yamashita, Y., & Iramina, K. (2016). Quantitative Evaluation System of Soft Neurological Signs for Children with Attention Deficit Hyperactivity Disorder. *Sensors*, 16(1), 116.

[330] Le Moing, A. G., Seferian, A. M., Moraux, A., Annoussamy, M., Dorveaux, E., Gasnier, E., ... & Servais, L. (2016). A movement monitor based on magneto-inertial sensors for non-ambulant patients with Duchenne muscular dystrophy: A pilot study in controlled environment. *PloS one*, 11(6), e0156696.

[331] O'neil, M. E., Fragala-Pinkham, M., Lennon, N., George, A., Forman, J., & Trost, S. G. (2016). Reliability and validity of objective measures of physical activity in youth with cerebral palsy who are ambulatory. *Physical therapy*, 96(1), 37-45.

[332] Coker-Bolt, P., Downey, R. J., Connolly, J., Hoover, R., Shelton, D., & Seo, N. J. (2017). Exploring the feasibility and use of accelerometers before, during, and

after a camp-based CIMT program for children with cerebral palsy. *Journal of pediatric rehabilitation medicine*, 10(1), 27-36.

Acknowledgements

This work has been funded by TIM S.p.A., Services Innovation Department, Joint Open Lab Milano, Italy.

I would like to express my gratitude to my supervisor prof. Laschi and to my tutor Dr. Cecchi, for their scientific guidance and support during my PhD studies.

Thanks to Dr. Cianchetti, for his help, presence and scientific support along this period.

Thanks to Dr. Tropea and Irene Mannari for their precious assistance and scientific support in the technical phases of my work.

Many thanks to all my friends and colleagues Elisa M., Emanuela, Ilaria, Elisa B., all the people with I had the pleasure of working together, and all the people I met during this experience.

Finally, all my gratitude goes to my family and Carmine for always standing by my side and trusting me along this experience.